جامعة سيدي محمد بن عبد الله بفاس
ⵜⴰⵙⴷⴰⵡⵉⵜ ⵙⵉⴷⵉ ⵎⵓⵃⵎⵎⴰⴷ ⴱⵏ ⵄⴱⴷⵍⵍⴰⵀ ⵏ ⴼⴰⵙ
UNIVERSITÉ SIDI MOHAMED BEN ABDELLAH DE FES

كلية العلوم والتقنيات فاس
ⵜⴰⵖⵉⵡⴰⵏⵜ ⵏ ⵜⵎⴰⵙⵙⴰⵏⵉⵏ ⴷ ⵜⵙⵏⵉⴳⵉⵜⵉⵏ - ⴼⴰⵙ
FACULTÉ DES SCIENCES ET TECHNIQUES DE FÈS

Centre d'Etudes Doctorales : Sciences et Techniques et Sciences Médicales

N° d'ordre 37 /2022

THESE DE DOCTORAT

Présentée par

Mme : Laila Ouazzani Chahidi

Spécialité : Génie énergétique

Sujet de la thèse : Energy-saving strategies in protected agriculture under Mediterranean climate conditions

Thèse présentée et soutenue le 28 mai 2022 devant le jury composé de :

Nom Prénom	Titre	Etablissement	
Ali Ahaitouf	PES	Faculté des Sciences et Techniques, USMBA, Fès, Maroc	Président
Roberto Sacile	Full Professor	Ecole Polytechnique, Université de Genova, Italie	Rapporteur
Nacer Kouider M'Sirdi	PES	Polytech de Marseille, Université Aix Marseille, France	Rapporteur
Abdelmajid Jamil	PES	Ecole Supérieure de Technologie, USMBA, Fès, Maroc	Rapporteur
Marco Fossa	Full Professor	Ecole Polytechnique, Université de Genova, Italie	Examinateur
Mohammed Rougui	PES	Ecole National des Arts et des Métiers, UM5, Rabat, Maroc	Examinateur
Najia Es-Sbai	PES	Faculté des Sciences et Techniques, USMBA, Fès, Maroc	Examinatrice
Abdellah Mechaqrane	PES	Faculté des Sciences et Techniques, USMBA, Fès, Maroc	Directeur de thèse

Laboratoire d'accueil : Systèmes intelligents, Géoressources, et Energies Renouvelables (SIGER).

Etablissement : Faculté des Sciences et Techniques de Fès (FSTF).

To my precious pearl, my lovely mom,

words cannot be enough to express what you deserve,

you have wished so much that I reached this goal,

that this work be the fruit of your efforts,

that I am always the source of your pride.

Acknowledgements

I would like to express my sincerest thanks to all people who have contributed to the achievement of this work. To all who have crossed my path, giving me time, listening, advice, and experience, and who have allowed me in their own way to progress, to move forward, to mature, to learn and to discover myself better.

Foremost, I would like to express my gratitude to my supervisor Prof. Abdellah Mechaqrane, for the confidence, the support he gave me and the knowledge he shared with me. His ample experience and human qualities have accompanied me all the time of this academic research and daily life. I would also like to thank the head of the Intelligent Systems, Georesources and Renewable Energies (SIGER) Laboratory, Prof. Ali Ahaitouf, for his availability and his enthusiasm. He never hesitated to support and encourage me.

My sincerest thanks to Prof. Marco Fossa for integrating me into his research team, for his confidence, for his continuous support since our first meeting and for sharing his immense knowledge. I am very grateful for all he taught me, humanly and scientifically. I would also like to express my gratitude to Prof. Antonella Priarone for her availability, support and precious help in the most delicate moments, kindness and human qualities. She always had time to listen to me, advise me, and satisfy my curiosity. Meeting and working with a brilliant team allowed me to progress and to feel supported and surrounded.

The EU INTERREG ALCOTRA Project No. 11039 “ANTEA” is acknowledged for granting the SamLab greenhouse project. Prof. R. Sacile (Unige/Dibris Dept) and the Cersaa center (Dr. G.Minuto and F.Tinivella) that shares with Unige the SamLab greenhouse and Erde company are also acknowledged for their fundamental contribution to building the SamLab greenhouse.

I would also like to thank the honorable thesis committee, Prof. Ali Ahaitouf, Prof. Roberto Sacile, Prof. Abdelmajid Jamil, Prof. Nacer Kouider M’sirdi, Prof. Marco Fossa, Prof. Mohammed Rougui and Prof. Najia Sbai for accepting to read the manuscript, evaluate this Ph.D. thesis, participate in the defense and share their relevant remarks, thus contributing to the improvement of the present research.

My special and heartily appreciation to all my professors from Sidi Mohamed Ben Abdellah and Sultan Moulay Sliman Universities, who assisted, encouraged, and supported me during my studies. Especially Prof. Abdelmajid Jamil and Prof. Youssef Mourad (professors at Higher

School of Technology of Fez), Prof. Mohammed Sajieddine, Prof. Rachid El Ayachi, and Prof. Mohammed Erraji (Professors at Faculty of Science and Techniques of Beni Mellal) who have been exemplary professors and idols to me.

Without forgetting, the members of the Intelligent Systems, Georesources and Renewable Energies (SIGER) Laboratory, the professors and the Ph.D. students (former and current). My warm thanks for the unforgettable moments, the friendly atmosphere, the productive discussions and mutual motivation. It would not have been possible to realize this thesis in the best conditions without their kind involvement.

Finally, yet importantly, I would like to thank my whole family and my friends for being there for me, for their unconditional love and support. My deepest thanks to my parents, the pearls of My Heart, for all the sacrifices they made on my behalf, the reason I am who I am today; words cannot express how grateful I am. Many thanks to my sister, the greatest life gift, and my brother, my guardian angel and my faithful companion, for their presence, encouragement and support. I would also like to thank my cousin Nihal Ouazzani Chahdi, a Ph.D. student in Interdisciplinary Social Sciences (at International Graduate School of African Studies, Bayreuth, Germany and Ibn Tofail University, Kenitra, Morocco) for English reviewing of the present thesis report. My warmest thanks to my dearest friend and soulmate, Deyae Badri, who was always by my side to encourage and support me. She assisted me in difficult times and supported me to cross them together.

Abstract

Greenhouse cultivation is one of the most effective and widely used methods in the world, which provides a suitable environment for plants growth. The persisting demand for energy in greenhouses presents the primary constraint for this cultivation method. Thus, the rational use of energy can lead to the development of this method and to a significant decrease in its operational costs. The main purpose of this doctoral thesis is to investigate and quantify the potential of energy-saving obtained by adopting different strategies in greenhouse cultivation. In the first instance, a literature survey is conducted on greenhouse crops production, focusing on greenhouse modeling and energy-efficient operating mode for new greenhouse buildings and greenhouse renovation. Subsequently, dynamic models have been created in the EnergyPlus environment, based on the energy balance of all the greenhouse components. The greenhouse is considered as a single zone that interacts with the outside environment as well as with different interior components (plants, soil and internal masses). The models are manipulated in order to select the optimal greenhouse design (shape, cover and orientation) and to study different energy-saving strategies (integration of passive techniques and renewable energies) in different climate conditions of the Mediterranean region (Albenga, Northwest Italy (as a part of a traineeship in the Department of Mechanical, Energy, Management and Transportation at the University of Genova, Italy) and the six Moroccan climatic zones). Finally, to adequately manage the greenhouse energy needs and resources, different artificial intelligence methods are used, namely artificial neural networks, gaussian process regression, support vector machine, boosting and hybridization of artificial neural networks and boosting methods. The obtained results reveal the importance of the integration of passive techniques, renewable energies and intelligent management strategies.

Keywords: greenhouse cultivation, greenhouse design, energy-saving strategies, machine learning, dynamic modeling.

Résumé

La culture sous serre est l'une des méthodes les plus efficaces et les plus utilisées dans le monde, permettant de créer un environnement approprié pour la croissance des plantes. La demande persistante d'énergie dans les serres représente la principale contrainte de celle-ci. Ainsi, l'utilisation rationnelle de l'énergie peut encourager au développement de cette méthode et conduire à une diminution significative de leurs coûts opérationnels. L'objectif principal de cette thèse est d'étudier et de quantifier le potentiel d'économie d'énergie obtenu en adoptant différentes stratégies appliquées à la culture sous serre. Dans un premier temps, une étude bibliographique est menée avec une attention particulière sur la modélisation des serres et les opérations d'efficacité énergétique pour la construction de nouvelles serres (sélection des caractéristiques de conception) ou pour leur rénovation (intégration des techniques passives et des énergies renouvelables). Pour atteindre les objectifs prédéfinis, des modèles dynamiques ont été créés à l'aide du logiciel EnergyPlus. Les modèles sont basés sur le bilan énergétique des différents composants de la serre. Où cette dernière est considérée comme une seule zone thermique interagissant avec l'environnement extérieur ainsi qu'avec les différents composants intérieurs (plantes, sol et masses internes). Les modèles ont été manipulés afin de sélectionner la conception optimale de la serre (forme, couverture et orientation) et d'étudier différentes stratégies d'économie d'énergie (intégration des techniques passives et des énergies renouvelables) dans différentes conditions climatiques de la région méditerranéenne : Albenga, nord-ouest de l'Italie (dont le choix a été fait dans le cadre d'un stage effectué au Département de Mécanique, Energie, Management et Transport à l'Université de Genova, Italie) et les six zones climatiques du Royaume du Maroc. Enfin, pour gérer de manière adéquate les besoins et les ressources énergétiques des serres, différentes méthodes d'intelligence artificielle ont été utilisées, à savoir réseaux de neurones artificiels, régression par processus gaussien, séparateurs vaste marge, « boosting » et l'hybridation des méthodes réseaux de neurones artificiels et « boosting ». Les résultats obtenus montrent l'importance de l'intégration des techniques passives, des énergies renouvelables et des stratégies de gestion intelligente.

Mots clés : culture sous serre, conception de serre, stratégies d'économie d'énergie, modèle d'apprentissage automatique, modélisation thermique dynamique.

Table of Contents

Acknowledgements iii

Abstract v

Résumé vi

List of figures xii

List of tables xv

Nomenclature xvii

General introduction 21

1. General context 21

2. Problem statement and objectives 21

3. Methodology 22

4. Thesis organization 23

Chapter 1: Background and literature review 26

1.1 Introduction 26

1.2 Background 27

1.2.1 Greenhouse effect 27

1.2.2 Greenhouse climate parameters 29

1.2.2.1 Temperature 29

1.2.2.2 Humidity 30

1.2.2.3 Irradiance level 30

1.2.2.4 Carbon dioxide concentration 30

1.2.2.5 Water need 31

1.3 Research methodology 32

1.3.1 Review objective 32

1.3.2 Search strategy 32

1.4 Review 35

1.4.1 Greenhouse modeling 35
1.4.1.1 Physics-based modeling 35
1.4.1.2 Data-driven (artificial intelligence) modeling 45
1.4.2 Greenhouse design selection 48
1.4.2.1 Greenhouse shapes 49
1.4.2.2 Greenhouse envelope materials 55
1.4.2.3 Greenhouse orientations 58
1.4.3 Energy-saving strategies 61
1.5 Conclusions 64
Chapter 2: Modeling, experimental validation, and energy-saving estimate of SamLab greenhouse 67
2.1 Introduction 67
2.2 SamLab greenhouse description 68
2.3 Data acquisition 71
2.4 Dynamic energy model 71
2.4.1 Geometric model 71
2.4.2 System specifications 72
2.4.2.1 Internal masses 72
2.4.2.2 Windows shading/reflecting system 73
2.4.2.3 Natural ventilation by operable windows 73
2.4.3 Greenhouse energy balance 74
2.4.3.1 Energy balance of glazing surfaces 74
2.4.3.2 Energy balance of opaque surfaces: 75
2.4.3.3 Energy balance of vegetation and soil 77
2.4.3.4 Energy balance of the air 78
2.4.4 HVAC modeling 78
2.4.5 PV modules 80

2.4.6 Performance evaluation 82
2.5 Validation of SamLab greenhouse model 82
2.5.1 External weather conditions 82
2.5.2 HVAC system 84
2.5.3 PV modules 86
2.5.4 Model performance 87
2.6 Greenhouse thermal behavior and energy-saving strategies 88
2.6.1 Effect of plants and internal masses 89
2.6.2 Effect of passive techniques 91
2.6.3 Renewable energy resources 92
2.6.3.1 The HVAC system: the ground-coupled heat pump 92
2.6.3.2 PV modules' production 94
2.7 Conclusions 95
Chapter 3: Selection of optimal greenhouse design in Moroccan climate conditions 98
3.1 Introduction 98
3.2 Study methodology 99
3.3 Moroccan climatic zones 100
3.3.1 Description of the Moroccan climatic zones 100
3.3.2 External temperatures 101
3.4 Greenhouses specifications 102
3.4.1 Greenhouse shapes 102
3.4.2 Greenhouse cover materials 103
3.4.3 Greenhouse orientations 104
3.4.4 Plants 104
3.5 Selection of optimal greenhouse shape and cover material 105
3.5.1 Impact of shape and cover material on greenhouse thermal loads 105

3.5.2 Impact of greenhouse shape and envelope material on annual air-conditioning cost 110

3.5.3 Impact of shape and envelope material on greenhouse floor incident radiation 111

3.6 Selection of optimal greenhouse orientation 113

3.6.1 Impact of orientation on greenhouse thermal loads 113

3.6.2 Impact of greenhouse orientation on annual air-conditioning cost 116

3.7 Improvement of the greenhouse energy efficiency 118

3.7.1 Thermal blankets insulation 118

3.7.2 Controlled natural ventilation 120

3.8 Conclusions 121

Chapter 4: Prediction of greenhouse energy demand and production using machine-learning methods 125

4.1 Introduction 125

4.2 Data sets 126

4.3 Models description 127

4.3.1 Artificial neural networks ANN 127

4.3.2 Gaussian process regression GPR 128

4.3.3 Support vector machine SVM 129

4.3.4 Boosting 130

4.4 Performance analysis 131

4.5 Comparison of four machine-learning models 132

4.5.1 Prediction of the air-conditioning electrical consumption 132

4.5.2 Prediction of the PV modules' electrical production 135

4.5.3 Comparison and analysis of the four methods 137

4.6 Impact of number of neurons in the hidden layer on ANN performance 138

4.7 Performance assessment of a hybrid model ANN-BST 140

4.7.1 Series hybrid model 141

4.7.2 Parallel hybrid model 143
4.7.3 Comparison and analysis of the hybrid approaches 145
4.8 Conclusions 146
General conclusions and perspectives 148
Publications 150
References 152

List of Figures

Figure 1.1. Greenhouse system. 26
Figure 1.2. Flowchart of chapter organization. 27
Figure 1.3. The schematization of the greenhouse effect. 28
Figure 1.4. Terrestrial solar spectral irradiance [12]. 29
Figure 1.5. The schematization of evapotranspiration process. 32
Figure 1.6. Distribution of studies showing the plants involved in the greenhouse model (years from 2000 to 2021). 45
Figure 1.7. Distribution of studies on Data-Driven methods used in greenhouse modeling (years from 2000 to 2021). 48
Figure 1.8. Distribution of greenhouse covering materials in greenhouse selection papers (years from 2000 to 2021). 57
Figure 1.9. Energy-saving strategies for sustainable greenhouse cultivation. 63
Figure 2.1. SamLab greenhouse external view. 68
Figure 2.2. SamLab ground-coupled heat pump and bench alimentation system. 70
Figure 2.3. SamLab air and cultivation bench energy alimentation system. 70
Figure 2.4. SamLab greenhouse 3D model. 72
Figure 2.5. Measured external global horizontal solar irradiance and temperature. (a) Month of March 2020. (b) Mid-August to mid-September 2020. 83
Figure 2.6. Measured and predicted hourly GCHP electrical consumption (per greenhouse surface) in March 2020. 84
Figure 2.7. Measured and predicted hourly borehole heat exchangers heat transfer rate (per greenhouse surface) in March 2020. 85
Figure 2.8. Measured and predicted hourly GCHP electrical consumption (per greenhouse surface) from mid-August to mid-September 2020. 85
Figure 2.9. Measured and predicted hourly borehole heat exchangers heat transfer rate (per greenhouse surface) from mid-August to mid-September 2020. 86
Figure 2.10. Measured and predicted hourly PV modules energy production (per greenhouse surface). (a) Month of March 2020. (b) Month of August 2020. 87
Figure 2.11. Daily average greenhouse indoor air temperature according to different modeling strategies. 89

Figure 2.12. Daily values of greenhouse thermal loads according to different modeling strategies. 90
Figure 2.13. Daily average greenhouse indoor air temperature (from May to the end of September) according to different energy consumption mitigation strategies. 91
Figure 2.14. Daily greenhouse thermal loads (from May to end September) according to different energy consumption mitigation strategies. 92
Figure 2.15. Daily average greenhouse inner air temperature for different modeling strategies. 93
Figure 2.16. Daily greenhouse primary energy consumption for different HVAC strategies. 94
Figure 3.1. Moroccan climatic zoning map. 100
Figure 3.2. Monthly minimal, mean, and maximal outside air temperatures for the six representative cities of the Moroccan climatic zones. 101
Figure 3.3. Greenhouse shapes considered for comparison in the present study. 102
Figure 3.4. "Even span" greenhouse oriented at 0°. 104
Figure 3.5. Annual heating loads of the different combinations shape/cover. 106
Figure 3.6. Annual cooling loads of the different combinations shape/cover. 107
Figure 3.7. Daily average floor incident solar radiation of the optimal combination (shape (8, gothic arch) with BPE material). 112
Figure 3.8. Daily average floor incident solar radiation for zone 4 (Ifran). 113
Figure 3.9. Monthly heating loads of the greenhouse with different orientations. 114
Figure 3.10. Monthly cooling loads of the greenhouse with different orientations. 115
Figure 3.11. Annual energy cost for the greenhouse air-conditioning according to the orientations. 117
Figure 3.12. Monthly heating loads of the greenhouse with and without nightly thermal blankets insulation. 119
Figure 3.13. Monthly cooling loads of the greenhouse with and without operable windows. 121
Figure 4.1. SamLab greenhouse data acquisition and monitoring subsystems. 126
Figure 4.2. Artificial Neural Networks the ANN model architecture. 128
Figure 4.3. Support vector machine SVM model. 130
Figure 4.4. Boosting trees model. 131
Figure 4.5. Measured and predicted air-conditioning elec. consumption for March (Validation set). 133

Figure 4.6. Measured and predicted air-conditioning elec. consumption of Mid-August to Mid-September (Validation set). 134
Figure 4.7. Measured and predicted PV modules elec. production of March (Validation set). 135
Figure 4.8. Measured and predicted PV modules elec. production of Mid-August to Mid-September (Validation set). 136
Figure 4.9. Models' normalized root mean square error (*nRMSE*). 137
Figure 4.10. ANN model normalized root mean square error (*nRMSE*) depending on the number of neurons in the hidden layer. 140
Figure 4.11. Series hybridization of ANN and Boosting models (ANN-BST). 142
Figure 4.12. Parallel hybridization of ANN and boosting models (ANN-BST). 144
Figure 4.13. Hybrid models normalized root mean square error (*nRMSE*) depending on the approach (series and parallel). 145

List of Tables

Table 1.1. Search keywords and criteria. 34
Table 1.2. Summary of physic-based method for greenhouse modeling (years from 2000 to 2021). 43
Table 1.3. Details on the studies conducted on greenhouse shapes selection (years from 2000 to 2021). 51
Table 1.4. Details on the studies conducted on greenhouse orientation selection (years from 2000 to 2021). 60
Table 2.1. SamLab greenhouse localization, climatic and geometrical parameters. 69
Table 2.2. SamLab greenhouse envelop material properties. 72
Table 2.3. SamLab greenhouse plant and soil proprieties. 77
Table 2.4. Thermal response test (TRT) method parameters. 79
Table 2.5. Model predicting performance. 88
Table 2.6. SamLab greenhouse monthly electrical energy consumption and PV modules' production. 94
Table 3.1. Sites geographical coordinates 101
Table 3.2. Greenhouses dimensions 103
Table 3.3. Cover material properties [211]. 104
Table 3.4. Plant and soil model parameters. 105
Table 3.5. Average heating and cooling loads of shapes (1, even span), (6, quonset) and (8, gothic arch), for the six climatic zones. 108
Table 3.6. Heating and cooling loads of shapes (8, gothic arch) with different cover materials for the six climatic zones. 110
Table 3.7. Annual air-conditioning cost for different combinations (Shape/cover material) for the six climatic zones. 111
Table 3.8. Heating and cooling loads of the greenhouse with the different orientations for the six climatic zones. 116
Table 3.9. Thermal insulation blankets' parameters. 118
Table 3.10. Benefit of the nighttime thermal insulation blankets for the six climatic zones. 119
Table 3.11. Financial gains of the controlled natural ventilation for the six climatic zones. 120

Table 4.1. Models' performance in predicting the air-conditioning elec. consumption (March, Mid-August to Mid-September). 134
Table 4.2. Models' performance in predicting the PV modules' electrical production (March, Mid-August to Mid-September). 137
Table 4.3. ANN performance in predicting the greenhouse energy demand and production, depending on the number of neurons in the hidden layer. 139
Table 4.4. Series hybrid model performance in predicting the air-conditioning electrical consumption and PV modules' electrical production. 142
Table 4.5. Parallel hybrid model performance in predicting the air-conditioning electrical consumption and PV modules' electrical production. 144

Nomenclature

$A_{surf,act}$	Active PV module area (m^2) ;
A_i, B_i, D_i, E_i	Equation fit coefficients for the cooling and heating modes ;
b	Bias ;
B	Borehole spacing (m) ;
c_f	Fractional vegetation coverage ;
d	Deficiency of the model ;
e	Residuals ;
E_{in}, E_{ext}	External and internal longwave radiations incident on the glazing surfaces ;
$f(x)$	Random function ;
F_o	Dimensionless time $(-)$;
g	Temperature response factor or g function $(-)$;
G_o	Hourly horizontal extraterrestrial solar irradiation (W/m^2) ;
G_{on}	Hourly normal extraterrestrial solar irradiation (W/m^2) ;
$G_{b,H}, G_{d,H}, G_{g,H}$	Hourly beam, diffuse, and global solar irradiation on horizontal surface (W/m^2) ;
G_{ir}, G_{sw}	Total incoming long and short wave irradiance respectively (W/m^2) ;
G_{sc}	Solar constant (1367 W/m^2) ;
G_T	Total solar irradiance incident on PV modules (W/m^2) ;
h	Convective coefficient ;
H	Borehole length (m) ;
k	Thermal conductivity $(W/m.K)$;
K_d	Hourly diffuse ratio $(-)$;
k_g	Ground thermal conductivity $(W/m.K)$;
K_t	Hourly clearness index $(-)$;
$k(x, x')$	Kernel function ;
$m(x)$	Mean function ;
n	Day of the year ;
$RMSE, nRMSE, RRMSE$	Root mean square error, normalized RMSE $(\%)$, relative RMSE $(\%)$;
P	PV modules power generation (W) ;
P_0	PV maximal power (W) ;
P_c, P_h	Power consumption in cooling and heating modes (W) ;
$\dot{Q}'$	Total heat extraction rate per borehole length (W/m) ;
$\dot{Q}_c, \dot{Q}_h$	Load side heat transfer rate in cooling and heating modes (W) ;

$\dot{Q}''_f, \dot{Q}''_g$	Net heat flux to foliage layer and ground surface (W/m^2) ;
$\dot{Q}''_{lat,f}, \dot{Q}''_{lat,g}$	Foliage and ground latent heat flux (W/m^2) ;
$\dot{Q}''_{sens,f}, \dot{Q}''_{sens,g}$	Foliage and ground sensible heat flux (W/m^2) ;
R	Coefficient of correlation ;
R^2	Coefficient of determination;
r_{bh}	Borehole radius (m) ;
r_f, r_g	Shortwave reflectivity (albedos) of the foliage and the ground surface ;
R_b, R_d, R_r	Beam, diffuse and reflected solar irradiance tilt factors $(-)$;
$T_{a,in}$	Greenhouse mean internal air temperature (K) ;
T_b	Borehole wall temperature (K) ;
T_f	Foliage layer temperature (K) ;
T_g	Ground surface temperature (K) ;
$T_{L,in}$	Inlet load side water temperature (K) ;
T_{panel}	PV panel temperature (K) ;
T_{ref}	Reference temperature, 298.15 (K) ;
T'_{ref}	Reference temperature, 283.15 (K) ;
$T_{S,in}$	Inlet source side water temperature (K) ;
TC	Temperature coefficient of the maximal power ;
VF	View factor ;
V_{wind}	Wind velocity ;
w	Weight ;
x	Inputs ;
y	Outputs ;

Abbreviations

ANN	Artificial Neural Network ;
AI	Artificial intelligence ;
AM	Air mass ;
BHE	Borehole heat exchanger ;
BES	Building energy simulation ;
BP	Back propagation ;
BST	Boosting trees ;
CFD	Computational fluid dynamics ;
COP	Coefficient of performance;
EER	Energy efficiency ratio ;
ELM	Extreme learning machine ;
EVA	Ethylenevinyl acetate ;
FASST	Fast all season soil strength ;
GCHP	Ground Coupled Heat Pump ;
GPR	Gaussian process regression ;
HVAC	Heating, ventilation and air conditioning ;

IoT	Internet of things ;
IPSO	Improved particle swarm optimization algorithm ;
IR	Infrared radiation ;
iRTG	Integrated rooftop greenhouse ;
ML	Machine learning ;
MLP	Multilayers perceptron ;
MLR	Multiple linear regression ;
NZEB	Near zero energy building ;
PE, D-PE, TPE, LDPE, HDPE, BPE	Polyethylene, double layer PE, thermal PE, low-density PE, high-density PE, bubbled PE ;
PLF	Partial load factor ;
PMMA	Polymethylmethacrylate ;
PMC	Phase change material ;
PV, CPV, PVT, OPV	Photovoltaic, concentrated PV, thermal PV, organic PV ;
PVC, VPVC	Polyvinylchloride, rose PVC based fluorescent ;
RBF	Radial basis function ;
RNN	Recurrent neural networks ;
SamLab	Smart agro-manufacturing laboratory ;
SVM, LSSVM	Support vector machine, least squares SVM ;
TC	Thermochromics ;
UV	Ultra violet ;
VAV	Variable air volume ;
WAHP	Water-to-air heat pump ;

Greek letters

$\alpha_{PAR}, \alpha_{NIR}$	Absorptance in the photosynthetically active and near infrared radiation ;
β	Tilt angle ;
δ	Solar declination ;
ε	Emissivity ;
$\gamma = 0.43$	
$\emptyset$	Latitude of the considered location ;
η_{cell}	Active surface conversion efficiency at the reference temperature ;
ω	Solar hour angle ;
ρ_{PAR}, ρ_{NIR}	Reflectance in the photosynthetically active and near infrared radiation ;
σ	Stefan-Boltzmann constant $5.67 \times 10^{-8}\ W/(m^2 \cdot K^4)$;
σ^2	Covariance noise ;
θ	Incidence angle ;
θ_z	Solar zenith angle ;
τ_{PAR}, τ_{NIR}	Transmittance in the photosynthetically active and near infrared radiation ;

Subscripts

act	Active ;
b	Beam ;

bh	Borehole ;
c	Cooling ;
$cell$	Cells ;
$cond$	Conduction ;
$conv$	Convection ;
d	Diffuse ;
f	Foliage layer ;
g	Global ;
h	Heating ;
H	Horizontal ;
in	Inlet ;
ir	Longwave ;
L	Load ;
M	Measured ;
P	Predicted ;
r	Reflected ;
ref	Reference ;
sw	Short-wave ;
T	Total ;

General Introduction

1. General context

Two billion people worldwide experienced moderate or severe food insecurity in 2019 [1]. Climate change with the continuous population growth will undoubtedly make the situation worse. In 2020, the average population increase was estimated to be 81 million people per year [2]. Moreover, population growth will increase the world food demand, which is expected to increase by 60% in 2050, above the 2006 value [3]. Conventional agricultural methods show clear restrictions and are not proficient enough to create adequate and sufficient food for the world population. One of the most prominent and interesting cultivation techniques that can be considered as a relevant solution for sustainable agriculture, one that able to face world development is protected agriculture or the so-called greenhouse cultivation; this cultivation technique represents many benefits e.g., assuring yearlong production, crop rotation, water saving, pesticide reduction. At present, greenhouse crop production is growing more and more. It is spread throughout the world, with an area of 405 000 ha [4].

The Mediterranean region has a promising agricultural potential; one-third of the world's food is produced in this region [5]. In order to face the actual challenges, the countries of the Mediterranean Basin have progressively become competitive producers of greenhouse crops. This crops production method significantly contributes to supporting the move towards sustainable agriculture in the Mediterranean climate environment. That leads to efficient use of natural resources and better control of product quantity and quality.

Currently, the politic of energy transition is of interest to different world countries, including the Mediterranean region countries. This transition is considered as a necessity given the increase of energy demand, while the decrease of conventional energy resources and the climate change issues. This energy transition must cover all human activities, including greenhouse cultivation, where the use of conventional energy resources is still present. Switching to renewable and sustainable energies and developing new energy-saving strategies are the suitable solutions for reducing the agricultural sector's carbon footprint.

2. Problem statement and objectives

Greenhouses are one of the most important agricultural buildings types that can help to face the climate change. They allow continuous production throughout the year by providing a suitable

environment for plant growth. This technique refers to creating a suitable microclimate for plant growth by modifying the natural environment using many technologies and systems. However, it has been shown by many studies [6]–[8] that a high amount of energy is needed for creating an adequate microclimate. Thus, the rational use of energy in greenhouses can lead to a significant decrease in operational costs.

Being one of the energy-intensive systems, the agricultural greenhouse should be a part of the energy transition strategies. In this context, our contribution aims to optimize the energy consumption of agricultural greenhouses in the Mediterranean region. This will contribute promoting the energy, economic and environmental valuation of agricultural and agrifood-industry products, mainly by bringing down their energy production costs. The objectives of this Ph.D. thesis are the followings:

(1) Presentation of an overview and an understanding of protected agriculture researches;

(2) Selection of suitable greenhouse design for new greenhouse building, including shape, envelope material and orientation;

(3) Integration of passive techniques, namely thermal insulation blankets; shading/reflecting system, and operable windows for controlled natural ventilation;

(4) Integration of renewable energies, namely by the use of semi-transparent photovoltaic panels for the production of greenhouse electrical energy needs and of ground-coupled heat pump for the greenhouse air-conditioning;

(5) Integration of intelligent management by the use of artificial intelligence methods to predict the air-conditioning electrical consumption and the photovoltaic module electrical production in order to have a preliminary idea of the energy needs and resources of the greenhouse for a better management.

3. Methodology

This Ph.D. thesis started with a literature survey on greenhouse crop production, focusing on greenhouse modeling and energy-efficient operations for new greenhouse buildings (design features selection) and greenhouse renovation (integration of passive techniques and renewable energies). The main purpose of this literature survey is to present an overview and an understanding of the research corpus on protected agriculture. The database was selected using the Scopus platform, filtered by excluding initially, irrelevant titles and irrelevant abstracts and finally according to inclusion criteria. The selected papers are then analyzed and summarized

in order to obtain an in-depth understanding, to draw general conclusions and to outline research perspectives.

For selecting the optimal greenhouse design and the definition of energy-saving potential by integrating passive techniques and renewable energies, dynamic models (SamLab greenhouse model, Albenga and the different greenhouse models, Morocco) have been created in the EnergyPlus environment, the worldwide known dynamic simulator software, usually used in thermal building physics and HVAC systems simulation. The 3D greenhouse geometries are created in SketchUp graphical interface and manipulated using the OpenStudio Plugins before being implemented as an input to the EnergyPlus software. The models are based on the energy balance of the greenhouse components, where the greenhouse is considered as a single zone that interacts with the outside environment as well as with different interior components (plants, soil and internal masses).

To predict the air-conditioning electrical consumption and the PV modules' electrical production different machine learning methods have been used: artificial neural networks (ANN), gaussian process regression (GPR), support vector machine (SVM), boosting and hybridization of artificial neural networks (ANN) and boosting methods. The prediction is conducted following four steps summarized as follows: data preprocessing, random split of the dataset (70% for training and 30% for validation), implementation of the different models, optimization of the chosen models' hyperparameters to improve their performance, and comparison of the models' performance in terms of some statistical indicators.

A great part of this Ph.D. thesis was conducted as a part of a traineeship period in Europe spent by the present Ph.D. candidate during the year 2019 in the department of Mechanical, Energy, Management and Transportation at University of Genova, Italy.

4. Thesis organization

This research work is presented in four chapters:

The **first chapter** introduces a fair assessment of research studies with greenhouse energy modeling and technologies as the primary analysis point. The chapter is split into three main parts; at first, a theoretical background on the research topic is provided in order to build an understanding of the agricultural greenhouse system, its microclimate and its characteristics; then, the research methodology adopted in this study is presented; finally, the literature review

of the current field of research is conducted (greenhouse modeling, design features and energy-saving strategies).

The **second chapter** presents a dynamic model created in the EnergyPlus environment considering the interaction among all the greenhouse components, including crops, soil, and internal masses. The model is then validated using measurements from a high-efficiency greenhouse (SamLab) located in Albenga, Italy, which was selected for the present thesis analysis since part of the traineeship period in Europe spent by the present Ph.D. candidate during the year 2019 at the University of Genova, Italy. The model is then explored to quantify the potential of energy-saving strategies (passive techniques and renewable energies) and to study the effect of greenhouse internal masses and plants on the greenhouse microclimate.

The **third chapter** aims to evaluate different greenhouse designs (shapes, covering materials and orientations) in order to select the most suitable for each of the six Moroccan climatic zones. The models are created in the EnergyPlus environment. The results regarding the selection of the greenhouse shape, cover and orientation are presented and discussed. Then the potential of energy-saving resulting from the use of nightly thermal insulation operating during the heating period and controlled natural ventilation operating during the cooling period is also investigated.

Finally, the **fourth chapter** focuses on predicting the air-conditioning electrical consumption and the photovoltaic modules' electrical production using different machine-learning algorithms, namely: artificial neural networks (ANN), gaussian process regression (GPR), support vector machine (SVM) and boosting. Then, further investigations on the artificial neural networks are conducted and a hybrid model combining ANN and boosting methods is proposed. The models' performance is evaluated and discussed based on two statistical indicators.

Chapter 1

Background and literature review

Chapter 1: Background and literature review

1.1 Introduction

A greenhouse system (**Figure 1.1**) can be defined as an agricultural building, having a transparent cover (glass, plastic, etc.,) and supported generally by a metallic or wooden structure. The propose of this building is to create an artificial microclimate (adequate temperature, humidity, irradiance level, etc.,) allowing for throughout year production of high quality and produces. Understanding the agricultural greenhouse system, its microclimate, and its characteristics is an essential element in creating and being able to maintain the right conditions for plant growth while having an efficient system. Different systems are needed to ensure a stable and suitable microclimate for the plant, namely heating, cooling, ventilation, proper watering and artificial lighting. Each depending on the plant type, the greenhouse design and location, and the season involved. Indeed, an important amount of energy is needed to maintain indoor controlled conditions, which is often the critical problem of this cultivation technique.

The present chapter aims to introduce a fair assessment of research studies having greenhouse energy modeling and technologies as the primary point of analysis: the main research fields are discussed, and sectors for research works are suggested. The aim is to provide an overview of the studies made over recent years so that researchers, engineers, designers, growers and any

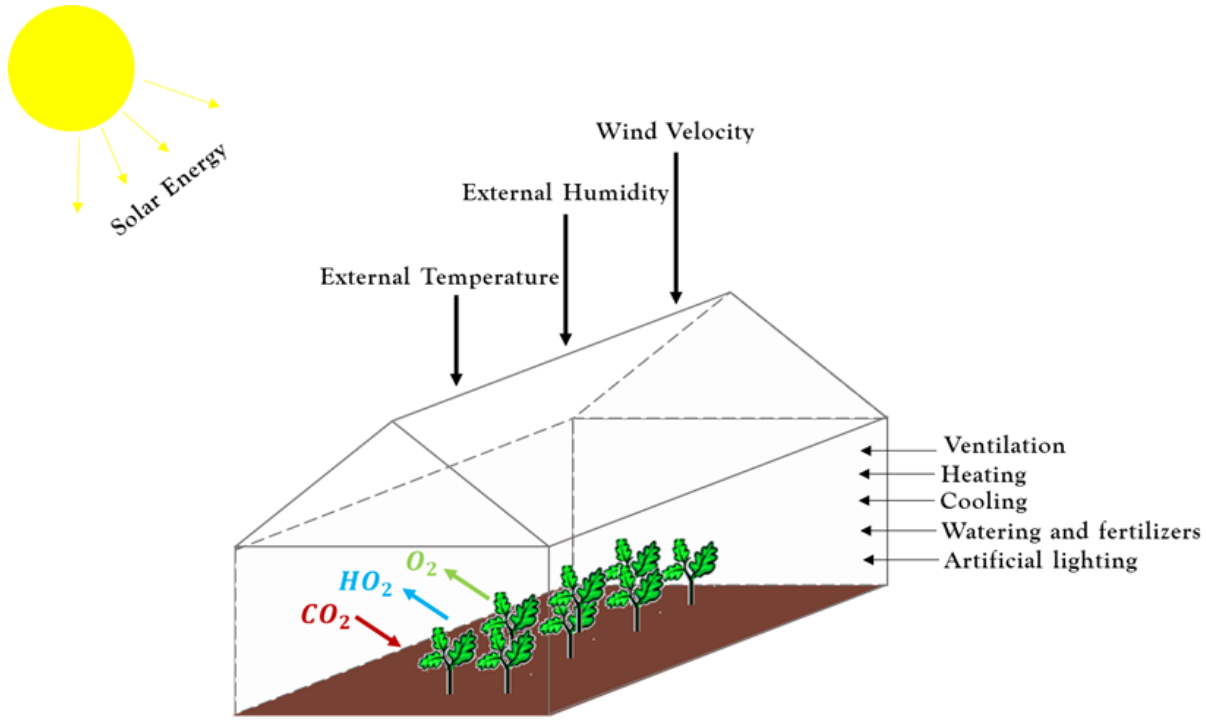

Figure 1.1. Greenhouse system.

concerned party can quickly obtain essential and sufficient information about the greenhouse systems allowing them to develop and complete ongoing studies.

The chapter is split into three main parts (**Figure 1.2**); at first, a background on the research topic is provided in order to build an understanding of the agricultural greenhouse system, its microclimate and its characteristics; then, the research methodology adopted in this study is presented; finally, the literature review of the current field of research is conducted. A particular focus has been devoted to greenhouse modeling, including; physics-based modeling and data-driven modeling. Physics-based modeling is essential for understanding the thermal behavior of greenhouse components, describing the evolution of the indoor microclimate, and comparing different energy-saving and management strategies to optimize energy consumption. Data-driven modeling is of great interest in developing intelligent management strategies and reducing potential energy and financial losses. In the present chapter, a specific focus is also dedicated to the greenhouse design features, which could be considered as a key factor of the protected agriculture process, given its impact on the amount of solar irradiance captured and therefore on the inside microclimate. Finally, some energy-saving strategies used to optimize system's efficiency are presented.

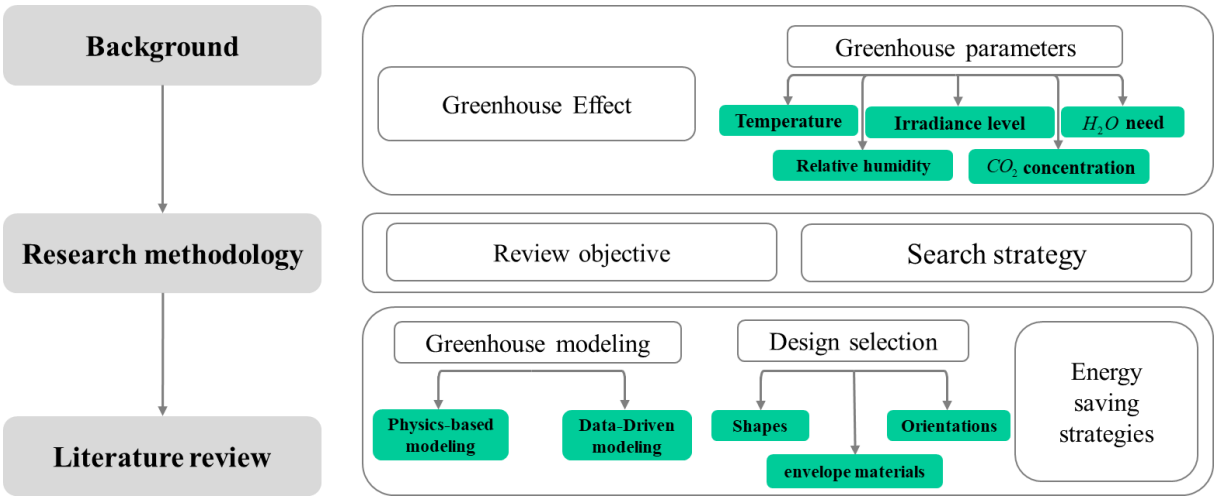

Figure 1.2. Flowchart of chapter organization.

1.2 Background

1.2.1 Greenhouse effect

In agricultural applications, the so-called greenhouse effect follows the same concept as for the earth. The energy coming from the sun passes through the cover and heats the soil, the crops, etc., inside the greenhouse. The air is then heated mainly by convection with the internal

surfaces while the longwave radiation cannot pass through the greenhouse envelope. Most of this radiation is "enclosed" in the structure, as presented in **Figure 1.3**. This phenomenon occurs because of the specific characteristics of the covering material: generally transparent to the shortwave components of solar radiation and "opaque" to the longwave radiation [9] emitted by low-temperature bodies inside the greenhouse, according to the well-known law of Wien[i] [10], [11].

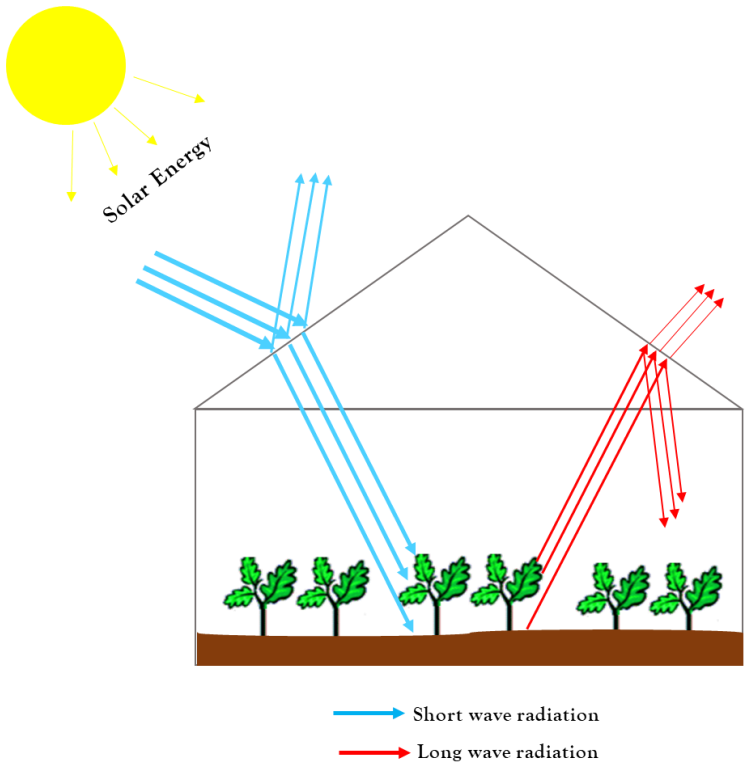

Figure 1.3. The schematization of the greenhouse effect.

The sun can be considered as a blackbody radiating at a temperature of 5800 K outside of the Atmosphere (extraterrestrial solar irradiance). Thus, reference Air Mass (AM) 1.5 Spectra is used to refer to terrestrial solar irradiance. The American Society for Testing and Materials (ASTM) developed an AM 1.5 reference spectrum ASTM G173-03 to represent terrestrial solar spectral irradiance (inclined plane at 37° tilt toward the equator, facing the sun) [12]. **Figure 1.4** represents the power distribution of terrestrial solar irradiance depending on wavelength.

The plants react differently depending on the light wavelength. Waaijenberg [13] discussed the aspects of natural light and the influence of each light strip on the greenhouse environment. The photosynthetically active radiation (PAR) arriving on earth (after solar radiation has traveled through the atmosphere AM 1.5) controls the plant growth in terms of energy transfer needed for photosynthesis.

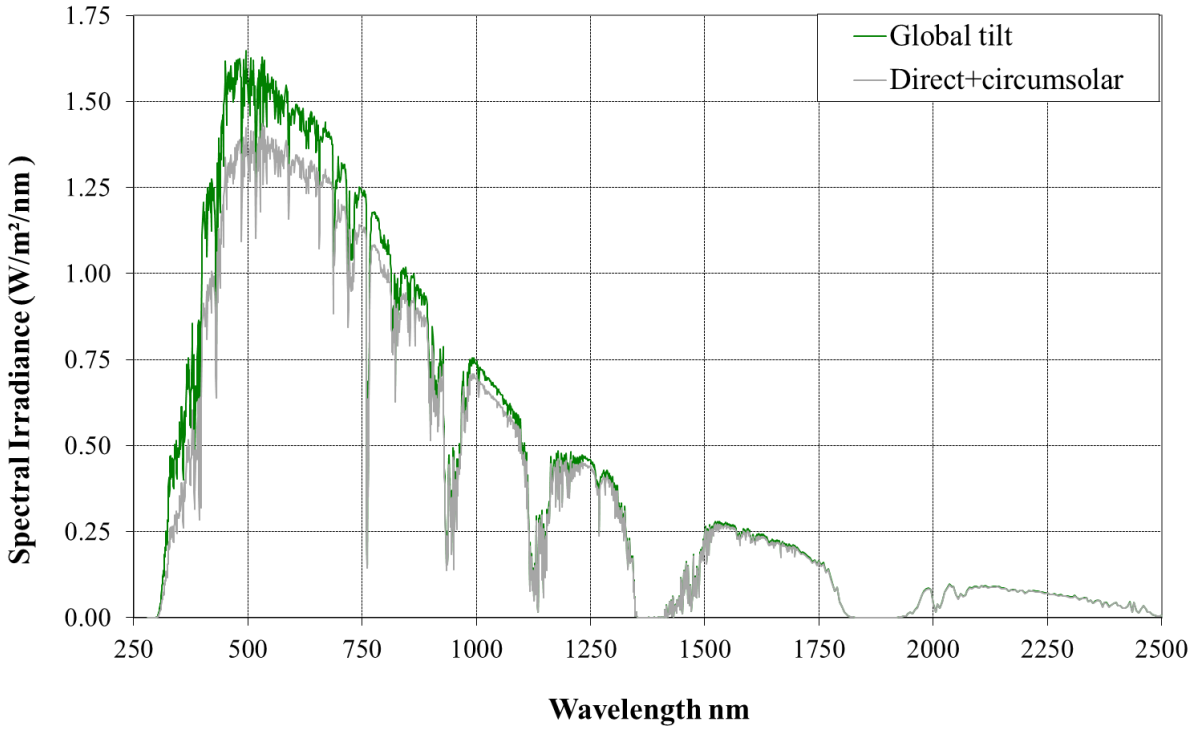

Figure 1.4. Terrestrial solar spectral irradiance [12].

1.2.2 Greenhouse climate parameters

1.2.2.1 Temperature

Temperature is a climatic factor having a meaningful impact on the plant's physiological development stages (germination, development, and growth of the vegetative system (roots, stems and leaves), flowering, and fruitset). It also directly affects the plant's transpiration process of and thus its water content during photosynthesis. According to Went [14], the impacts of temperature on plant growth are primarily mediated by chemical processes. Several studies have been conducted in order to clearly understand the effect of temperature on different plants and at different development stages [15]–[19]. The optimal temperature in the greenhouse depends mainly on the plants' type since each plant (in each process) responds differently to temperature variation [20].

Protected agriculture is a good solution to control the indoor air and soil temperatures for a better environmental conditions for the plant's growth. Very high or very low temperatures cause harmful effects. Just as other living beings, plants react against inadequate environmental factors in order to regulate their temperature. High temperatures cause an important water loss in the plant due to excessive transpiration [20]. In contrast, low temperatures disturb the chemical processes since a part of the energy used in those processes is exploited to regulate the plant temperature [21].

1.2.2.2 Humidity

As well as temperature, relative humidity also has an important effect on the plants' well-being [20]. Indeed, at constant humidity ratio, relative humidity is directly linked to the temperature; an increase of temperature leads to a decrease of relative humidity and vice versa. In protected agriculture, it is crucial to maintain a correct and balanced set-point temperature and humidity [22]. A high temperature and a low relative humidity lead the plant to transpire more water than it absorbs, thus causing water stress and an increase of stomatal resistance[ii] of the plant [23]. The increase or decrease of stomatal resistance directly influences the photosynthesis process. On the contrary, a high relative humidity, instead of influencing the plants' physiological processes, promote an unfavorable development of some microorganism, i.e., bacteria.

1.2.2.3 Irradiance level

For plants, like for all living beings, light is one of the most important elements of life [24]. In fact, light is the principal energy source for plants and constitutes a living need for them, having profound impacts on their chemical constituents, physical properties and vital processes [25]. The development of plants is constrained by mainly three light cycles, namely photosynthesis[iii], photomorphogenesis[iv] and photoperiodism[v].

The photosynthesis is the well-known and fundamental plant process responsible for the great majority of life on Earth. During this process, the plants synthesize the organic matter using luminous energy. The photosynthesis process occurs, in general, in two steps, namely: first, water (H_2O) draws up through the plant's roots, and the leaves absorb carbon dioxide (CO_2) from the air; then, the leaves trap the luminous energy and use it to convert water and carbon dioxide (CO_2) into sugar ($C_6H_{12}O_6$) and oxygen (O_2) [29], [30]. **Equation 1.1** presents the chemical formula of the photosynthesis process.

$$6CO_2 + 6H_2O \rightarrow C_6H_{12}O_6 + 6O_2 \qquad \textbf{1.1}$$

A significant number of researches studied the effect of light variation (during the day or the year) on the plant's growth whether it would be sunlight or artificial light [31]–[33].

1.2.2.4 Carbon dioxide concentration

As mentioned in **section 1.2.2.3**, Carbon dioxide (CO_2) is one of the important components in the photosynthesis process. Carbon dioxide is absorbed by the plant through its stomatal

openings that depends on several factors: irradiance level, temperature, humidity, CO_2 concentration itself, etc.,. The air contains (the year of 2021) approximately 414 ppm of carbon dioxide [34]. In greenhouse production, it has been shown that the plant's growth increases as the carbon dioxide concentration increases. In fact, carbon dioxide enrichment leads to a decrease of oxygen inhibition of photosynthesis and an increase of net photosynthesis [35]. The positive effect of atmosphere enrichment by carbon dioxide on plants production [36]–[39], drives to the use of carbon dioxide supplementary systems, i.e., combustion of carbon-based fuels (hybrid systems) or directly from carbon dioxide generator. A carbon dioxide level between 700 and 900 ppm is considered as the optimal concentration and is generally recommended in greenhouse production [35]. Instead, several studies showed that carbon dioxide levels exceeding 1000 ppm could disturb plant growth [35], [40].

1.2.2.5 Water need

The availability of water is an essential condition for the existence of life and a vital need for all living beings, including plants. In addition to the importance of water in the photosynthesis process (**section 1.2.2.3**), water is a medium to transfer nutrients from soil to the plant. Furthermore, water is involved in the plant's evapotranspiration process. For well-balanced growth, plants need a specific amount of water, depending on climatic parameters (temperature, humidity, irradiance level…), soil characteristics, plants type and growth stage. Too little water causes water stress and too much water removes air from the soil making roots transpiration difficult. Thus, it is important to ensure to the plant the exactly sufficient amount of water that prevents water and energy wastage. The quantity of water needed for plant irrigation depends on the quantity of water vapor released into the atmosphere during "evapotranspiration". **Figure 1.5** provides an overview of the evapotranspiration process: evapotranspiration means the quantity of water transferred from the soil, by evaporation and plants transpiration, to the atmosphere. Therefore, the evapotranspiration process is driven by the difference between the partial pressure of water vapor on leaves and soil and that of the ambient air.

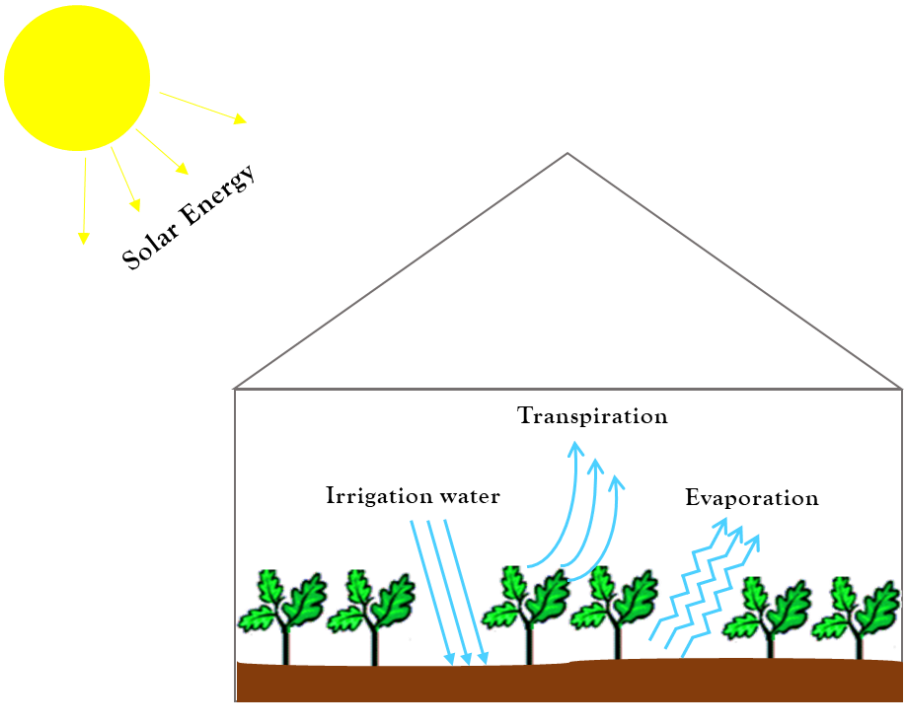

Figure 1.5. The schematization of evapotranspiration process.

1.3 Research methodology

1.3.1 Review objective

The main goal of the present study is to present an overview and an understanding of the researches on protected agriculture in the period from 2000 to 2021. The literature review deals with greenhouse crops production focusing specifically on greenhouse modeling and energy-efficient operations for new greenhouse buildings (design features selection) and greenhouse renovation (integration of passive techniques and renewable energy). The purpose of this literature review is; 1) to introduce a fair assessment of the research topic; 2) to help recognize any gaps in the current research topics in order to suggest further enhancement; 3) to sum up and provide background for future research studies.

1.3.2 Search strategy

According to the objective of this review, the researches reporting greenhouse modeling (including physics-based modeling and data-driven modeling), greenhouse design features, and energy-efficient operation, were selected. After fixing the study objectives, a search strategy is developed to collect the database for review, according to two approaches; first, the use of the Scopus platform using specific keywords and selection criteria (**Table 1.1**); second, the analysis

of references inside the selected relevant publications. Different document types have been considered namely journal articles, reviews, conference papers, and book chapters.

The flowchart presented in **Figure 1.6** summarizes the literature review process. Following the search carried out on the Scopus platform, a database was selected and then filtered by excluding initially irrelevant titles, subsequently irrelevant abstracts and finally, according to inclusion criteria. The selected papers are then analyzed and summarized. Finally, general conclusions have been drawn and future research perspectives have been outlined.

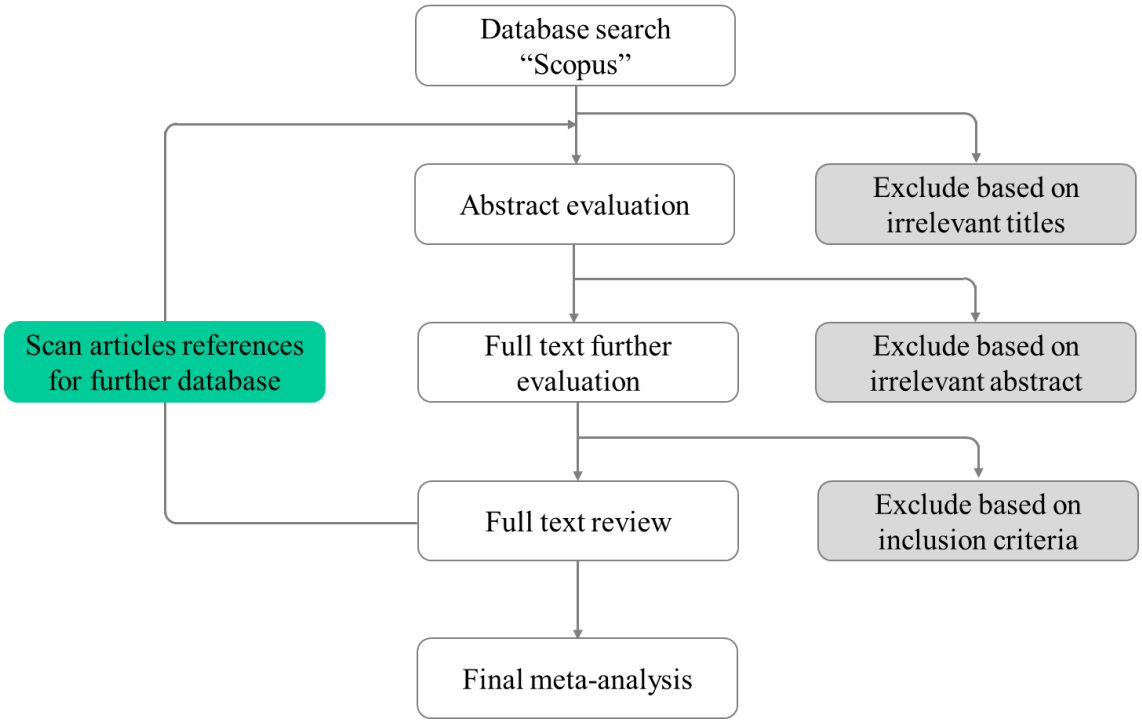

Figure 1.6. Literature review process.

Table 1.1. Search keywords and criteria.

Keywords		Criteria			
		Type	Subject Area	Language	Period
Physics-based modeling	Agriculture AND Greenhouse AND Physics AND Modeling	Journal article, Review, Conference paper, and book chapter	Energy, Engineering, Agricultural sciences, and Multidisciplinary	English	From 2000 to 2021
Data-driven modeling	Agriculture AND Greenhouse AND Machine learning				
Design features	Agriculture AND Greenhouse AND (Design OR Covering Material OR Shape OR Orientation)				
Energy-efficient operation	Agriculture AND Greenhouse AND (Energy-efficient operation OR Energy-saving strategies)				

A quantitative analysis of the research studies conducted in this field per year (from 2000 to 2021) was performed, as presented in **Figure 1.7**. The majority of papers belong to the five last years, with a coverage of 53%, showing an increasing research interest in the greenhouse sector and hence confirming the importance of the present investigation.

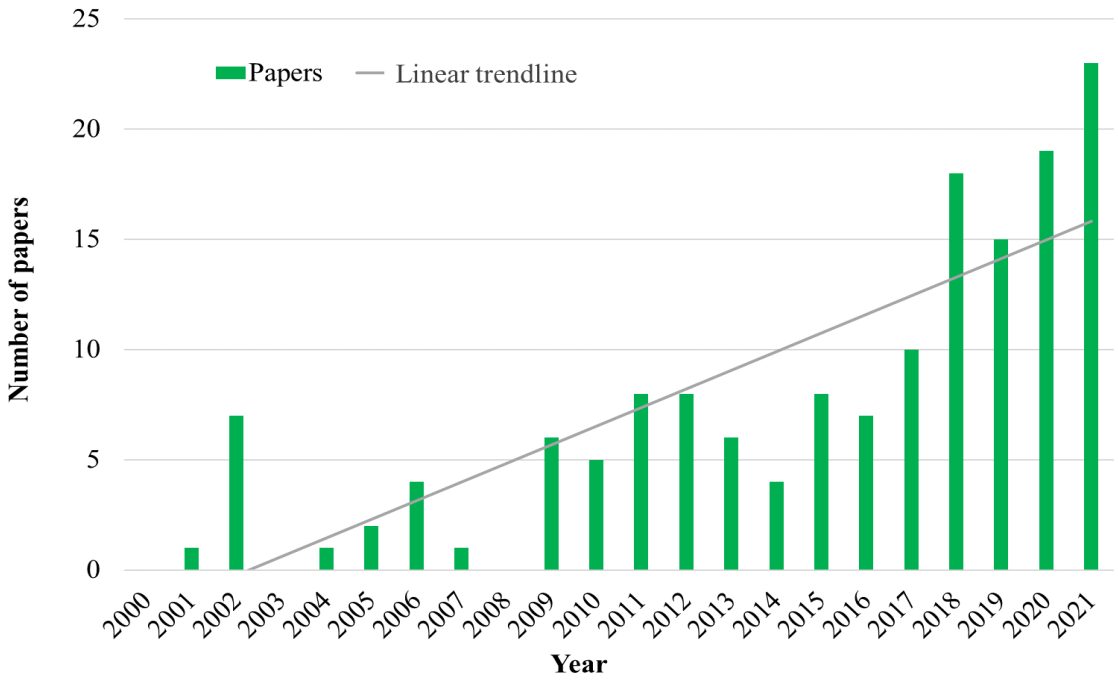

Figure 1.7. Number of papers published in the period from 2000 to 2021.

1.4 Review

1.4.1 Greenhouse modeling

Modeling the greenhouse microclimate is considered as a key factor for understanding the system behavior, developing energy management strategies and reducing the amount of energy requested. Greenhouse microclimate modeling can be classified into two general main types: physics-based whole modeling and data-driven modeling, as presented in the sub-sections below.

1.4.1.1 Physics-based modeling

Physics-based models require the knowledge of the weather parameters and the greenhouse component specifications. With this method, it is possible to understand the thermal behavior of the components, describe the evolution of the indoor microclimate, and compare different energy-saving and management strategies at different levels depending on the complexity of the model. Physics-based modeling can be divided into three approaches, namely steady-state, quasi-steady-state and dynamic. The steady-state approach neglects any time-varying terms of the energy balance equation, including energy storage. On the contrary, the quasi-steady-state approach considers the heat storage phenomenon through an adjusted parameter. The most complex approach is dynamic energy modeling since it considers a short time step variation of the model parameters. This latter approach, despite being more complicated (it requires the knowledge of the hourly or sub-hourly weather parameters and more data on thermal properties of the greenhouse components), allows for a deeper analysis of the system, and it has higher accuracy [43].

The greenhouse environment could be considered as a complex dynamic system composed of two main entities: the microclimate and the plant [44]. This system is governed by a large number of parameters interacting with each other, and the physics-based modeling relies on energy balances. In this context, several studies have been presented in the literature, and different methods or tools have been used. Moreover, some assumptions have been made depending on the model complexity and the analyzed case study: some studies considered only the greenhouse microclimate without considering any plant inside, while others take into account the presence of plants.

a. CFD method

The computational fluid dynamics method (CFD) was widely used to study airflow and climate inside greenhouses[45]–[52]. Several reviews were specially carried out for this purpose [53].

With the objective of greenhouse microclimate control, Ma et al. [54] created a physics-based model in Comsol-Multiphysics environment and validated it using the measurement from a greenhouse equipped with a vegetation conveyor belt system whose objective is to eliminate the effect of microclimate heterogeneity on the vegetation. The studied greenhouse is located in West Lafayette, Indiana, USA and the model validation was carried out considering data of a clear sky conditions day with constant wind speed according to their assumptions. Furthermore, predicted and measured daily accumulated light radiation and temperature (integration over time, among 20 space samples covering low to high radiation greenhouse regions) were compared, obtaining a coefficient of determination (R^2) of 0.91 and 0.88, respectively.

The thermal performance of a greenhouse located in Batna, Algeria, was analyzed using again CFD method [55]. The predicted indoor air temperature was found to be lower than the measured one. The measurements were conducted during the two days, namely a windy overcast day on March 10, 2010, and a clear day on March 11, 2010. On the first day, a difference of 2 to 5 K was noted in the period from 2 p.m. to 7 p.m., while on the second day, a difference of 5 to 10 K was noted in the period from midday to 5 p.m.. The authors stated that the predictive accuracy of the model should be further studied, and more experiments are needed for a veritable validation.

Using Comsol-Multiphysics, Oskin et al. [56] proposed a numerical model of a quonset greenhouse in the climate conditions of Krasnodar, Russia at the beginning of the year. The main object of their study was to compare the efficiency of two heating methods, namely air heater and cable heating systems. The authors stated that the proposed model could be used for further research on other heating methods and on actions to increase the efficiency of the greenhouse.

El Jazouli et al. [57] studied the airflow, temperature and humidity distribution inside a multispan greenhouse covered by insect-proof nets and located in coastal area of southern Morocco. For this aim, the authors used a CFD model and considered the dynamic effect of their cover using the approach proposed by Darcy and Forchheimer for porous medium. Outside temperature and relative humidity of about 27.54 °C and 46.18% was considered for the

calculations. A good agreement was found between the measured and predicted indoor air temperature and humidity. The authors concluded that, despite of the high ventilation rate of the greenhouse, high heterogeneity of the internal climate was detected.

In order to study the effect of roof-integrated PV panels arrangements (checkerboard and straight line) on the greenhouse microclimate, a numerical CFD model of the greenhouse was presented by Fatnassi et al. [58]. An analysis of the distribution of indoor air temperature, airflow and solar radiation was provided. The outside temperature was considered to be constant, 33 °C and 10 °C for typical summer (June 21) and winter (January 10) days, respectively, and only direct external radiation was considered.

In the same context, He et al. [59] studied the effect of removable back walls on the airflow and temperature distribution inside the greenhouse, based on a 2D CFD transient model. Measurements were collected from July 13 to August 15, 2016, inside a greenhouse located in Jiangsu, China. A good agreement was found between predictions and measurements with root mean square error (RMSE) of about 0.39 °C and 0.05 m/s for temperature and air velocity, respectively. The results showed also that the back wall vent has a significant effect on greenhouse cooling.

In order to show up the effect of dynamic solar gains and wind profile and direction on the greenhouse microclimate, a 3D CFD model was developed for a greenhouse located in Ahvaz, Iran [60]. A correlation coefficient (R) between 0.78 and 0.68 was obtained when comparing the measured and predicted temperature distributions inside the greenhouse (from June 2017 to June 2018).

A coupling approach, between a CFD model and an energy balance simulation model was used to study the effect of ventilation on indoor air temperature, humidity and condensation of a greenhouse [61]. Night-time clear sky and overcast sky conditions were considered in an unheated greenhouse. According to their findings, the ventilation was recommended under clear-sky conditions, and it was found that a slight opening of the rooftop ventilators could be adequate. The ventilation was mostly recommended under cloudy sky conditions, and it was found to be unnecessary when the air humidity outside the greenhouse exceeds 85%.

In order to study the effect of vent opening on the air humidity ratio inside a Chinese solar greenhouse, Zhang et al. [62] developed a 3D CFD model. Simulations were conducted for different vent opening rates (20%, 40%, 60%, 80%, and 100%), and the humidity distribution inside the greenhouse was obtained. The model results were compared to the measurements

from a greenhouse scale model (scale of 40:1). The gap between actual and theoretical values increases when the vent opening rate increases: the gap was 0.97% and 23.31% for an opening rate of 20% and 100%, respectively.

Dhiman et al. [63] studied the effect of two different heating systems (hot water and flue gas heat sink pipe networks) on the indoor air temperature of a greenhouse by means of a 3D CFD model. The simulation results were compared to experimental measurements (during a winter night) from a 100 m² greenhouse located in Ludhiana City, India, with a RMSE of 1% between predicted and measured temperatures.

Based on a 2D CFD model, Baxevanou et al. [64] studied the performance of different greenhouse materials. Considering the optical properties of the plant in the four wavelength bands, the radiation transfer was simulated to calculate the available PAR, indoor air temperature and velocity. The model was validated using the measurements of PAR collected from a greenhouse having the same geometry and orientation as the simulated one. RMSE values range from 7.2 W/m² to 15.2 W/m² for the day 27/6/2015 and from 14.5 W/m² to 23.7 W/m² for the day 23/9/2015 (considered, respectively, similar to the typical days of 21 June and 21 September).

Sdringola et al. [65] studied the thermal performance of an urban bioclimatic greenhouse (connected to an apartment) located in Perugia, Italy. The energy benefit related to the greenhouse (thermal insulation, solar control glass and external shading) and to the apartment was quantified. The results obtained from the proposed model were compared to other methods, namely Sunspace, Ecotect, STIMA 10 TFM. The authors stated that the proposed model showed comparable results with those obtained using the other methodologies from both qualitative and quantitative points of view.

b. Mathematical models

Different greenhouse modeling studies used mathematical methods for different aims, analyzing the greenhouse thermal behavior [66], selecting the optimal greenhouse design [67], proposing an open-source tool for greenhouse modeling [68], and others.

A greenhouse thermal model was proposed by Abdel-Ghany and Hilal [69] by considering the greenhouse as a solar collector having three semi-transparent parallel covers, namely the actual cover of the greenhouse, the humid air and the plants. The soil was considered as the absorber of the solar collector. The validation of the developed model was performed using measurements (conducted during the daytime of May 15, 2009) from a tomato greenhouse

located in Riyadh, Saudi Arabia. According to the authors, absorbed and lost energies were predicted with a maximal error of 2% and 0.7% for plant leaf index area (LAI) less than 1.5 and 5, respectively.

Joudi and Farhan [70] presented a dynamic model of an uneven span greenhouse with roof-mounted solar air heaters (facing the south with a slope of 26.6◦) located in Baghdad, Iraq. The model was implemented in Matlab environment, and experimental measurements were collected within a period of 9 months. Both winter clear sky and partially cloudy sky conditions were selected to compare between the predicted and measured temperatures of air and soil. The results showed a good agreement in both analyzed conditions, with an average absolute error of 8% and 6% for the indoor air and the soil temperatures, respectively.

Using Matlab/Simulink environment, Ben Ali et al. [71] proposed a dynamic greenhouse model which considers the thermal behavior of all the greenhouse components, i.e., cover, air, soil and crops. The model was validated by comparing the calculated indoor air temperature with the one measured in two greenhouse types in Northern Tunisia for nine days in March. In particular, they considered transparent and insulated greenhouses (movable blinds used from the sunset on the south face, and double cover in the northern roof and sidewalls) in the same site and having the same dimensions. The results showed a fair agreement between the measured and predicted indoor air temperature, with correlation coefficients (R) of 0.95 and 0.92 in the insulated and transparent greenhouses, respectively.

A dynamic model based on heat exchange between three greenhouse components (indoor air, soil and cover) was compared to multilayers perceptron (MLP) neural network [72]. To do so, a dynamic model was developed and validated using data collected from a real greenhouse located in Tabriz, Iran. The model neglected the presence of plants and evaporation from the soil and revealed to have low accuracy in predicting temperature fluctuations.

With a quite similar model, Mohammadi et al. [73] predicted the greenhouse indoor air and soil temperatures by considering the soil surface, indoor air and roof cover as the interactive components. Using data from the same greenhouse as Taki et al. [72], the RMSE of the proposed model was found to be around 5.3 °C and 3.45 °C for indoor air and soil temperatures, considering clear sky conditions during a summer day (in June 2015).

Based on heat and mass transfer balance, Taki et al. [74] estimated different microclimate variables inside a single slop greenhouse with north wall insulation and night operating thermal screen, located in Northwest Iran. The model was developed in Matlab environment,

considering in this case also the plant evapotranspiration. The model was validated using experimental data of indoor air (above and below the thermal screen), crop, soil, cover, and thermal screen temperatures. The results proved the good performance of the model with an RMSE ranging from 1 °C to 2 °C for the different estimated temperatures.

Another dynamic model was proposed by Vanthoor et al. [75], [76], considering the effect of the greenhouse microclimate on tomato product yield. The model validation was conducted for different climatic regions, namely temperate marine climate (northwest Netherlands), Mediterranean climate (Sicily, Italy) and semi-arid climate (Texas and Arizona, USA). The comparison between predictions and measurements, during specific winter and summer days, showed a good agreement in the majority of cases with a relative RMSE (RRMSE) of less than 10%.

Ahamed et al. [77] developed a quasi-steady-state model in order to predict the heating requirements of a greenhouse. Monthly actual heating loads (from March to October 2014) of a commercial greenhouse under the cold climate of Saskatoon, Canada, were used to validate the model. According to the authors, the proposed model was found to be accurate in predicting the greenhouse heating needs, with errors of less than 9% for winter months and an average error of around 4.6%.

In another work [78], a typical Mediterranean greenhouse located in Almería, southeast Spain, has been modeled based on mass and energy balance and using the object-oriented modeling with Modelica language (Dymola). For the greenhouse, four variables have been defined (cover temperature, indoor air temperature, indoor air humidity, and soil temperature), for each one, a submodel has been developed and independently validated. The components were then linked, and the whole model was validated based on data obtained by 13 days of measurements from the real greenhouse.

In order to assess the impact of ground inertia on the thermal behavior of a quonset greenhouse, Ben Younes and Ayeb [79] have used a numerical model based on the green functions theory (GFT). Their model considers the thermal interactions between three components, namely the cover, the air and the soil without any plants inside the greenhouse. The authors highlighted the ability of soil in absorbing the solar radiation acting as a thermal wheel of inertia for the greenhouse.

To investigate energy performance and microclimate control of a fully mechanically ventilated greenhouse, a dynamic energy model was proposed by Costantino et al. [43]. The model was

composed of nine calculation modules, namely “preliminary calculation module” (calculation of input variables used in other modules), “solar radiation module” (calculation of the incident solar radiation on the canopy), “plant transpiration module” (calculation of water vapor rate and sensible heat reduction due to the plant transpiration), “thermal balance modules” (based on thermal/electrical analogy, this module has intereffect with all other modules), “moisture balance module” (calculation of relative humidity), “heating system module” (calculation of thermal loads and thermal energy consumption for heating purpose), “cooling pad efficiency module” (evaporative pad activation based on cooling loads), “dehumidification ventilation system model” (calculation of electrical energy required for dehumidification if needed), “cooling ventilation system module” (calculation of ventilation airflow rate based on cooling loads). A comparison of simulation results and their actual values, measured in a multispan greenhouse (Northeast Italy), showed that the model properly predicted greenhouse variables.

In order to evaluate the suitability of a traditional Colombian greenhouse, Diaz et al. [80], first validated a greenhouse climate model (GCM) using actual measurement (recorded from March 28 to August 9) from a traditional tomato greenhouse located in Santa Sofia, Colombia. Then, the model was used to evaluate the thermal behavior of traditional tomato greenhouses under six different Colombian climate conditions. According to the authors, the predicted temperature and vapor pressure fit well with the measured ones with RRMSE of 11.7% and 13.7%, respectively.

c. Building energy simulation

Different building energy simulation tools were used to model greenhouse system, for instance TRNSYS [81], [82], EnergyPlus [83], [84], Design Builder [85].

The thermal behavior of a mango greenhouse located in South Korea was studied by Lee et al. [86] using the building energy simulation (BES) software TRNSYS. The model considers the heat transfer of the plants, including latent and sensible contributions. Their study aimed to estimated energy-saving potential using a thermal effluent (provided from Boreyeong power complex, south Korea) coupled heat pump. Their proposed model was experimentally validated by comparing the predicted and measured indoor air temperature and plants transpiration (from May 28 to June 1, 2016). A good agreement was found with determination coefficients (R^2) of 0.94 and 0.96 for indoor air temperature and plants transpiration, respectively. Using again TRNSYS tool, Henshaw [87] studied the performance of unheated Iqaluit Community Greenhouse (ICG), Canada. The model considered that the convection heat transfer coefficients were constant for the internal and external sides of the wall. An analysis of eight scenarios

(modification of the greenhouse design) was performed based on growing season duration. The results showed that north wall and roof insulation, nighttime covers, and adding thermal mass and vestibule allow for extending the growing season considered as the consecutive days having an indoor air temperature above 4 °C.

Gao et al. [88] created in the EnergyPlus environment a Chinese solar greenhouse. The object of the study was to define the optimal greenhouse north wall configuration under the climate conditions of Lanzhou, China. The north wall of the greenhouse was made up of a phase change material (PCM) wallboard layer, a block brick layer and a heat preservation layer. The heat storage/ release capacity and the shadow (of the east and west walls) were calculated. According to the authors, the optimal north wall length for the analyzed case was found to be about 90 m.

In order to assess the thermal performance of an integrated rooftop greenhouse (iRTG), Nadal et al. [89] used the EnergyPlus environment to create a dynamic model of iRTG incorporated in ICTA-ICP buildings, University of Barcelona, Spain. The crop transpiration was considered using empirical equations provided by Bonachela et al. [90] for greenhouses under Mediterranean climate conditions. The created model was first validated by comparing measured and predicted indoor air temperature and humidity obtaining a cumulative variation of RMSE (CV(RMSE)) of about 11.5% and 15.9%, respectively. The iRTG performances were compared to a similar greenhouse design in freestanding conditions and the results showed that iRTG is an advantageous concept.

In order to assess the thermal performance and energy needs of a greenhouse located in Crotone, Italy, Baglivo et al. [91] proposed a TRNSYS model that was validated by comparing the results to the ones of an EnergyPlus model. A comparison of the indoor air temperature obtained by TRNSYS and EnergyPlus showed a relative error of 11.1%. The results were not experimentally validated.

Alvarez-Sanchez et al. [85] used Design Builder to compare three greenhouse configurations under the climate conditions of Mexico City. Their study aimed to select the optimal greenhouse configuration by considering its operating and construction costs.

Table 1.2 presents an overview of studies carried out on physics-based modeling, specifying their field of interest, the used modeling tool, if the model is experimentally validated or not, and if plants are considered or not. It can be observed from the table that the CFD method has been extensively used in greenhouse modeling research works. Moreover, it should be noted that many studies do not consider the effect of the plant on the greenhouse microclimate, as it

is clearly presented in **Figure 1.8**. It can as well be remarked that the most assessed plant is the tomato, which could be explained by its wide use in protected agriculture and also the availability of tomatoes' physiological data compared to other plants.

Table 1.2. Summary of physic-based method for greenhouse modeling (years from 2000 to 2021).

Year	Study reference	Study's interest area	Numerical tool	Experimental validation	Plant
2021	Boccalatte et al. [84]	Savona, Italy	EnergyPlus	No	No plant
2021	Costantino et al. [43]	Verona (Italy), Nantes (France), Seville (Spain)	__	Yes	Flowers
2021	El Jazouli et al. [57]	Agadir, Morocco	__ (CFD)	Yes	Tomato
2021	Lee et al. [86]	South Korea	TRNSYS	Yes	Irwin mangoes
2021	Oskin et al. [56]	krasnodar, Russia	Comsol Multiphysics	No	No plant
2020	Baglivo et al. [91]	Crotone, Italy	TRNSYS	No	Chrysanthemum
2020	Ben Ali et al. [71]	Northern Tunisia	Simulink/ Matlab	Yes	Tomato
2019	Altes-Buch et al. [68]	__	Dymola	No	Tomato
2019	Dhiman et al. [63]	Ludhiana, India	Ansys Fluent	Yes	No plant
2019	Ma et al. [54]	West Lafayette, Indiana	Comsol Multiphysics	Yes	Not defined (thermal properties was considered as those of "wood" material)
2019	Saberian and Sajadiye [60]	Ahvaz, Iran	Ansys Fluent	Yes	No plant
2019	Zhang et al. [62]	Northern China	Ansys	Yes	No plant
2018	Ahamed et al. [77]	Saskatoon, Canada	MATLAB	Yes	Tomato
2018	Baxevanou et al. [64]	Central Greece	Ansys Fluent	Yes	Tomato
2018	Diaz et al. [80]	Santa Sofia, Colombia	__	Yes	Tomato
2018	He et al. [59]	Jiangsu, China	Ansys Fluent	Yes	No plant
2018	Mohammadi et al. [73]	Tabriz, Iran	Matlab	Yes	No plant
2018	Taki et al. [72]	Tabriz, Iran	Matlab	Yes	No plant
2017	Gao et al. [88]	Lanzhou, China	EnergyPlus	No	No plant
2017	Henshaw [87]	Iqaluit, Canada	TRNSYS	No	No plant
2017	Nadal et al. [89]	Barcelona, Spain	EnergyPlus	Yes	Tomato and two successive crops of lettuce (only in experiment)
2016	Taki et al [74]	Azerbaijan, Iran	Matlab	Yes	Not defined

2015	Fatnassi et al. [58]	__	Ansys Fluent	No	Tomato
2015	Joudi and Farhan [70]	Baghdad, Iraq	Matlab	Yes	No plant
2015	Piscia et al. [61]	__	Ansys	No	Not defined
2014	Alvarez-Sanchez et al. [85]	Mexico City	DesignBuilder	No	No plant
2014	Sdringola et al. [65]	Perugia, Italy	Comsol	No	No plant
2013	Mashonjowa et al. [82]	Zimbabwe	Fortran/ TRNSYS	Yes	Rose crop
2013	Mesmoudi et al. [55]	Batna, Algeria	Fluent	Yes	No plant
2013	Wang et al. [52]	Jinmen, Central China	Fluent	Yes	Cherrytomatoe
2012	Candy et al. [81]	Humla, Nepal region	TRNSYS	Yes	Spinach
2012	Fabrizio [83]	Northwest Italy (Turin and San Remo)	EnergyPlus	No	No plant
2012	Nebbali et al. [50]	__	Ansys Fluent	No	Tomato
2012	Piscia et al. [49]	__	Ansys Fluent	Yes	Lettuce
2011	Abdel-Ghany and Hilal [69]	Riyadh, Saudi Arabia	__	Yes	Tomato (considered as semi-transparent cover)
2011	Nebbali et al. [48]	__	Fluent	No	Tomato
2011	Vanthoor et al. [75], [76]	Temperate marine climate (northwest Netherlands), Mediterranean climate (Sicily, Italy) and semi-arid climate (Texas and Arizona, USA)	Matlab	Yes	Tomato
2010	Fidaros et al. [47]	Central Greece	Ansys Fluent	No	Tomato
2009	Ben Younes et al. [79]	__	__	No	No plant
2009	Majdoubi et al. [46]	Agadir, Morocco	__ (CFD)	Yes	Tomato
2009	Sethi et al. [67]	Ludhiana, India	C++	Yes	Capsicum
2006	Ould Khaoua et al. [45]	__	__ (CFD)	Yes	Kalanchoe (only in experiment)
2005	Montero et al. [51]	__	Fluent	No	No plant
2002	Rodríguez et al. [78]	Almería, Spain	Dymola	Yes	No plant

2001	Tavares et al. [66]	Lisbon, Portugal	Maple V	Yes	No plant

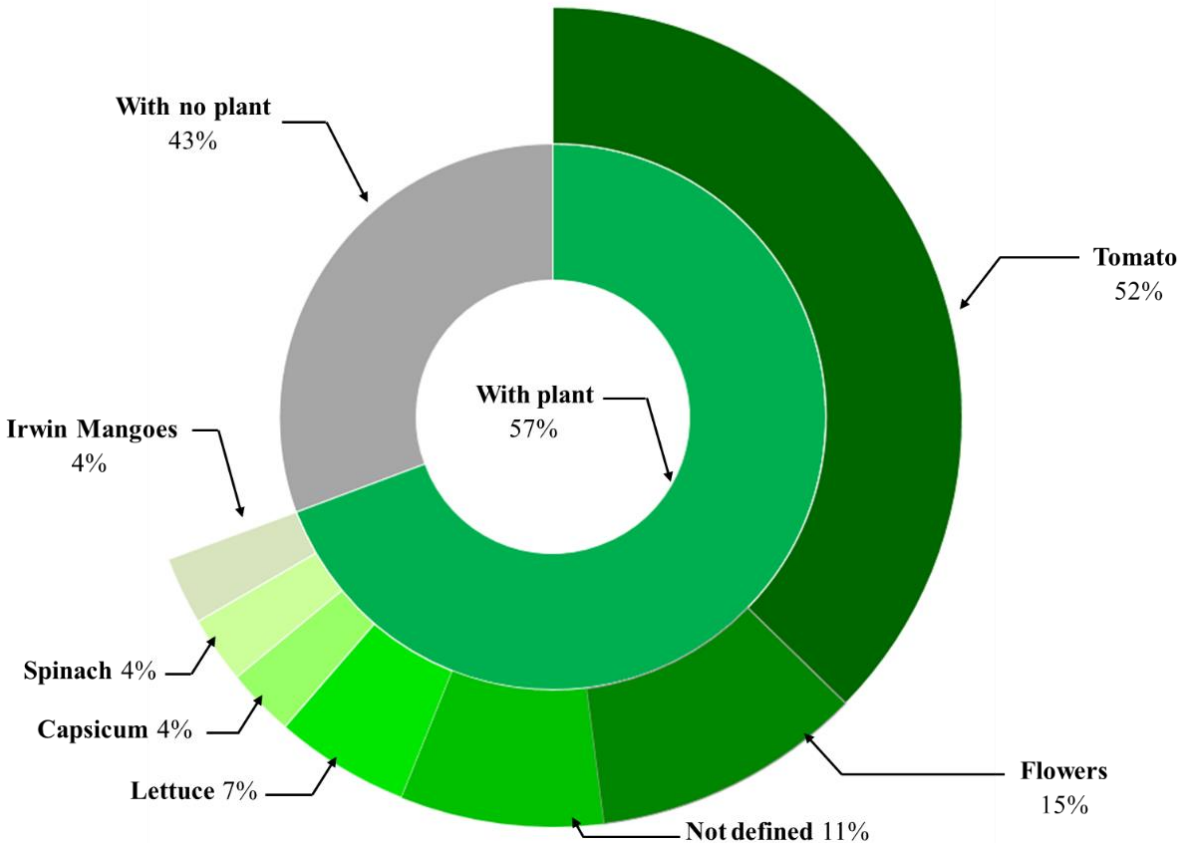

Figure 1.8. Distribution of studies showing the plants involved in the greenhouse model (years from 2000 to 2021).

1.4.1.2 Data-driven (artificial intelligence) modeling

Data-driven energy modeling methods do not require detailed information on greenhouse components, environmental conditions and system specifications. However, a large set of measured data is needed for training and validating the models. Currently, the agricultural sector faces a real revolution in modeling, thanks to the data-driven approach. The advent of technologies and the implementation of artificial intelligence (AI) play a crucial role in this revolution and have taken the agriculture framework to an advanced level [92]. Artificial intelligence can lead to real-time monitoring and decision-making, which can be of considerable interest to further improve and develop this sector. Substantial research has been devoted to this target. Jha et al. [93] presented a comprehensive review of the present state of automation in agriculture and discussed the applications of artificial neural networks (ANN), machine-learning (ML) and the internet of things (IoT) for precision farming. In another review paper, Patrício and Riederb [94] evaluated the approaches and the issues of computer vision

and artificial intelligence applied to precision grain crops agriculture. Pantazi et al. [95] described in an exhaustive manner different artificial intelligence methods and their applicability in precision farming. In particular, machine-learning methods can be applied in protected agriculture in many ways, such as to optimize greenhouse microclimate control [96], to optimize the irrigation process [97], to properly apply pesticides and herbicides [98], to detect plant disease [99]–[102], to optimize the energy consumption, and many others.

To predict the agricultural greenhouses variables, different machine-learning (ML) methods can be used. Artificial Neural Networks (ANN) have been largely used for this purpose [103]–[109].

Ferreira et al. [110] predicted the indoor air temperature of a hydroponic vegetable production greenhouse using radial basis function neural networks method (RBFNN). Outside air temperature, solar radiation and indoor air relative humidity were selected as model inputs. Compared to the hybrid batch and adaptive methods, the authors reported that the algorithm based on a levenberg-marquardt method has the minimal computational cost and the best performance, considering the error performance and parameter convergence.

A multilayer perceptron ANN (ANN-MLP) with a cascade architecture was used to predict the electrical power consumption of a greenhouse located at Querétaro State University, Mexico [111]. The model performance was compared to a conventional regression model and the results showed that the MLP model has better performance with a mean absolute percentage error (MAPE) of 0.0626 against 0.0921 for the other model.

Taki et al. [72] compared the performance of multiple linear regression (MLR) and dynamic models with ANN models in predicting the indoor air and roof temperatures, and energy loss of a single slop greenhouselocated in the North-West of Iran. According to the results, the ANN method showed the best performance, with RMSE of 0.23 and 0.17 for air and roof temperatures.

Using multilayer perceptron neural network (MLP-ANN) with different hidden layers, Neugebauer et al. [112] predicted the indoor air temperature (after 10 hours of heating) of a tunnel greenhouse located in northeastern Poland and heated by a bioreactor. According to the authors, MLP structures 4-15-1 and 4-19-1 showed the best performance based on RMSE values (5.61 and 5.44, respectively). They concluded that the proposed models could be considered as an efficient method to control the indoor air temperature of the greenhouse and switch to alternative heating when necessary.

The other machine-learning methods have been scarcely tackled up. Taki et al. [113] studied the feasibility of controlling greenhouse climate conditions and energy consumption for a polyethylene greenhouse located in the Isfahan Province, Iran. In their study, a comparison of ANN (multilayer perceptron (MLP) with radial basis function (RBF)) and support vector machine (SVM) methods was conducted. The results showed that the RBF neural network model is more accurate in estimating the parameters inside the greenhouse (air, soil and plant temperatures) with a range of root mean square error of about 0.07–0.12 °C.

In another work, Yu et al. [114] predicted the indoor air temperature of a Chinese solar greenhouse using a least squares support vector machine (LSSVM) optimized by the improved particle swarm optimization algorithm (IPSO). The LSSVM model showed suitable accuracy compared to standard SVM and backpropagation ANN (BPANN), with a lower mean square error of about 0.0281 °C.

Zou et al. [115] predicted the indoor air temperature and relative humidity of a solar greenhouse in the "institution vegetable and fruit of the Chinese academy of agricultural sciences" using the convex bidirectional extreme learning machine (CB-ELM) method. This method showed the highest accuracy (root mean square error of about 1.4409 °C and 2.4988% for temperature and relative humidity, respectively) compared to bidirectional extreme learning machine (B - ELM), backpropagation neural network (BPNN), support vector machine (SVM) and radial basis function (RBF). Chen et al. [116] proposed hybrid particle swarm optimization (PSO) and genetic algorithms (GA) techniques to predict the energy demand of a greenhouse located in Jiangsu Province, China. Their study aimed to compare the proposed model with the separated PSO and GA methods. According to the authors, the HPSO-GA shows better performance regarding the accuracy and calculation time.

In order to predict the greenhouse indoor air temperature, Allouhi et al. [117] compared four machine-learning methods (MLR, SVR, GPR, ensemble of trees) using as inputs outside temperature, relative humidity, global solar radiation and air velocity. The data collection was conducted in a canarian greenhouse located in Agadir, Morocco, for a period of four months (January to May 2019). The results showed that the GPR model is the best in predicting greenhouse indoor air temperature, with a coefficient of determination (R^2) of about 0.94. The authors stated that the GPR model was the most computational time-consuming among the four learning methods.

Figure 1.9 shows the distribution of the studies conducted in data-driven modeling of greenhouse variables, published in the period from 2000 to 2021. It can be remarked from the

graph that the artificial neural networks method (with its different types, namely BP-ANN, ELM, RNN, and others) is the more investigated field, with a rate of 54%. Moreover, several machine-learning methods have not been sufficiently exploited. Nevertheless, their use for predicting greenhouse variables is of great interest and shows good performance. Machine-

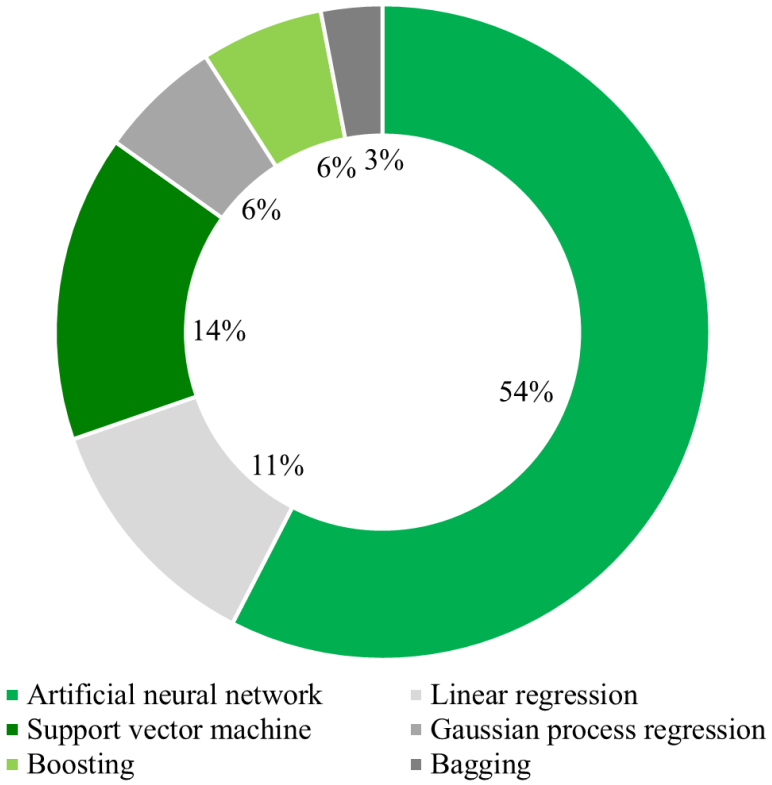

Figure 1.9. Distribution of studies on Data-Driven methods used in greenhouse modeling (years from 2000 to 2021).

learning methods could be an affordable solution for developing intelligent management strategies and reducing potential energy and financial losses.

1.4.2 Greenhouse design selection

The greenhouse design is a key factor in the protected agriculture process. Thus, the shape, the covering material, and the orientation must be carefully chosen, given their impact on the amount of solar irradiance captured and, therefore, the inside microclimate. The optimal greenhouse design helps approach as much as possible the adequate microclimate and leads to a decrease in the heating and cooling loads, thereby reducing the greenhouse operating cost. Several efforts have been undertaken to address this issue and exhaustive reviews on this field have been presented. Odesola and Ezekwem [118] reviewed the studies related to the effect of greenhouse shapes and orientation. Choab et al. [119] presented a comprehensive review of greenhouses researches from different standpoints: greenhouse design, thermal modeling and

simulation, and climate-controlling technologies. Ghani et al. [120] reviewed greenhouse design issues in a hot and arid environment, including shapes, covering materials and orientations.

1.4.2.1 Greenhouse shapes

Several greenhouse shapes were studied in the literature in different regions. In order to optimally choose the greenhouse shape, a compromise must be found between its ability to take advantage of passive energy (solar energy) and its ability to resist to external stresses (e.g., wind force). **Table 1.3** shows, in the first column, sketches of some different greenhouse shapes.

Groener et al. [121] conducted several geometric tests on the software Solidworks Flow Simulation. Quonset shape is, according to them, the best one because it allows for mitigating the effects of wind load, thus reducing the need for expensive structural materials and simplifying the on-site assembly process. In another work, Aissa and Boutelhig [122], [123] compared three greenhouse shapes (even span, modified quonset and dome) from a safety point of view under climate conditions of Ghardaia, Algeria. CFD simulation results lead the authors to select the dome shape as the best one. In a more comprehensive work, Kim et al. [124] evaluated the structural safety of even span and modified quonset greenhouses accordingly to design standards for wind load in different countries: USA, EU, Korea, China and Japan. According to the authors and based on the design standards of the USA and Korea, the even span design was found to be possibly destroyed due to a strong wind environment in the target areas. Whereas it was considered to be safe according to design standards of the EU, China, and Japan. The modified quonset greenhouse was considered unsafe and vulnerable to strong wind, based on design standards of the USA, the EU and China. At the same time, it was considered structurally safe based on the standards of Korea and Japan.

From an energy optimization point of view, several studies have been carried out [125]–[127]. Ahamed et al. [128] evaluated, five shapes under the climate conditions of Canadian prairies, namely even span, uneven span, mansard roof, quonset, and gothic arch. The authors concluded that the uneven span shape receives the highest amount of solar energy but has insignificant heating saving potential. They recommended, for high latitudes, quonset and even span shapes for single span and multispan greenhouses, respectively.

The energy consumption of six most commonly used greenhouse shapes (even span, uneven span, mansard roof, single slop, gothic arch and quonset), with the same length, width and

height, was evaluated under climate conditions of Tabriz, Iran [129], [130]. The results showed that a single slop greenhouse (with north wall insulation) is the optimal shape.

In the climate conditions of Bayburt City, Turkey, Çakır and Şahin [131] compared five commonly used shapes (even span, uneven span, mansard roof, quonset and modified quonset) in terms of solar energy gain. The modified quonset was selected as the best shape in all evaluated cases.

In another study, Choab et al. [132] evaluated the performance of three greenhouse shapes, namely even span, quonset and modified quonset. The comparison was carried out based on the greenhouse heating and cooling energy needs under climate conditions of Agadir City, Morocco. The results showed that quonset is the optimal greenhouse shape in the target area by considering the annual energy cost of an air-conditioning system.

Numerous studies selected India as an interest area where most climatic zones of the country were considered [133]–[136]. Sethi [67], [137] compared different greenhouses shapes (even-span, uneven-span, mansard roof, modified arch and quonset) with the same dimensions (6 m length, 4 m width, 3 m ridge height). The results showed that the greenhouse shapes selection depends on the geographic characteristics of the site; in fact, during all year months and at all latitudes, an uneven-span greenhouse receives the maximum of solar radiation and a quonset greenhouse receives the minimum. For other shapes and at 10°N, they receive more solar energy in winter and less in summer, while the opposite at 30°N and 50°N latitudes. Tiwari and Gupta [138] evaluated the impact of five greenhouse shapes (even span, uneven span, modified arch, mansard roof, and modified IARI) in New Delhi climate conditions. Based on greenhouse indoor air temperature and thermal loads, modified quonset and mansard roof were found to be the best shapes in summer and winter, respectively.

Table 1.3 summarizes the conclusions drawn by each study for the different greenhouse shapes. For greenhouse plants production, it can be remarked from the literature that even span is the most studied shape. That can be explained by the fact that this shape has been used for a very long time worldwide. It can also be inferred from the literature that the majority of studies have been conducted under the climate conditions of India. In cold climate conditions, uneven span or sawtooth greenhouse shapes could be recommended, while quonset or gothic arch shapes could be preferred in hot or moderate climate conditions.

Table 1.3. Details on the studies conducted on greenhouse shapes selection (years from 2000 to 2021).

Shape	Study Reference	Study interest area	Main conclusions of the study
Even span 	Ahamed et al. [128]	Canadian Prairies	Recommended as multispan greenhouse for the studied region.
	Chen et al. [125]	Haikou, Fuzhou, and Wuhan, southern China	Regarding the amount of solar radiation captured, this shape was rated 5th after sawtooth, modified quonset, modified gothic arch, and uneven span shapes.
	Rasheed et al. [126]	Daegu, South Korea	Requires 2% more annual energy than modified a gothic arch shape.
	Mobtaker et al. [129], [130]	Tabriz, Iran	Rated 4th after single slop, mansard roof and gothic arch shapes, regarding the amount of energy requirement during the winter period.
	Çakır and Şahin [131]	Bayburt, Turkey	Rated 3rd after gothic arch and uneven span shapes, regarding the amount of solar energy gain.
	Choab et al. [132]	Agadir, Morocco	It has the lowest energy requirements for cooling purposes.
	Belkadi et al. [127]	Tunisia, Tunis	The best shape considering the overall greenhouse energy consumption.
	Gupta and Chandra [133]	North India	It has a heating requirement of 8.37 MJ/m^2.
	Sethi [67]	10°N, 31°N and 50°N latitudes, India	It receives 14.7%, 12.9%, and 11.3% less yearly average solar energy than uneven span, at 10°N, 31°N, and 50°N, respectively.
	Kumari et al. [135]	Kolkata, New Delhi, Jodhpur, Chennai, and Srinagar cities, India	—
	Singh and Tiwari [136]	Delhi, India	Requires the highest amount of energy for heating purposes.
	Tiwari and Gupta [138]	New Delhi, India	Could be suitable for summer conditions.
Uneven span 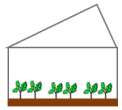	Ahamed et al. [128]	Canadian Prairies	It has insignificant heating saving potential. It captures the highest solar radiation except for November to January. Requires high capital cost.
	Chen et al. [125]	Haikou, Fuzhou, and Wuhan, Southern China	Regarding the amount of solar radiation captured, this shape was rated 4th after sawtooth, modified quonset and modified gothic arch shapes in Haikou. And 3rd, after sawtooth, modified quonset in Fuzhou and Wuhan.
	Mobtaker et al. [129], [130]	Tabriz, Iran	Rated 5th after single slop, mansard roof, gothic arch shapes, and even span regarding the amount of energy requirement during the winter period.
	Çakır and Şahin [131]	Bayburt city, Turkey	Rated 2nd after gothic arch shape, regarding the amount of solar energy gain.
	Belkadi et al. [127]	Tunisia, Tunis	Could be suitable considering only heating requirements.
	Sethi [67]	10°, 31° and 50° latitudes, India	Captures the highest amount of solar energy at all latitudes.

	Gupta and Tiwari [134]	New Delhi, Jodhpur, Chennai, and Srinagar cities, India	Selected as the best shape regarding heating needs.
	Kumari et al. [135]	Kolkata, New Delhi, Jodhpur, Chennai, and Srinagar cities, India	Selected as optimal design from a heating point of view for cold and cloudy climate (Srinagar).
	Singh and Tiwari [136]	Delhi, India	Selected as suitable shape regarding heating requirements.
	Tiwari and Gupta [138]	New Delhi, India	Rated 2nd after mansard roof from heating requirement point of view.
Single slop 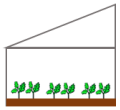	Mobtaker et al. [129], [130]	Tabriz, Iran	Receives maximum solar radiation during cold periods and can be considered as the suitable choice in cold climates as for Tabriz. (with a north wall)
Mansard roof 	Ahamed et al. [128]	Canadian Prairies	Shows its efficiency in Canadian Prairies climates. Cannot be used as multispan greenhouse.
	Chen et al. [125]	Haikou, Fuzhou, and Wuhan, southern China	Receives less amount of solar radiation.
	Mobtaker et al. [129], [130]	Tabriz, Iran	Rated 2nd after single slop shape, regarding the amount of energy requirements during the winter period.
	Çakır and Şahin [131]	Bayburt city, Turkey	Receives the lowest solar energy gain.
	Sethi [67]	10°, 31° and 50° latitudes, India	It receives 16.1%, 10.3% and 9.4% less yearly average solar energy than even span, at 10°N, 31°N and 50°N, respectively.
	Singh and Tiwari [136]	Delhi, India	Rated 3rd after uneven span and quonset shapes, regarding heating requirements.
	Tiwari and Gupta [138]	New Delhi, India	Selected as the best shape during the winter period.
	Gupta and Tiwari [134]	New Delhi, Jodhpur, Chennai, and Srinagar cities, India	It is preferred regarding cooling needs.
	Kumari et al. [135]	Kolkata, New Delhi, Jodhpur, Chennai, and Srinagar cities, India	—
	Tiwari and Gupta [138]	New Delhi, India	Could be suitable for summer conditions.
	Ahamed et al. [128]	Canadian Prairies	More efficient in climate conditions of the target area. Recommended as single span since it cannot be used as multispan greenhouse.
	Mobtaker et al. [129], [130]	Tabriz, Iran	It has the highest energy requirement. (with north wall)

Quonset 	Çakır and Şahin [131]	Bayburt city, Turkey	Rated 4th after gothic arch, uneven span and even span shapes, regarding the amount of solar energy gain.
	Choab et al. [132]	Agadir, Morocco	Selected as the optimal shape in the target area by considering the annual energy cost for heating and cooling needs.
	Gupta and Chandra [133]	North India	It has the highest heating requirements (8. 51 MJ/m²) compared to single slop and gothic arch shapes.
	Sethi [67]	10°, 31° and 50° latitudes, India	Captures the lowest amount of solar energy at all latitudes.
	Singh and Tiwari [136]	Delhi, India	Rated 2nd after uneven span shape, regarding heating requirements.
Modified quonset 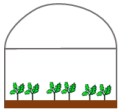	Chen et al. [125]	Haikou, Fuzhou, and Wuhan, southern China	For all the studied regions, this shape was rated 2nd after the sawtooth shape regarding the amount of solar radiation captured.
	Rasheed et al. [126]	Daegu, South Korea	Requires 8% more annual energy than the modified gothic arch.
	Choab et al. [132]	Agadir, Morocco	Has the lowest energy requirement for heating purposes.
	Belkadi et al. [127]	Tunisia, Tunis	The least efficient in terms of daylight.
	Tiwari and Gupta [138]	New Delhi, India	Selected as the best shape during the summer period.
Gothic arch 	Ahamed et al. [128]	Canadian Prairies	Has less solar radiation gain in the summer season. Could be beneficial for cooling purposes, but in the studied region, the cooling is mainly provided by natural ventilation.
	Mobtaker et al. [129], [130]	Tabriz, Iran	Rated 3rd after single slop and mansard roof shapes, regarding the amount of energy requirement during the winter period. (with a north wall)
	Çakır and Şahin [131]	Bayburt city, Turkey	The best shape regarding solar energy gain.
	Gupta and Chandra [133]	North India	Has a heating requirement of 8. 15 MJ/m². Considered as the best shape since its heating requirement is less by 2.6% and 4.2% than single slop and quonset, respectively.
	Sethi [67]	10°, 31° and 50° latitudes, India	Receives 2.3%, 0.5% and 0.6% less yearly average solar energy than even span, at 10°N, 31°N and 50°N, respectively.
	Gupta and Tiwari [134]	New Delhi, Jodhpur, Chennai, and Srinagar cities, India	Preferred regarding cooling needs.
	Chen et al. [125]	Haikou, Fuzhou, and Wuhan, Southern China	Regarding the amount of solar radiation captured, this shape was rated 3rd after sawtooth, modified quonset shapes in Haikou. And 4th after sawtooth, modified quonset, and even span in Fuzhou and Wuhan

Modified gothic	Rasheed et al. [126]	Daegu, South Korea	The most suitable shape in the target area; thus, it requires less annual energy. Receives more solar radiation during the winter and less during the summer.
 arch	Singh and Tiwari [136]	Delhi, India	Rated 4nd after uneven span, quonset and mansard roof shapes regarding heating requirements.
Sawtooth 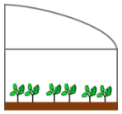	Chen et al. [125]	Haikou, Fuzhou, and Wuhan, southern China	Receives the highest amount of solar radiation in winter at all latitudes. Considered as the best shape.
Rectangle 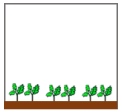	Belkadi et al. [127]	Tunisia, Tunis	Could be suitable considering only lighting system energy consumption.

1.4.2.2 Greenhouse envelope materials

The envelope (transparent cover) material is the boundary between the inside greenhouse and the external environment. It can be considered as the element that allows for controlling the external/internal flows. Thus, it must be optimally selected to protect the plants from the external weather and to control the exchanges between the outdoor and the indoor environments while letting through the necessary solar irradiation for plant's photosynthesis process. The optical, thermal and mechanical properties of the greenhouse covering materials considerably affect the choice.

Under hot climate conditions, the suitable covering material should have the characteristics of reflecting the infrared (IR) and ultraviolet (UV) radiations coming from the external environment [139], and letting through only the visible strip of light. On the contrary, it should be utterly transparent to infrared radiation from inside the greenhouse. Conversely, under cold climate conditions, the suitable cover is the one that lets through all radiation wavelength from outside except UV and blocks all radiation from the inside [140][141].

Katsoulas et al. [142] reviewed UV blocking greenhouse covering materials and their effect on plants' physiological processes. The authors presented the advantages and disadvantages of this type of cover; the UV blocking materials positively affect the plants' physiological processes (photosynthesis, transpiration and growth). However, it reduces the antioxidant content and other health-related phytochemicals. Abdel-Ghany et al. [143] analyzed the effect of cover type on the greenhouse indoor air temperature, the transmittance of photosynthetically active radiation (PAR) and the reflectance of near-infrared radiation (NIR). The authors also presented the benefits of NIR reflecting covers in minimizing greenhouse cooling energy requirements under arid conditions.

As there is no ideal greenhouse cover for all combinations of plants and climate conditions, several researches were conducted in order to select the optimal greenhouse covering material in different target conditions, for instance, Japan [144], [145], Italy [146], United Arab Emirates [147], [148] and Morocco [132].

Under Korean climate conditions, Rasheed et al. [126] compared different covering materials (polyethylene (PE), polyvinylchloride (PVC), glass (G), polymethylmethacrylate (PMMA), and polycarbonate (PC)) in order to select the most suitable one from a heating requirements point of view. According to the authors, the least heating requirement was obtained using

PMMA cover compared to the others, and a reduction of 40% was obtained when using PE in double-layer configuration compared to single-layer.

In another study, Erhioui et al. [149] compared the growth, yield, photosynthesis and leaf carbohydrate synthesis of Tomato plants cultivated in three mini-greenhouses under spring climate conditions of Ontario, Canada. The study considered different covers, namely single glass, double inflated polyethylene film (D-PE), and rigid twin acrylic panels (PMMA). The results showed that the best environment is obtained in greenhouses covered with D-PE and PMMA materials.

Baxevanou et al. [64] created a 2D tunnel greenhouse model based on radiation transfer in order to evaluate four covering materials (three-layer co-extruded film (3L), ethylenevinyl acetate film (EVA), thermal polyethylene film (TPE) and rose polyvinylchloride-based fluorescent (VPVC)) in climate conditions of Larissa, located in Central Greece. The four materials were classified based on a comparison between the plant agronomic needs and the indoor obtained parameters, namely visible spectrum irradiance, temperature and air velocity.

The effect of three covering materials (clear glass, diffuse glass and polycarbonate sheet) on the cucumber greenhouse microclimate in Riyadh, Saudi Arabia, is investigated by Alharbi et al. [150]. Cucumber yield was found to be quite similar in glass-covered greenhouse (clear and diffuse) and higher by about 50% compared to polycarbonate.

In the climate conditions of Tunisia, five covering materials (glass, low-emissivity glass, polyethylene, polycarbonate, acrylic) were investigated in terms of lighting, heating and cooling energy requirements [127]; the authors finally proposed polyethylene as the more appropriate greenhouse cover.

Moreover, a new generation of greenhouse covering materials (thermochromic, photochromic, photoelectric, photoselective film (i.e., IR and UV reflecting materials, etc.,) have appeared and current research trends in this field are involved [151]–[154]. Lamnatou and Chemisaba [155] reviewed and presented some critical comments on some categories of the new generation of greenhouse covers.

Hu and Yu [156] evaluated the energy performance of greenhouses covered with thermochromic materials (thermochromic glazing, thermochromic film and combined TC-film/TC-glazing) by comparing them with a simple and low emissivity glass-covered greenhouse. The analysis was conducted especially for cold climates; Ottawa, Canada and

Cleveland, United States. The results showed that combined TC-film/TC-glazing improves the energy efficiency of the greenhouse compared to the other covers.

In order to assess the impact of polyethylene incorporated organic semi-transparent PV (OPV) cover on the greenhouse microclimate, Baxevanou et al. [157] compared three polyethylene incorporated OPV densities and polyethylene sheets without PV. In their study, the climate conditions of Agchialos, Greece, were considered. Based on the required minimum PAR level, the case with 47% of greenhouse roof coverage (with a PAR transmittance of 60%) was found to be the optimal one.

Finally, based on the literature review conducted for greenhouse cover selection studies, published in the period between 2000 and 2021, it can be observed that the most studied covering materials are polyethylene film, followed by glass and polycarbonate film (**Figure 1.10**), which can be explained by the wide use of those materials as greenhouse cover given their relatively low price. Another conclusion could be drawn: the choice of the appropriate cover depends significantly on the climate conditions of the location and there is not a perfect cover for all cases.

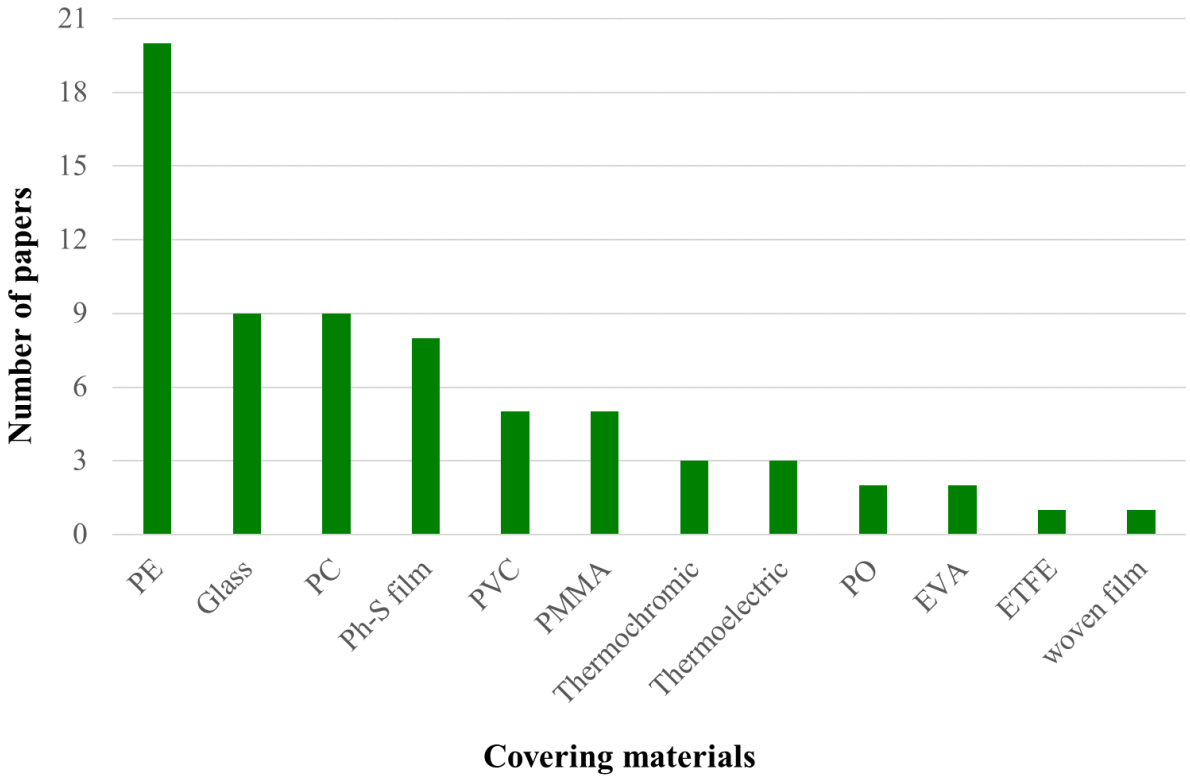

Figure 1.10. Distribution of greenhouse covering materials in greenhouse selection papers (years from 2000 to 2021).

1.4.2.3 Greenhouse orientations

The greenhouse orientation may significantly influence the solar heat gains and thus the internal climate. Its optimal selection could help reduce the amount of energy consumption in a passive way, which promotes the interest of the scientific community. Numerous researchers were interested in optimizing the greenhouse orientation [158], [128], [126], [159], [132], [160].

Sethi [67], [137] compared the North-South and East-West orientations in terms of the total solar radiation captured by an even span greenhouse at different geographical localization in India (10°N, 31°N, 50°N). The East-West orientation resulted in a higher amount of solar radiation captured during winter and a lower during summer compared to the North-South orientation. Thus, the author recommended it as the optimal orientation at all latitudes and for year-round operating greenhouse.

In nine regions of northern China, Chen et al. [161] studied the effect of orientation on solar radiation energy received in a Chinese solar greenhouse. According to the authors, the orientation degree should increase from the true south to the west when the latitude is higher.

East-West and North-South orientations were compared under the climate conditions of Tabriz, Iran [129], [130]. The authors reported that East-West and North-South orientations capture more solar radiation during winter and summer, respectively, and that East-West orientation is the optimal one considering additional energy requirements.

In climate conditions of Bayburt, Turkey, Çakır and Şahin [131] tested different orientation angles (from East-West to North-South with a step of 1°) for different greenhouse shapes. The authors reported that the optimal orientation depends not only on the shape but also on the size of the greenhouse, except for quonset shape where North-South was found to be the optimal orientation for different sizes.

El-Maghlany et al. [162] provided the solar energy captured and heating energy-saving cost generated from selecting the optimal quonset shaped greenhouse orientation. Different Egyptian locations were considered, namely Aswan, Assuit, Cairo, Alexandria and the North-South orientation (longer axis) involved the maximum amount of solar energy captured for the different studied locations.

Gupta et al. [158] and Çakır and Şahin [131] showed that the optimal orientation depends not only on the site latitude, as stated in the other studies, but also on the greenhouse shape and size. It could be added that it also depends on the plant type, operating time, and heating and cooling techniques.

It can be remarked from **Table 1.4** that the majority of papers considered as evaluation criteria the solar radiation availability on the greenhouse. However, it cannot be considered as the only criteria for defining the best orientation. When the greenhouse is oriented at East-West (longer axis), it makes quite a lot of sense that the solar energy captured during winter is higher than when the greenhouse is oriented at North-South, since one of the larger faces is facing the south. On the contrary, the other larger face is facing the north, which could increase the heat loss due to north wind, if there is any. In the authors' opinion, it would be preferable to consider the air-conditioning annual energy cost as a figure of merit for greenhouse orientation selection.

Table 1.4. Details on the studies conducted on greenhouse orientation selection (years from 2000 to 2021).

Study reference	Study interest area	Studied orientation	Evaluation criteria	Efficient orientation (longer axis)
Gupta et al. [158]	New Delhi, India	(0°, 30°, 45°, 60°, 90°)	Total solar fraction transmitted to the greenhouse on typical clear days in winter and summer	45° clockwise (Relative East–West)
Sethi [67], [137]	10°N, 31°N, 50°N, India	North-South and East-West	Captured solar radiation	East-West
Gupta and Chandra [133]	Northern India	North-South and East-West	Captured solar radiation	East-West
Ahamed et al. [128]	Prairies, Canada	North-South and East-West	Heating requirement	East-West
Rasheed et al. [126]	Daegu, south Korea	(0°, 15°, 30°, 45°, 60°, 75°, and 90°)	Solar energy gain	East-West
Chen et al. [125]	Haikou, Fuzhou, and Wuhan, southern China	(0°, 15°, 30°, 45°, 60°, 75°, and 90°)	Heating requirement	East-West
Chen et al. [161]	9 regions in northern China $34.3°N \leq latitude \leq 43.9°N$	From -12° to 12° (clockwise, 0° equivalent East-West)	Captured solar radiation	Increases from the true south to the west when the latitude increase (from East-West to North-South)
Dragićević [159]	24°N, 34°N, 44°N, 54°N Serbia	North-South and East-West	Total solar radiation availability on a typical day of each month	East-West
Stanciu et al. [163]	Bucharest, Romania	North-South and East-West	Total solar radiation on typical days in winter and summer	East-West
Mobtaker et al. [129], [130]	Tabriz, Iran	North-South and East-West	Total solar radiation availability	East-West
Çakır and Şahin [131]	Bayburt, Turkey	90 different orientations	Total solar energy gain	Depends on greenhouse shape and size
El-Maghlany et al. [162]	Aswan, Assuit, Cairo and Alexandria, Egypt	(0°, 45°, - 45°, 90°)	Total solar energy gain during winter (1st November- end of April) and heating cost saving	North-South
Choab et al. [132]	Agadir, Morocco	North-South and East-West	Thermal loads and annual air-conditioning cost	East-West

1.4.3 Energy-saving strategies

In order to improve greenhouse energy efficiency, several strategies were studied in the literature, including the use of passive techniques and the integration of renewable energy systems. Some researchers [164]–[166] presented a comprehensive review on renewable and sustainable based strategies, for instance; PV technologies (conventional photovoltaic technology (PV), hybrid photovoltaic thermal technology PVT, concentrated photovoltaic technology CPV, hybrid concentrated photovoltaic thermal technology CPVT), Solar thermal collectors (flat and concentrating collectors), heat pumps, thermal energy storage and others.

Ghani et al. [120] presented investigations on effective greenhouse cooling methodologies in hot and arid conditions allowing for maintaining adequate climate conditions inside the greenhouse. Another review [167] focused, in particular, on shading systems, their combination with other cooling methods (natural ventilation and evaporative cooling), their impact on greenhouse microclimate, and their contributions to energy and water saving.

For cold climates, Ahamed et al. [168] reviewed energy-saving techniques for heating purposes, including microclimate management techniques and efficient heating systems. Vadiee and Martin [169] analyzed several energy-efficient strategies for a more promising commercial greenhouse sector, with particular attention to Nordic climate conditions.

The integration of solar energy in protected agriculture has been developed as part of the greenhouse crops production trend. Several studies have been conducted in this context, particularly for roof-integrated PV panels [170]–[173]. Ezzaeri et al. [174] evaluated the effects of the PV modules shade in two canarian tomato greenhouses (shaded (40% covered) and unshaded) having the same dimensions. The results showed an improvement in the production during the summer period in the shaded greenhouse compared to the unshaded one because the PV shade helps reduce the indoor air temperature. On the contrary, a low production during winter is due to the delay of tomato maturity caused by the reduction of solar radiation reaching the plants. Under climate conditions of Pyrgos, Greece, Trypanagnostopoulos et al. [175] investigated the effect of greenhouse roof-integrated PV modules on energy production and plant growth. For this purpose, two greenhouses with lettuce production were considered: the first one covered with pc-Si panels and the second one without any PV system. The authors concluded that roof-integrated PV shading of about 20% or lower does not present a considerable effect on plant growth while having a significant contribution to fulfilling greenhouse energy demand. Chen et al. [176] analyzed the distribution of solar radiation inside

a greenhouse with roof-integrated PV panels. Checkerboard, crisscross and straight-line layouts were compared based on the radiation distribution uniformity, the radiation intensity and the electricity yield. The best annual electricity yield was obtained with checkerboard layouts and a covering rate of 25% was found not to have a meaningful impact on the daily radiation and plant growth. It can be observed from the literature analysis that there is a disagreement on the optimal PV panels shading rate to cover as much as possible the greenhouse electrical needs without influencing the plant growth. This seems to make sense since the optimal PV panels shading rate depends mainly on the plant type and the climate conditions of the target area.

In order to assess the effectiveness of biomass-based heating systems, several studies were conducted [177], [178]. Ali et al. [179] developed crop residues biomass furnace to meet the greenhouse heating needs. Comparing the proposed system with a diesel heater, the authors concluded that the biomass furnace is an attractive and proficient solution for greenhouse heating because its operating cost is 50% lower than that of a diesel heater.

Numerous studies considered hybrid systems based on different renewable energy sources and/or passive techniques. In order to ensure the heating and ventilation requirements of a greenhouse, a multi-source power system was proposed [180], combining a PV field and wind turbine generator with a battery energy storage system. Moreover, particular attention has been devoted to the control of the different greenhouse systems. The simulation results were compared to measurements for a small-scale tomato greenhouse located in the Faculty of Sciences in Tunis, Tunisia. According to the authors, the proposed solution was found to be efficient in controlling the greenhouse microclimate during different periods of the year.

A nearly zero-energy building (NZEB) greenhouse was designed and constructed under the climate conditions of Savona, Italy [84]. The greenhouse is equipped with roof-integrated semi-transparent PV modules connected to a battery system. The air-conditioning requirements of the greenhouse were provided by an air source heat pump and the transparent surface are low emission double glazing. The study results showed that the use of reflective shading and controlled natural ventilation can save around 30% of the greenhouse yearly energy demand and that the PV system can provide up to 94% of the heat pump electrical consumption.

Esen and Yuksel [181] studied the advantages of using various renewable energy sources to meet the greenhouse heating needs. A system combining a ground-coupled heat pump (GCHP) (with spiral heat exchanger), biogas, and solar collector was designed and experimentally investigated. The hybrid system was used to heat a real greenhouse located in Elazig, Turkey.

The analysis leads the authors to conclude that the combination of the GCHP and biogas system could be used as a greenhouse standalone heating system.

Thomas et al. [182] evaluated the energy-saving potential provided by using industry heat waste (local sugar plant) as the heating source for a greenhouse located in Lovell Wyoming, United States. A water-to-air heat pump (WAHP) was used for recovering the waste heat and transfer it to the greenhouse. The proposed system was compared to an electrical heater coupled with a variable air volume system (VAV). According to the authors, the annual electrical energy consumed to heat the greenhouse decreased by about 57% when using the WAHP system compared to the VAV system.

Costantino et al. [43] studied the effect of using variable angular speed fans for greenhouse ventilation on electrical energy consumption. The study considered different climate conditions, namely (Verona (Italy), Seville (Spain), Nantes (France)). It has been shown that the variable speed fans save around 25% of energy compared to fixed speed fans.

Figure 1.11 summarizes the different energy-saving strategies investigated in the literature for sustainable greenhouse production. The energy-saving strategies can be classified as integrating renewable energies and integrating passive techniques. Different types of renewable energies showed their efficiency in greenhouse cultivation, including photovoltaic systems, solar thermal collectors, biomass, wind energy, and renewable energy-based heat pumps. Furthermore, passive techniques (ventilation, evaporative cooling, thermal screens, reflective shading, nighttime insulation) were found to contribute significantly to optimizing greenhouse energy needs. PV technologies (PV, PVT, CPV and CPVT) were largely investigated in the

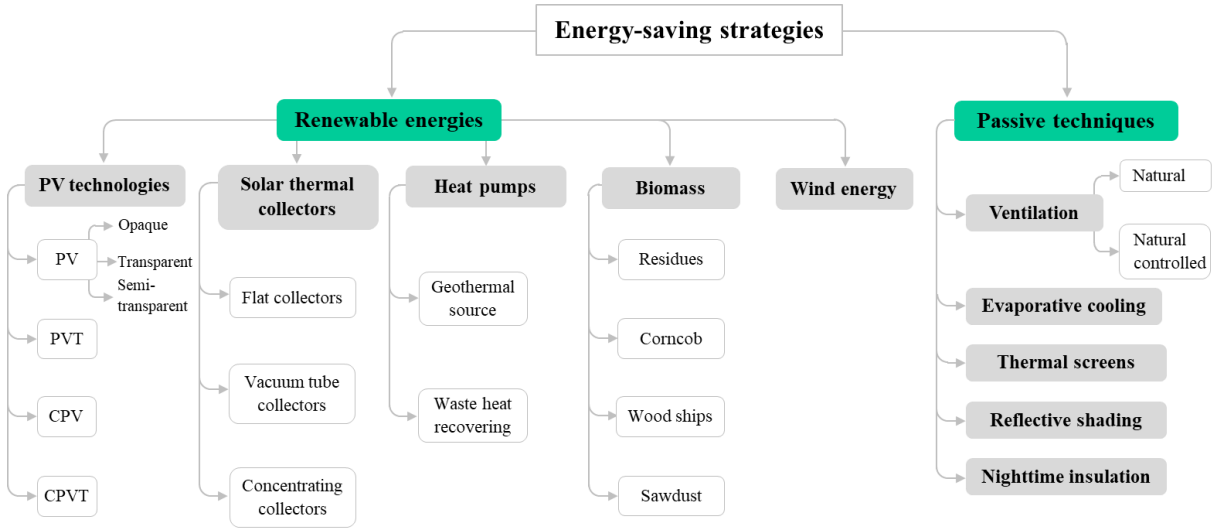

Figure 1.11. Energy-saving strategies for sustainable greenhouse cultivation.

literature, 68% of the presented papers studied the benefits/ challenges of integrating PV systems in greenhouse agriculture.

1.5 Conclusions

The increasing demand for food around the world has prompted the development of different agricultural techniques. Greenhouse production is one of the world's promising and widely used techniques. However, to create an adequate microclimate for plant growth, an important amount of energy is needed, making the greenhouse an energy-intensive system. As a consequence of the current energy availability and costs challenges, it is crucial to correctly address the energy and food relationships. The main goal of this work is to provide a comprehensive overview of the researches carried out in the last two decades, namely from the years 2000 to 2021, with a particular focus on energy issues. Based on the present review, some main conclusions can be drawn as follows:

(1) Physics-based modeling proved its importance in understanding the thermal behavior of the greenhouse system, describing the evolution of the indoor microclimate, and comparing different energy-saving and management strategies. Several numerical tools are available and have shown their good performance in predicting greenhouse microclimate. The selection of the adequate tool should consider, depending on the final objects of the study, the desired level of analysis. Therefore, it should be noted that it is important to consider the presence of plants inside the greenhouse and their contribution to varying the microclimate. It was as well observed that the CFD method has been extensively used in research works on greenhouse physics-based modeling; by up to 43% of the reported studies compared to the other methods.

(2) Machine-learning methods could be an affordable solution to develop intelligent management strategies and reduce energy and financial losses. Despite the great interest and good performance, they showed, the use of machine-learning methods in predicting greenhouse variables remains limited. Based on reported works, the artificial neural networks (ANN) method was found to be the more investigated one with a percentage of 54%, compared to the other methods. Thus, several machine-learning methods have not been sufficiently exploited and should prompt more attention.

(3) The greenhouse design selection (shape, cover and orientation) is a crucial step toward sustainable systems since their impact on solar collection is significant. Nevertheless, solar radiation availability should not be considered as the only criterion in greenhouse

design selection. In authors' opinion, it would be advisable to address greenhouse design investigations to overall yearly energy demand estimations at given indoor climate conditions.

(a) Based on the literature, even span is the most studied shape (in 93% of the presented papers). In cold climate conditions, uneven span or sawtooth greenhouse shapes could be recommended, while quonset or gothic arch shapes could be preferred in hot or moderate climate conditions.

(b) The most studied covering material is polyethylene film with a percentage of 29%, followed by glass and polycarbonate film (13% each one). Based on the presented studies in the review, there is not a perfect cover for all cases because the choice of the appropriate cover depends significantly on the climate conditions of the location and the plant needs. It could be noted that, for hot climate conditions, a suitable covering material should have the characteristic of reflecting the infrared (IR) and ultraviolet (UV) radiations coming from the external environment and letting through only the visible strip of light. In addition, the cover should be completely transparent to IR radiation from inside the greenhouse. Conversely, during cold climate conditions, a suitable cover is the one that lets through all radiation wavelengths from outside except UV and blocks all radiations from the inside.

(c) The optimal orientation depends not only on the site latitude but also on the greenhouse shape and size. It also depends on the plant type, operating time, and heating and cooling techniques.

(4) The integration of renewable energies and passive techniques in greenhouse agriculture showed a significant potential of energy-saving and could be a promising solution for sustainable agriculture able to face the energy/food conflict. Based on the present literature review, PV technologies (PV, PVT, CPV and CPVT) were largely investigated, thus 68% of the presented papers studied the benefits/ challenges of integrating PV systems in greenhouse agriculture. It is therefore recommended to give more attention and to study, in addition to PV technologies, other energy saving strategies.

The extended version of this chapter has been submitted to "Renewable and Sustainable Energy Reviews"

Chapter 2

Modeling, experimental validation, and energy-saving estimate of SamLab greenhouse

Chapter 2: Modeling, experimental validation, and energy-saving estimate of SamLab greenhouse

2.1 Introduction

Greenhouse is a complex system governed by a large number of parameters interacting with each other. This system could be considered as two principal subsystems, namely the plant and the inside environment. As stated in **section 1.4.1.1**, greenhouse modeling is of great interest to build an understanding of the system and to be able to improve its efficiency. Furthermore, physics-based modeling has shown its importance in describing the evolution of indoor microclimate variables, understanding the thermal behavior, analyzing greenhouse features and recommending different energy-efficient strategies.

In this chapter, a dynamic model created in the EnergyPlus environment is presented. The dynamic approach is selected as it is more accurate and takes into account more physical phenomena (for example, the heat storage capacities) compared to the other approaches (steady-state and quasi-steady-state). Despite its shortcomings (i.e., requires the knowledge of the hourly weather parameters and greenhouse components specifications), the dynamic approach allows for a deeper analysis of the system, which further explains its choice. The presented model considers the interaction among all the greenhouse components, including crops, soil, and internal masses.

The model validation is performed using experimental data from a high-efficiency greenhouse (SamLab) located in Albenga, in the Northwest Italy (https://samlab.dibris.unige.it/). Thus, actual weather data, namely ambient air temperature and solar irradiance are used to appropriately modify the weather file implemented as input in the EnergyPlus model. Different outputs are compared to actual monitored data, namely the actual electrical consumption of the air-conditioning system, the boreholes heat transfer rate and the electrical production of PV modules.

The model is then explored to quantify the potential of energy-saving strategies (passive techniques and renewable energies) and to study the effect of greenhouse internal masses and plants on the greenhouse microclimate.

The chapter is organized as follows: first, a description of the case study greenhouse is provided; then, the model of the greenhouse developed in the EnergyPlus environment is presented; after that, the proposed model is validated by considering different weather conditions, namely March 2020 and August/ September 2020; finally, the model was exploited to assess the effect

of internal masses and plants and to quantify the potential of energy-saving of passive techniques and renewable energies.

2.2 SamLab greenhouse description

The "Smart Agro-Manufacturing Laboratory" (SamLab) greenhouse [183] is a research laboratory devoted to experimenting innovative methods and technologies for precision agriculture for vegetables and flower plants. The greenhouse (**Figure 2.1**) was built in 2015 at the Regional Agriculture Research Center (CeRSAA) located in Albenga, Italy, in the framework of a Liguria Region research program involving the University of Genova (Dime and Dibris Departments) and the Erde Enterprise [184].



Figure 2.1. SamLab greenhouse external view.

The greenhouse has a standard even-span shape with a floor area of 151.47 m² (9.90×15.30) and a height at the rooftop of 5.60 m. The supporting structure is made of galvanized steel and is anchored in a concrete footing of 0.03 m. The greenhouse side containing the main entrance is faced - 60° in the direction of the relative South. The building envelope is made up of glass windows with an aluminum frame. The selected material for the glazed surfaces is a low-emissivity K-glass type N characterized by an overall heat transfer coefficient of 3.30 W/m².K and a thickness of 4 mm. The greenhouse is equipped with four concrete benches for plants cultivation purposes.

Table 2.1 summarizes the localization, climatic and geometrical parameters of the greenhouse. The climatic parameters are calculated from the hourly weather data used for the modeling. The HDD (heating degree day) and CDD (cooling degree day) are calculated based on the mean daily degree-hours method [185], with balance temperatures of 15.5 °C and 21°C, respectively. The winter and summer periods considered here are, respectively, from the 1st of November to the 15th of April and from the 1st of May to the 15th of October.

Table 2.1. SamLab greenhouse localization, climatic and geometrical parameters.

Location	
City	Albenga
Longitude	8.1°E
Latitude	44.1°N
Altitude	3 m
Time zone	+1 CET
Climatic parameters	
HDD (balance temperature 15.5 °C)	671.8
CDD (balance temperature 21 °C)	420.1
Hourly average temperature (Winter / Summer)	11.8 °C / 22.2 °C
Hourly maximum temperature (Winter / Summer)	23.5 °C / 33.9 °C
Hourly minimum temperature (Winter / Summer)	-2.2 °C / 7.3 °C
Dimensions	
Length	15.2 m
Width	9.9 m
Eave height	3.5 m
Rooftop height	5.6 m
Roof pitch	23°

The passive techniques implemented in the real greenhouse for cooling purposes are an internal shading/reflecting system (able to cover on-demand most of the inner surface) and operable windows on lateral sides and roof. One pitch of the greenhouse roof (facing southwest) is equipped with semi-transparent PV modules, having a peak power of about 2 kW. PV modules are made by a sandwich of crystalline silicon cells and glass and they occupy some 22 m^2 of the roof with a shaded area (cells) of about 50%.

The air-conditioning system of the greenhouse is associated to a water-to-water ground-coupled heat pump (GCHP). GCHPs are one of the most interesting solutions for air-conditioning in buildings and even in greenhouses cultivation that can fulfill both the heating and cooling needs. Furthermore, these systems help reduce the air-conditioning cost because they are characterized by high and stable efficiency as a result of the stable ground temperature.

In the SamLab greenhouse, the geothermal heat pump is coupled with six borehole heat exchangers (BHEs); each one is a double-U PE100 pipe with an external diameter of 32 mm and a length of nearly 100 m. The selected HP (Ecoforest brand, model Ecogeo B3) has a nominal heating capacity at a partial load factor $PLF = 95\%$ of 28 kW for $T_{in} = 10$ °C and $T_{out} = 55$ °C with a $COP = 3.7$ and a nominal cooling capacity at $PLF = 100\%$ of 34.4 kW for $T_{in} = 20$ °C and $T_{out} = 7$ °C with $EER = 5.29$.

In the real greenhouse HVAC system (**Figure 2.2**), the GCHP feeds a water tank (300 liters) for heat storage and flow rate decoupling. From the tank, hot water during winter and cold water during summer feeds an air handling unit (AHU) with a system of textile ducts for the conditioned air distribution. The ducts are located under the first three benches. The tank also directly feeds two benches with hot/cold water using a coil that passes below the plants. The other two benches are equipped with electrical resistances to ensure fulfilling of bench setpoint temperatures. **Figure 2.3** is a simplified scheme representing the whole system.



Figure 2.2. SamLab ground-coupled heat pump and bench alimentation system.

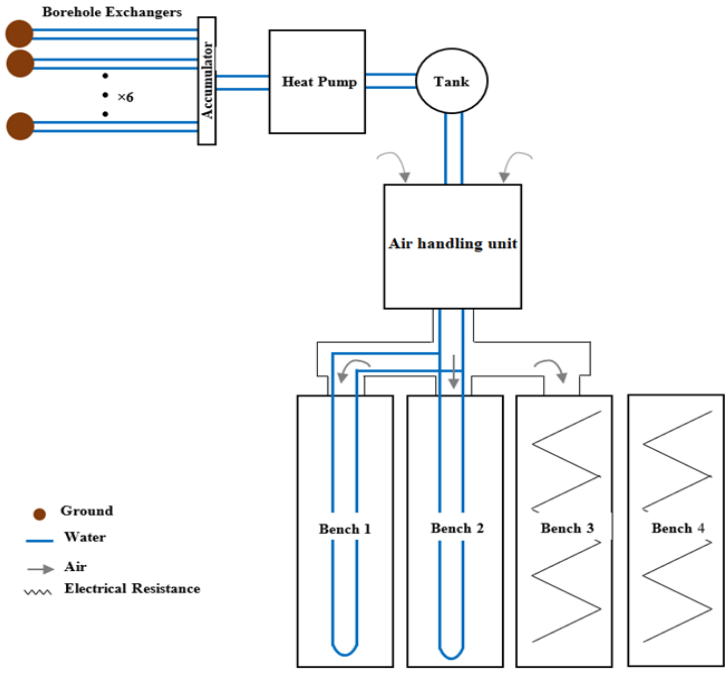

Figure 2.3. SamLab air and cultivation bench energy alimentation system.

2.3 Data acquisition

Actual weather data related to the selected periods (March and mid-August to mid-September 2020) are necessary to validate the model. The data for the analyzed location (i.e., Albenga) are partially measured on-site (temperature) and partially deduced from the Liguria Region Agency for the Environment webpage [186] (solar irradiance) and are used to properly modify the weather file adopted as input in the EnergyPlus model.

The SamLab greenhouse is equipped with a complete data acquisition and monitoring system that measures and records different parameters related to the PV modules, the HVAC plant, the passive techniques (operable windows and shading system) and the climate conditions inside the greenhouse. Many pressure, temperature and mass flow rate sensors allow acquiring a huge amount of hourly and sub-hourly data. This data acquisition system is composed of different subsystems: the ground-coupled heat pump (GCHP) datalogger (webserver inside the HP), the Bbone datalogger and the Raspberry datalogger.

2.4 Dynamic energy model

The greenhouse modeling and simulation are carried out in the EnergyPlus environment, the worldwide known dynamic simulator software, usually used in thermal building physics and HVAC systems simulation. In the present model, the greenhouse is a single zone that interacts with the outside environment as well as with different interior components, including plants, soil and internal masses.

2.4.1 Geometric model

The SketchUp graphical interface is used to create the 3D greenhouse geometry represented in **Figure 2.4**. The 3D model is manipulated using the OpenStudio Plugins and then implemented as an input to the EnergyPlus software. In the model, the aluminum, steel and concrete surfaces are considered as walls, and the glazing surface as windows (fixed and operable windows) and glazed doors. **Table 2.2** summarizes the materials properties used for the modeling. The internal masses are presented in the 3D model using "*interior partition surface*", then considered with their construction as "*internal mass*" and taken into account in the overall energy balance of the zone.



Figure 2.4. SamLab greenhouse 3D model.

Table 2.2. SamLab greenhouse envelop material properties.

	Glass	Steel	Aluminum	Concrete
Total area (m²)	256.2	53.1	25.8	76.6
Thickness (m)	0.004	0.2	0.17	0.3
Thermal conductivity (W/m. °C)	0.9	-	-	0.9
Conductance per unit length (W/m. °C)	-	173.3	619.8	-
Specific heat capacity (Wh/kg. °C)	-	138.8×10^{-3}	257.7×10^{-3}	244.4×10^{-3}
Visible transmittance	0.83	-	-	-
Visible reflectivity	0.11	-	-	-

2.4.2 System specifications

Annex 1 summarizes the parameters used to model the passive techniques (shading/reflecting system and operable windows) and renewable energy equipment (PV modules and the ground-coupled heat pump).

2.4.2.1 Internal masses

The internal masses of the greenhouse have a considerable heat capacity that undoubtedly affects the transient thermal behavior of the zone. Hence, it is essential to consider them in the model. In the present case study, the considered internal masses are the four concrete benches and all the HVAC system elements. In the "*internal mass*" feature, the physical properties of the construction materials are taken into consideration. This also leads to an increase in the number of surfaces that participate in the zone air heat balance and the longwave radiant exchange.

2.4.2.2 Windows shading/reflecting system

The shading /reflecting system is a passive technique used in the SamLab greenhouse to reduce cooling loads during the summer. Its effect influences the overall heat balance of the zone and depends on several parameters, namely transmittance, inter-reflection between the shading material and glass, and the amount of radiation absorbed by the shading.

The shading system is modeled as an interior shading surface with a thickness of 5 mm, solar transmissivity of 0.50 and solar reflectivity of 0.40, located 5 cm away from the glazing surface. The thermal model considers different thermal interactions, i.e., the thermal interaction between the shading layer and the glazing surfaces, and between the shading layer and the zone. Moreover, the shading surface model also calculates the natural convection airflow between the shading layer and the glazing surface.

The shading system's opening and closing are controlled based on the zone indoor air temperature; when the temperature exceeds 30 °C, the shading device is closed in order to minimize the solar gains.

2.4.2.3 Natural ventilation by operable windows

The second passive technique used to control the indoor temperature is an operable window system that provides natural ventilation inside the greenhouse. The system is modeled as a fraction area of the shell that can be opened; the ventilation flow rate is governed by wind and stack effect.

The natural ventilation is managed during the whole year based on a maximum exterior air velocity (5.4 m/s), a minimum and a maximum temperature for both indoor (16 °C – 60 °C) and outdoor (16 °C – 30 °C) conditions. Those parameters are the limits that set the shutoff of the ventilation. The control method helps avoid the heat losses from the zone to the exterior environment during the coldest days by closing the windows when the exterior or interior temperatures get down to 16 °C. Thus, their opening is applied when a high interior temperature is detected, fixed at a maximum of 60 °C (strictly higher than the maximum indoor temperature throughout the year) while the exterior temperature is still lower than 30 °C. If the exterior temperature exceeds 30 °C, the windows are shut down and the cooling is provided by the HVAC system. This system allows for minimizing energy consumption and avoiding the peaks of temperature in the hottest hours of the day due to an excessive greenhouse effect that is unsustainable for the plants' growth.

2.4.3 Greenhouse energy balance

In the model, as stated in **section 2.4.1**, the aluminum, steel and concrete surfaces are considered as walls, and the glazing surface as windows (fixed and operable windows) and glazed doors. The energy balances of the glazing and opaque surfaces are presented in **equation 2.1** and **equation 2.9**, respectively.

2.4.3.1 Energy balance of glazing surfaces

$$\dot{Q}''_{ir,glz} + \dot{Q}''_{sw,glz} + \dot{Q}''_{cond,glz} + \dot{Q}''_{conv,glz} = 0 \qquad \textbf{2.1}$$

$$\dot{Q}''_{ir,glz} = \dot{Q}''_{ir,glz\_ext} + \dot{Q}''_{ir,glz\_in} = \varepsilon_{glz\_front}(E_{ext} - \sigma T^4_{surf,glz\_ext}) + \varepsilon_{glz\_back}(G_{ir} + E_{in} - \sigma T^4_{surf,glz\_in}) \qquad \textbf{2.2}$$

$$\dot{Q}''_{sw,glz} = \dot{Q}''_{sw,glz\_ext} + \dot{Q}''_{sw,glz\_in} = \alpha_{d,glz\_front}(G_b \cos(\theta) + G_d) + G_{SW}\alpha_{d,glz\_back} \qquad \textbf{2.3}$$

$$\dot{Q}''_{cond,glz} = k_{glz}(T_{surf,glz\_in} - T_{surf,glz\_ext}) \qquad \textbf{2.4}$$

$$\dot{Q}''_{conv,glz} = \dot{Q}''_{conv,glz\_ext} + \dot{Q}''_{conv,glz\_in} = h_{glz\_ext}(T_{air\_ext} - T_{surf,glz\_ext}) + h_{glz\_in}(T_{air\_in} - T_{surf,glz\_in}) \qquad \textbf{2.5}$$

$$h_{glz\_ext} = 8.07 \cdot V_{wind}^{0.605} \quad \text{if } V_{Wind} > 2\ m/s$$

$$h_{glz\_ext} = 12.27 \quad \text{if } V_{Wind} < 2\ m/s$$

Windward surfaces **2.6**

$$h_{glz\_ext} = 18.64(0.3 + 0.05 \cdot V_{wind})^{0.605}$$

Leeward surfaces **2.7**

$$h_{glz\_in} = Nu\frac{k_{air}}{H} \qquad \textbf{2.8}$$

where:

$\dot{Q}''_{ir,glz}$ is the longwave radiation exchanges in glazing surfaces, composed of external $\dot{Q}''_{ir,glz\_ext}$ and internal longwave radiation exchanges $\dot{Q}''_{ir,glz\_in}$ that depend on the external E_{ext} and internal E_{in} longwave radiations incident on the external and internal glazing surfaces, respectively. T_{surf,glz_ext} and T_{surf,glz_in} are the temperatures of the external and internal glazing surface faces,

respectively. G_{ir} is the longwave radiation from internal sources (light and equipment), incident on glazing from inside. σ is the Stefan-Boltzmann constant $5.67\times10^{-8}\ W/(m^2\cdot K^4)$.

$\dot{Q}''_{sw,glz}$ is the shortwave radiation flux on the glazing surface. The external shortwave radiation flux $\dot{Q}''_{sw,glz-ext}$ considers the heat flux absorption of the incident beam and diffuse solar radiation on the outer glazing faces. $\dot{Q}''_{sw,glz-in}$ is the interior shortwave radiation, from internal sources and from reflected diffuse solar, incident and absorbed at glazing inner face.

$\dot{Q}''_{cond,glz}$ is the conduction flux through glazing surfaces.

$\dot{Q}''_{conv,glz}$ is the convective flux exchanges depending on the external T_{air_ext} and the internal T_{air_in} air temperatures.

The external convective coefficient h_{glz_ext} depends on the wind direction and velocity [187]. It is calculated using **equations 2.6** and **2.7** for windward surfaces and leeward surfaces, respectively; The internal convective coefficient h_{glz_in} depends mainly on the air thermo-physical properties and surface geometry [188]. It is calculated using **equation 2.8**, where: k_{air} is the air thermal conductivity, H is the glazing surface height, and Nu is the Nusselt number. Nu is calculated using four correlations that vary according to the surface tilt angle $\beta_{surf,glz}$, and are based on heating conditions. For cooling conditions (where $T_{surf,glz\_in} > T_{air\_in}$), the tilt angle used for calculation is obtained by $\beta_{surf,glz} = 180 - \beta_{surf,glz}$;

2.4.3.2 Energy balance of opaque surfaces:

$$\dot{Q}''_{ir,opq} + \dot{Q}''_{sw,opq} + \dot{Q}''_{conv,opq} + \dot{Q}''_{cond,opq} = 0 \qquad \textbf{2.9}$$

$$\dot{Q}''_{ir,opq} = \dot{Q}''_{ir,opq\_ext} + \dot{Q}''_{ir,opq\_in} \qquad \textbf{2.10}$$

$$\dot{Q}''_{ir,opq\_ext} = \varepsilon\sigma\cdot VF_{gnd}\left(T^4_{gnd} - T^4_{srf,opq\_ext}\right) + \varepsilon\sigma\cdot VF_{sky}\left(T^4_{sky} - T^4_{srf,opq\_ext}\right) + \varepsilon\sigma\cdot VF_{air}\left(T^4_{air} - T^4_{srf,opq\_ext}\right) \qquad \textbf{2.11}$$

$$\dot{Q}''_{ir,opq\_in} = VF_{i,j}\left(T^4_{i,opq\_in} - T^4_{j,opq\_in}\right) \qquad \textbf{2.12}$$

$$\dot{Q}''_{sw,opq} = \dot{Q}''_{sw,opq\_ext} + \dot{Q}''_{sw,opq\_in} \quad \textbf{2.13}$$

$$\dot{Q}''_{conv,opq} = \dot{Q}''_{conv,opq\_ext} + \dot{Q}''_{conv,opq\_in} = h_{opq\_ext}(T_{srf,opq\_ext} - T_{air\_ext}) + h_{opq\_in}(T_{srf,opq\_in} - T_{air\_in}) \quad \textbf{2.14}$$

where:

$\dot{Q}''_{ir,opq}$ is the external and internal longwave radiation exchanges on opaque surfaces. In the external longwave radiation heat flux $\dot{Q}''_{ir,opq\_ext}$ exchanges with the ground, the sky, and the air are considered as presented in **equation 2.11**, where: VF_{gnd}, VF_{sky}, VF_{air} are the surface to ground, sky and air view factors [189], respectively. The calculation of the internal longwave radiation $\dot{Q}''_{ir,opq\_in}$ considers the exchanges between the internal surfaces because the zone air is considered as completely transparent to longwave radiation (i.e., the greenhouse indoor air does not participate in the internal longwave radiation exchange); $VF_{i,j}$ is the view factor between surface *i* and *j* [190].

$\dot{Q}''_{sw,opq}$ includes the external and the internal shortwave radiation fluxes. The external shortwave radiation flux $\dot{Q}''_{sw,opq\_ext}$ considers the heat flux absorption of the incident direct and diffuse solar radiation on the external face of opaque surfaces. The internal shortwave radiation flux $\dot{Q}''_{sw,opq\_in}$ considers the heat flux due to the transmitted solar radiation to the zone (from transparent surfaces) and the shortwave radiation from internal sources, absorbed at surfaces.

$\dot{Q}''_{conv,opq\_ext}$ and $\dot{Q}''_{conv,opq\_in}$ are the external and internal convective fluxes exchanges, respectively, calculated according to **equation 2.14**. In the literature, several methods for calculating the exterior h_{opq_ext} [191] and interior h_{opq_in} [192] convection coefficients can be found and several of them are included in EnergyPlus. In this study, the adaptive convection algorithm is used for both the outside and inside coefficients [193], [194] because it allows for assigning the appropriate correlation for each specific surface.

Finally, $\dot{Q}''_{cond,opq}$ is the conduction flux through opaque surfaces. The conduction transfer function coefficients (CTFs) method, which takes into account both the thermal resistance and capacity of the surface, has been selected for the calculation.

2.4.3.3 Energy balance of vegetation and soil

Even though vegetation is the most important element in the greenhouse system, several studies on greenhouse models do not consider it, thus neglecting the evapotranspiration phenomenon in the overall energy balance. The plants contribute, through the evaporation process, to decreasing the greenhouse indoor air temperature. This would modify the energy needs both for heating and cooling. It is therefore important to consider them, especially when sizing the air-conditioning system.

The soil and the vegetation are defined, successively, as the outer layers of the construction material of the four benches (the side facing inside the greenhouse).**Table 2.3** presents the properties of the plant and soil used in the modeling. The energy analysis is divided into two heat balances: the heat balance of the foliage layer and the heat balance of the soil layer, as described in **equations 2.15** and **2.16**, respectively.

Table 2.3. SamLab greenhouse plant and soil proprieties.

Plant	
Type	Begonia
Height	0.12 m
Leaf index area	1
Minimum stomatal resistance	135 s/m
Leaf reflectivity	0.22
Soil	
Conductivity of dry soil	0.35 W/m. °C
Density of dry soil	1100 kg/m^3
Specific heat of dry soil	600 J/kg. °C
Solar absorptance	0.7

Foliage layer energy balance:

$$\dot{Q}_f^{"} = c_f \left[G_{sw}(1-r_f) + \varepsilon_f G_{ir} - \varepsilon_f \sigma T_f^4 \right] + \frac{r_f \varepsilon_g \varepsilon_f \sigma}{\varepsilon_1}(T_g^4 - T_f^4) + \dot{Q}_{sens,f}^{"} + \dot{Q}_{lat,f}^{"} \qquad \textbf{2.15}$$

Soil layer energy balance:

$$\dot{Q}_g^{"} = (1-c_f)[G_{sw}(1-r_g) + \varepsilon_g G_{ir} - \varepsilon_g \sigma T_g^4] - \frac{r_f \varepsilon_g \varepsilon_f \sigma}{\varepsilon_1}(T_g^4 - T_f^4) + \dot{Q}_{sens,g}^{"} + \dot{Q}_{lat,g}^{"} + k_g \frac{\partial T_g}{\partial z} \qquad \textbf{2.16}$$

where c_f is the fractional vegetation coverage; r_f and r_g are the shortwave reflectivity (albedos) of the foliage and the ground surface, respectively; ε_f and ε_g are the emissivities of the foliage and the ground surface, respectively; $\varepsilon_1 = \varepsilon_g + \varepsilon_f - \varepsilon_f \varepsilon_g$; G_{sw} and G_{ir} are the total incoming short and longwave radiations, respectively; T_f and T_g are the foliage and the ground

surface temperature, respectively; $\dot{Q}''_{sens,f}$ and $\dot{Q}''_{sens,g}$ are the foliage and the ground sensible heat flux, respectively; $\dot{Q}''_{lat,f}$ and $\dot{Q}''_{lat,g}$ are the foliage and the ground latent heat flux, respectively; and σ is the Stefan-Boltzmann constant.

The EnergyPlus vegetation and soil model is based on the "fast all season soil strength" (FASST) model [195] with some assumptions, and takes into account the radiative exchanges (longwave and shortwave) within the plant canopy, the evapotranspiration (latent heat flux) related to both soil and plants, the effects of the canopy on convective heat transfer (sensible heat flux) as well as the heat transfer by conduction in the soil layer. FASST model neglects any energy supply or dissipation due to phase changes of soil water, precipitation or vertical transport of water in the soil.

2.4.3.4 Energy balance of the air

The air energy balance considers the zone loads (including convection heat flux from the greenhouse components ($\sum \dot{Q}_{conv}$), the contribution due to infiltration of the outside air ($\dot{Q}_{\inf}$) and the heat transfer rate provided by the HVAC system ($\dot{Q}_{HVAC}$), as presented in **equation 2.17**. This is solved in the time domain (6 times per hour) based on a third-order backward approximation of the zone air temperature derivative.

$$\rho_{air} C_p \frac{dT_{air,in}}{dt} = \sum \dot{Q}_{conv} + \dot{Q}_{\inf} + \dot{Q}_{HVAC} \qquad \textbf{2.17}$$

2.4.4 HVAC modeling

The HVAC system considered in this study includes a ground-coupled heat pump (GCHP). Its source side is composed of six vertical borehole heat exchangers (BHEs) and modeled based on the temperature response factor (TRF) approach [196], [197], according to **equation 2.18**.

$$T_{bh} = T_g - \frac{\dot{Q}'}{2\pi k_g} \cdot g(F_o, r_{bh}/H, B/H) \qquad \textbf{2.18}$$

where $g(F_0, r_{bh}/H, B/H)$ is the dimensionless temperature response factor (or *g-function*), which depends on the dimensionless time F_0, the dimensionless borehole radius r_{bh}/H, and the bore-field dimensionless aspect ratio B/H.

The average boreholes wall temperature T_{bh} depends on the ground undisturbed temperature T_g, the heat extraction rate per borehole length $\dot{Q}'$, the non-dimensional temperature "g-function", and the proper thermal conductivity of the ground (k_g) that has been evaluated using the Thermal Response Test (TRT) method. This latter is an efficient experimental procedure that consists of injecting or extracting a constant heat rate in the ground while the carrier fluid circulates inside a reference borehole heat exchanger. The aim is to measure the average ground thermal conductivity and the effective thermal resistance of the BHE. More details can be found in [198], [199], and **Table 2.4** summarizes the test parameters. It is worth mentioning that the (apparent) ground conductivity at the greenhouse site resulted to be higher than expected, as the presence of groundwater circulation in the alluvial site plane enhances the heat transfer with respect to pure conduction. Details on TRT analysis with non-zero Peclet conditions are given in [198].

Table 2.4. Thermal response test (TRT) method parameters.

$\dot{\boldsymbol{Q}}$ $(\boldsymbol{W})$	5000
$\boldsymbol{H}$ $(\boldsymbol{m})$	98
Evaluated slope (for $8.4h < t < 74.5h$)	0.8105
Evaluated k_g $(\boldsymbol{W}/\boldsymbol{m}.\boldsymbol{K})$	5.01

In EnergyPlus, the water-to-water heat pump behavior is modeled based on the "Curve Fit Method" [200]. The effects of both source and load side water temperature on the performance of the heat pump are considered. The cooling and heating modes are described by **equations 2.19**, **2.20** and **2.21**, **2.22**, respectively. The equations present a simplified version of the model [201] by neglecting the effect of the volumetric flow rates at the source and load sides. The equation fit coefficients A_i, B_i, D_i, E_i are determined using the generalized least square method based on the available manufacturer data.

Cooling mode:

$$\frac{\dot{Q}_c}{\dot{Q}_{c,ref}} = A_1 + A_2\left(\frac{T_{L,in}}{T'_{ref}}\right) + A_3\left(\frac{T_{S,in}}{T'_{ref}}\right) \qquad \textbf{2.19}$$

$$\frac{P_c}{P_{c,ref}} = B_1 + B_2\left(\frac{T_{L,in}}{T'_{ref}}\right) + B_3\left(\frac{T_{S,in}}{T'_{ref}}\right) \qquad \textbf{2.20}$$

Heating mode:

$$\frac{\dot{Q}_h}{\dot{Q}_{h,ref}} = D_1 + D_2\left(\frac{T_{L,in}}{T'_{ref}}\right) + D_3\left(\frac{T_{S,in}}{T'_{ref}}\right) \quad \textbf{2.21}$$

$$\frac{P_h}{P_{h,ref}} = E_1 + E_2\left(\frac{T_{L,in}}{T'_{ref}}\right) + E_3\left(\frac{T_{S,in}}{T'_{ref}}\right) \quad \textbf{2.22}$$

where, $\dot{Q}_c$ and $\dot{Q}_h$ are the load side heat transfer rates (cooling and heating capacities); P_c and P_h are the power consumptions; $T_{L,in}$ and $T_{S,in}$ are the load and the source sides inlet water temperatures, respectively.

2.4.5 PV modules

The electrical production of the PV modules is estimated using **equation 2.23**, taking into account the actual active surface $A_{surf,act}$ and the power decrease of PV modules due to the variation of the cell temperature (temperature coefficient of the maximal power $TC = 0.43\%/K$).

$$P = A_{surf,act} \cdot G_T \cdot \eta_{cell} \cdot \left[1 - TC \cdot (T_{cell} - T_{ref})\right] \quad \textbf{2.23}$$

η_{cell} is the active surface conversion efficiency at the reference temperature ($T_{ref} = 298.15\,\mathrm{K}$), and in this study, it is about 17%.

The PV surfaces' incident solar radiation G_T is calculated by means of **equation 2.24**.

$$G_T = R_b \cdot G_{b,H} + R_d \cdot G_{d,H} + R_r \cdot G_{g,H} \quad \textbf{2.24}$$

The irradiance data of Albenga are the global irradiance on horizontal surface, while for the modeling in EnergyPlus, beam and diffuse solar irradiances are also need. Based on the measured global solar irradiance on a horizontal surface $G_{g,H}$, the calculated solar angles and considering the solar constant $G_{SC} = 1367\ W/m^2$, the clearness index K_t is evaluated according to **equations 2.25** to **2.28**:

$$G_{on} = G_{SC} \cdot \left(1 + 0.033 \cdot \cos\left(\frac{360 \cdot n}{365}\right)\right) \quad \textbf{2.25}$$

$$\cos(\theta_z) = \sin(\phi) \cdot \sin(\delta) + \cos(\phi) \cdot \cos(\delta) \cdot \cos(\omega) \quad \textbf{2.26}$$

$$G_o = G_{on} \cdot \cos(\theta_z) \quad \textbf{2.27}$$

$$K_t = \frac{G_{g,H}}{G_o} \quad \textbf{2.28}$$

where n is the day of the year, θ_z is the solar zenith angle, δ is the solar declination, $\emptyset$ is the latitude of the considered location, and ω is the solar hour angle.

Then, the hourly diffuse ratio K_d is estimated, using **equations 2.29**, by considering cloudy, partially cloudy and sunny days [202].

$$K_d = 0.995 - 0.081 \cdot K_t \quad \text{for} \quad K_t \leq 0.21 \quad \text{(cloudy)}$$

$$K_d = 0.724 + 2.738 \cdot K_t - 8.32 \cdot K_t^2 + 4.967 \cdot K_t^3 \quad \text{for} \quad 0.21 < K_t < 0.76 \quad \text{(partially cloudy)} \quad \textbf{2.29}$$

$$K_d = 0.18 \quad \text{for} \quad K_t > 0.76 \quad \text{(sunny)}$$

Thus, the hourly diffuse $G_{d,H}$ and beam $G_{b,H}$ horizontal solar irradiances, in **equation 2.24**, are calculated using **equations 2.30** and **2.31**, respectively.

$$G_{d,H} = K_d \cdot G_{g,H} \quad \textbf{2.30}$$

$$G_{b,H} = G_{g,H} - G_{d,H} \quad \textbf{2.31}$$

Finally, the beam R_b, diffuse R_d and reflected R_r solar irradiance tilt factors are estimated based on **equations 2.32**.

$$R_b = \frac{\cos(\theta)}{\cos(\theta_z)} \quad \textbf{2.32}$$

$$R_d = \frac{1+\cos(\beta)}{2}$$

$$R_r = \rho_g \frac{1-\cos(\beta)}{2}$$

$$\cos(\theta) = \cos(\alpha_s) \cdot \cos(\gamma_s - \gamma).\sin(\beta) + \sin(\alpha_s).\cos(\beta) \quad \textbf{2.33}$$

2.4.6 Performance evaluation

As previously stated, the EnergyPlus model of the SamLab greenhouse has been validated against measurements. In particular, the predicted GCHP electrical consumption, the boreholes heat transfer rate, and the PV modules' electrical production, are compared to the corresponding measured parameters.

To evaluate the performance of the model, the coefficient of correlation (R) is used. R is widely used in literature to analyze the performance of physics based models. It aims to measure the agreement between predicted and measured values. This coefficient is calculated according to **equation 2.34**.

$$R = \frac{\sum_{i=1}^{n}(M_i - \overline{M}).(P_i - \overline{P})}{\sqrt{\left[\sum_{i=1}^{n}(M_i - \overline{M})^2\right].\left[\sum_{i=1}^{n}(P_i - \overline{P})^2\right]}} \cdot 100 \quad \textbf{2.34}$$

where P_i and M_i are the predicted and measured values, respectively.

2.5 Validation of SamLab greenhouse model

In this section, the validation of the EnergyPlus model of the SamLab greenhouse is provided by comparison with the data measured by the monitoring system.

2.5.1 External weather conditions

Among weather data, two parameters mainly influence the behavior of the greenhouse system, namely the external global solar irradiance and the external air temperature. In the analysis devoted to the validation of the EnergyPlus model by means of measured data, weather data for Albenga are partially measured on-site (temperature) and partially downloaded from the Liguria Region Agency for the Environment webpage (solar irradiance). In particular, **Figure 2.5** presents the variation of the external global horizontal solar irradiance and the external air

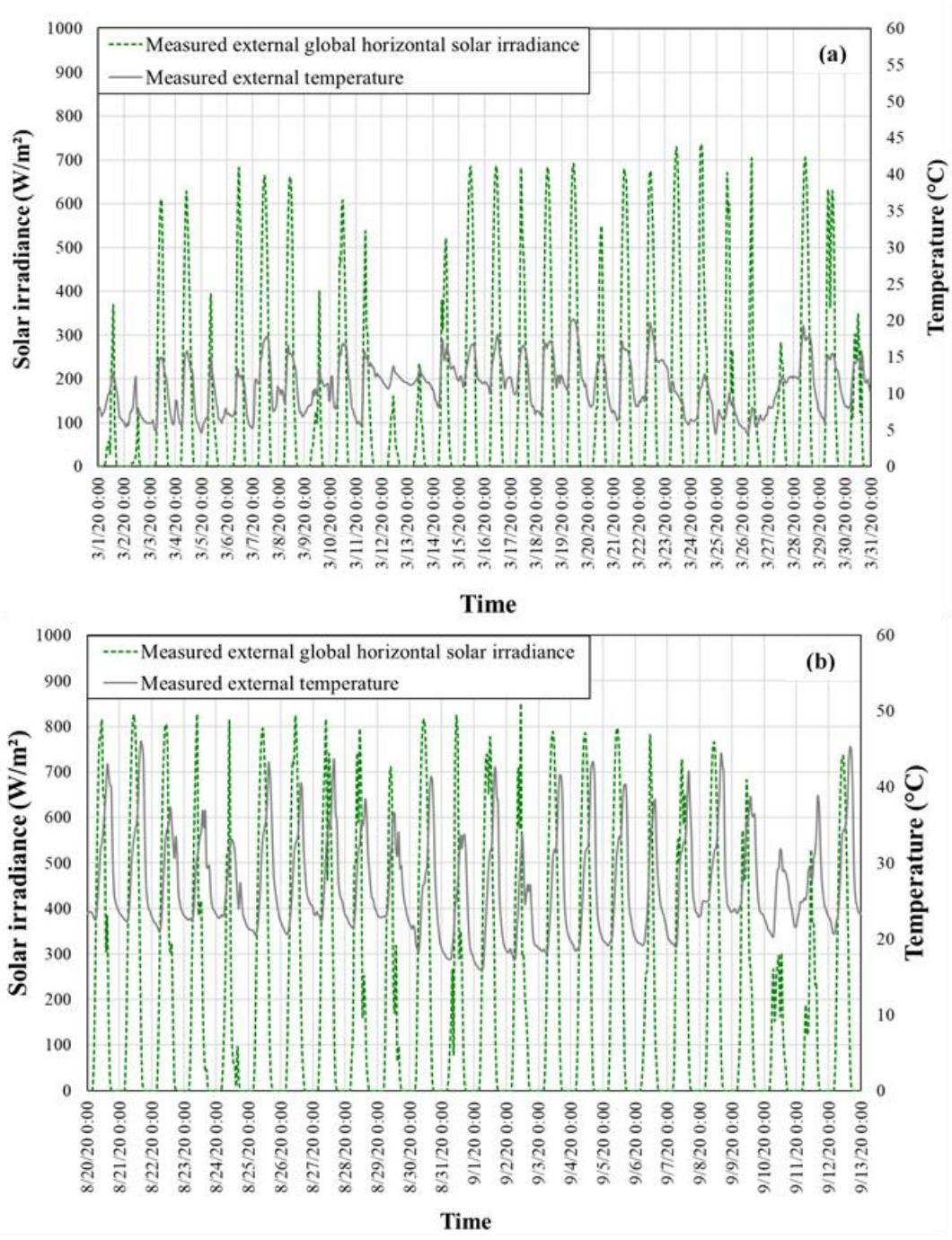

Figure 2.5. Measured external global horizontal solar irradiance and temperature. (a) Month of March 2020. (b) Mid-August to mid-September 2020.

temperature for the selected periods (i.e., the month of March (a) and mid-August to mid-September (b) 2020). During March 2020, the solar irradiance varies between 0 and 736 W/m² reaching its maximum on 3/24. The temperature varies between 4.5 and 20.2 °C and the maximum and minimum temperatures are observed on 3/19 and 3/24, respectively. During the period from mid-August to mid-September, the solar irradiance varies between 0 and 900 W/m²

reaching its maximum on 8/4. The temperature varies between 15.88 and 46 °C. The maximum and minimum temperatures are observed on 8/21 and 9/1, respectively.

2.5.2 HVAC system

In this sub-section, the attention is focused on the HVAC system performance. In particular, the comparison between model and measured data is presented for the ground-coupled heat pump (GCHP) electrical consumption and the borehole heat exchangers (BHE) heat transfer rate (the heat extracted or injected to the ground by the heat pump), considering both the heating (March 2020) and the cooling (mid-August to mid-September 2020) periods. The same operating conditions (during considered periods) as the real greenhouse are set in the EnergyPlus model for the HVAC system; in particular, the temperature setpoint is 24.8 °C for the heating and 29.8 °C for the cooling period.

Figure 2.6 represents the comparison between the actual and the predicted hourly GCHP electrical consumption during the heating period (March 2020). Based on the graph, it can be remarked that there is a quite good agreement between the estimated consumption (EnergyPlus model) and the greenhouse measured one with a coefficient of correlation of about 0.91, with an underestimation is noted for the extreme values. The borehole heat exchangers and the ground characteristics are implemented in the EnergyPlus model. Thus, the BHE heat transfer rate into the ground is calculated and then compared to the available measurements for the

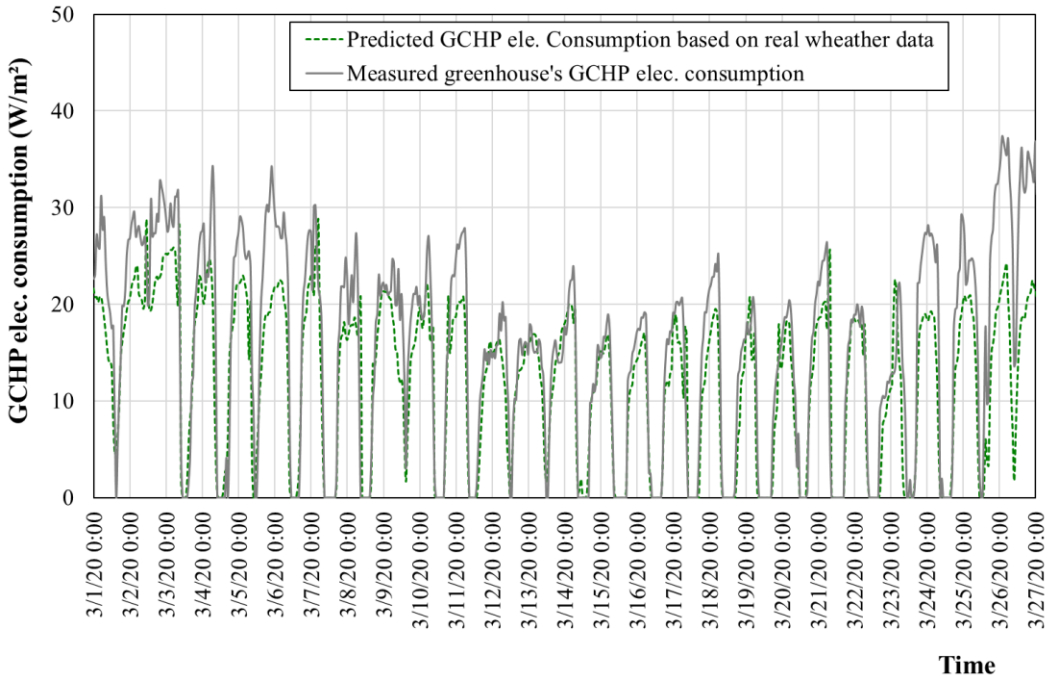

Figure 2.6. Measured and predicted hourly GCHP electrical consumption (per greenhouse surface) in March 2020.

heating period, as displayed in **Figure 2.7**. The results show a coefficient of correlation of about 0.88.

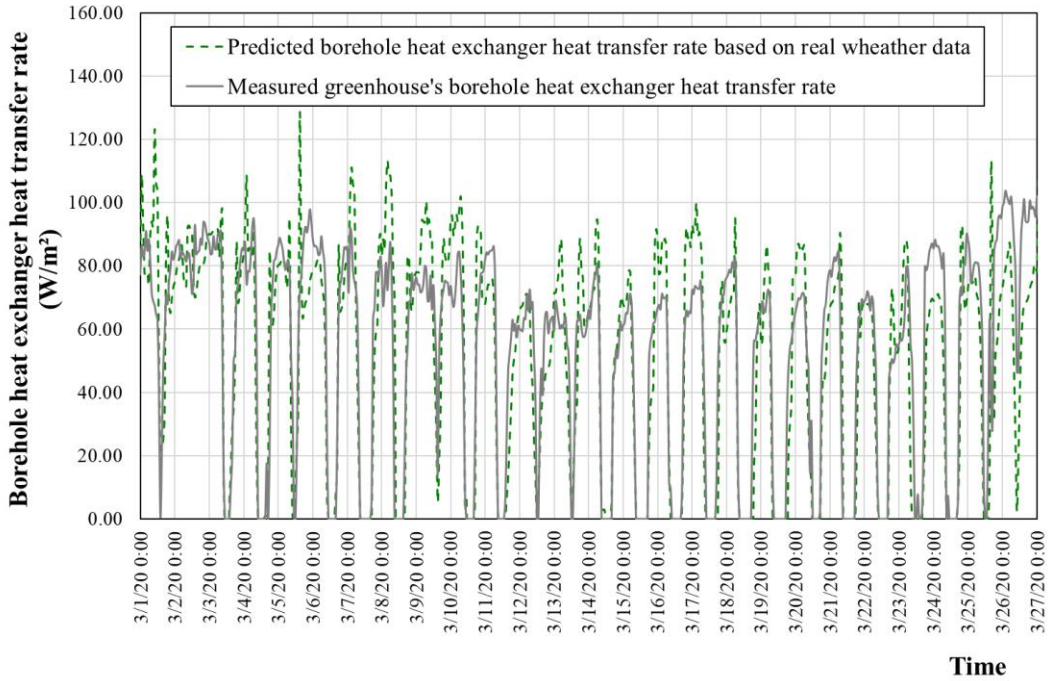

Figure 2.7. Measured and predicted hourly borehole heat exchangers heat transfer rate (per greenhouse surface) in March 2020.

In addition, the cooling period has been analyzed, in particular from mid-August to mid-September 2020. In **Figure 2.8**, the real and predicted hourly electrical consumptions of the GCHP are presented. The estimations follow quite well the measurements with a coefficient of

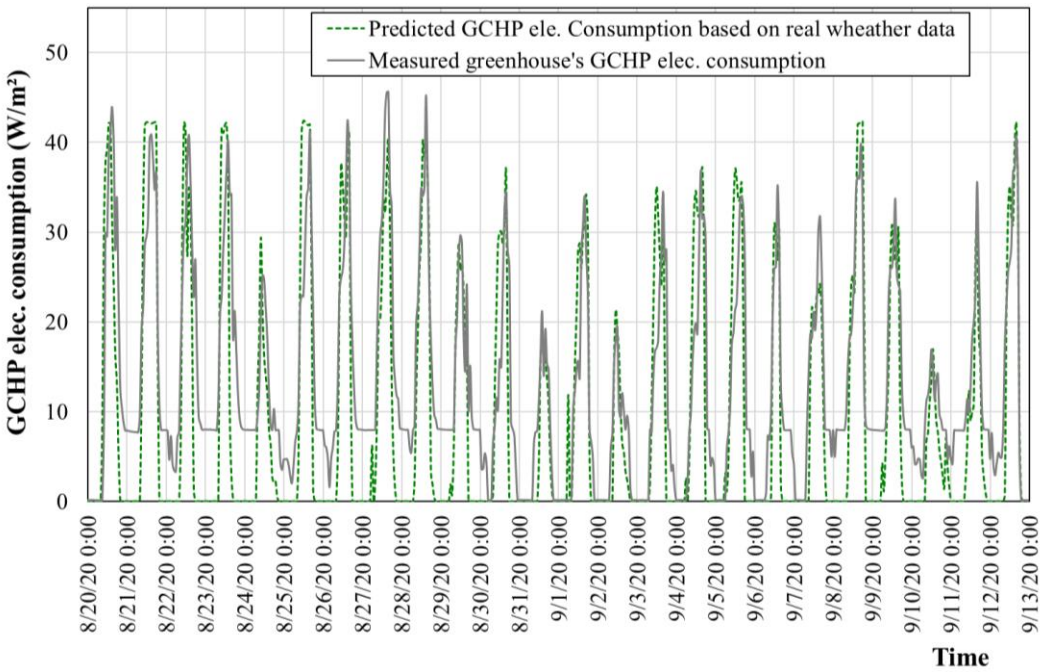

Figure 2.8. Measured and predicted hourly GCHP electrical consumption (per greenhouse surface) from mid-August to mid-September 2020.

correlation of about 0.86. Moreover, the measured and calculated hourly BHE heat transfer rates are compared from mid-August to mid-September 2020 as presented in **Figure 2.9**, with a related coefficient of correlation of about 0.82.

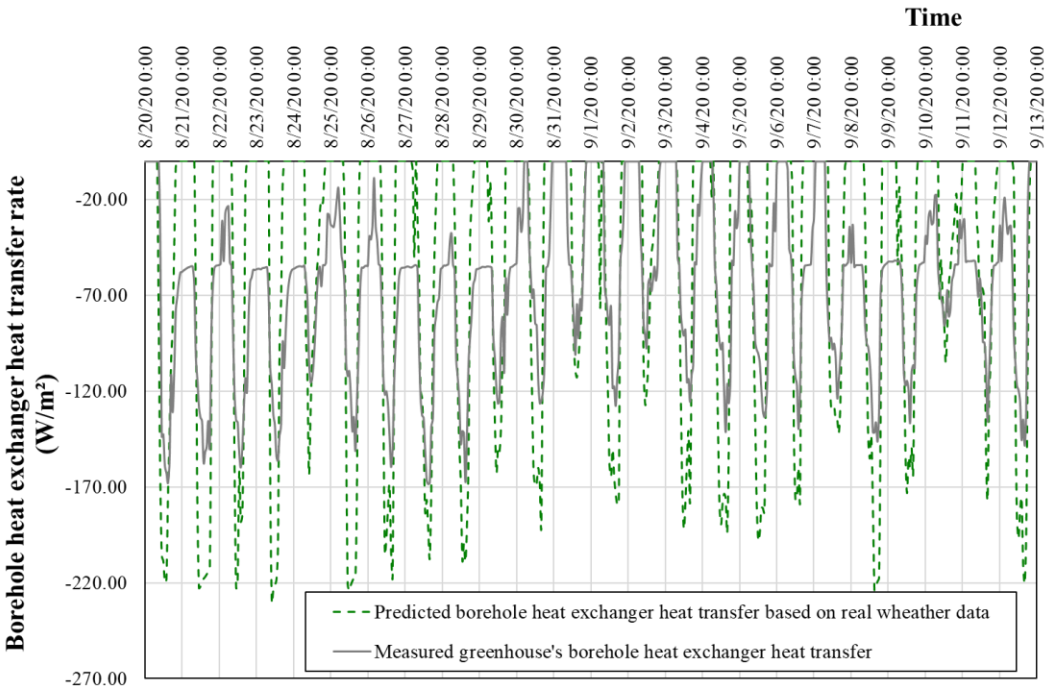

Figure 2.9. Measured and predicted hourly borehole heat exchangers heat transfer rate (per greenhouse surface) from mid-August to mid-September 2020.

2.5.3 PV modules

In this section, the validation of the PV system model is presented. For this aim, the measured PV modules hourly electrical production is compared to the predicted one by considering different weather conditions: March 2020 and August 2020. The weather file is updated with respect to the measured external temperature and the solar irradiance by considering cloudy, partially cloudy and sunny days, defined using the clearness index as presented in **section 2.4.5**.

The incident solar radiation on the PV modules is calculated based on **equations 2.23** to **2.31**. On the contrary, the cell temperature is estimated using the EnergyPlus model. Then the PV modules' electrical production is calculated according to **equation 2.22**.

represents the hourly PV modules' electrical production during moderate (March) (a) and hottest (August) (b) periods. The graphs show a good fit between measurements and estimations with a correlation coefficient of about 0.91 and 0.87 during moderate and hottest periods, respectively.

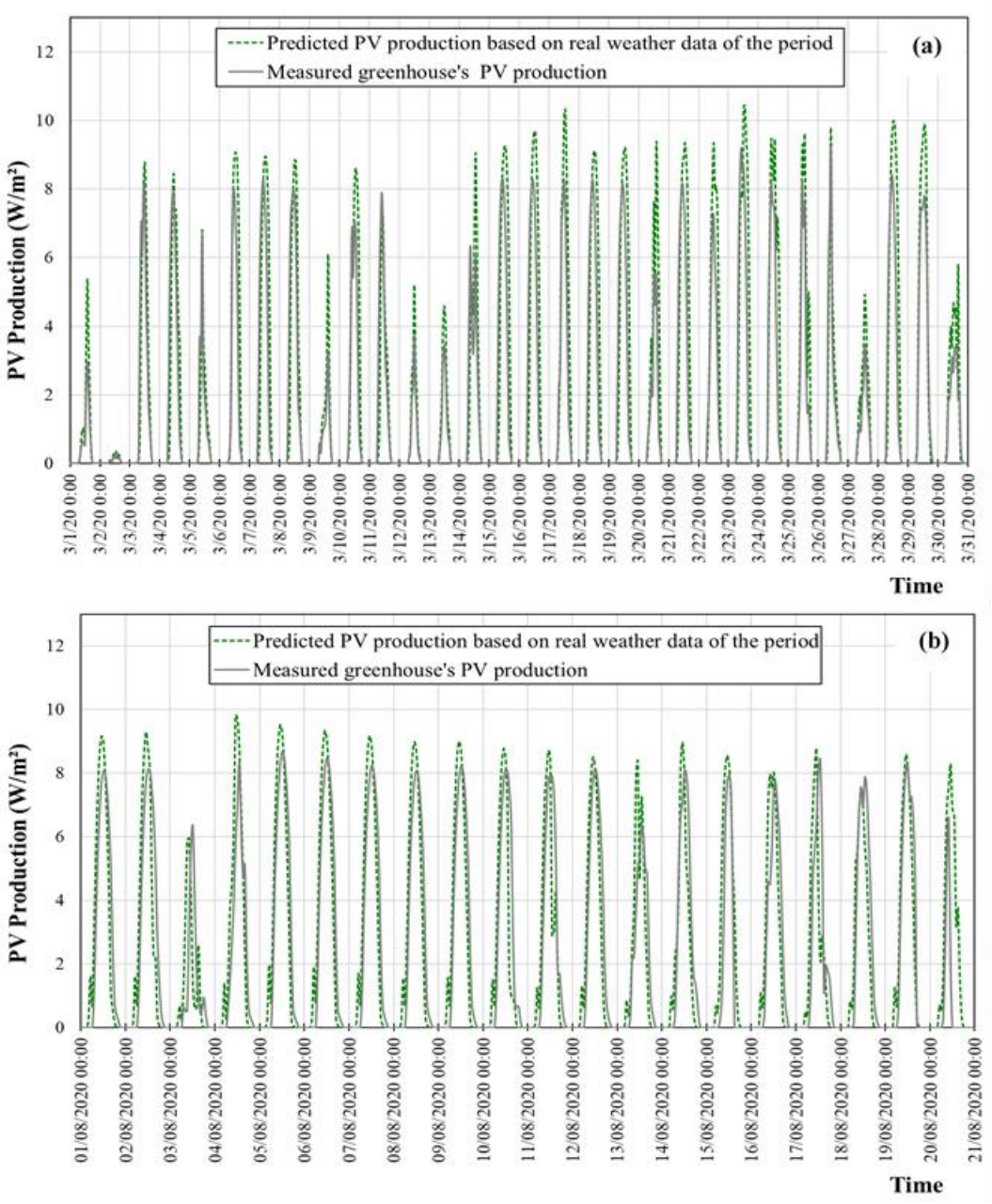

Figure 2.10. Measured and predicted hourly PV modules energy production (per greenhouse surface). (a) Month of March 2020. (b) Month of August 2020.

2.5.4 Model performance

As presented in section 2.4.6, the model performance is evaluated using the correlation coefficient R. **Table 2.5** summarizes the performance of the model in predicting the GCHP electrical consumption (R about 0.91 in March 2020 and 0.86 in August/September 2020), the BHE heat transfer rate (R about 0.88 in March 2020 and 0.82 in August/September 2020), and the PV modules' production (R about 0.91 in March 2020 and 0.87 in August/September 2020).

Table 2.5. Model predicting performance.

	Coefficient of correlation R	
	March 2020	**August/September 2020**
GCHP electrical consumption	0.91	0.86
Borehole heat exchangers heat transfer rate	0.88	0.82
PV modules' production	0.91	0.87

2.6 Greenhouse thermal behavior and energy-saving strategies

In order to analyze the thermal behavior of the studied greenhouse and to quantify the energy-saving potential resulting from the integration of passive techniques and renewable energy resources, weather data of a whole year is used. Since the measured annual weather data is not available (only data for March and August/September is available), they are provided by means of the suitable TMY weather file for Albenga obtained from Meteonorm software.

The first set of simulations analyzes the greenhouse without considering the detailed HVAC model and is devoted to estimating of the heating and cooling loads of the greenhouse. For this purpose, the EnergyPlus feature called "*Ideal Loads*" has been considered. The "*Ideal Loads*" is a special option in EnergyPlus used to simulate the building without focusing on the HVAC system in detail. This system is an ideal unit that takes air at the zone exhaust condition and then adds or removes heat and moisture at 100% efficiency to produce a supply airstream at specified conditions, according to imposed indoor air temperature set-points. For this part of the analysis, the indoor air temperature set-points are 16 °C during winter and 30 °C during summer. In this way, the obtained results depend only on the greenhouse envelope thermal properties, on the internal and solar gains and do not depend on the HVAC system variable performance. The outputs of this type of model are the heating and cooling loads of the greenhouse and not the primary or electrical energy consumption of the thermal plants. This part of the study aims to analyze the effect of crops, internal mass and passive techniques on the greenhouse thermal behavior.

The second part of the study analyzes the HVAC system and its interaction with the greenhouse system. Finally, an evaluation of the energy-saving associated to the use of renewable energies (GCHP and PV modules) is carried out.

2.6.1 Effect of plants and internal masses

The first set of simulations was carried out to evaluate the effects of the internal masses and plants on the greenhouse mean indoor air temperature $T_{air,in}$ and on the ideal loads. As a reference, the case of the greenhouse without any masses or plants inside has been considered. The internal masses are then included in the model (the four benches and all the HVAC system elements). The effect of the plants has also been considered with their evapotranspiration by means of the FASST model [195].

Figure 2.11 shows the annual profile of daily indoor air temperature $T_{air,in}$ for different studied cases: the reference model, the model including internal masses and the one including both internal masses and plants inside the zone.

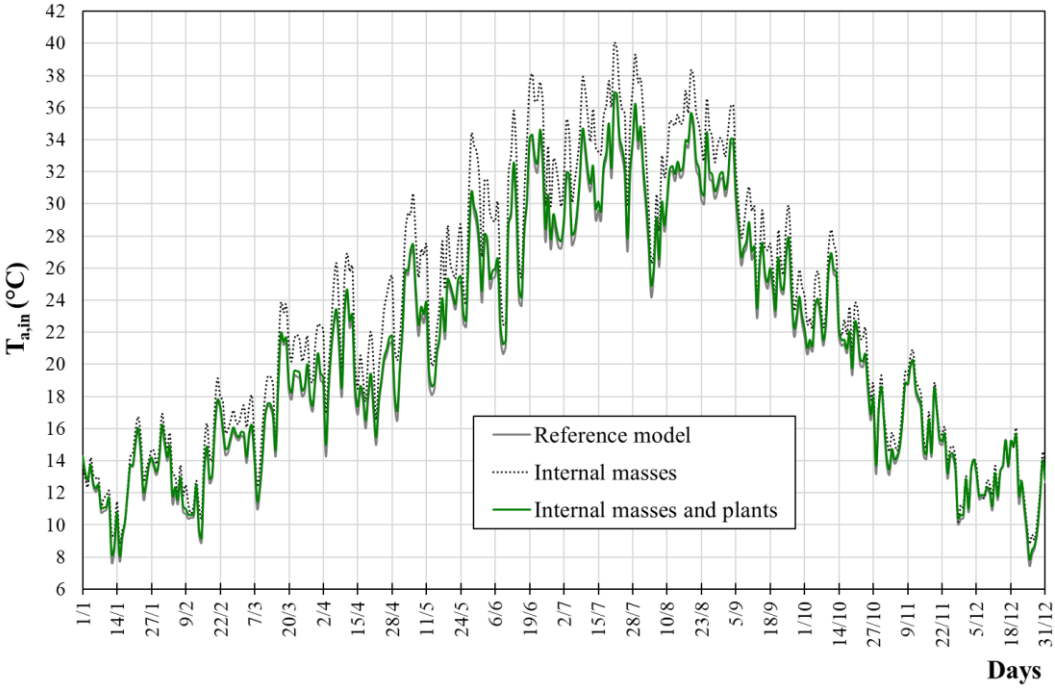

Figure 2.11. Daily average greenhouse indoor air temperature according to different modeling strategies.

The obtained results show that both internal masses and plants have a significant impact on the inside air temperature of the greenhouse. Compared to the reference model, the temperature $T_{air,in}$ generally rises when the internal masses are included, especially during summer, with a maximum temperature increase of nearly 5 °C in June. On the contrary, the presence of the plants acts in the opposite direction, reducing the previous increase down to less than 1 °C in July if compared to the reference model. This is due to the phenomenon of evapotranspiration

of the plants. Thus, those results confirm that it is important to consider these contributions when analyzing the greenhouse microclimate and sizing the HVAC system.

Figure 2.12 shows the greenhouse energy needs (i.e., the ideal loads) for different studied cases. The energy needs raise when including internal masses during the cooling period and slightly decrease during the heating period. That can be explained by the fact that the internal masses are heated by solar thermal intakes. Owing to their absorption and heat storage properties, the insertion of internal masses generates a temperature increase (a clear increase during the summer when the solar thermal intakes are very important, and a very slight increase during the winter). Thus, the energy needs slightly decrease during winter and increase during summer. Conversely, the final energy needs reduce when also considering plants and their soil. Compared to the reference model, the annual energy need increases by around 56.4 kWh/m² when including the interior masses and decreases by about 2.7 kWh/m² when including also plants and soil.

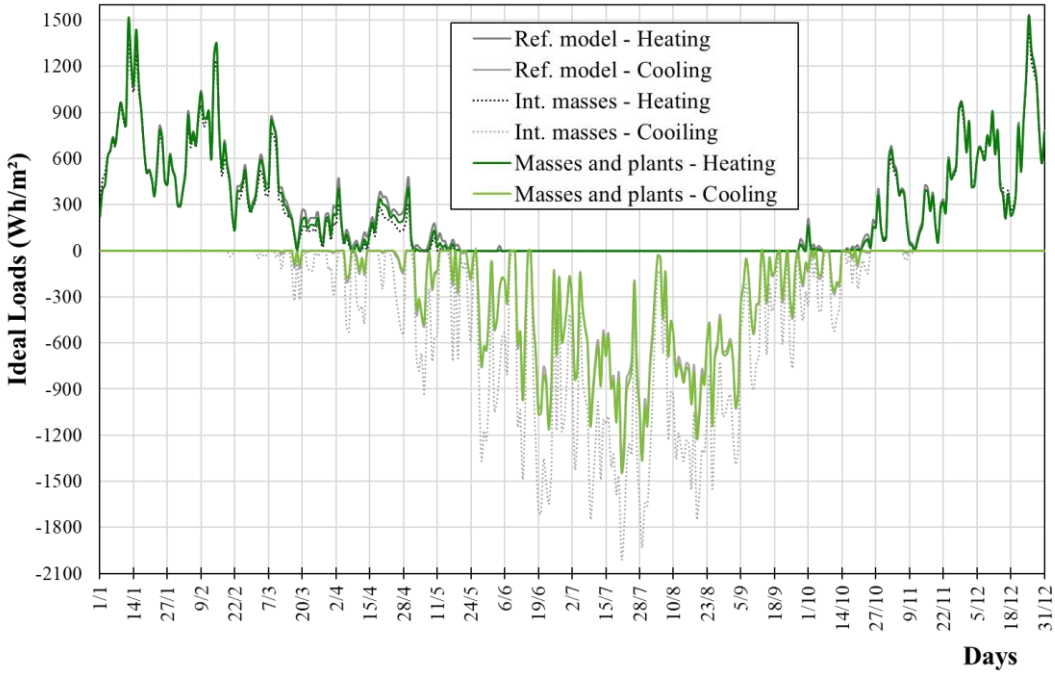

Figure 2.12. Daily values of greenhouse thermal loads according to different modeling strategies.

The main objective of this comparison is to demonstrate, in general, the impact of integrating masses and plants in a greenhouse modeling study. The results obtained here cannot be generalized since the impact level depends on several parameters, namely the internal masses properties, the type of plants and their stage of maturity.

2.6.2 Effect of passive techniques

This section summarizes the effects of passive techniques on reducing the cooling load. The considered technologies are a shading/reflecting system and an operable windows system. In this analysis, the reference case is the greenhouse, including internal masses and plants and the simulations are devoted to determining the potential of energy-saving using passive techniques. The comparison is based on the daily greenhouse inside air temperature $T_{air,in}$ and in terms of the daily energy needs of the greenhouse (ideal loads).

Focusing on the moderate and hottest periods (cooling period), **Figure 2.13** presents the daily inside air temperature profiles for the period from the first of May to the end of September. The temperature remarkably decreases when using the passive techniques, with a maximum hourly reduction of 2.8 °C using the shading/reflecting system and 16 °C when using the operable windows system. It is worth mentioning that the strong effect of natural ventilation is related to the large opening area (in both the real greenhouse and its model) that accounts for some 63 m².

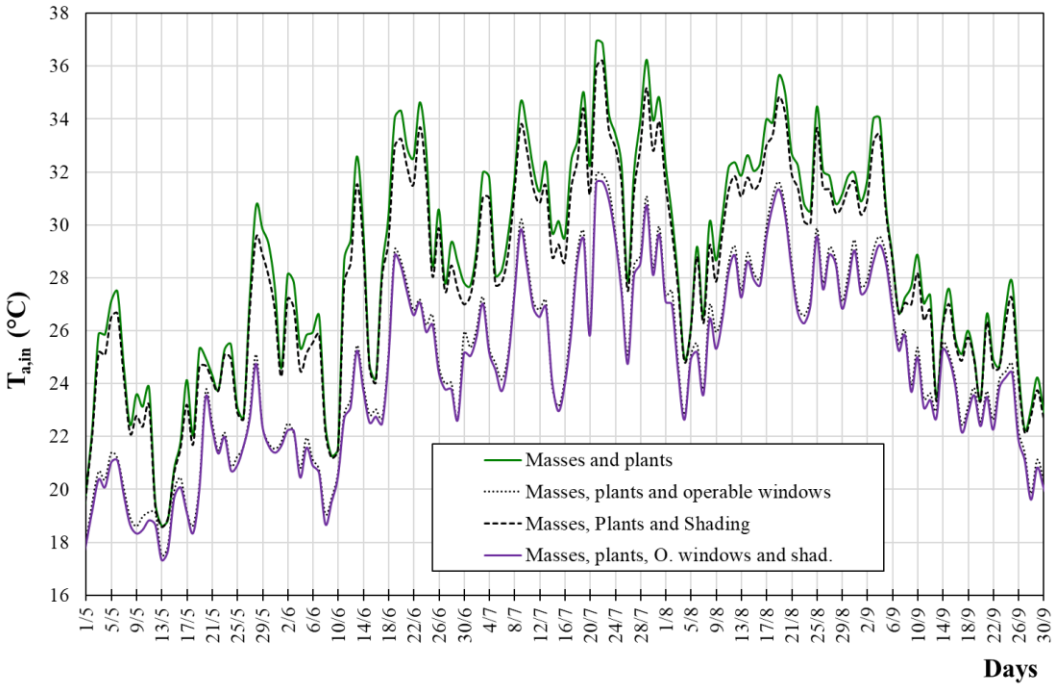

Figure 2.13. Daily average greenhouse indoor air temperature (from May to the end of September) according to different energy consumption mitigation strategies.

Figure 2.14 shows the greenhouse energy needs (i.e., the ideal loads) in cooling: the passive techniques significantly contribute to the reduction of the greenhouse cooling load during both hot and moderate seasons. Based on the graph, it can be observed that during the moderate weather conditions period, both the heating and cooling are needed on the same day, which can be explained by the fact that during this period, the heating and cooling needs vary hourly. As

for temperatures, the shading system effect is limited, whereas the operable windows system considerably reduces the need for cooling and even eliminates it during days with mild outdoor temperature.

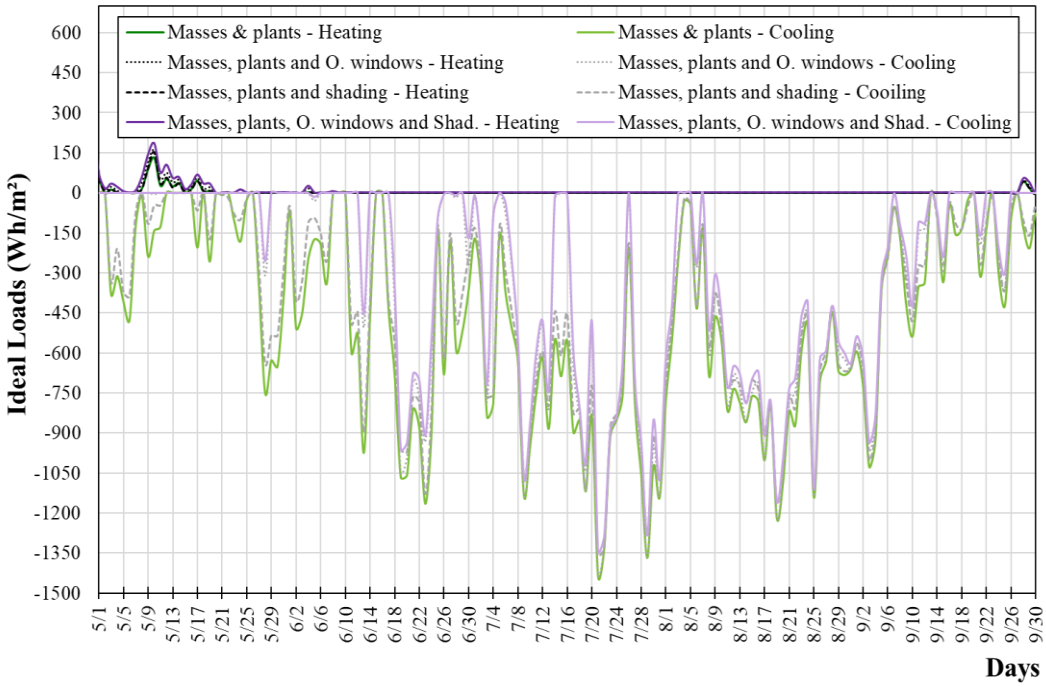

Figure 2.14. Daily greenhouse thermal loads (from May to end September) according to different energy consumption mitigation strategies.

Finally, on an annual basis, the shading system can save about 5% of the greenhouse energy needs, the operable windows system saves nearly 14% and the combined use of the two systems almost saves annually 25.6 kWh/m², which represents 16% of energy needs.

2.6.3 Renewable energy resources

2.6.3.1 The HVAC system: the ground-coupled heat pump

After evaluating the energy needs of the greenhouse in cooling and heating, the detailed HVAC model has been included in the EnergyPlus simulation. This section presents the main results regarding inside air temperature $T_{air,in}$ and primary energy consumption. In particular, the GCHP has been considered with its variable performance, as described in **section 2.4.4.**

Figure 2.15 shows the daily inside air temperature $T_{air,in}$ in three different cases. The first one, considered as a reference, presents the trend of inside air temperature without any internal comfort control (i.e., with only passive techniques). The other two cases impose both the same set-points (16 °C during winter and 30 °C during summer) and compare the results obtained using the "ideal loads" feature of EnergyPlus and the detailed HVAC system model. The

imposed internal set-points in the greenhouse, favorable for plants growing purpose, positively influence the load side temperature of the plant and increase the conversion performance of the heat pump.

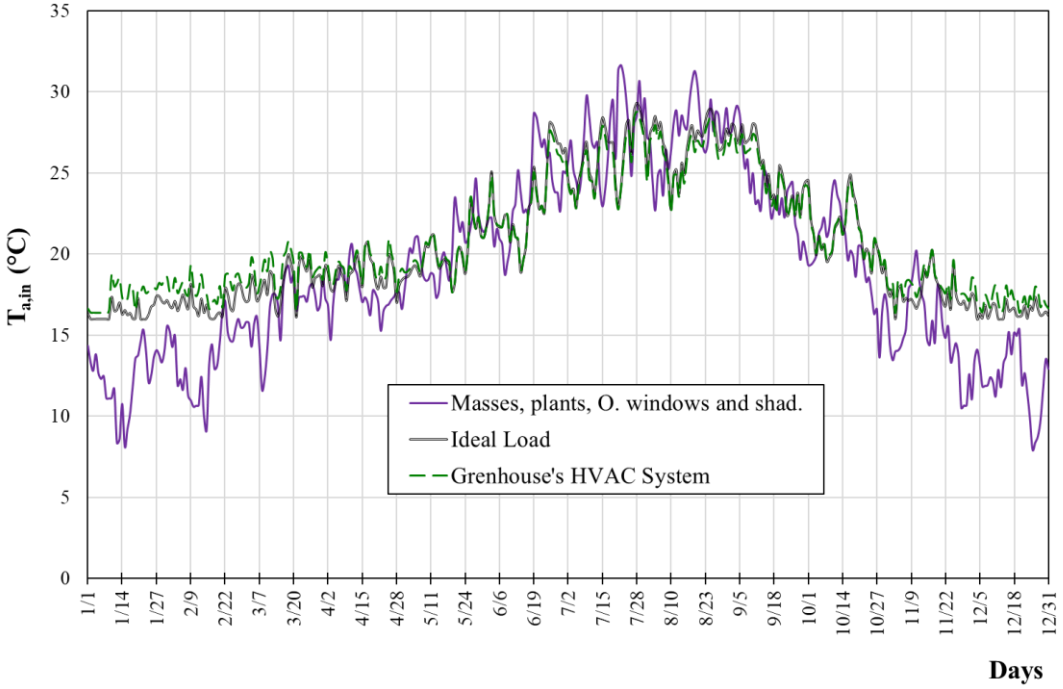

Figure 2.15. Daily average greenhouse inner air temperature for different modeling strategies.

A comparison on an annual basis has been performed to quantify the reduction of primary energy consumption with the use of the ground-coupled heat pump (GCHP). In particular, the daily primary energy consumption of the GCHP has been compared to the one associated to a standard conventional system composed of a boiler with top efficiency $\eta = 0.96$ and, for cooling purposes, a chiller with $EER = 3.5$. A primary energy/electricity ratio of 2.5 has been used.

From **Figure 2.16**, it is clear that the GCHP provides a significant contribution on energy-saving, especially at peak load conditions, thanks to the favorable nearly constant value of the ground temperature that represents the source side of the GCHP both in winter and summer. Considering the annual primary energy consumption, the energy-saving, with respect to the standard conventional system case, exceeds 50.1 kWh/m² with a relative reduction of nearly 21%.

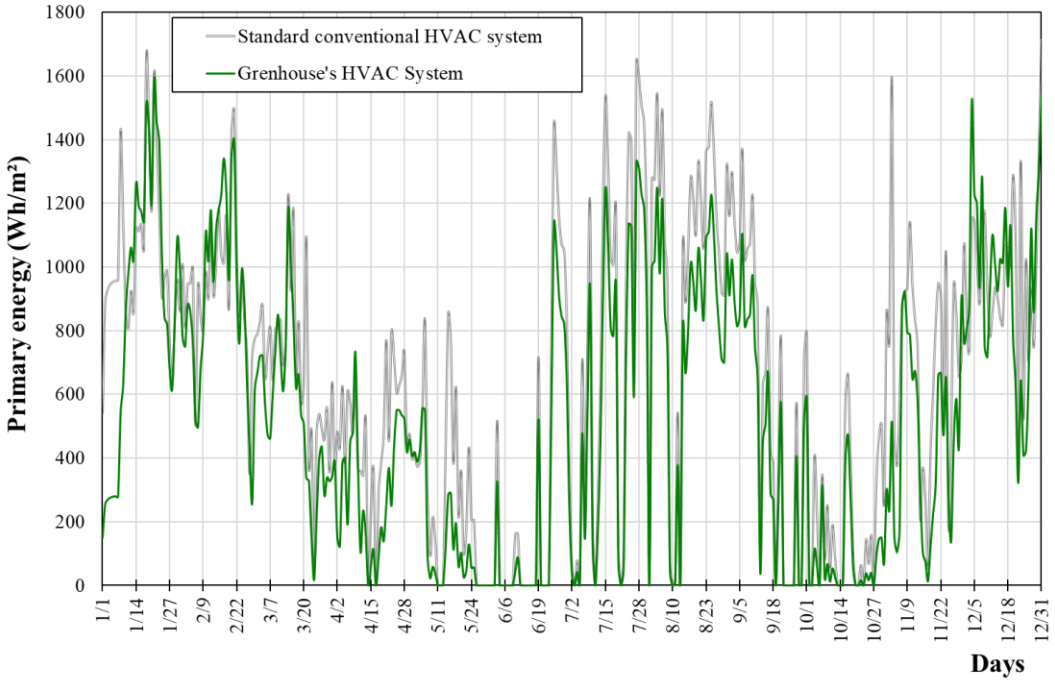

Figure 2.16. Daily greenhouse primary energy consumption for different HVAC strategies.

2.6.3.2 PV modules' production

The monthly energy produced by the semi-transparent PV modules is evaluated according to the procedure described in **section 2.4.5** and presented in **Table 2.6,** together with the total electricity consumption of the greenhouse.

Table 2.6. SamLab greenhouse monthly electrical energy consumption and PV modules' production.

Months	PV energy production (Wh/m²)	Greenhouse electricity consumption (Wh/m²)	Electricity covered by PV (%)
January	634	18583	3
February	901	16852	5
March	1469	10798	14
April	1684	5361	31
May	2165	2690	81
June	2392	3635	66
July	2534	9590	26
August	2363	12606	19
September	1764	7433	24
October	1470	1734	85
November	863	8219	11
December	625	18024	3

From the table, it can be concluded that during spring and autumn (e.g., May and October), the production can cover more than 80% of the consumption. However, the electrical energy

consumption exceeds the PV modules' production during the whole year. Consequently, the use of PV modules as the only electricity source in such a case seems not to be sufficient. The PV system can supply around 16% of the greenhouse's total electrical demand throughout the year.

2.7 Conclusions

This chapter presents a dynamic energy model that is created in the EnergyPlus environment with reference to the case study of the innovative high-efficiency SamLab greenhouse, located in Albenga, Italy. The model is validated using data from the actual greenhouse. The hourly ground-coupled heat pump electrical consumption, the hourly borehole heat exchangers heat transfer rate and the electrical production of photovoltaic modules predicted by the model have been compared to the measured data collected during March and August/September 2020. For the validation purpose, the weather file used as input into the EnergyPlus model has been modified to consider the actual weather conditions of the site. In particular, the external air temperature and the global solar irradiance have been updated. Then the model was exploited in order to quantify the energy-saving potential of integrating passive techniques and renewable energies in greenhouse cultivation, and to study, as well, the effect of plants and internal masses on the thermal behavior of the greenhouse. For that, annual weather data from Meteonorm software for a whole year is used.

The validation results show that the model provides a good estimation and it can be used to test and validate new energy management strategies. To quantify the agreement between predicted and measured values, the coefficient of correlation (R) is used. The results also quantify the energy-saving potential of the studied strategies and show the importance of integrating passive techniques and renewable energies in greenhouse cultivation for sustainable agriculture. The main conclusions are made as follows:

(1) The coefficient of correlation for the hourly measured and predicted:

   (a) GCHP electrical consumption is around 0.91 and 0.86 during heating and cooling periods, respectively;

   (b) Borehole heat exchangers heat transfer rate is around 0.88 and 0.82 during heating and cooling periods, respectively;

   (c) PV modules' electrical production is around 0.91 and 0.87 during heating and cooling periods, respectively.

(2) By analyzing the effects of the internal masses and the plants on the greenhouse inside air temperature and its energy needs, it has been shown that their effects are relevant, and that it is important to include them in the energy modeling of greenhouses.

(3) Passive techniques are investigated and, in particular, the effect of shading system and operable windows on the cooling load by considering the greenhouse with internal masses and plants as reference. Based on the results, it can be deduced that the controlled shading system can save around 5% of the energy needs during the cooling period, thanks to the low thermal emissivity of the shading material. Regarding the operable windows, the amount of energy-saving represents nearly 14% of the total energy needs during the cooling period.

(4) The detailed HVAC plant of the SamLab greenhouse has been included inside the model, namely the air handling unit associated with a ground-coupled heat pump. Comparing the primary energy consumption of the reversible ground-coupled heat pump to the one of a standard conventional plant (boiler + medium performance chiller), considering standard conversion factors, it is possible to conclude that the geothermal heat pump allows for saving nearly 21% of primary energy.

(5) The greenhouse semi-transparent photovoltaic modules can supply around 16% and 44% of the total electrical annual demand and the yearly air-conditioning electrical needs.

The work presented in this chapter has been published in the following papers:

1. Ouazzani Chahidi, L., Fossa, M., Priarone, A., & Mechaqrane, A. (2021). Energy saving strategies in sustainable greenhouse cultivation in the mediterranean climate–A case study. Applied Energy, 282, 116156.
2. Ouazzani Chahidi, L., Fossa, M., Priarone, A., & Mechaqrane, A. (2021). Greenhouse cultivation in Mediterranean climate: Dynamic energy analysis and experimental validation. Thermal Science and Engineering Progress, 26, 101102.

Chapter 3

Selection of optimal greenhouse design in Moroccan climate conditions

Chapter 3: Selection of optimal greenhouse design in Moroccan climate conditions

3.1 Introduction

The Kingdom of Morocco, which is part of the Mediterranean region of North Africa[vi], has a significant potential and diversified natural resources thanks to its particular geographical position. Despite all these assets, Morocco is the most energy-dependent country in the region since it does not own fossil energy resources [203]. In 2016, an energy dependency ratio of around 93% was reported [204]. Consequently, Morocco decided to follow a sustainable development policy to increase energy efficiency in different sectors of activity and the portion of renewable energies in its energy mix [205]. Among those sectors, agriculture must be placed in the central priorities of the national energy transition strategy. In 2008, Morocco launched a strategy to improve agricultural productivity and related social and sustainable development issues, called the "Green Morocco Plan" [206]. Moreover, this sector is one of the cornerstones of the kingdom's economy. It contributes by nearly 13% of the national economy with a Gross Domestic Product of 125 billion dirhams in 2017 [207]. The efforts provided in this framework have made it possible to go from a coverage rate (export/import) of 37.18% in 2008 to 55.81% in 2017, that represents a significant improvement but still has a negative agricultural trade balance [207].

Being one of the energy-intensive systems, the agricultural greenhouse ought to be a part of this Moroccan strategy. In particular, since it was planned to dispose of 59,000 ha for vegetable production, including 27,500 ha of protected cultivation in 2020, which represents a very high rate of almost 47% [208]. Therefore, energy optimization must be considered at the earliest stages of the construction of the greenhouses. The greenhouse heating and cooling energy needs undoubtedly depend on its design and geographic localization. Thus, in specific climate conditions and for a particular type of cultivation, the design of the greenhouses should be chosen to maintain adequate microclimate parameters as much as possible.

As a result of these challenges and the circumstances linked to the Covid-19 pandemic, it has been important to think about autonomous regions, able to produce and meet their needs. As part of this vision, the work carried out in this chapter aims to evaluate different greenhouse designs (shapes, cover materials and orientations) to select the most suitable for each of the six Moroccan climatic zones. The models are created in the EnergyPlus environment and are based on heat balance equations as presented in **section 2.4.3**. The present chapter starts by describing the considered zones. Then a presentation of the considered specifications (shapes, cover

materials, orientation and crops) is provided. Finally, the results are presented and discussed regarding the selection of the greenhouse shape, cover material and orientation. The potential of energy-saving resulting from the use of nightly thermal insulation operating during the heating period and controlled natural ventilation is also studied.

3.2 Study methodology

The greenhouse design can directly influence the interior microclimate and, therefore, the heating and cooling loads. This study aims to assess the impact of the greenhouse design (i.e., the shape and the cover material) on its thermal loads (during both the heating and cooling periods) and on the floor incident solar radiation, to select the optimal one under the climate conditions of six Moroccan climatic zones (**section 3.3.1**). The weather data is provided from Meteonorm software.

In this study, the modeling and simulations are carried out in the EnergyPlus software. The greenhouse is modeled as a single zone interacting with its outside environment as well as with its interior components (plants and soil). The calculation of loads is based on energy balance (**section 2.4.3**) of the zone and the different greenhouse components, where the transparent surfaces are considered as windows and opaque ones as walls. The heat balance equation is solved in the time domain based on a third-order backward approximation of the zone temperature derivative with six times per hour a time step calculation. Moreover, the soil and plants are defined in EnergyPlus as the floor material layers, respectively. Their effect is considered based on the FASST model [195], as presented in **section 2.4.3.3**.

Thirty-six different combinations are first compared; nine shapes (standard span, uneven span, single slope, mansard, modified IARI, quonset, modified quonset, gothic-arch, modified gothic arch) and four cover materials (glass, low-density polyethylene LDPE, Bubbled polyethylene BPE, Ethylenevinyl acetate EVA). After selecting the optimal shape and cover material, four greenhouse orientations (relative to the north-south axis) are compared: 0°, 90°, 45° and - 45° (longer axis). Finally, a further improvement of the selected design is studied, namely the use of thermal insulation blankets operating from sunset to sunrise, to reduce the heating demand. To minimize the cooling demand, operable windows are used for controlled natural ventilation.

3.3 Moroccan climatic zones

3.3.1 Description of the Moroccan climatic zones

Being one of the Mediterranean regions of North African countries, Morocco is mainly dominated by a temperate climate in the north of the country and a tropical climate in the south part. Based on the weather data collected during 10 years (from 1999 to 2008) in 37 meteorological stations, the national territory was divided into six climatic zones. **Figure 3.1** is the map representing the Moroccan climatic zones. This zoning is a result of several studies conducted by the Moroccan agency of energy efficiency (AMEE) [209], [210]. Six cities were selected as the representative climate for each zone, namely Agadir (zone 1), Tangier (zone 2), Fez (zone 3), Ifran (zone 4), Marrakech (zone 5), and Errachidia (zone 6). **Table 3.1** presents the geographical coordinates of the representative city of each zone.

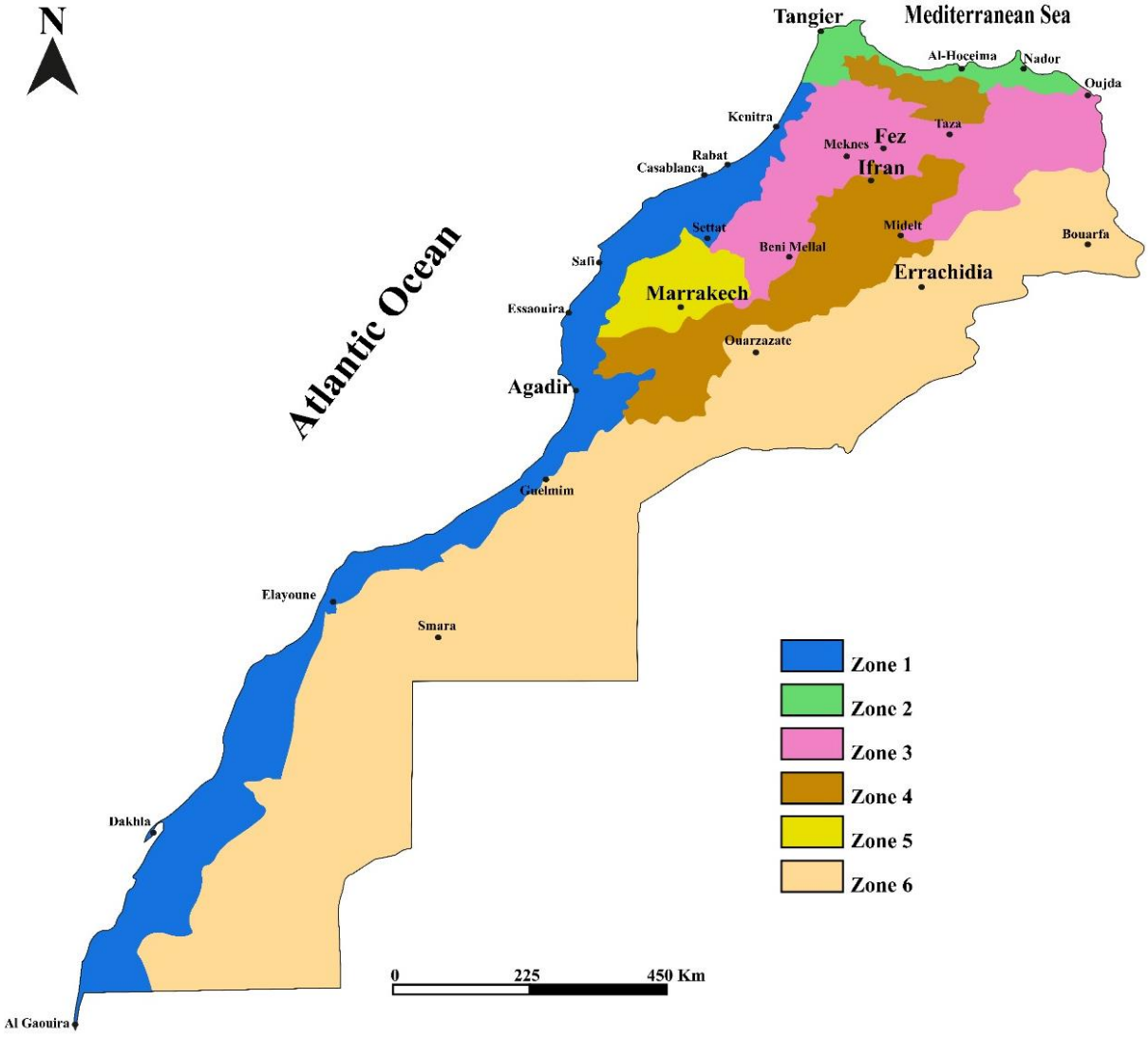

Figure 3.1. Moroccan climatic zoning map [210].

Table 3.1. Sites geographical coordinates

	Longitude	Latitude	Altitude
Zone 1 (Agadir)	9.60°W	30.43°N	23 m
Zone 2 (Tangier)	5.83°W	35.76°N	21 m
Zone 3 (Fez)	4.98°W	33.93°N	579 m
Zone 4 (Ifran)	5.11°W	33.52°N	1665 m
Zone 5 (Marrakech)	7.98°W	31.63°N	466 m
Zone 6 (Errachidia)	4.43°W	31.93°N	1045 m

In order to select the most suitable greenhouse design for tomato plant production in the different climatic zones, the six representative cities were considered. For each zone, we evaluate the effect of various greenhouse designs on the inside microclimate and the potential of energy-saving resulting from the use of thermal insulation and operable windows.

3.3.2 External temperatures

Figure 3.2 presents the monthly variation of the minimal, mean and maximal temperatures of the representative cities of the Moroccan climatic zones (Agadir, Tangier, Fez, Ifran, Marrakech, and Errachidia). For Agadir City, the monthly mean temperature varies between 13.53 °C in January and 23.91 °C in July. During the whole year, the minimal and maximal monthly temperatures are around 8.86 °C and 34.88 °C observed, in January and July, respectively. For Tangier City, the monthly mean temperature varies between 11.79 °C in January and 25.01 °C in August. During the whole year, the minimal and maximal monthly temperatures are around 5.68 °C and 30.66 °C, observed in January and July, respectively. For Fez City, the monthly mean temperature varies between 9.37 °C in January and 27.19 °C in July. During the whole year, the minimal and maximal monthly temperatures are around 3.82 °C and 35.12 °C, observed in January and July, respectively. For the City of Ifran, the monthly mean temperature varies between 6 °C in January and 26.25 °C in August. During the

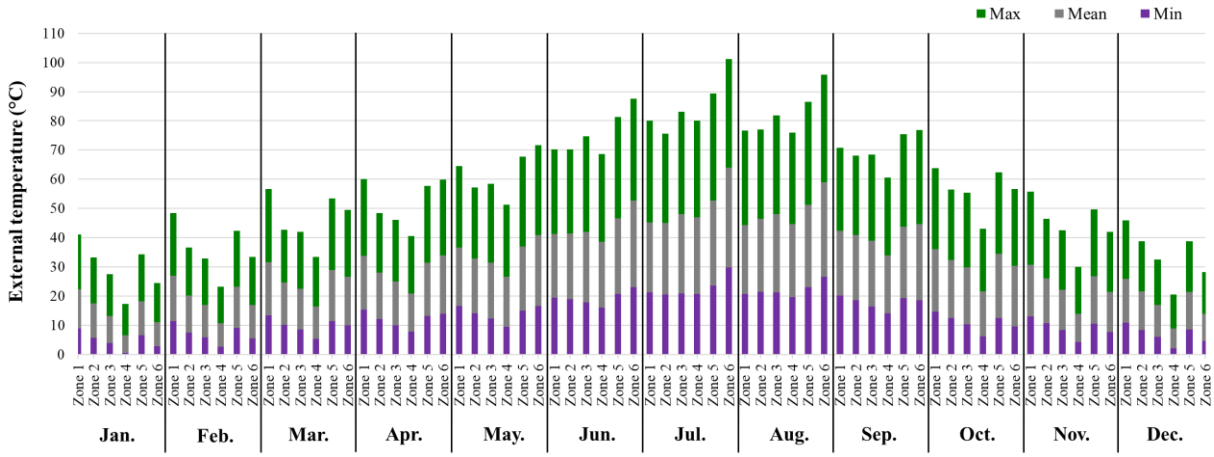

Figure 3.2. Monthly minimal, mean, and maximal outside air temperatures for the six representative cities of the Moroccan climatic zones.

whole year, the minimal and maximal monthly temperatures are around 0.53 °C and 33.16 °C, observed in January and July, respectively. For the City Marrakech, the monthly mean temperature varies between 11.66 °C in January and 29.17 °C in August. During the whole year, the minimal and maximal monthly temperatures are around 6.57 °C and 36.64 °C, observed in January and July, respectively. For Errachidia, the monthly mean temperature varies between 8.11 °C in January and 34.08 °C in August. During the whole year, the minimal and maximal monthly temperatures are around 2.88 °C and 37.18 °C, observed in January and July, respectively. Given the extreme temperatures, it can be considered that January is the coldest month and July is the hottest one in the six Moroccan zones.

3.4 Greenhouses specifications

3.4.1 Greenhouse shapes

Nine different greenhouse shapes (as presented in **Figure 3.3**: (1) even span, (2) uneven span, (3) single slop, (4) mansard roof, (5) modified IARI, (6) quonset, (7) modified quonset, (8) gothic-arch, (9) modified gothic-arch), with the same length, width and roof-top height, are studied. As a first step, the 3D geometric models were separately created using SketchUp

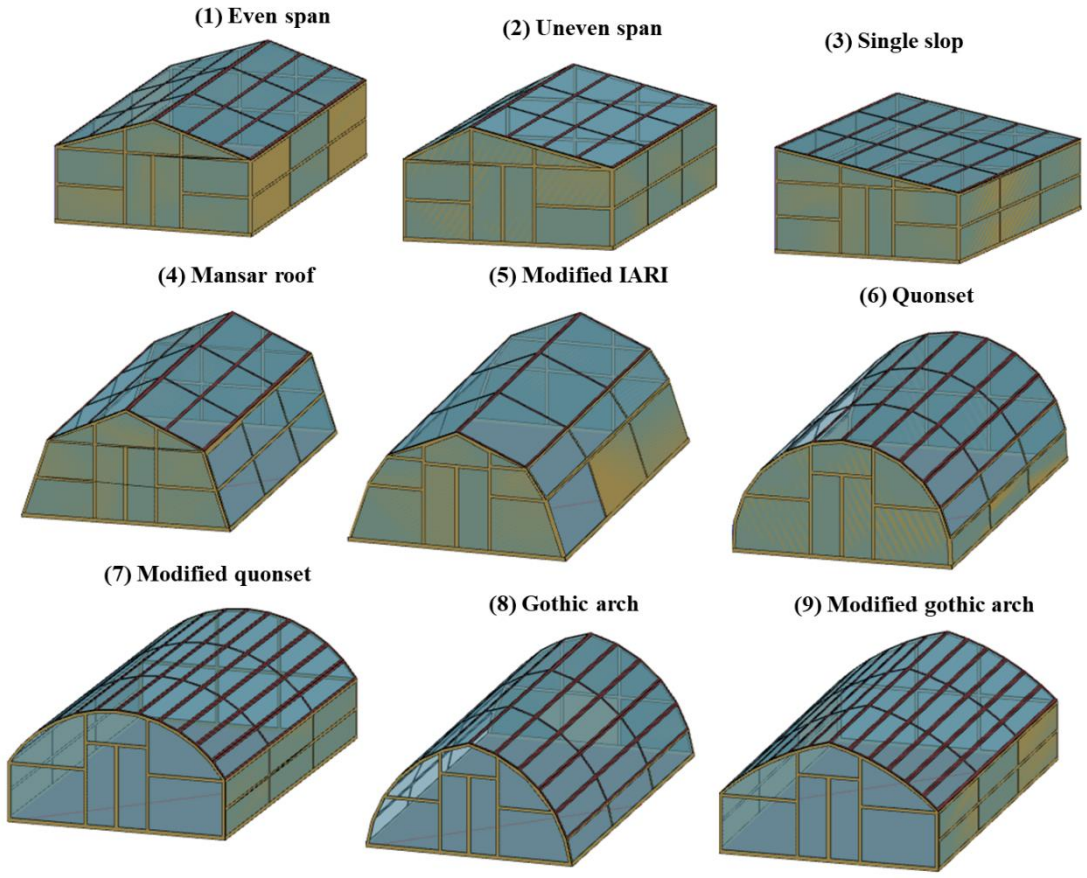

Figure 3.3. Greenhouse shapes considered for comparison in the present study.

graphical interface and OpenStudio Plugins, then implemented as inputs to the EnergyPlus software, where each greenhouse is considered as a single thermal zone. In the second step, the studied cover materials were integrated into the model.

Table 3.2 presents the greenhouses dimensions, including length, width, roof-top height and overall external wall area. The difference between the studied shapes is mainly presented in the difference of the overall external wall area and their inclination/orientation. Since the greenhouses are built on the basis of the availability of a horizontal surface and since it is unfeasible to fix the surface of the external faces, it has been chosen to fix the horizontal surface for the comparison.

Table 3.2. Greenhouses dimensions

shapes	Length (m)	Width (m)	Roof-top height (m)	Overall external wall area (m^2)
Even span	20	11 m	6 m	511.68
Uneven span				513.17
Single slop				533.61
Mansard roof				361.28
Modified IARI				445.42
Quonset				469.95
Modified quonset				493.15
Gothic arch				441.81
Modified gothic arch				479.34

3.4.2 Greenhouse cover materials

After creating the geometric models, the cover material effect is tested for each shape, by analyzing the variation of the mean annual floor incident solar radiation and the mean annual thermal loads (during heating and cooling periods) for each studied climatic zone.

Table 3.3 summarizes the physical properties of the studied materials, where τ is the transmittance, ρ is the reflectance, and α is the absorptance in PAR (photosynthetically active radiation) and NIR (near infrared radiation) wavebands. Low-density polyethylene film (LDPE) and glass are among the widely used greenhouse cover materials, which explains their choice in this study. Bubbled polyethylene plastic (BPE) is an improved type of Polyethylene film by integrating air bubbles which raises its thermal resistance thus decreases the heat exchanges between the greenhouse and the external environment. Ethylenevinyl acetate film (EVA) material is chosen by referring to a previous study [64], in which it was classified the first among three other ones, based on a comparison between needs and the real inside parameters (visible spectrum irradiance, temperature and air velocity).

Table 3.3. Cover material properties [211].

Material	τ_{PAR}	ρ_{PAR}	α_{PAR}	τ_{NIR}	ρ_{NIR}	α_{NIR}	k $(W/m^2.K)$
Glass	84%	6%	10%	73%	7%	20%	0.9
LDPE	83%	8%	9%	87%	8%	5%	0.33
BPE	63%	14%	23%	68%	14%	18%	0.22
EVA	89%	8%	3%	89%	7%	4%	0.23

3.4.3 Greenhouse orientations

The selection of the optimal greenhouse orientation could help maintain an adequate microclimate and lead to a decrease in heating and cooling loads, thereby the operating cost. For this aim, different greenhouse orientations (0°, 90°, 45° and - 45°), relatively to the Nord-Sud (N-S) direction are evaluated to select the most suitable one in terms of energy optimization in each climatic zone. For the sake of clarity, the analysis of greenhouse orientation is conducted by fixing the optimal greenhouse shape and cover material (the previously selected ones in the previous analysis). **Figure 3.4** specifies the orientation of 0° (N-S longer axis).

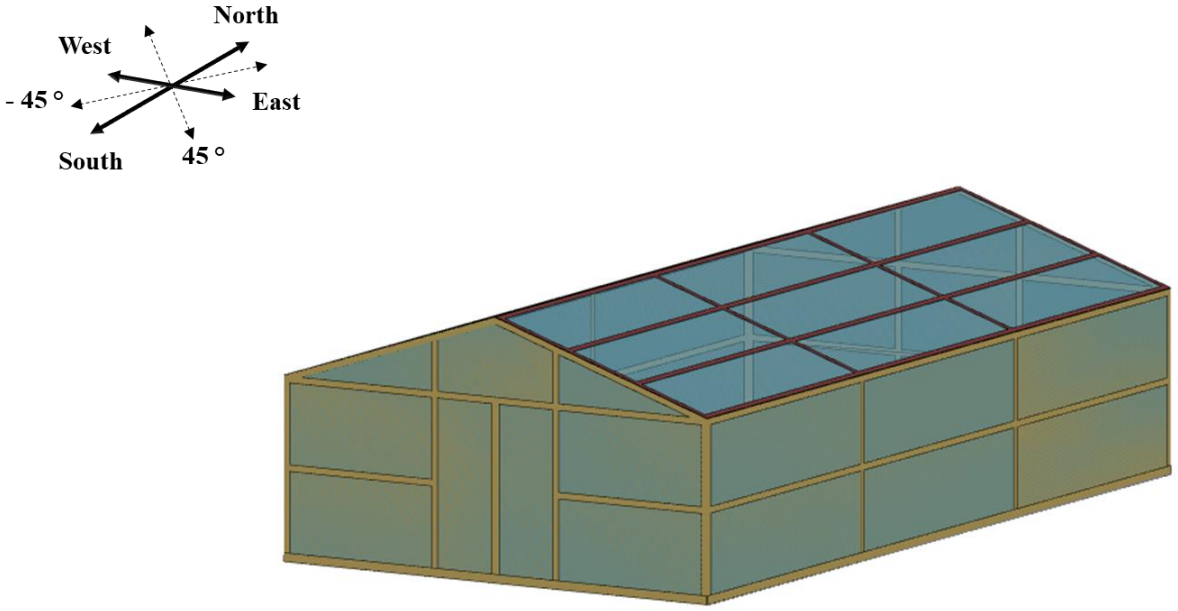

Figure 3.4. "Even span" greenhouse oriented at 0°.

3.4.4 Plants

Tomato is the crop considered in the present study. It can be considered as one of the most important vegetable crops in the whole world, whose production and consumption have increased by 164% and 314%, respectively, during 40 years [212]. The production of tomatoes in controlled greenhouses is a technique that has demonstrated great success, whether for the

quality of the product or the quantity. Indeed it has been shown that this technique generates an average yield of around four times greater than cultivation in open fields (500-600 t/ha against 120-150 t/ha in open fields) [213]. Tomato is considered as a fast-developing plant with an optimum mean day time temperature ranging from 18 °C to 25 °C and a mean nighttime temperature between 10 °C to 20 °C [214].

The plant and the soil are modeled in the EnergyPlus environment by considering them as the outer layer of the floor construction. Their impact on the overall heat balance is implemented based on the FASST model [215], as detailed in **section 2.4.3.3**. **Table 3.4** summarizes the essential parameters of the soil and plant models used in this study.

Table 3.4. Plant and soil model parameters.

Plant		**Soil**	
Height of the plant	1 m	Conductivity of dry soil	0.35 W/m.K
Leaf area index	4	Density of dry soil	1100 kg/m^3
Minimum stomatal resistance	120 s/m	Specific heat of dry soil	600 J/kg.K

3.5 Selection of optimal greenhouse shape and cover material

In order to investigate the impact of the greenhouse design on its microclimate, the climate conditions of the representative cities of the six Moroccan climatic zones are considered. Simulations are conducted for nine shapes and four cover materials and the analysis focuses mainly on three variables: the floor incident solar radiation, thermal loads during both the cooling and heating periods and the annual air-conditioning cost.

For the sake of clarity and to avoid a complex presentation of the results, only annual data is presented. The first part of the analysis compares the different studied shapes based on the annual thermal loads during heating and cooling periods. In the second part, a comparison of the four cover materials regarding the annual loads is carried out. Finally, an analysis of the floor incident solar radiation in different combinations (shape/material) is represented.

3.5.1 Impact of shape and cover material on greenhouse thermal loads

Figure 3.5 and **Figure 3.6** present the mean annual thermal loads of the studied combinations of shapes and cover materials during heating and cooling periods, respectively, for the six considered climatic zones. According to the obtained results, combinations (shape/cover material) can be classified in the same order for the six climatic zones. Regarding shapes and as a general observation of the graphs, it can be remarked that, for all zones, the shape (8, gothic

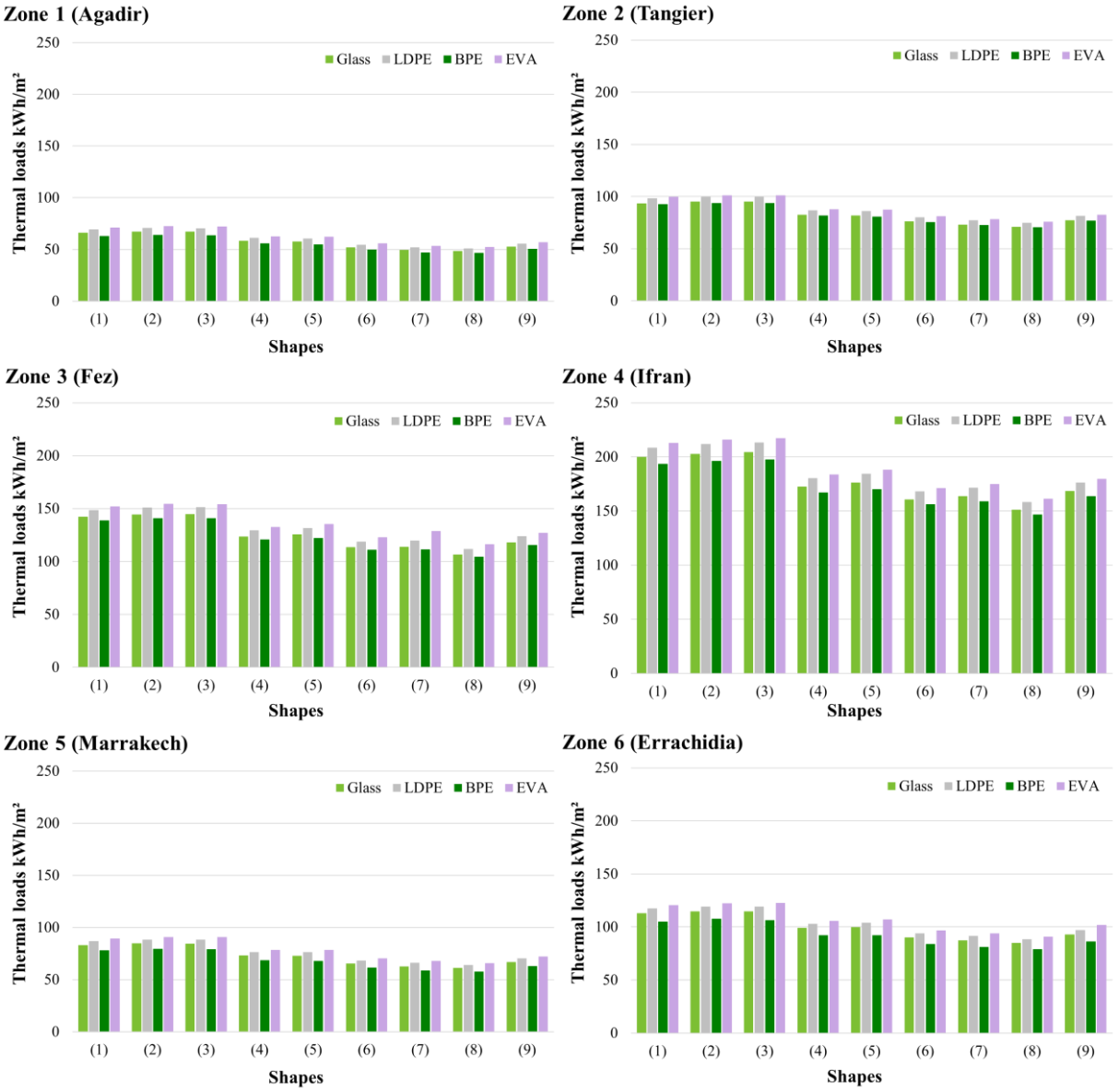

Figure 3.5. Annual heating loads of the different combinations shape/cover.

arch) is the best one, considering both heating and cooling thermal loads. Shapes (1, even span), (2, uneven span) and (3, uneven span) have close thermal loads compared to each other. Their thermal loads rise, regarding shapes, in the following order: (1, even span), (2, uneven span), then (3, uneven span), which can be explained by the surface of the roof facing the southeast comparing one to another. During the heating period, maximum differences (between shapes (1, even span), (2, uneven span) and (3, single slop)) of about 1.1 kWh/m^2, 1.5 kWh/m^2, 2.6 kWh/m^2, 4.5 kWh/m^2, 1.5 kWh/m^2, and 1.9 kWh/m^2 are obtained in zones 1, 2, 3, 4, 5, and 6, respectively. Regarding the cooling period, maximal differences around 32.2 kWh/m^2, 30 kWh/m^2, 33 kWh/m^2, 4.5 kWh/m^2, 34.8 kWh/m^2, and 32.4 kWh/m^2 are obtained in zones 1, 2, 3, 4, 5 and 6, respectively.

The other five shapes, i.e., (4, mansar roof), (5, modified IARI), (6, quonset), (7, modified quonset), and (9, modified gothic arch) have also close thermal loads, with maximum differences of about 9.2 kWh/m^2, 11.5 kWh/m^2, 12.7 kWh/m^2, 17.1 kWh/m^2, 10.7 kWh/m^2 and 12.9 kWh/m^2 are obtained in zones 1, 2, 3, 4, 5 and 6, respectively, during the heating period. For the cooling period, maximal differences of about 42.3 kWh/m^2, 36.1 kWh/m^2, 32.7 kWh/m^2, 26.5 kWh/m^2, 46.6 kWh/m^2 and 46.7 kWh/m^2 are obtained in zones 1, 2, 3, 4, 5 and 6, respectively. These five shapes are classified differently according to the materials, the climatic zones, and the period (heating and cooling).

The optimal shape (8, gothic arch) is compared to the two commonly used ones in Moroccan protected agriculture: shapes (1, even span) and (6, quonset). For zone 1 (Agadir) and during

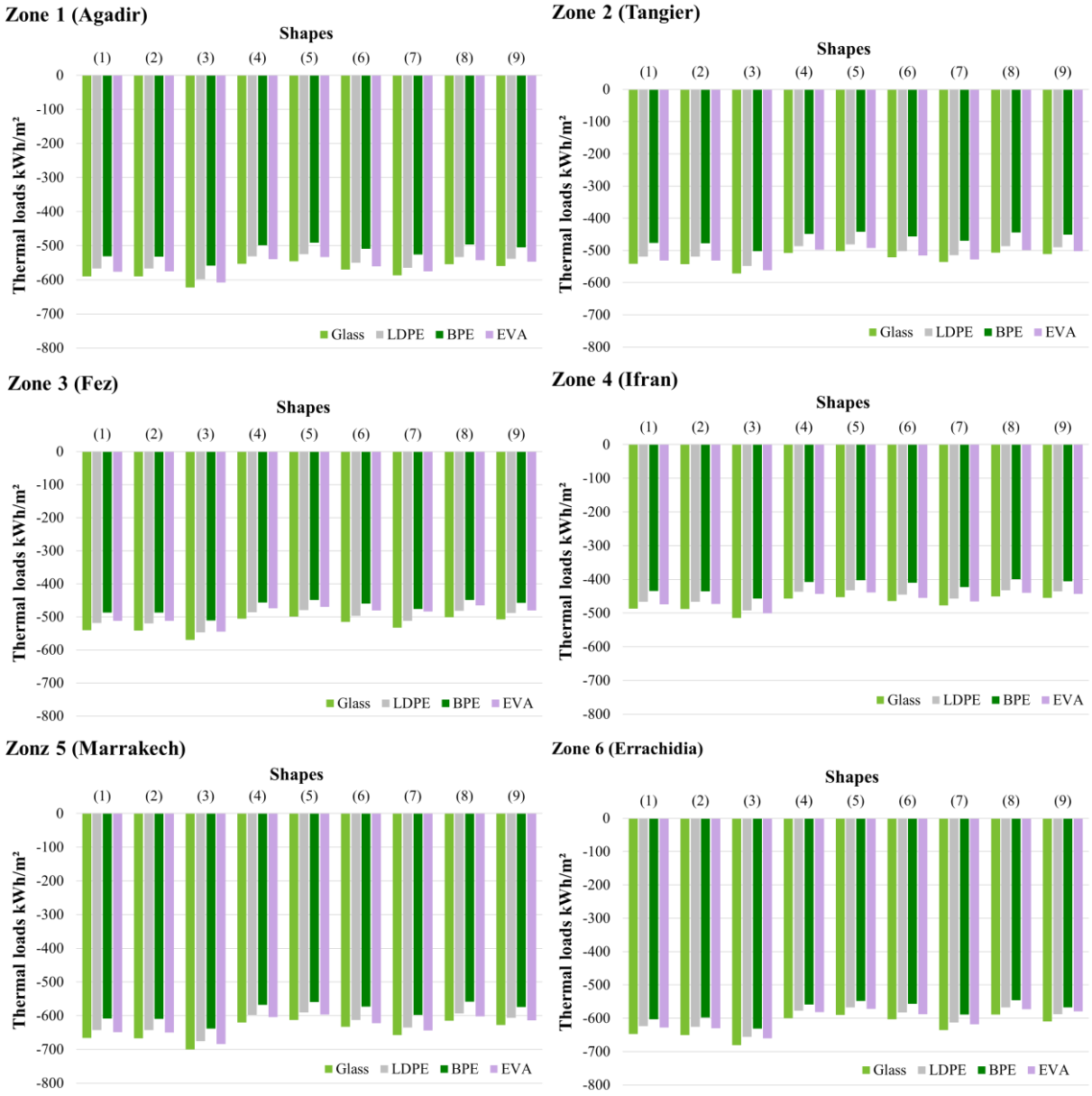

Figure 3.6. Annual cooling loads of the different combinations shape/cover.

the heating period, the thermal loads of shape (8, gothic arch) are around 26% and 7% less than shapes (1, even span) and (6, quonset), respectively. A relative reduction of about 6% and 3% can be noticed regarding the cooling period compared to shape (1, even span) and (6, quonset), respectively. For zone 2 (Tangier) and during the heating period, the thermal loads of shape (8, gothic arch) are around 24% and 7% less than shapes (1, even span) and (6, quonset), respectively. A relative reduction of about 6% and 3% can be noticed regarding the cooling period compared to shapes (1, even span) and (6, quonset), respectively. For zone 3 (Fez) and during the heating period, the thermal loads of shape (8, gothic arch) are around 25% and 6% less than shapes (1, even span) and (6, quonset), respectively. Regarding the cooling period, a relative reduction of about 8% and 3% can be noticed compared to shapes (1, even span) and (6, quonset), respectively. For zone 4 (Ifran) and during the heating period, the thermal loads of shape (8, gothic arch) are around 24% and 6% less than shapes (1, even span) and (6, quonset), respectively. Regarding the cooling period, a relative reduction of about 7% and 3% can noticed compared to shapes (1, even span) and (6, quonset), respectively. For zone 5 (Marrakech) and during the heating period, the thermal loads of shape (8, gothic arch) are around 26% and 6% less than shapes (1, even span) and (6, quonset), respectively. Regarding the cooling period, a relative reduction of around 8% and 3% can be noticed compared to shapes (1, even span) and (6, quonset), respectively. For zone 6 and during the heating period, the thermal loads of shape (8, gothic arch) are around 25% and 6% less than shapes (1, even span) and (6, quonset), respectively. Regarding the cooling period, a relative reduction of around 9% and 2% can be noticed compared to shapes (1, even span) and (6, quonset), respectively. Note that these percentages are the average values of the ones obtained for the four materials (**Table 3.5**).

Table 3.5. Average heating and cooling loads of shapes (1, even span), (6, quonset) and (8, gothic arch), for the six climatic zones.

		Zone 1	Zone 2	Zone 3	Zone 4	Zone 5	Zone 6
Heating loads (kWh/m²)	**Shape (1)**	67.31	96.02	145.34	203.68	84.21	113.90
	Shape (6)	53.05	78.17	116.56	163.94	66.38	91.17
	Shape (8)	49.53	73.01	109.61	154.35	62.20	85.83
Cooling loads (kWh/m²)	**Shape (1)**	566.09	517.50	514.46	465.37	641.42	625.65
	Shape (6)	547.20	499.32	488.37	443.74	609.90	582.75
	Shape (8)	531.53	484.41	474.42	430.64	592.36	568.68

For all shapes and climatic zones, the BPE material seems to be the best one, both in the heating and cooling periods. During the heating period, the EVA material induces higher loads, followed by LDPE material, then glass, and finally, the BPE material. For the cooling period, glass is the one that induces higher loads, followed by EVA then LDPE. The BPE material is still the best one. An exception is for zone 3 (Fez), where the materials are inversely classified for heating loads (Glass, LDPE, EVA) with respect to their classification in the cooling loads (EVA, LDPE, Glass).

Table 3.6 summarizes thermal loads of shape (8, gothic arch) with different cover materials during heating and cooling periods in the six climatic zones. Regarding shape (8, gothic arch), for zone 1 (Agadir), heating loads are less by 11%, 9% and 4% using BPE material than EVA, LDPE and glass, respectively. The thermal loads in the cooling period decrease by 10%, 9% and 7% compared to glass, EVA and LDPE, respectively. For zone 2 (Tangier), heating loads are less by 7%, 6% and 1% using BPE material than EVA, LDPE and glass, respectively. The thermal loads in the cooling period decrease by 12%, 11% and 9% compared to glass, EVA and LDPE, respectively. For zone 3 (Fez), heating loads are less by 10%, 7% and 2% using BPE material than EVA, LDPE and glass, respectively. The thermal loads in the cooling period decrease by 10%, 7% and 4% compared to glass, LDPE and EVA, respectively. For zone 4 (Ifran), heating loads are less by 9%, 7% and 3% using BPE material than EVA, LDPE and glass, respectively. The thermal loads in the cooling period decrease by 11%, 9% and 7% compared to glass, EVA and LDPE, respectively. For zone 5 (Marrakech), heating loads are less by 12%, 10% and 6% using BPE material than EVA, LDPE and glass, respectively. The thermal loads in the cooling period decrease by 9%, 7% and 6% compared to glass, EVA and LDPE, respectively. For zone 6 (Errachidia), heating loads are less by 13%, 11% and 7% using BPE material than EVA, LDPE and glass, respectively. The thermal loads in the cooling period decrease by 7%, 5% and 4% compared to glass, EVA and LDPE, respectively.

Table 3.6. Heating and cooling loads of shapes (8, gothic arch) with different cover materials for the six climatic zones.

		Zone 1	Zone 2	Zone 3	Zone 4	Zone 5	Zone 6
Heating loads (kWh/m²)	**Glass**	48.49	71.01	106.43	151.12	61.19	84.90
	LDPE	50.95	74.76	111.64	158.20	64.10	88.47
	BPE	46.52	70.55	104.28	146.82	57.63	78.99
	EVA	52.15	75.72	116.08	161.26	65.86	90.97
Cooling loads (kWh/m²)	**Glass**	533.75	506.56	501.04	450.58	614.69	588.56
	LDPE	533.35	487.09	482.28	432.09	594.00	567.82
	BPE	496.13	444.80	448.86	399.87	558.78	545.97
	EVA	542.91	499.18	465.49	440.00	601.95	572.37

3.5.2 Impact of greenhouse shape and envelope material on annual air-conditioning cost

To evaluate the economical advantages obtained from the optimal selection of the greenhouse shape and envelope material, a comparison on an annual basis is conducted. The annual energy operating cost is calculated for each combination of shape/envelope material and considered as the main indicator to select the optimal one (as recommended in **section 1.4.2**). In this study, a standard conventional system for greenhouse air-conditioning is selected. This system is composed of a boiler with top efficiency $\eta = 0.96$ and a chiller for cooling purposes with $EER = 3.5$. In Morocco, electricity consumers associated to the agricultural sector benefit from a special pricing "green tariff" [216]. In this pricing mode, the electrical kWh price depends on several parameters; season, time of the day, and others. The electrical kWh price considered in this study is 0.9 MAD/kWh.

Table 3.7 summarizes the annual cost of the air-conditioning in greenhouses with different combinations of shape and cover material. Based on this indicator, the more suitable combination is highlighted. It can be concluded that shape (8, gothic arch) combined with BPE material is the most suitable combination for the six studied zones (reduction of annual air-conditioning cost by about 23%, 24%, 25%, 27%, 24% and 24% for zone 1 (Agadir), 2 (Tangier), 3 (Fez), 4 (Ifran), 5 (Marrakech) and 6 (Errachidia), respectively). **Annex 2** represents the annual cost of the air-conditioning in greenhouses (shape/cover material) normalized by the overall external surface of walls.

Table 3.7. Annual air-conditioning cost for different combinations (Shape/cover material) for the six climatic zones.

		Shape (1)	Shape (2)	Shape (3)	Shape (4)	Shape (5)	Shape (6)	Shape (7)	Shape (8)	Shape (9)
Cost MAD/m²/year	**Zone 1 (Agadir)**									
	Glass	209.03	210.20	218.21	192.97	190.50	191.64	193.81	184.49	189.77
	LDPE	205.87	206.98	214.80	189.76	187.45	188.69	190.55	181.37	186.65
	BPE	191.23	192.34	198.93	176.72	173.79	174.09	176.16	167.95	173.50
	EVA	209.65	210.72	218.89	193.06	190.99	192.61	194.37	184.87	190.04
	Zone 2 (Tangier)									
	Glass	220.36	221.71	229.39	202.23	199.95	200.15	201.35	191.83	198.46
	LDPE	218.77	220.06	227.53	200.39	198.34	198.59	199.51	190.06	196.84
	BPE	202.88	204.18	210.49	186.14	183.50	182.97	183.88	175.52	182.44
	EVA	223.07	224.33	232.12	204.20	202.36	202.90	203.82	193.99	200.73
	Zone 3 (Fez)									
	Glass	262.02	264.15	271.87	237.17	237.12	230.75	235.57	221.04	232.86
	LDPE	262.17	264.26	271.79	236.89	237.18	230.68	235.35	220.71	232.84
	BPE	245.21	247.24	253.65	221.81	221.26	214.52	219.17	205.75	217.79
	EVA	263.18	265.54	273.62	236.92	237.99	230.22	235.69	220.24	233.84
	Zone 4 (Ifran)									
	Glass	298.28	301.04	309.10	266.83	268.86	258.35	264.41	246.71	262.85
	LDPE	300.45	303.17	311.06	268.29	270.75	260.04	265.96	248.07	264.66
	BPE	279.22	281.81	288.61	249.51	250.89	240.59	246.38	229.93	246.07
	EVA	305.97	308.69	316.83	273.09	275.91	265.14	271.06	252.75	269.45
	Zone 5 (Marrakech)									
	Glass	243.20	244.84	253.41	222.92	220.74	219.39	223.50	211.17	219.56
	LDPE	240.34	241.91	250.30	219.96	217.94	216.76	220.52	208.35	216.77
	BPE	224.02	225.58	232.75	205.50	202.73	200.75	204.77	193.70	202.29
	EVA	244.28	245.80	254.53	223.38	221.63	220.79	224.42	211.93	220.25
	Zone 6 (Errachidia)									
	Glass	264.35	266.41	274.37	240.17	238.27	233.22	239.26	224.95	237.22
	LDPE	262.05	264.01	271.77	237.71	236.01	231.21	236.86	222.70	235.02
	BPE	245.88	247.07	254.45	223.59	221.04	216.08	221.90	208.87	220.97
	EVA	266.02	267.97	276.01	241.10	239.67	235.00	240.52	226.03	237.24

3.5.3 Impact of shape and envelope material on greenhouse floor incident radiation

The amount of solar radiation that must reach the plants is crucial when selecting the optimal design. It is one of the parameters having a direct and major influence on the plant growth process. In the present study, as mentioned in **section 3.4.4**, tomato plants are considered as the reference. Their recommended minimum solar radiation need is 2.34 kWh/m².day [10]. Based on this value, the minimum daily average floor incident radiation over a year of the studied greenhouses is investigated.

Following the same approach as for the thermal loads' comparison and continuing ahead, keeping the most suitable combination (shape (8, gothic arch) with BPE material) preliminary

selected. Having a look at the daily average floor incident solar radiation of this combination **(Figure 3.7)**, it can be mentioned that only on a few days during the whole year, the values are under the nominal value (2.34 kWh/m²/day, tomato). For zone 1 (Agadir), the minimum incident radiation largely exceeds the minimum recommended value. While for zones 2, 3, 5 and 6, the incident radiation is under the recommended value only for less than seven days.

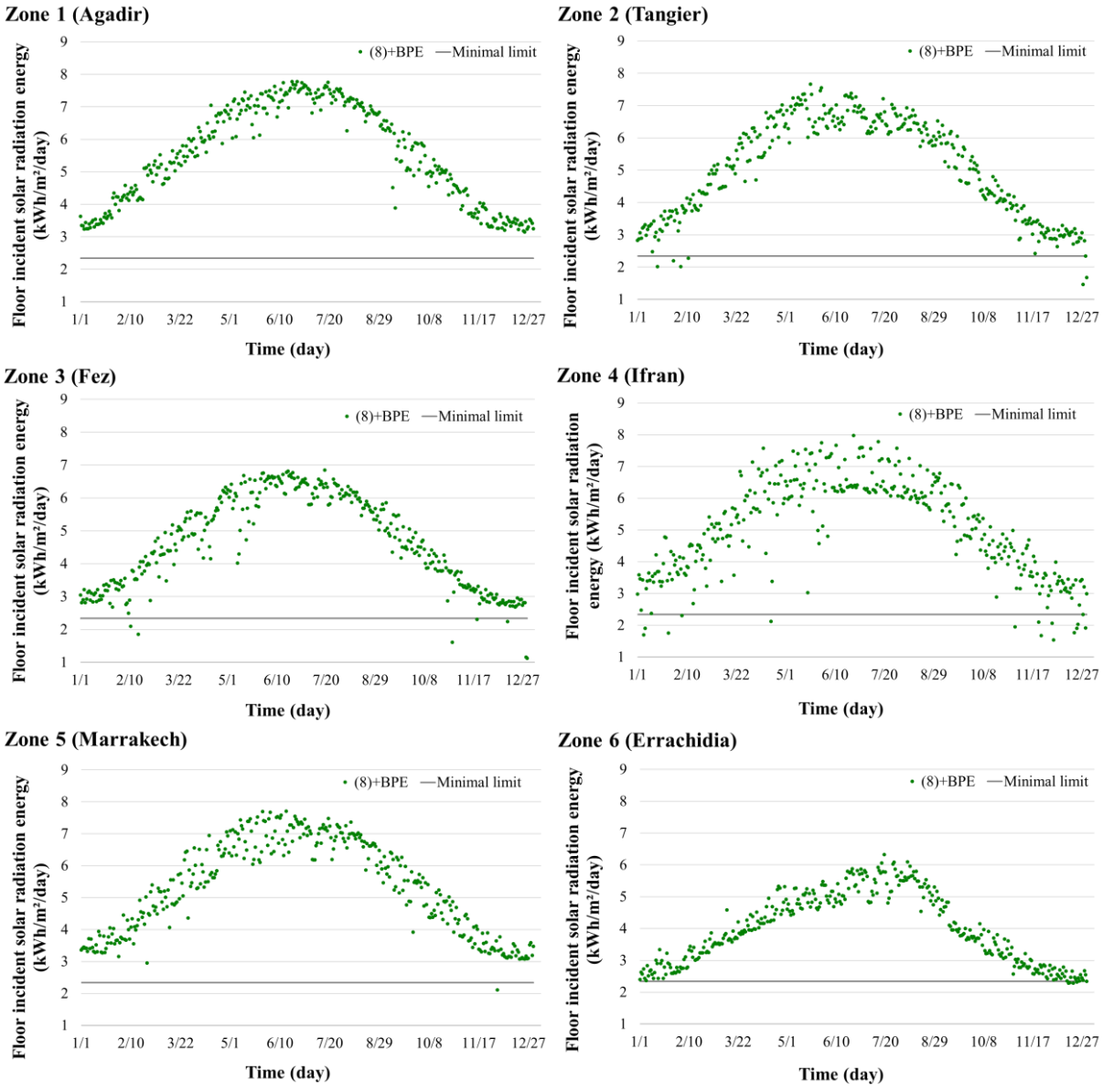

Figure 3.7. Daily average floor incident solar radiation of the optimal combination (shape (8, gothic arch) with BPE material).

For zone 4 (Ifran), the incident radiation is under the recommended value during a period of 14 days. For this reason, we evaluate the floor incident radiation of another combination classified directly after the preliminary selected one regarding thermal loads, which is shape (6, quonset) with BPE material. It has been noticed that this combination has the same range of days having a deficit as the combination of shape (8, gothic arch) with BPE material (Figure 3.8). Therefore,

this latter is still the most optimal one, and it is recommended to compensate the deficit of solar radiation with a lighting system.

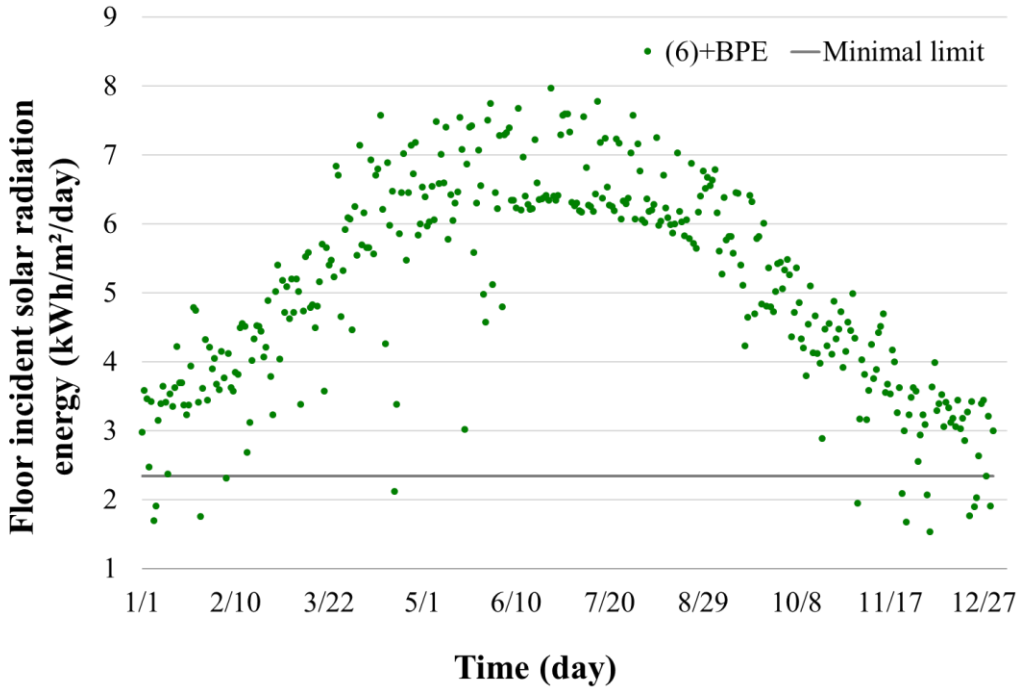

Figure 3.8. Daily average floor incident solar radiation for zone 4 (Ifran).

3.6 Selection of optimal greenhouse orientation

Based on the results presented in **section 3.5**, the combination of gothic arch and bubbled polyethylene (BPE) plastic has been selected as the optimal one for the 6 studied zones. This combination has been fixed in order to assess the impact of greenhouse orientation on its thermal loads. For that, four orientations are studied, namely 0°, 90°, 45° and - 45° (longer axis vs North-South direction).

Simulations are first performed separately for the four greenhouse orientations. Thereafter, the impact of the orientation on the greenhouse thermal behavior is evaluated. The thermal loads for heating and cooling are analyzed by considering the adapted microclimate for tomato plant. Then, the annual energy cost of the air-conditioning system is estimated and the operational cost reduction generated from the right selection of the greenhouse orientation is evaluated.

3.6.1 Impact of orientation on greenhouse thermal loads

Figure 3.9 and **Figure 3.10** show the monthly greenhouse heating and cooling loads, respectively, in the six climatic zones. Based on the graphs, the maximal heating and cooling requirements occur during January and July, respectively. As expected, the cooling load is bigger than the heating load and the effect of orientation is bigger in summer.

On an annual basis, in zone 1 (Agadir), minimal heating loads are observed in the greenhouse oriented at 0°. For the other orientations, heating loads are bigger than the greenhouse oriented at 0° by about 1.03%, 4.6% and 8.6%, at 45°, - 45° and 90°, respectively. Although, minimal cooling loads occur when the greenhouse is oriented at 90°. For the other orientations, cooling loads increase by about 2.4%, 6.2% and 7.9% when the greenhouse is oriented at - 45°, 45°, and 0°, respectively, compared to 90°. In zone 2 (Tangier), minimal heating loads are observed in the greenhouse oriented at 90°. For the other orientations, heating loads are more important than the greenhouse oriented at 90° by about 1.3%, 4.3% and 4.7% at 45°, - 45° and 0°, respectively. Although, minimal cooling loads occur when the greenhouse is oriented at 0°. For the other orientations, cooling loads increase by about 4.1%, 8.5% and 10.4% when the greenhouse is oriented at - 45°, 45°, and 90°, respectively, compared to 0°. In zone 3 (Fez),

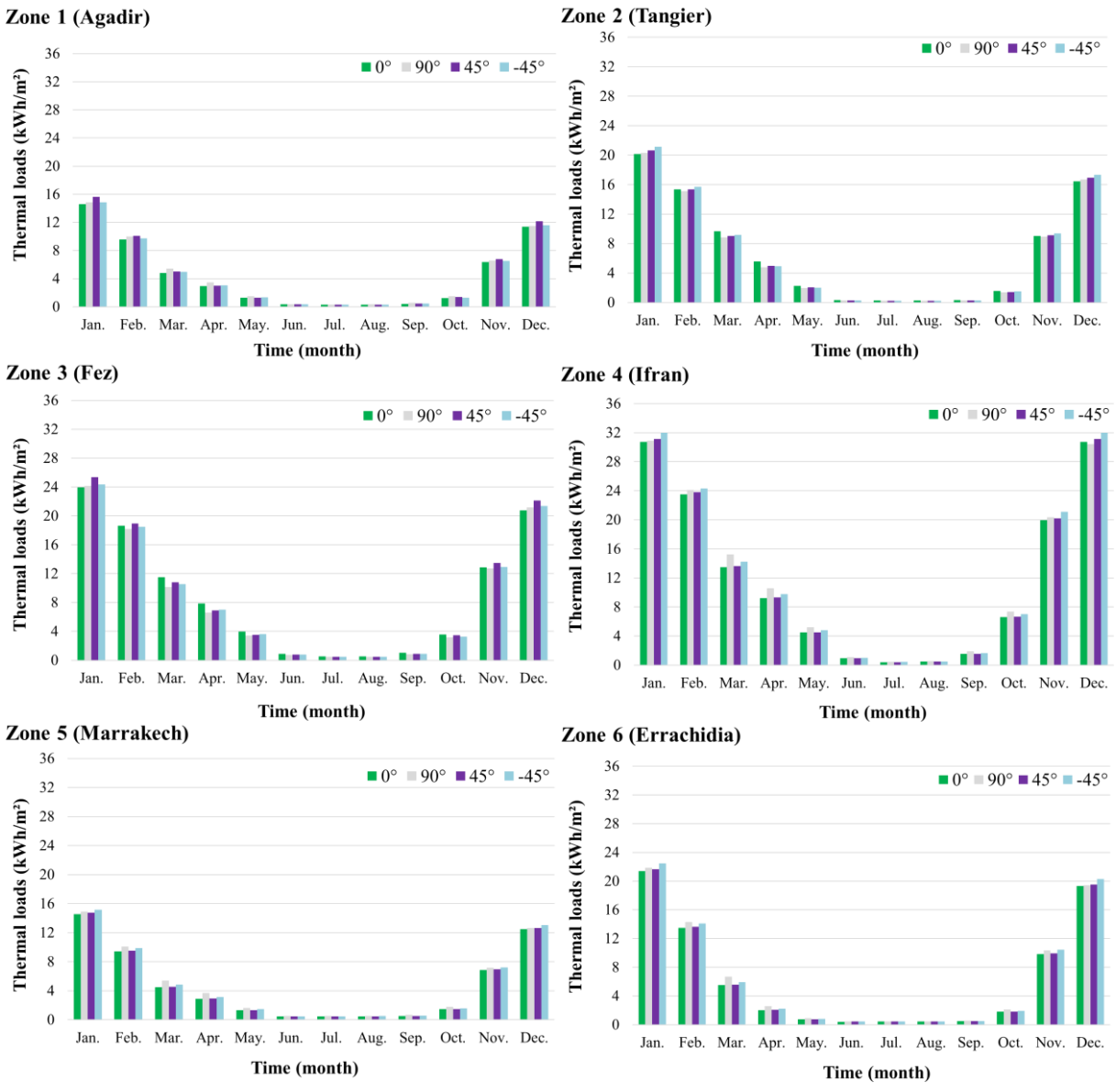

Figure 3.9. Monthly heating loads of the greenhouse with different orientations.

minimal heating loads are observed in the greenhouse oriented at 90°. For the other orientations, heating loads are more important than the greenhouse oriented at 0° by about 2%, 4% and 5% at - 45°, 0° and 45°, respectively. Although, minimal cooling loads occur when the greenhouse is oriented at 0°. For the other orientations, cooling loads increase by about 5%, 5.5% and 8.4% when the greenhouse is oriented at - 45°, 45°, and 90°, respectively, compared to 0°. In zone 4 (Ifran), minimal heating loads are observed in the greenhouse oriented at 0°. For the other orientations, heating loads are more important than the greenhouse oriented at 0° by about 1.23%, 4.3% and 4.75% at 45°, 0° and - 45°, respectively. Although, minimal cooling loads occur when the greenhouse is oriented at 90°. For the other orientations, cooling loads increase by about 6.1%, 11.5% and 13.4% in the greenhouse oriented at - 45°, 45°, and 0°, respectively, compared to 90°. In zone 5 (Marrakech), minimal heating loads are observed in the greenhouse

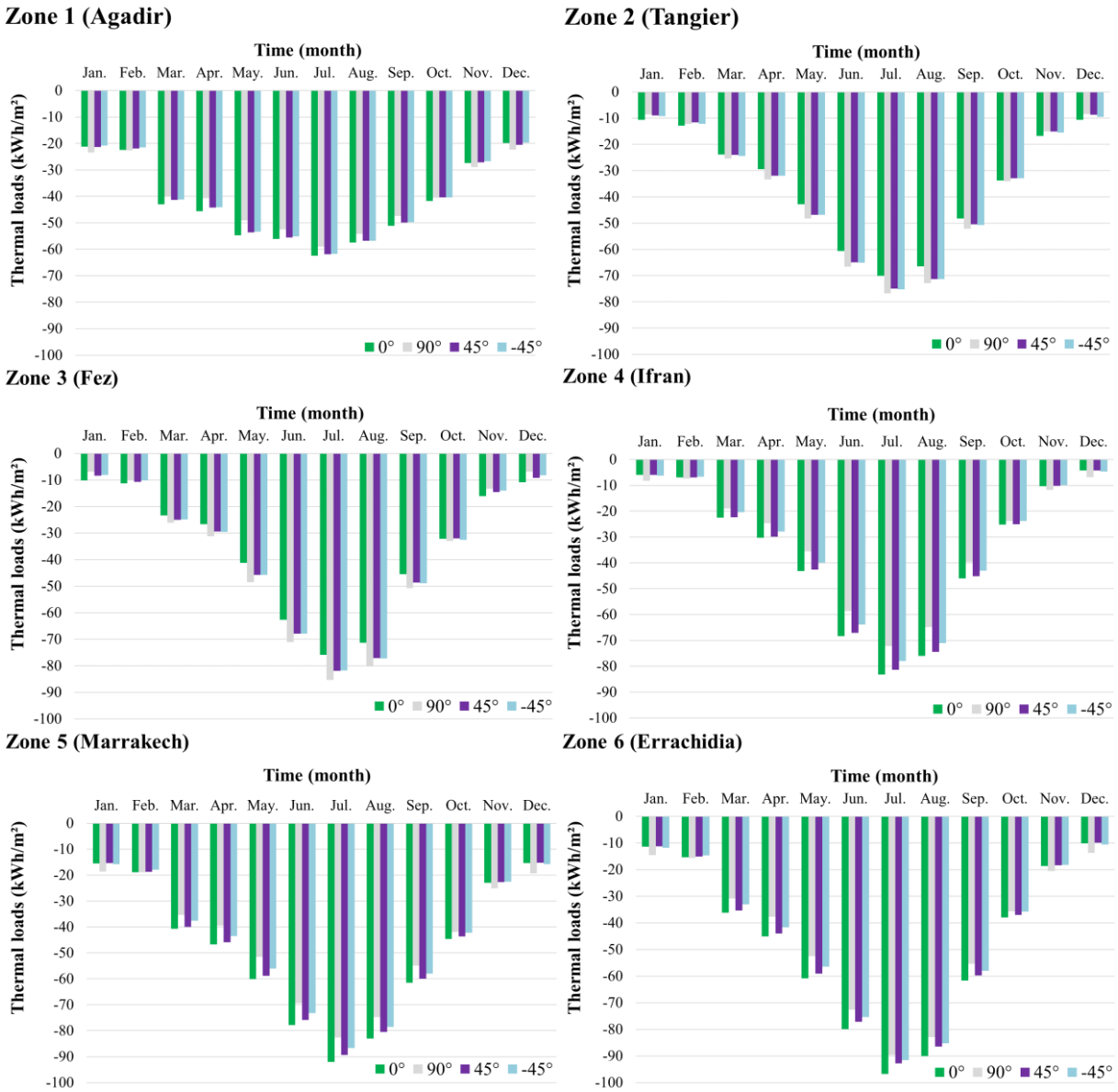

Figure 3.10. Monthly cooling loads of the greenhouse with different orientations.

oriented at 0°. For the other orientations, heating loads are more important than the greenhouse oriented at 0° by about 1.1%, 5% and 7.1%, compared to 0°, for 45°, - 45° and 90°, respectively. Although, minimal cooling loads occur when the greenhouse is oriented at 90°. For the other orientations, cooling loads increase by about 3.1%, 6.5% and 9% at - 45°, 45°, and 0°, respectively, compared to 90°. In zone 6 (Errachidia), minimal heating loads are observed in the greenhouse oriented at 0°. For the other orientations, heating loads are more important than the greenhouse oriented at 0° by about 1.13%, 5.33% and 5.54% at 45°, - 45° and 90°, respectively. Although, minimal cooling loads occur when the greenhouse is oriented at 90°. For the other orientations, cooling loads increase by about 2%, 4.7% and 8.1% at - 45°, 45°, and 0°, respectively, compared to 90°. **Table 3.8** summarizes heating and cooling loads of the greenhouse depending on the studied orientations.

Table 3.8. Heating and cooling loads of the greenhouse with the different orientations for the six climatic zones.

		Zone 1	Zone 2	Zone 3	Zone 4	Zone 5	Zone 6
Heating loads (kWh/m²)	**0°**	45.04	71.87	106.13	142.13	55.58	75.91
	45°	45.51	69.52	107.26	143.87	56.17	76.76
	- 45°	47.13	71.58	104.28	148.88	58.36	79.96
	90°	48.89	68.65	102.05	148.24	59.54	80.12
Cooling loads (kWh/m²)	**0°**	515.99	422.49	427.20	422.43	581.77	566.29
	45°	508.24	458.40	450.42	415.11	568.62	548.51
	- 45°	489.89	439.68	448.86	395.16	550.24	534.41
	90°	478.40	466.33	463.24	372.39	533.72	523.86

3.6.2 Impact of greenhouse orientation on annual air-conditioning cost

Following the same method as presented in **section 3.5.2**, the impact of greenhouse orientation on annual air-conditioning costs is quantified. **Figure 3.11** represents the annual energy cost (MAD/m²) variation depending on the greenhouse orientation for the six climatic zones. For zone 1 (Agadir), it can be observed from the graph that the orientation of 90° is the best one with an annual energy cost of about 169.04 MAD/m². For the other orientations, - 45°, 45° and 0°, the annual energy cost increases by around 0.8%, 2.6% and 3.5% compared to the orientation of 90°, respectively. For zone 2 (Tangier), the orientation of 0° is the optimal one with an annual energy cost of about 176.21 MAD/m². For the other orientations; - 45°, 45° and 90°, the annual energy cost increases by around 2.3%, 3.8% and 4.5% compared to the

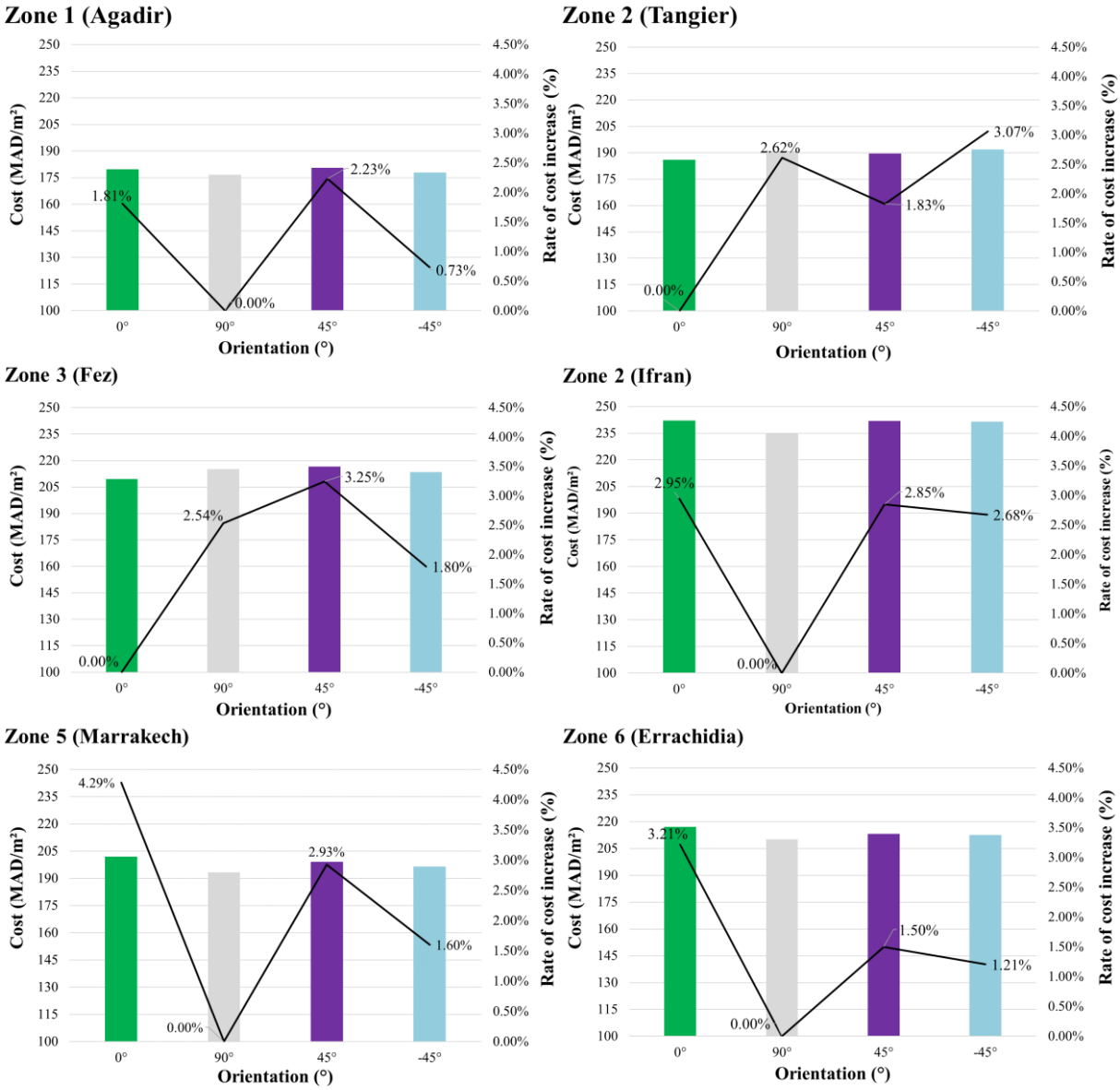

Figure 3.11. Annual energy cost for the greenhouse air-conditioning according to the orientations.

orientation of 0°, respectively. For zone 3 (Fez), the orientation of 0° is the optimal one with an annual energy cost of about 209.60 MAD/m². For the other orientations, - 45°, 90° and 45°, the annual energy cost increases by about 1.80%, 2.54% and 3.25% compared to 0°, respectively. For zone 4 (Ifran), the orientation of 90° is the optimal one with an annual energy cost of about 235 MAD/m². For the other orientations, - 45°, 45° and 0°, the annual energy cost increases by about 2.68%, 2.85% and 2.95% compared to 90°, respectively. For zone 5 (Marrakech), the orientation of 90° is the optimal one with an annual energy cost of about 193.30 MAD/m². For the other orientations, - 45°, 45° and 0°, the annual energy cost increases by about 1.60%, 2.93% and 4.29% compared to 90°, respectively. For zone 6 (Errachidia), the orientation of 90° is the optimal one with an annual energy cost of about 210.05 MAD/m². For the other orientations, -

45°, 45° and 0°, the annual energy cost increases by about 1.21%, 1.50% and 3.21% compared to 90°, respectively.

3.7 Improvement of the greenhouse energy efficiency

After analyzing the impact of the greenhouse design (shape, cover material, and orientation) on energy requirements, the optimal design obtained for each zone is selected. To further improve the greenhouse energy efficiency, two systems are studied: nighttime thermal blankets insulation operating during the heating period and controlled ventilation to minimize greenhouse cooling needs.

3.7.1 Thermal blankets insulation

To minimize the greenhouse heating loads, a thermal insulation blankets system operating from sunset to sunrise is investigated. The system is active only during the months when heating loads are important: from November to April. The thermal insulation blankets material, used in this study, is the high-density polyethylene (HDPE) opaque material with a relatively low thermal conductivity that is used to protect the greenhouse from the potential heat losses during the night of the coldest period. **Table 3.9** presents the thermal insulation blankets' thermo-physical properties.

Table 3.9. Thermal insulation blankets' parameters.

Thermal insulation blankets	
Material	HDPE
Thickness	5 mm
Thermal Conductivity	0.5 W/m.K
Density	960 kg/m^3

The monthly thermal loads of the greenhouse with and without the nighttime operating insulation blankets are presented in **Figure 3.12**. In all the six climatic zones, the insulation contributes to minimizing heating loads. On an annual basis, a reduction of about 6.18 kWh/m², 11.6 kWh/m², 18.45 kWh/m², 21 kWh/m², 7.7 kWh/m², and 11.13 kWh/m² have been obtained in zones 1, 2, 3, 4, 5, and 6, respectively.

Table 3.10 represents the financial gains and the payback period of the nighttime thermal insulation blankets operating during the heating period. A heating needs reduction of about 13%, 16%, 17%, 14%, 13% and 14% with a payback period of about five years and six months, two years and 11 months, one year and ten months, one year and seven months, four

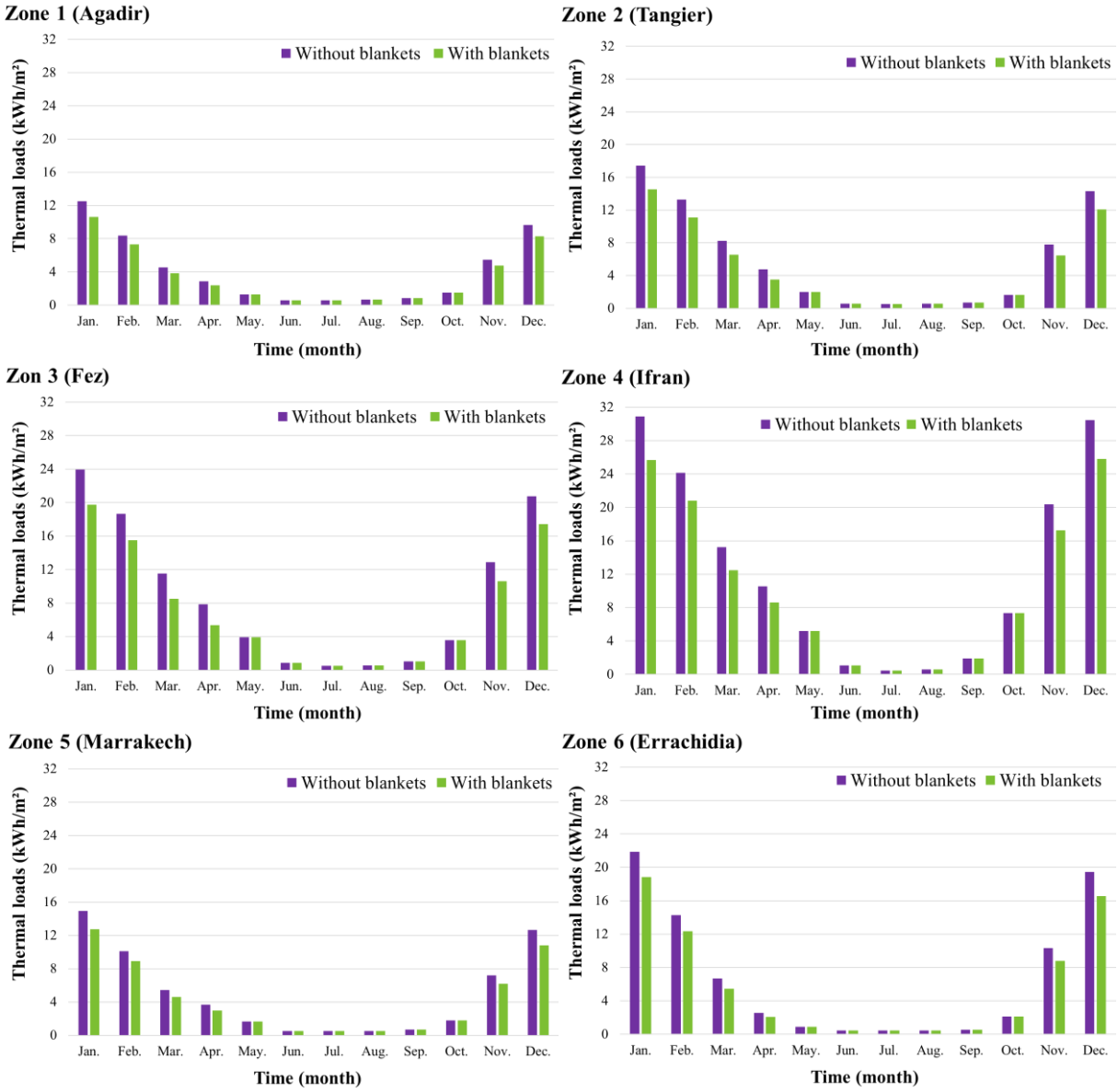

Figure 3.12. Monthly heating loads of the greenhouse with and without nightly thermal blankets insulation.

years and five months and three years are obtained for zone 1 (Agadir), 2, 3, 4, 5 and 6, respectively. For the six climatic zones, the payback period seems to be good compared to a lifetime period of up to eight years.

Table 3.10. Benefit of the nighttime thermal insulation blankets for the six climatic zones.

	Annual heating loads (kWh/m²)	Financial gain (MAD/year)	Payback period
Zone 1	42.71	1276.44	5 years, six months
Zone 2	60.27	2395.05	2 years, 11 months
Zone 3	87.68	3809.44	1 year, ten months
Zone 4	127.23	4337.42	1 year, seven months
Zone 5	51.86	1586.10	4 years, five months
Zone 6	68.99	2297.74	3 years

3.7.2 Controlled natural ventilation

A controlled natural ventilation system is used to regulate the inside temperature and minimize the cooling needs. The system is modeled as a fraction area of the shell that can be opened (about 32% of the total transparent area); the ventilation flow rate is governed by the wind and stack effect. The natural ventilation is managed during the whole year based on minimum and maximum temperatures for both indoor (18 °C – 80 °C) and outdoor (18 °C – 25 °C) conditions. Those parameters are the limits that set the closing of the opening surfaces and thus the shutoff of the ventilation. The control method helps avoid the heat losses from the zone to the exterior environment during the coldest days by closing the windows when the exterior or interior temperature gets down to 18 °C. Thus, their opening is applied when a high interior temperature is detected, fixed at a maximum of 80 °C (strictly higher than the maximum indoor temperature throughout the year) while the exterior temperature is still lower than 25 °C. If the exterior temperature exceeds 25 °C, the windows are shut down and the cooling is provided by the HVAC system. This system allows for minimizing energy consumption and avoiding the peaks of temperature in the hottest hours of the day an unsustainable greenhouse effect for the plants' growth.

The monthly thermal loads of the greenhouse with and without the operable windows are presented in **Figure 3.13**. In the six climatic zones, the controlled natural ventilation contributes to minimizing cooling loads. On an annual basis, a reduction of about 79.15 kWh/m², 85.48 kWh/m², 69.98 kWh/m², 81.19 kWh/m², 61.88 kWh/m², and 54.17 kWh/m² equivalent to 16.5%, 20.2%, 16.4%, 21.8%, 11.6%, and 10.3% are obtained in zones 1, 2, 3, 4, 5, and 6, respectively. **Table 3.11** summarizes the financial gains of controlled natural ventilation.

Table 3.11. Financial gains of the controlled natural ventilation for the six climatic zones.

	Annual cooling loads (kWh/m²)	Financial gain (MAD/year)
Zone 1	399.25	4482.69
Zone 2	337.01	4841.17
Zone 3	357.22	3963.35
Zone 4	291.20	4598.16
Zone 5	471.84	3504.50
Zone 6	469.68	3067.99

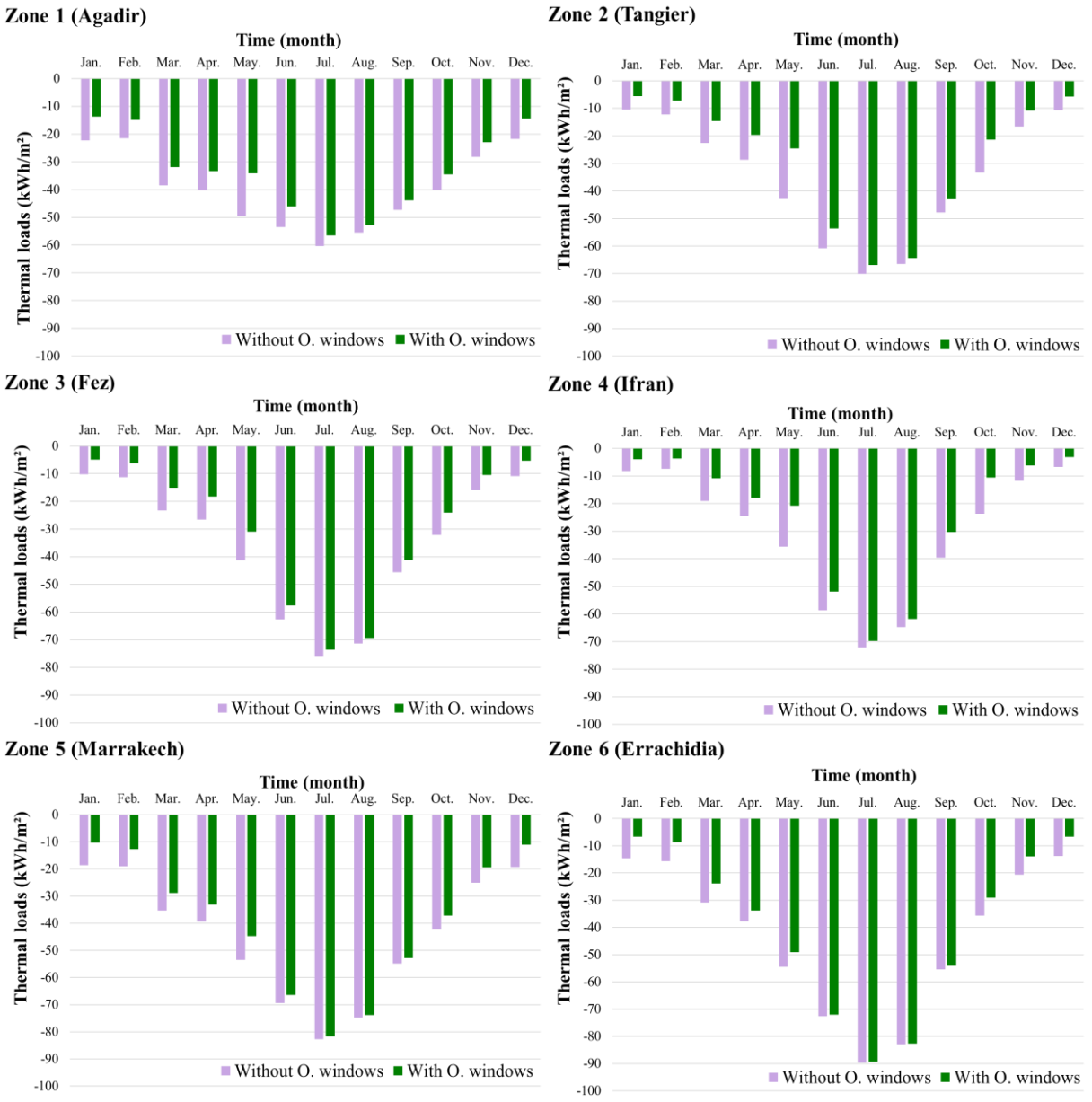

Figure 3.13. Monthly cooling loads of the greenhouse with and without operable windows.

3.8 Conclusions

This chapter evaluates different greenhouse designs (shape, cover material and orientation) in order to select the most suitable one for each Moroccan climatic zones. For that, different shape/cover material combinations are considered, namely nine shapes (standard even span, uneven span, single slop, mansard roof, modified IARI, quonset, modified quonset, gothic arch, and modified gothic arch) and four materials (glass, LDPE, EVA, and BPE). After the selection of the suitable combination, four orientations were investigated, namely 0°, 90°, 45° and - 45° (longer axis vs North-South axis). The greenhouse energy efficiency is further improved by

using nighttime thermal insulation operating during the heating period and natural controlled ventilation to reduce the cooling needs. Different parameters are considered to select the optimal design and to define the potential of energy-saving in each climatic zone: the greenhouse thermal loads during heating and cooling periods and the greenhouse floor incident solar radiation depending on the considered plant needs. The main conclusions can be made as follows:

(1) The greenhouse shape has a significant impact on the thermal loads; thus, the right choice can generate until 26% and 9% of energy-saving during heating and cooling periods, respectively.

(2) The greenhouse cover material significantly affects the greenhouse thermal loads and the optimal selection can reduce until 13% and 12% of heating and cooling energy needs, respectively.

(3) The combination of gothic arch shape and BPE material is a good compromise for tomato plants' greenhouse under the different considered Moroccan climatic zones based on the minimal thermal loads, all-around year, and the plant solar radiation needs.

(4) The selection of the optimal greenhouse orientation can save until 8.6% and 13.4% of heating and cooling energy requirements, respectively. The optimal greenhouse orientation was found to be 0° for zones 2 and 3 and 90° for the other Moroccan climatic zones.

(5) In the six climatic zones, the nighttime insulation contributes to minimizing the greenhouse heating loads. The energy-saving potential varies between 13% and 17%, depending on the climatic zone.

(6) The controlled natural ventilation was found to have an important impact in minimizing cooling loads, with an energy-saving potential ranging between 10.3% and 21.8%, depending on the climatic zone.

(7) Combining the proposed design (shape, cover material, orientation, thermal insulation blankets and operable windows), the annual energy cost for tomato greenhouse air-conditioning is 142.88, 143.32, 174.25, 194.67, 170.14 and 185.66 MAD/year/m² for zone 1 (Agadir), 2 (Tangier), 3 (Fez), 4 (Ifran), 5 (Marrakech), and 6 (Errachidia), respectively.

A part of the work presented in this chapter has been published in the following papers:

1. Ouazzani Chahidi, L., & Mechaqrane, A. (2022). Greenhouse Design Selection in Moroccan Climatic Conditions. In WITS 2020, Lecture Notes in Electrical Engineering (pp. 639-648). Springer, Singapore.
2. Ouazzani Chahidi, L., & Mechaqrane, A. (2021). Energetic and economic analysis for improving greenhouse energy efficiency. Journal of Energy Systems, 5(4), 296-305.

Chapter 4

Prediction of greenhouse energy demand and production using machine-learning methods

Chapter 4: Prediction of greenhouse energy demand and production using machine-learning methods

4.1 Introduction

The agricultural sector has undergone a clear and rapid evolution in recent years. The main objective is to make a compromise between the tremendously increasing food demand and decreasing natural resources while ensuring a good quality product. Protected agriculture has become more modern and competitive. It adopts, nowadays, innovative and impressive technologies that allow for rational use of resources and a high yield and quality production. This cultivation technique which become an integral part of the agricultural activity, allows for production throughout the year and off-season different kinds of plants. However, the protected agriculture is an energy-intense cultivation technique with an energy request of around 40% of the total production cost [217]. Thus, efficient management can significantly contribute not only to minimizing the energy needs but also to increasing the yield and the quality of the product. The use of intelligent techniques to predict the greenhouse inside microclimate and/or energy consumption can be of great importance to develop a good energy management strategy and to maintain the required inside air conditions for plant growth.

Currently, the agricultural sector faces a real revolution. The advent of technologies and the implementation of artificial intelligence (AI) play a key role in this revolution and have taken the agriculture framework to an advanced level [92]. Artificial intelligence (AI) can lead to real-time monitoring and decision-making, which can be of considerable interest to further improve and develop this sector of activity. Many researches have been devoted to this target [93]–[95]. The artificial intelligence (AI) can be applied in protected agriculture in many ways, namely to maintain an adapted microclimate to the plant growth, to optimize the irrigation process, to properly apply pesticides and herbicides, or also to optimize energy consumption.

The use of machine-learning methods for predicting greenhouses variables is of great interest to develop intelligent management strategies and reduce potential energy and financial losses. The conducted literature review (**section 1.4.1.2**) showed that several machine-learning methods have not been sufficiently exploited. The study presented in this chapter focuses on predicting the air-conditioning electrical consumption and the photovoltaic modules' electrical production using different supervised machine-learning algorithms, namely: artificial neural networks (ANN), gaussian process regression (GPR), support vector machine (SVM) and boosting trees. Then, further investigations on the artificial neural networks are conducted and

a hybrid model combining ANN and boosting methods is proposed. The models' performance is evaluated and compared based on the two statistical indicators: the coefficient of correlation (R) and the normalized RMSE (nRMSE).

4.2 Data sets

In this chapter, the data sets used to build the studied models is provided by the monitoring system of the "Smart Agro-Manufacturing Laboratory" (SamLab) greenhouse. As previously mentioned, this high-efficiency greenhouse is located in Albenga, Italy and occupies an area of 151.47 m^2 with an even span shape (15.30 m length, 9.9 m width, 3.5 m Eave height and 5.6 m rooftop height) and a glass envelope with galvanized steel structure and aluminium frame. The greenhouse is equipped with passive techniques (operable windows and shading/reflecting system) and renewable energy systems (semi-transparent PV panels and a ground-coupled heat pump, GCHP). A more detailed description of the greenhouse is presented in **section 2.2**.

The SamLab greenhouse is equipped with a complete data acquisition and monitoring system that measures and records different parameters related to the greenhouse systems and the inside climate conditions. Many pressure, temperature and mass flow rate sensors allow acquiring a huge amount of hourly and sub-hourly data. This data acquisition system is composed of different subsystems: the EcoForest Heat Pump (HP) Datalogger (webserver inside the HP), the Bbone Datalogger and the Raspberry Datalogger, as presented in **Figure 4.1**. Moreover, data

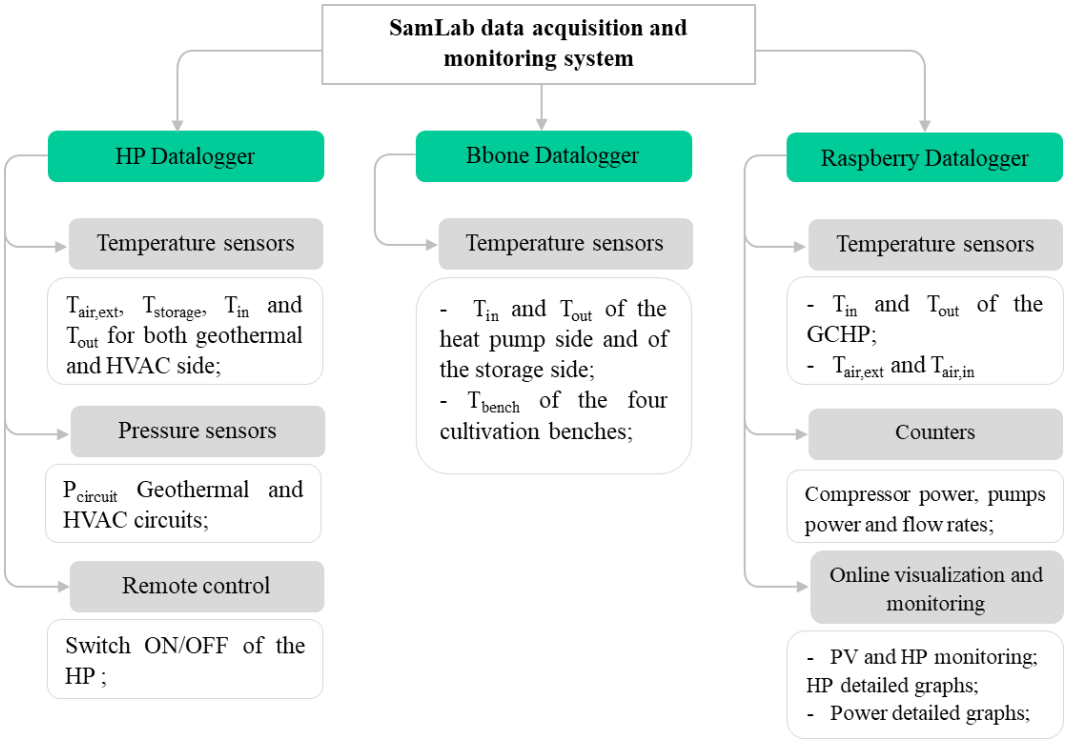

Figure 4.1. SamLab greenhouse data acquisition and monitoring subsystems.

related to the selected periods (March and Mid-August to Mid-September 2020) are used to train and validate the models. Some meteorological data for the analyzed location (i.e., Albenga) is partially measured on-site (temperature) and partially deduced from the Liguria Region Agency for the Environment webpage [186] (solar irradiance).

4.3 Models description

The study presented in this chapter aims to compare the performance of four techniques in predicting the air-conditioning electrical consumption and the PV modules' electrical production. The following methods were attempted: ANN, GPR, SVM and Boosting. To reach this goal, the present study follows four steps summarized as follows: data pre-processing Random split of the dataset (70% for training and 30% for validation), implementation of the four different models, optimization of the chosen models' hyperparameters to improve their performance, and comparison of the models' performance in terms of their statistical indicators (**section 4.4**).

The model's hyperparameters, defined as parameters allowing for controlling the learning process, strongly affect their performance. For GPR, SVM and boosting trees models, the selection of the optimal ones has been made by automatically trying different hyperparameter combinations based on an optimization scheme that aims to minimize the model's mean squared error (MSE), and finally, returns the model using optimized hyperparameters. The optimal ones depend on the predicted parameters.

4.3.1 Artificial neural networks ANN

Artificial neural networks (ANN) are powerful methods that have shown their ability to solve complex nonlinear problems and to found the relationship between inputs and outputs. The fundamentals of ANN were inspired by the structure of the human brain system [218].

This study uses a "back propagation" multi-layer perceptron neural networks. The network architecture (2-10-1) is constituted of one input layer with two neurons (external temperature and global solar radiation), one hidden layer with ten neurons and one output layer with one neuron (air-conditioning electrical consumption or PV modules' production), as presented in **Figure 4.2**. The selected activation functions are the hyperbolic tangent sigmoid function for the hidden neurons (**equation 4.2**) and the linear function for the output neuron (**equation 4.1**).

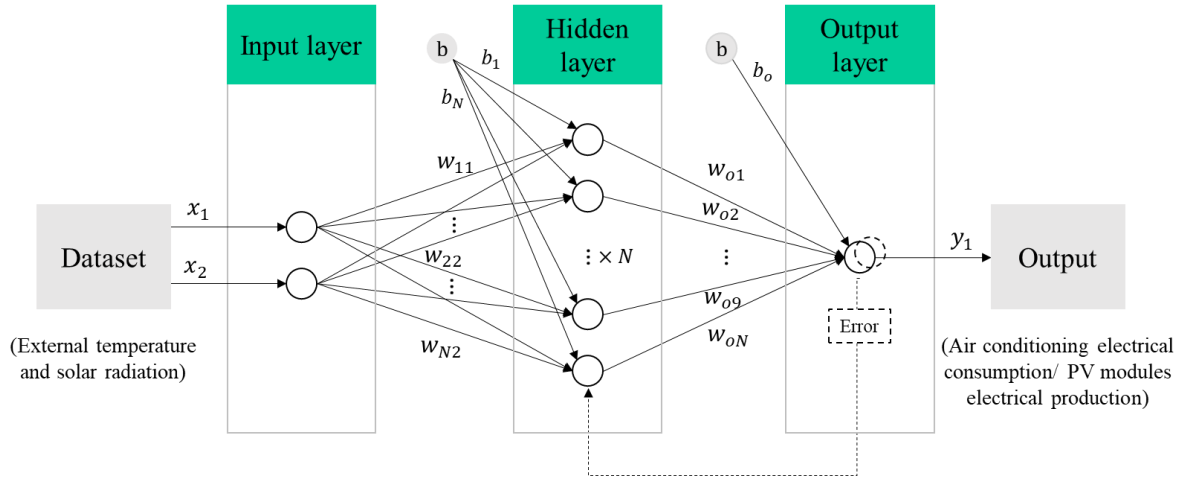

Figure 4.2. Artificial Neural Networks the ANN model architecture.

$$y = w_{oh}\, a\left(w_{hi}\, x + b_h\right) + b_o \qquad \textbf{4.1}$$

$$a\left(w_{hi}\, x + b_h\right) = \frac{2}{1 + e^{-2\left(w_{hi}\, x + b_h\right)}} - 1 \qquad \textbf{4.2}$$

where w_{hi} is the weights matrix of the connections between the inputs and the hidden neurons, w_{oh} the weights vector of the connections between the hidden and the output neurons, b_h is the vector of biases of the hidden neurons, and b_o is the bias of the output neuron.

4.3.2 Gaussian process regression GPR

Gaussian Process Regression is one of the powerful supervised machine-learning methods that showed its ability in learning and accurately predict from a small dataset. It is an application of the Gaussian Process to solve regression problems [219], defined as a collection of random variables in a way that any subset of them is jointly Gaussian. Furthersmore, Gaussian Process could represent distribution over a random function $f(x)$ evaluated at any specific input $x \in \mathbb{R}^d$. As presented in **equation 4.3**, the Gaussian process (GP) is specified by the mean function $m(x)$ (**equation 4.4**) and the kernel function or so-called covariance function $k(x, x')$ (**equation 4.5**).

$$f(x):\ GP\left(m(x), k(x, x')\right) \qquad \textbf{4.3}$$

$$m(x) = \mathrm{E}\left|\, f(x)\right| \qquad \textbf{4.4}$$

$$k(x,x') = \mathrm{E}\left[\left(f(x) - m(x)\right)\left(f(x') - m(x')\right)\right] = \mathrm{cov}\left(f(x), f(x')\right) \quad \textbf{4.5}$$

Considering that $\left\{x_i, y_i\right\}_{i=1}^{i=N} \in \left(\mathbb{R}^d, \mathbb{R}\right)$ is the training dataset and $\left\{x_{i,*}\right\}_{i=1}^{i=N} \in \mathbb{R}^d$ is the validation dataset, the distribution of Gaussian process functions is given in **equation 4.6**.

$$\begin{pmatrix} f(x) \\ f(x_*) \end{pmatrix} : N\left(\begin{pmatrix} m(x) \\ m(x_*) \end{pmatrix}, \begin{pmatrix} k(x,x) + \sigma^2 I & k(x,x_*) \\ k(x_*,x) & k(x_*,x_*) \end{pmatrix}\right) \quad \textbf{4.6}$$

with σ^2 is a GP hyper-parameter, indicating the covariance noise.

4.3.3 Support vector machine SVM

The support vector machine regression method was derived from the support vector machine early developed to solve classification problems [220]. This method seeks for a function that roughly maps the variation of the actual output parameters from the input parameters based on a training sample. The best function is the hyperplane that gathers a maximum number of points (**Figure 4.3**). Then the model becomes able to predict the variation of the output parameters from a new database containing only the input parameters.

Considering that $\left\{x_i, y_i\right\}_{i=1}^{i=N} \in \left(\mathbb{R}^d, \mathbb{R}\right)$ is the training dataset and $\left\{x_{i,*}\right\}_{i=1}^{i=N} \in \mathbb{R}^d$ is the validation dataset. The equation of the hyperplane is presented in **equation 4.7**. w and b are the model parameters.

$$f(x) = (w,x) + b \quad \textbf{4.7}$$

with w is a vector and b is a scalar. Support vector regression aims to find the best hyperplane characterized by w^* and b^* that minimizes the overall gap between f and y_i, and gives a better fitting model (**equation 4.8**).

$$\left(w^*, b^*\right) = \arg\min_{w,b} \sum_{i=1}^{n} \left(y_i - \left(w, x_i\right) - b^2\right) \quad \textbf{4.8}$$

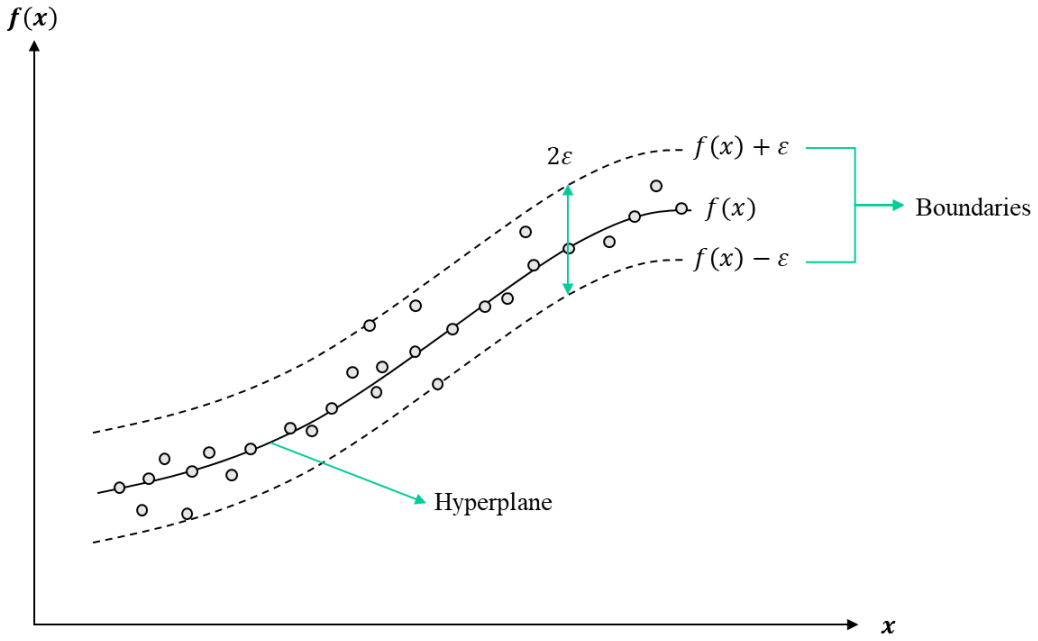

Figure 4.3. Support vector machine SVM model.

4.3.4 Boosting

Boosting is one of the competitive ensemble methods based on gathering multiple learners into an aggregate predictor, which undoubtedly leads to expanding the solutions domain [221]. Furthermore, each learner is individually different from the other and makes it possible to extract different relationships from a given data set, yielding to a much better result than a single individual predictor. Thus, it leads to a long training time. The particularity of boosting compared to the other techniques of ensemble methods is that each learner seeks to correct the weaknesses of the previous one by an iterative approach reducing then the bias, as presented in **Figure 4.4**.

Considering that $\left\{x_i, y_i\right\}_{i=1}^{i=N} \in \left(\mathbb{R}^d, \mathbb{R}\right)$ is the training dataset and $\left\{x_{i,*}\right\}_{i=1}^{i=N} \in \mathbb{R}^d$ is the validation dataset, M is the regression trees model and e is the residual (**equations 4.9** and **4.10**).

$$y_i = M_1\left(x_i\right) + d_{1i} \qquad \textbf{4.9}$$

$$d_{1i} = y_i - M_1\left(x_i\right) \qquad \textbf{4.10}$$

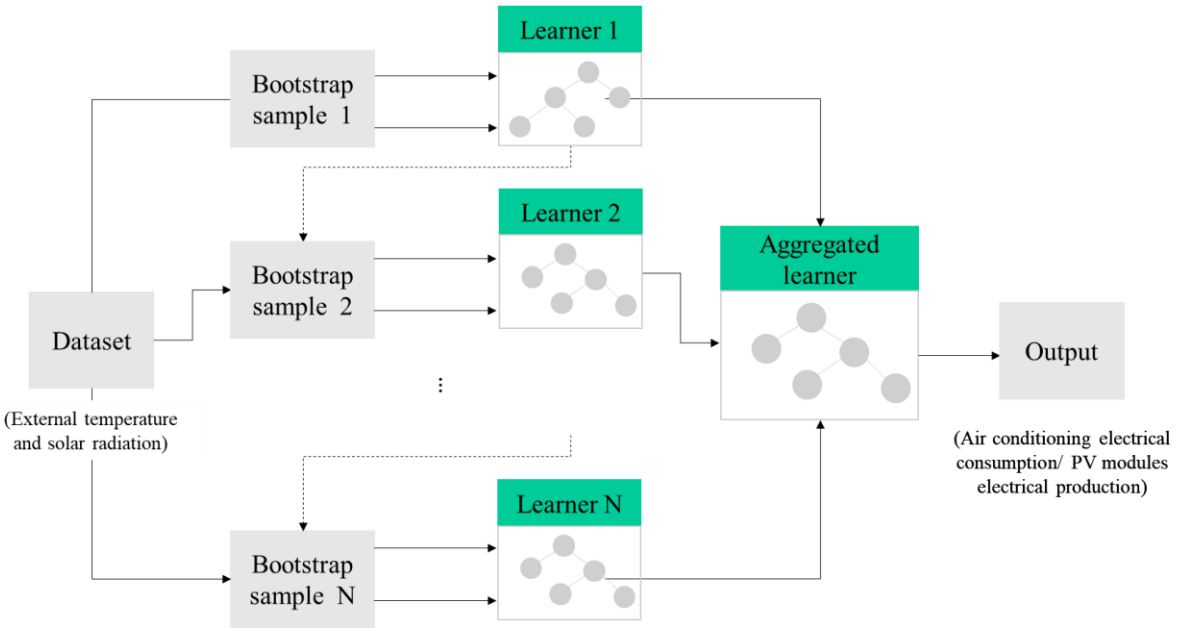

Figure 4.4. Boosting trees model.

The residual is modeled with a second one M_2, and then associated to the previous. The goal is to compensate the deficiency (d) of M_1 for a better prediction, as presented in **equations 4.11** and **4.12**. The same for the residual e_2

$$e_{1i} = M_2(x_i) + d_{2i} \qquad \textbf{4.11}$$

$$y_i^{'} = M_1(x_i) + M_2(x_i) \qquad \textbf{4.12}$$

4.4 Performance analysis

In order to assess the performance of the studied methods in predicting the desired outputs, two of the widely used statistical indicators in the literature, are used to compare the predicted and measured values: the coefficient of correlation (R) and the normalized root mean square error ($nRMSE$). These indicators are calculated based on **equations 4.13** and **4.14**, respectively.

$$R = \frac{\sum_{i=1}^{n}\left(M_i - \overline{M}\right)\cdot\left(P_i - \overline{P}\right)}{\sqrt{\left[\sum_{i=1}^{n}\left(M_i - \overline{M}\right)^2\right]\cdot\left[\sum_{i=1}^{n}\left(P_i - \overline{P}\right)^2\right]}} \cdot 100 \qquad \textbf{4.13}$$

$$nRMSE = \frac{\sqrt{1/n \sum_{i=1}^{n} (P_i - M_i)^2}}{\overline{M}} \cdot 100 \qquad \textbf{4.14}$$

with P_i and M_i are the ith predicted and measured values, and $\overline{P}$ and $\overline{M}$ are their mean values, respectively. The coefficient of correlation (R) measures the strength of the relationship between predicted and measured values; as much as the paces of the curves are similar, the correlation coefficient R is close to one. While the normalized root mean square error ($nRMSE$) allows for evaluating the dispersion of the predicted values with respect to measured ones. As much as the value of $nRMSE$ is close to zero, the models are considered better.

4.5 Comparison of four machine-learning models

4.5.1 Prediction of the air-conditioning electrical consumption

Figure 4.5 and **Figure 4.6** present the curves of variation of the air-conditioning electrical consumption during March and Mid-August to Mid-September, respectively, using the four studied machine-learning methods. The graphs show that the predicted values have a good agreement with the measured ones, with coefficients of correlation, in the validation phase and for the month of March, of about 92.46% for ANN, 91.57% for GPR, 90.76% for SVM and 91.17% for Boosting. For the period from Mid-August to Mid-September, the correlation coefficients are around 94.01%, 96.21%, 94.05% and 95.96% for ANN, GPR, SVM and Boosting, respectively.

The results obtained for the period from Mid-August to Mid-September are much better than those obtained for March. This could be explained by the fact that on summer days, the external temperature and solar radiation (inputs of the models) are the main parameters influencing the greenhouse inside microclimate and could be sufficient in predicting its air-conditioning electrical consumption. On the contrary, other climatic parameters are more intensive during March and can influence the greenhouse microclimate, e.g., wind, precipitations, sky

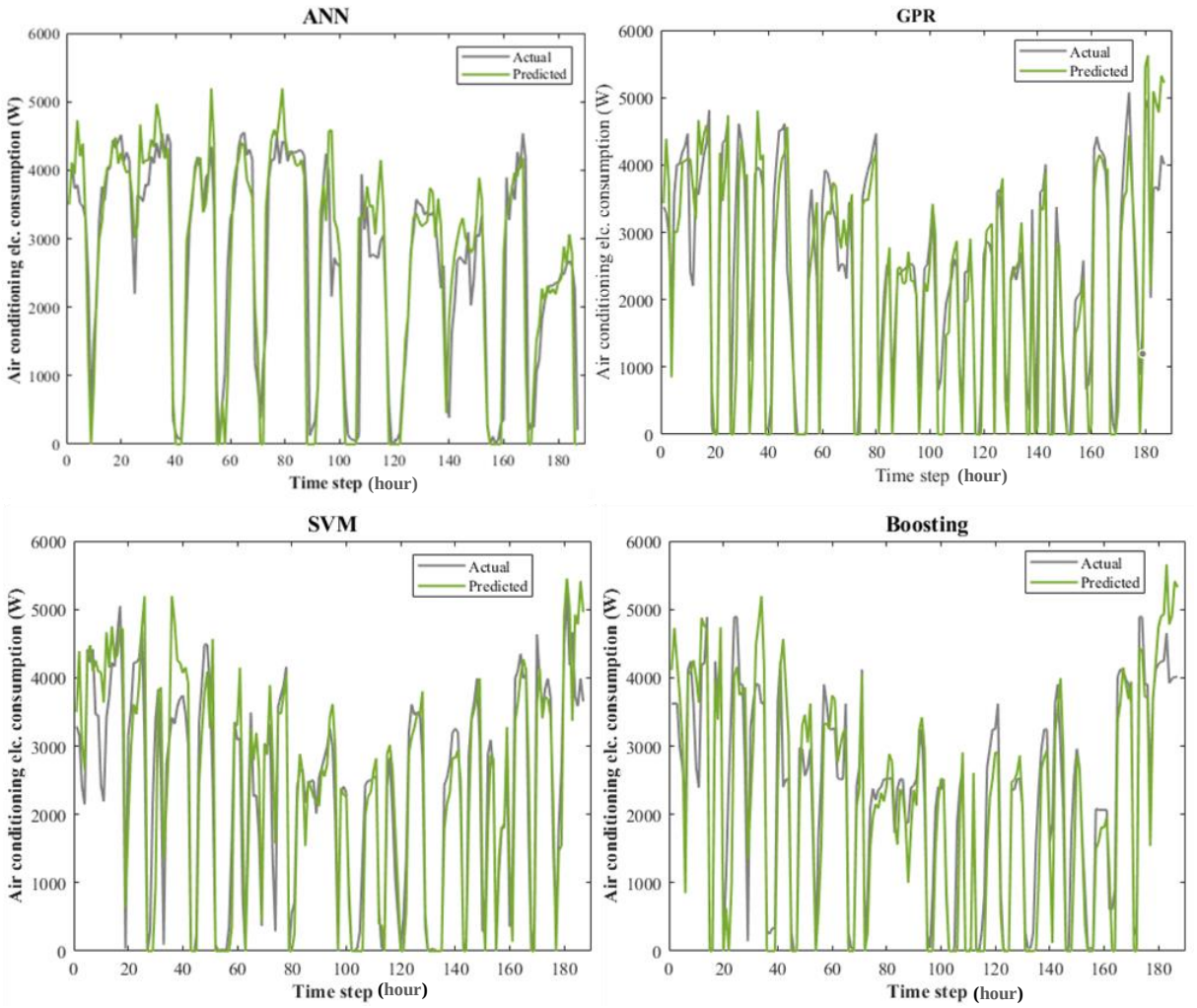

Figure 4.5. Measured and predicted air-conditioning elec. consumption for March (Validation set).

cloudiness. GPR outperforms all evaluated models in predicting the air-conditioning electrical consumption in the period from Mid-August to Mid-September. While, for March, the ANN model slightly outperforms the other models. **Table 4.1** summarizes the statistical indicators (R, and $nRMSE$) of the models in predicting the air-conditioning electrical consumption of March and Mid-August to Mid-September.

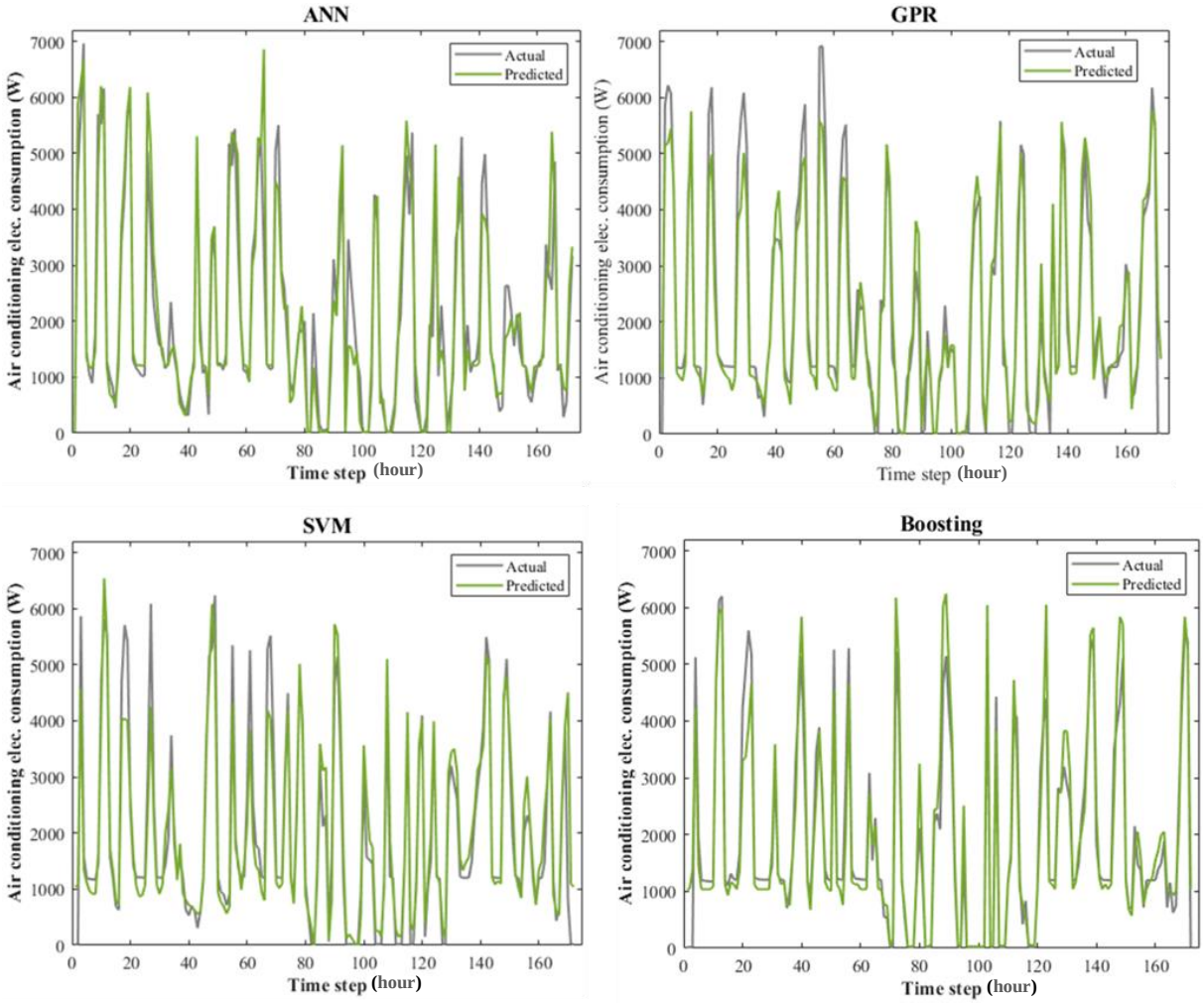

Figure 4.6. Measured and predicted air-conditioning elec. consumption of Mid-August to Mid-September (Validation set).

Table 4.1. Models' performance in predicting the air-conditioning elec. consumption (March, Mid-August to Mid-September).

Output	Period	Model		Training		Validation	
				R (%)	$nRMSE$ (%)	R (%)	$nRMSE$ (%)
Air-conditioning electrical consumption	March 2020	ANN	2-10-1	97.8712	18.8831	92.4610	12.9642
		GPR	$\sigma = 1.5$	91.2684	24.4969	91.5676	15.7289
		SVM	$\varepsilon = 6.35$	91.0673	24.0926	90.7590	15.4800
		Boosting	36 learners	91.6594	22.6429	91.1679	16.8750
	Mid-August/ Mid-September 2020	ANN	2-10-1	97.6209	24.9683	95.0121	15.0257
		GPR	$\sigma = 4.7$	96.3606	19.6298	96.2057	12.8562
		SVM	$\varepsilon = 2.49$	95.5177	22.3990	94.0457	15.4998
		Boosting	10 learners	97.7934	15.3439	95.9600	13.8336

4.5.2 Prediction of the PV modules' electrical production

Figure 4.7 and **Figure 4.8** present the curves of variation of the PV modules' electrical production, during the months of March and Mid-August to Mid-September, respectively, using the four studied machine-learning methods. The graphs show that the predicted values have a good agreement with the measured ones, with coefficients of correlation, in the validation phase and for the month of March, of about 96.12% for ANN, 92.38% for GPR, 91.29% for SVM and 91.88% for Boosting. For the period from Mid-August to Mid-September the coefficients of correlation are around 96.33%, 94.21%, 93.55% and 94.13% for ANN, GPR, SVM and Boosting, respectively.

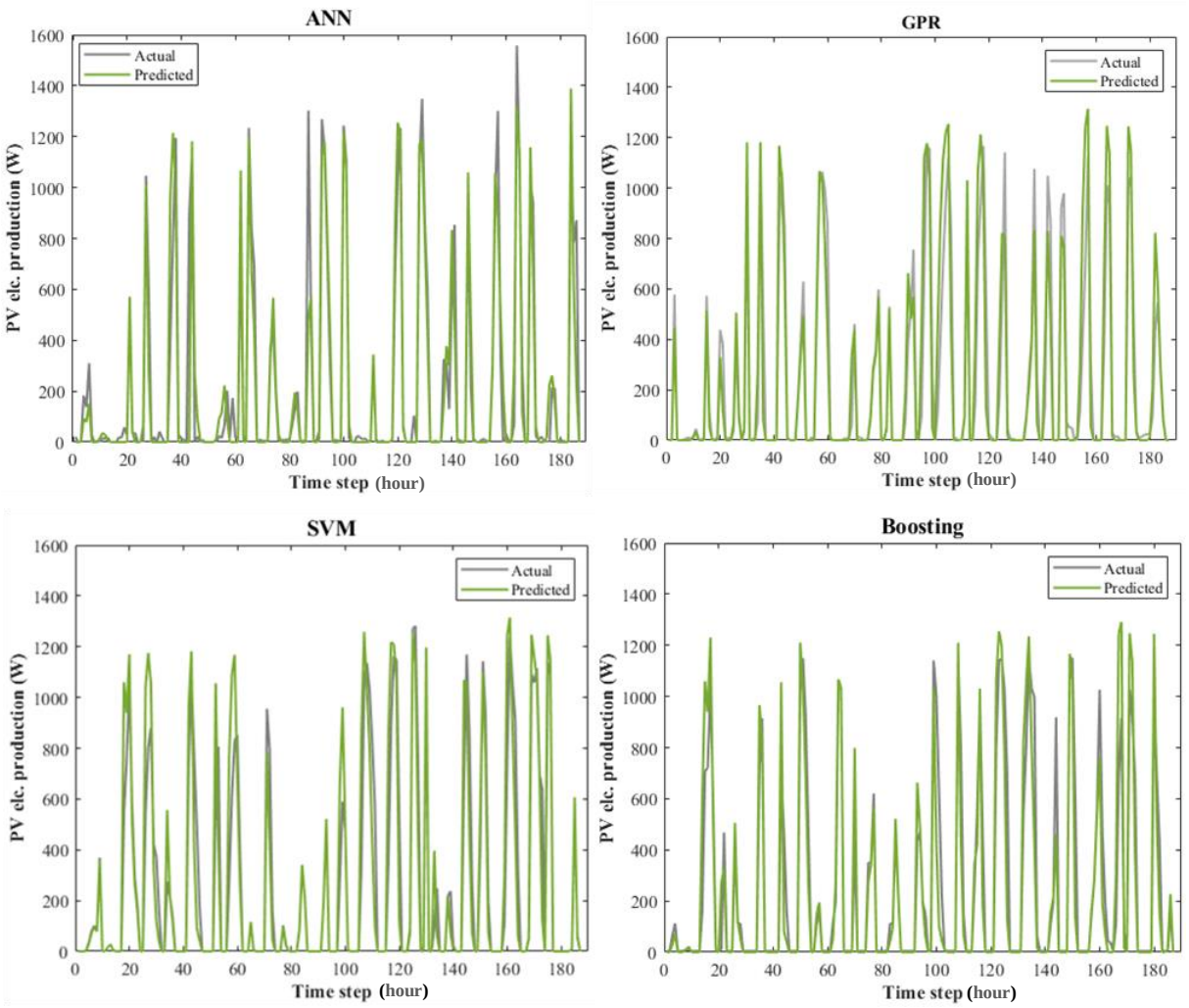

Figure 4.7. Measured and predicted PV modules elec. production of March (Validation set).

Comparing the coefficients of correlation and considering the validation sets, the ANN model outperforms the studied ones in predicting the PV modules' electrical production, in both periods, especially for the month of March. The ANN model is followed by GPR, then Boosting trees and finally SVM method. As for the prediction of the air-conditioning electrical consumption, the models have better performance in predicting the PV modules' electrical production during the period of Mid-August to Mid-September and the same explanation as previously could be provided.

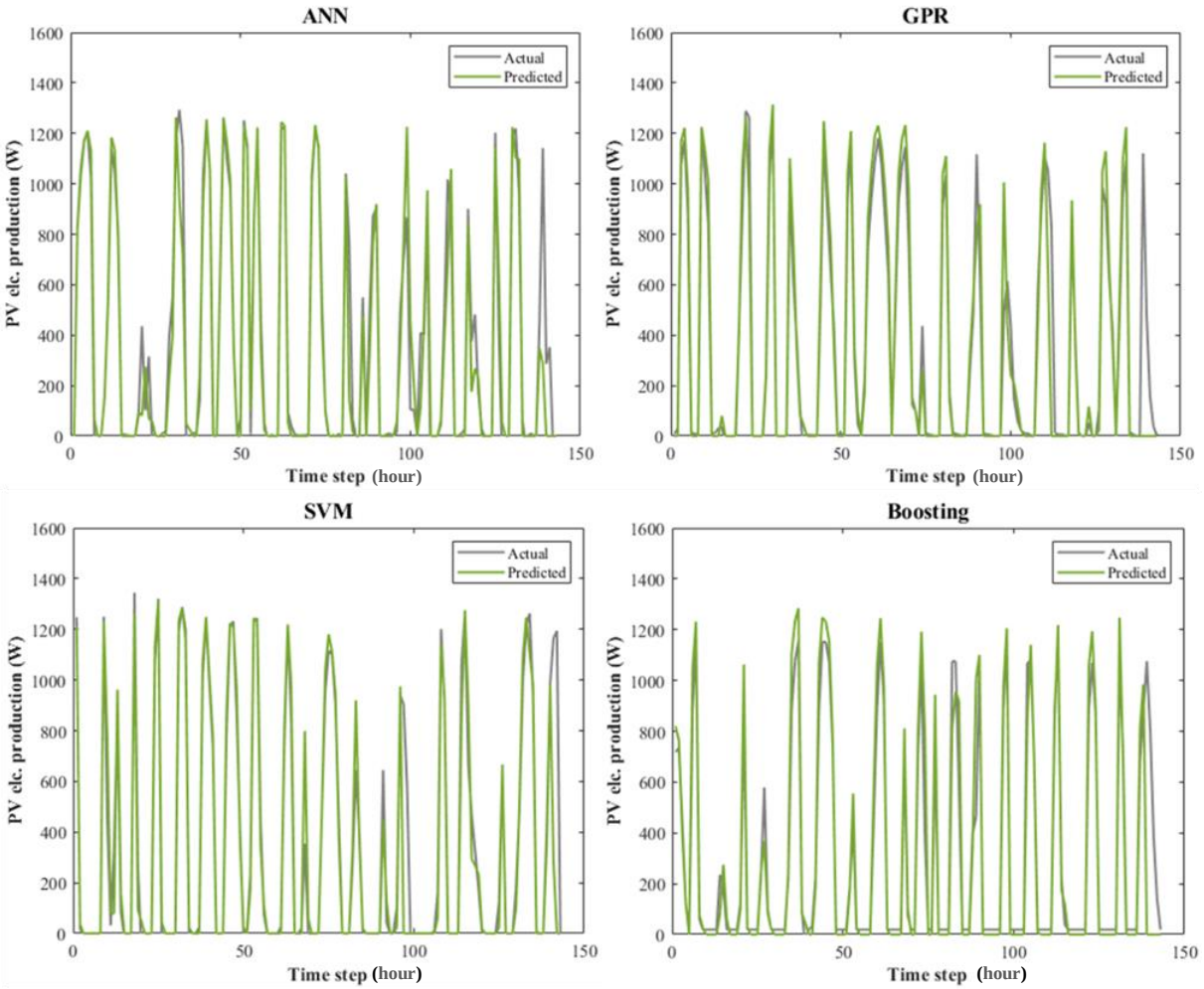

Figure 4.8. Measured and predicted PV modules elec. production of Mid-August to Mid-September (Validation set).

Table 4.2 presents the models' performance in predicting the PV modules' electrical production in the month of March and from Mid-August to Mid-September.

Table 4.2. Models' performance in predicting the PV modules' electrical production (March, Mid-August to Mid-September).

Output	Period	Model		Training		Validation	
				R (%)	$nRMSE$ (%)	R (%)	$nRMSE$ (%)
PV modules' electrical production	March 2020	ANN	2-10-1	97. 3864	33.1328	96. 3285	22.0497
		GPR	$\sigma = 3.97$	92.6129	42.7174	92.3836	21.4978
		SVM	$\varepsilon = 0.7150$	92.7159	42.7893	91.2903	23.3442
		Boosting	39 learners	94.1176	35.9266	91.8845	24.7175
	Mid-August/ Mid-September 2020	ANN	2-10-1	97. 6136	30.0094	96. 1150	20.2251
		GPR	$\sigma = 4.41$	95.0153	24.9565	94.2151	13.6115
		SVM	$\varepsilon = 7.65$	95.3025	23.6884	93.5519	17.3420
		Boosting	36 learners	95.6063	21.5596	94.1332	16.1418

4.5.3 Comparison and analysis of the four methods

The normalized root mean square error (nRMSE) is also a good statistical indicator in evaluating the models' performance. In this study (**Figure 4.9**), the nRMSE varies between 12.86% (prediction of the air-conditioning electrical consumption in the period from Mid-August to Mid-September using the GPR model) to 24.72% (prediction of the PV modules'

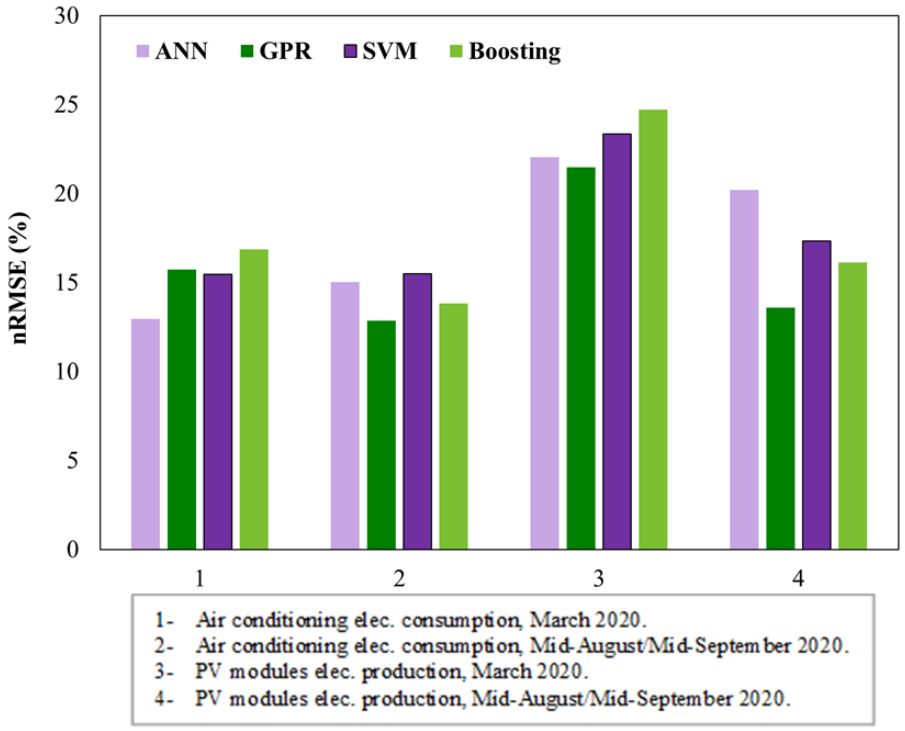

Figure 4.9. Models' normalized root mean square error (*nRMSE*).

electrical production in March using the Boosting trees method), as presented in **Figure 4.9**. According to several studies [222]–[224], the selected models have acceptable to good performances $(10\% < nRMSE < 30\%)$. The nRMSE values vary from 12.96% to 22.05% for the ANN, from 12.86% to 21.50% for the GPR, from 15.48% to 23.34% for the SVM and from 13.83% to 24.72% for the Boosting trees method.

As a general conclusion, the best performance is obtained when using the ANN and GPR models. Moreover, the SVM method has shown moderate performance. On the contrary, the boosting trees method has good performance in the training phase, but it decreases considerably in the validation phase compared to the other methods. Indeed, the basics on which the boosting trees method is based-on can lead to an over-fitting where the model also learns the noise of the measurements. This problem can be more noticeable when the size of the database is small, which is the case in this study. That explains the relatively low performance obtained using the boosting trees method compared to the other methods. Furthermore, it must be noted that the training time of the boosting trees method is longer than that of the others.

4.6 Impact of number of neurons in the hidden layer on ANN performance

Based on the results presented in **section 4.5**, the ANN model proved its ability to predict the greenhouse air-conditioning electrical consumption and PV modules' electrical production. For this reason, the ANN model is selected to further study its performance. In this section, the impact of the number of neurons in the hidden layer is investigated. The number of neurons has been varied from 1 to 35 (1 and 5 to 35 with a step of 5) and the performance of the different architectures is analyzed based on the two statistical indicators (coefficient of correlation (R), normalized root mean square error (nRMSE) (**section 4.4**)). The obtained results are presented in **Table 4.3**.

It can be observed from the obtained results that the model performance significantly depends on the number of neurons in the hidden layer. In some cases, an unpredictable drop in the model performance occurs. Considering the validation set and for predicting the air-conditioning electrical consumption during March, the coefficient of correlation varies between 87.6605% and 92.1973% for 35 and ten neurons in the hidden layer, respectively. For the period from Mid-August to Mid-September, the correlation coefficient varies from 95.1951% to 96.5731% when 35 and ten neurons in the hidden layer are used. An unpredictable model performance degradation has been observed in predicting the PV modules' electrical production. For the month of March, the correlation coefficients vary between 71.0645% for 20 neurons and

95.2634% for 10 neurons in the hidden layer. During the period from Mid-August to Mid-September, correlation coefficient values ranging from 23.5242% to 95.5006% are obtained using 25 and ten neurons, respectively.

Table 4.3. ANN performance in predicting the greenhouse energy demand and production, depending on the number of neurons in the hidden layer.

Output	Period	Number of neurons in the hidden layer	Training		Validation	
			R (%)	$nRMSE$ (%)	R (%)	$nRMSE$ (%)
Air-conditioning electrical consumption	March 2020	1	96.0876	21.2027	90.2031	15.0480
		5	96.4810	20.7149	90.5267	13.9264
		10	96.5702	20.5640	92.1973	12.6008
		15	95.6823	21.4773	91.5699	14.1104
		20	95.8284	21.2122	91.4663	14.1312
		25	95.7828	21.2740	91.3883	14.1935
		30	95.5885	21.5656	91.0010	14.6094
		35	95.6460	21.4440	87.6605	18.8746
	Mid-August/ Mid-September 2020	1	95.4220	20.9422	95.6013	14.2095
		5	95.8402	21.4503	96.1833	14.9054
		10	96.0392	19.5707	96.5731	12.9045
		15	95.8454	19.9808	96.1685	13.4425
		20	95.8781	19.8838	96.3588	12.9702
		25	96.3799	18.6924	96.5700	12.4985
		30	96.0796	19.4021	96.4795	12.8424
		35	96.2213	19.2038	95.1951	15.1745
PV modules' electrical production	March 2020	1	94.8820	41.6161	94.7744	28.1289
		5	96.3270	37.8355	94.8671	28.5181
		10	96.6762	35.4094	95.2634	27.7601
		15	83.6912	90.2940	79.8312	77.5459
		20	69.9525	93.3210	71.0645	76.5045
		25	92.8599	38.4554	92.5620	34.4430
		30	86.3625	95.3020	86.6745	83.5030
		35	93.2805	46.9585	92.3550	37.7044
	Mid-August/ Mid-September 2020	1	95.0300	34.1438	93.0794	27.5976
		5	97.2531	33.2603	94.8217	26.0549
		10	97.4269	32.8625	95.5006	25.4901
		15	80.3213	93.9483	76.9981	71.0043
		20	95.5039	32.8047	93.9073	26.3783
		25	20.1419	94.2160	23.5242	89.6823
		30	90.3367	63.5630	88.8636	52.2462
		35	86.3608	78.5831	82.4817	58.7822

Figure 4.10 represents the variation of nRMSE values of the studied the ANN model with different numbers of neurons in the hidden layer. As for the coefficient of correlation and based on the graph, it can be observed that the nRMSE strongly depends on the number of neurons in the hidden layer with a random variation. The nRMSE values range from 12.4958% in predicting the air-conditioning electrical consumption during March and 89.6823% in predicting the PV electrical production in the period from Mid-August to Mid-September using the ANN model with 25 neurons in the hidden layer in both cases. A suitable number of neurons cannot be established, regardless of the database; the optimal number of neurons in a specific case can be the worst one in another case. In the present study, ten neurons in the hidden layer are found to be the optimal number when predicting the air-conditioning electrical consumption in the period from Mid-August to Mid-September and the PV electrical production in both studied periods. While for predicting the air-conditioning electrical consumption during March, 25 is the optimal number of neurons.

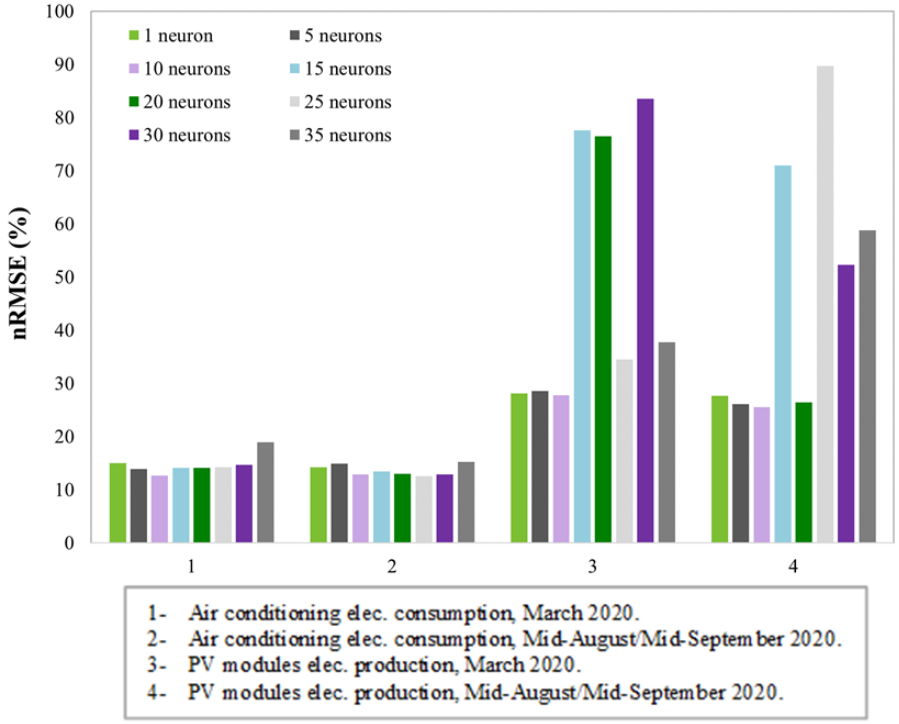

Figure 4.10. ANN model normalized root mean square error ($nRMSE$) depending on the number of neurons in the hidden layer.

4.7 Performance assessment of a hybrid model ANN-BST

According to the results presented in **section 4.5**, the boosting trees model has been found to have good performance in the training phase. However, it decreases considerably in the validation phase compared to the other methods. For this reason, a hybrid model of boosting

combined with ANN is proposed and tested. Two configurations are investigated, namely hybridization in series and in parallel.

A “back propagation” multi-layer perceptron neural network is considered, with an architecture (2-10-1) based on one input layer with two neurons (external temperature and global solar radiation), one hidden layer with ten neurons and one output layer with one neuron (air-conditioning electrical consumption or PV modules’ electrical production). For the boosting method, different combinations of the model’s hyperparameters are automatically tested. The combination generating a minimum mean squared error (MSE) is, then, selected. For the prediction of both the air-conditioning electrical consumption and the PV modules’ electrical production, the dataset is divided into 70% for training and 30% for validation.

4.7.1 Series hybrid model

First, the ANN model is used to predict the air-conditioning electrical consumption / the PV modules’ electrical production. Then the predicted variable in both training and validation phases has been inserted into the database used as input for boosting method. **Figure 4.11** provides an overview of the series hybridization approach.

In order to analyze the hybrid model performance, the correlation coefficient and the normalized root mean square error are calculated. **Table 4.4** summarizes the series model performance in predicting the air-conditioning electrical consumption and the PV modules’ electrical production in both considered periods: March and the period from Mid-August to Mid-September. For the validation phase, correlation coefficients of about 93.5760% and 97.7145% are obtained when predicting the air-conditioning electrical consumption during March and the period from Mid-August to Mid-September, respectively. While the PV modules’ electrical production is predicted with correlation coefficients of about 92.4286% and 98.9286% during March and the period from Mid-August to Mid-September, respectively. As for the previously studied models, the results obtained for the period from Mid-August to Mid-September are much better than those obtained for March.

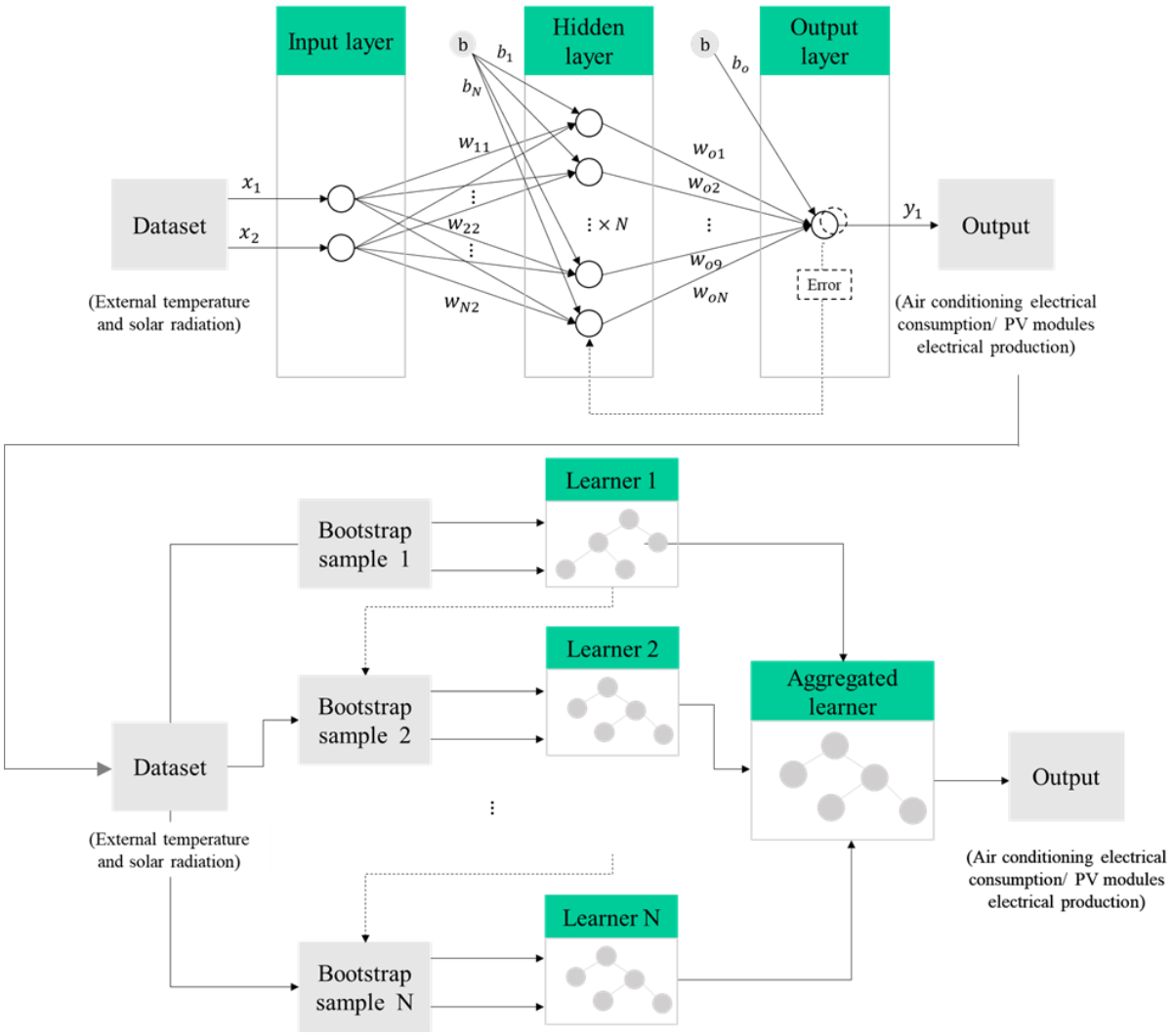

Figure 4.11. Series hybridization of ANN and Boosting models (ANN-BST).

Table 4.4. Series hybrid model performance in predicting the air-conditioning electrical consumption and PV modules' electrical production.

Output	Period	Training		Validation	
		R (%)	$nRMSE$ (%)	R (%)	$nRMSE$ (%)
Air-conditioning electrical consumption	**March 2020**	93.6888	20.0101	93.5760	14.8715
	Mid-August/ Mid-September 2020	98.6496	14.0946	97.7145	11.3474
PV modules' electrical production	**March 2020**	96.2552	29.5647	92.4286	29.6908
	Mid-August/ Mid-September 2020	98.7064	22.0117	98.9286	14.8769

The nRMSE values vary between 11.3474% and 29.6908% for the prediction of the air-conditioning electrical consumption during the period from Mid-August to Mid-September and the PV modules' electrical production in March. By comparing the nRMSE values obtained

using the hybrid model and the ones obtained using ANN and boosting models separately, the hybrid model gives better performance in the prediction of air-conditioning electrical consumption (11.3474% for the hybrid model, 12.9642% for ANN, and 16.8750% for boosting trees) and the PV modules' electrical production (14.8769% for the hybrid model, 20.2251% for ANN, and 16.1418% for boosting trees) during the period from Mid-August to Mid-September. It can also be observed that the common point between the two cases is that in the separated models, the boosting trees show lower nRMSE than the ANN model. For the prediction of the air-conditioning electrical consumption during March, the nRMSE value obtained using the hybrid model (14.8715%) is in between the values obtained using the ANN model (12.9642%) and boosting trees model (16.8750%). During the same period, a nRMSE of about 29.6908% is obtained when predicting the PV modules' electrical production.

4.7.2 Parallel hybrid model

In this study, the parallel hybrid model approach is the parallel prediction of the output (air-conditioning electrical consumption/ PV modules' electrical production) using two different predictors: the first one based on the artificial neural networks method and the second one based on boosting trees method. To follow, the predictors are aggregated by calculating the average of the predictions. **Figure 4.5** presents the parallel hybridization of ANN and boosting trees methods.

Table 4.5 summarizes the parallel hybrid model performance in predicting the air-conditioning electrical consumption and the PV modules' electrical production in both considered periods: March and the period from Mid-August to Mid-September. For the training phase, the correlation coefficient ranges from 92.5210% (prediction of air-conditioning electrical consumption during March) and 99.0828% (prediction of PV modules' electrical production during the period from Mid-August to Mid-September). While in the validation phase, correlation coefficients of about 93.7171% and 98.1997% are obtained when predicting the air-conditioning electrical consumption during March and the period from Mid-August to Mid-September, respectively. For the PV modules' electrical production is predicted with correlation coefficients of about 92.0188% and 97.5347% during March and the period from Mid-August to Mid-September, respectively. As for the previously studied models, the results obtained for the period from Mid-August to Mid-September are much better than those obtained for March.

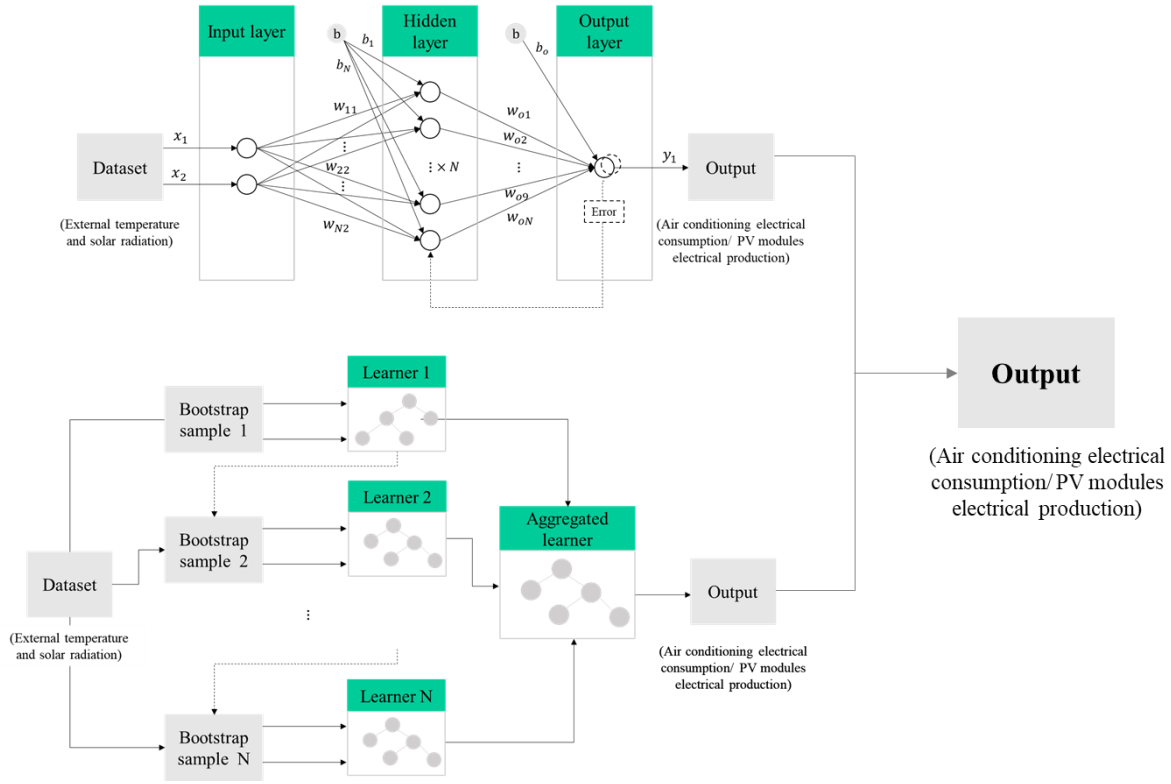

Figure 4.12. Parallel hybridization of ANN and boosting models (ANN-BST).

Table 4.5. Parallel hybrid model performance in predicting the air-conditioning electrical consumption and PV modules' electrical production.

Outputs	Period	Training		Validation	
		R (%)	$nRMSE$ (%)	R (%)	$nRMSE$ (%)
Air-conditioning electrical consumption	**March 2020**	92.5210	21.3770	93.7171	14.3820
	Mid-August/ Mid-September 2020	97.8790	16.4384	98.1997	10.6462
PV modules' electrical production	**March 2020**	96.2491	29.5348	92.0188	28.4283
	Mid-August/ Mid-September 2020	99.0828	13.8663	97.5347	19.8485

Regarding the nRMSE value and as for the series hybrid model, sometimes the parallel hybrid model gives better performance than ANN and boosting trees methods separately, sometimes less and sometimes between the two. For the prediction of the air-conditioning electrical consumption during the period from Mid-August to Mid-September, the hybrid parallel model has an nRMSE value of about 10.6462%, better than both ANN (15.0257%) and boosting

trees(13.8336%). A higher nRMSE value is obtained using the parallel hybrid model (28.4283%) compared to ANN (22.0497%) and boosting (24.7175%) separated when predicting the PV modules' electrical production. The nRMSE value of the parallel hybrid model is in between the ones of the two separated models in the cases of the prediction of the air-conditioning electrical consumption during March (14.3820%) and PV modules' electrical production in the period from Mid-August to Mid-September (19.8485%).

4.7.3 Comparison and analysis of the hybrid approaches

As presented in **Figure 4.13,** the nRMSE values vary from 11.3474% to 29.6908% for the series approach and from 10.6462% to 28.4283% for the parallel approach. The models have acceptable to good performances ($10\% < nRMSE < 30\%$). The parallel hybrid model slightly outperforms the series hybrid model in predicting the PV modules' electrical production in March, the air-conditioning electrical consumption during March and the period from Mid-August to Mid-September. Except for the prediction of PV modules' electrical consumption during the period from Mid-August to Mid-September, where the series hybrid model slightly outperforms the parallel hybrid model.

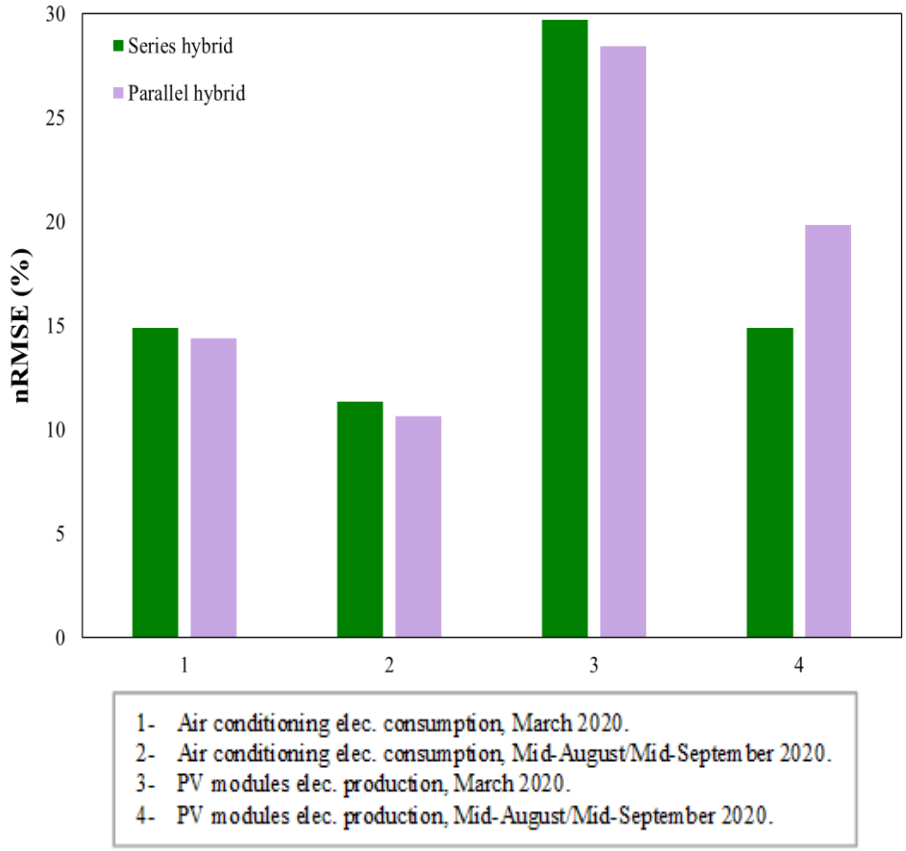

Figure 4.13. Hybrid models normalized root mean square error (*nRMSE*) depending on the approach (series and parallel).

4.8 Conclusions

Predicting the greenhouse microclimate and the energy uses is of great interest and can be used to adequately manage needs and resources. In addition, it can be useful to apply preventive measures to avoid extreme indoor climate parameters and protect crops from damage. This chapter focuses on predicting the air-conditioning electrical consumption and the photovoltaic modules' electrical production based on different supervised machine-learning methods, namely: Artificial Neural Networks (ANN), Gaussian Process Regression (GPR), Support Vector Machine (SVM) and boosting. Then, the effect of the number of neurons in the hidden layer of the ANN model is investigated. Thereafter a hybrid model based on ANN and boosting methods is proposed, adopting two approaches, series and parallel hybridization. The models' performance are compared based on two statistical indicators: the coefficient of correlation (R) and the normalized root mean square error (nRMSE). The main conclusions can be summarized as follows:

(1) The four considered models have acceptable to good performances with $10\% < nRMSE < 30\%$. The prediction of both air-conditioning electrical consumption and PV modules' electrical production showed better performance in the period of Mid-August to Mid-September compared to those obtained in the month of March. This can be explained by the fact that in the period of March the greenhouse microclimate and the PV module production are influenced by other weather parameters than external temperature and solar radiation (wind velocity, precipitations, sky cloudiness…). On the contrary, during the period of Mid-August to Mid-September the external temperature and solar radiation can be considered as the major influencing weather parameters.

(2) Considering the two statistical indicators, the ANN and GPR methods showed the best performances, while the boosting method the worst ones. It can be concluded that, the boosted learning can lead to an over-fitting, especially when a small dataset is available, with a longer training time. In fact, the model also learns the noise of the measurements, which decrease the performance in the validation phase. Thus, ANN and GPR methods can be recommended for controlling the greenhouse and predicting its energy uses when having a small dataset.

(3) The performance of the ANN model significantly depends on the number of neurons in the hidden layer; in some cases an unpredictable drop in the model performance occurs.

Thus to optimize the ANN model performance it is important to test different numbers of neurons in the hidden layer.

(4) The hybrid model, including series and parallel approaches, sometimes gives better performance than ANN and boosting trees methods separately, sometimes less and sometimes between the two.

A part of the work presented in this chapter has been published in the following paper:

1. Ouazzani Chahidi, L., Fossa, M., Priarone, A., & Mechaqrane, A. (2021). Evaluation of Supervised Learning Models in Predicting Greenhouse Energy Demand and Production for Intelligent and Sustainable Operations. Energies, 14(19), 6297.

General Conclusion

Greenhouse cultivation is one of the most effective and widely used methods, which allows for providing a suitable environment for plants growth. The persisting demand for energy in greenhouses represents the main constraint for this cultivation method. Thus, the rational use of energy in greenhouses can significantly decrease their operational costs. Integrating passive technologies, renewable energies and intelligent management strategies can significantly contribute reducing energy consumption.

This Ph.D. thesis aims to reduce the energy consumption and production costs of agricultural greenhouses in the Mediterranean region (Albenga, Northwest Italy (as a part of a traineeship in the Department of Mechanical, Energy, Management and Transportation at the University of Genova, Italy) and the six Moroccan climatic zones) in order to contribute to promoting the energy, economic and environmental valuation of agricultural and agrifood-industry products. Different energy-saving strategies are investigated: the selection of suitable greenhouse design (shape, envelope material and orientation); the integration of passive techniques (thermal insulation blankets, shading/reflecting system, and operable windows for controlled natural ventilation); the integration of renewable energies (semi-transparent photovoltaic panels and ground-coupled heat pump); the integration of intelligent management (artificial intelligence methods to predict the air conditioning electrical consumption and the photovoltaic modules electrical production).

The main conclusions of the present work can be drawn as follows:

(1) In the first chapter, a comprehensive review is presented, of some 200 recent studies conducted on greenhouse cultivation techniques devoted to energy-saving and environmental sustainability. The main research fields are discussed and sectors for research works are suggested.

(2) The second chapter presents a dynamic model created in EnergyPlus environment and validated with reference to the case study of the innovative high-efficiency SamLab greenhouse, located in Albenga, Italy. The validation results show that the model provides a good estimation and it can be used to test and validate new energy management strategies. The results also quantify the energy-saving potential of the studied strategies and show the importance of integrating passive technologies and renewable energies in greenhouse cultivation for a sustainable agriculture (the

controlled shading/reflecting system and the operable windows can save about 5% and 14% of the energy needs, respectively; the ground coupled heat pump saves around 21% of the primary energy consumption of a traditional air-conditioning system; the semi-transparent PV modules provide about 16% of the greenhouse energy demand, throughout the year).

(3) The third chapter evaluates different greenhouse designs (shapes, cover materials and orientations), in order to select the most suitable one for the six Moroccan climatic zones. After selecting the optimal combination in each zone, the greenhouses energy efficiency is further improved by using nighttime operating thermal insulation and operable windows. It has been found that the greenhouse design and the energy-saving strategies have a significant impact on the greenhouse annual air-conditioning cost: the optimal combination of greenhouse shape/cover material saves on average 24.5%; the optimal greenhouse orientation saves on average 3%; the nighttime insulation saves between 13% and 17% depending on the climatic zone; the controlled natural ventilation saves between 10.3% and 21.8% depending on the climatic zone. Finally, it has been shown that zone 1 (Agadir City) has a minimal air conditioning energy cost (142.88MAD/year/m²).

(4) Finally, the fourth chapter presents the prediction of the greenhouse energy uses, namely the semi-transparent PV panels' electrical production and the ground-coupled heat pump electrical consumption. This is of great interest to adequately manage greenhouse needs and resources. For this purpose, four machine-learning methods (ANN, GPR, SVM and boosting trees) are first compared. Furthermore, the effect of the number of neurons in the hidden layer of ANN model is investigated. Finally, a hybrid model based on the combination (in series and in parallel) of ANN and boosting trees methods is proposed and analyzed. The results showed that the studied models have acceptable to good performances with $10\% < nRMSE < 30\%$.

In terms of perspectives, this work can open new research horizons:

(1) Test and validate new energy management strategies in different climate conditions;

(2) Study the impact of other greenhouse parameters on energy consumption;

(3) Implementation of prediction methods in the greenhouse control system;

(4) Study and optimization of a hybrid solar system: heating of greenhouses-drying of agricultural products;

Publications

1. Ouazzani Chahidi, L., Fossa, M., Priarone, A., & Mechaqrane, A. (2021). Energy saving strategies in sustainable greenhouse cultivation in the mediterranean climate–A case study. Applied Energy, 282, 116156.
2. Ouazzani Chahidi, L., Fossa, M., Priarone, A., & Mechaqrane, A. (2021). Greenhouse cultivation in Mediterranean climate: Dynamic energy analysis and experimental validation. Thermal Science and Engineering Progress, 26, 101102.
3. Ouazzani Chahidi, L., Fossa, M., Priarone, A., & Mechaqrane, A. (2021). Evaluation of Supervised Learning Models in Predicting Greenhouse Energy Demand and Production for Intelligent and Sustainable Operations. Energies, 14(19), 6297.
4. Ouazzani Chahidi, L., & Mechaqrane, A. (2022). Greenhouse Design Selection in Moroccan Climatic Conditions. In WITS 2020, Lecture Notes in Electrical Engineering (pp. 639-648). Springer, Singapore.
5. Ouazzani Chahidi, L., & Mechaqrane, A. (2021). Energetic and economic analysis for improving greenhouse energy efficiency. Journal of Energy Systems, 5(4), 296-305.
6. Ouazzani Chahidi, L., & Mechaqrane, A. Selection of the suitable greenhouse orientation on the basis of energy saving. 9th Eur. Conf. Ren. Energy Sys. 21-23 April 2021, Istanbul, Turkey.
7. Bounoua, Z., Ouazzani Chahidi, L., & Mechaqrane, A. (2021). Estimation of daily global solar radiation using empirical and machine-learning methods: A case study of five Moroccan locations. Sustainable Materials and Technologies, 28, e00261.
8. Ait Ali, A., Ouazzani Chahidi. L., Mechaqrane, A., Charroud, M., Ouahzizi, & Y., Choukrad, J., (2022) Selection of suitable concentrated solar power farm's locations A Case study: Fez-Meknes Region, Morocco. In WITS 2021 (ID. 181). E3S Web of Conferences (eISSN: 2267-1242).
9. El ALAOUI, M., Ouazzani Chahidi, L., Rougui, M., Mechaqrane, A., & Senhaji, A. "Comparison of CFD and Machine Learning Methods on Predicting Greenhouse Microclimate Parameters with the Assessment of Seasonality Impact on Machine Learning Performance" (under review in journal of Biosystems Engineering).
10. El ALAOUI, M., Ouazzani Chahidi, L., Rougui, M., Lemrani, A., & Mechaqrane, A., "Evaluation of Machine Learning-Based Approach and Statistical-Based Approach in

predicting the energy consumption of an administrative building" (under review in journal of Building Engineering).

11. Ouazzani Chahidi, L., Fossa, M., Priarone, A., & Mechaqrane, A. A "Comprehensive Review on Greenhouse Cultivation Techniques devoted to energy saving and environmental sustainability" (submitted to Renewable and Sustainable Energy Reviews journal).

Oral presentations and posters

1. Poster presentation, "Energy saving strategies in protected agriculture". The 7th Doctoral Days, the Intelligent Systems, Georesources and Renewable Energies (SIGER) Laboratory, December 11, 2021, Fez, Morocco.
2. "Selection of the Suitable Greenhouse Orientation on the basis of Energy Saving". The 9th European Conference on Renewable Energy Systems (ECRES 2021). April 21-22, 2021, Istanbul, Turkey.
3. "Energy saving strategies in greenhouse cultivation" The 6th Doctoral Days, the Intelligent Systems, Georesources and Renewable Energies (SIGER) Laboratory, February 20, 2021, Fez, Morocco .
4. « Greenhouse Design Selection under the Climatic Conditions of Fez, Morocco ». The 6th International Conference on Wireless Technologies, Embedded and Intelligent Systems (wits-2020). October 14-16, 2020, Fez, Morocco.
5. Valorisation des produits agricoles par intégration des énergies renouvelables et des techniques de récupération. The 5th Doctoral Days, the Intelligent Systems, Georesources and Renewable Energies (SIGER) Laboratory, December 14, 2019, Fez, Morocco.

References

[1] *The State of Food Security and Nutrition in the World 2020*. FAO, IFAD, UNICEF, WFP and WHO, 2020. doi: 10.4060/ca9692en.

[2] *World Population Clock: 7.8 Billion People (2020) - Worldometer*. Accessed: Nov. 23, 2020. [Online]. Available: https://www.worldometers.info/world-population/

[3] FAO, "THE STATE OF FOOD AND AGRICULTURE," 2016.

[4] W. Baudoin *et al.*, *Good Agricultural Practices for greenhouse vegetable crops*. 2013. doi: 10.1201/b13737-8.

[5] Presses de Sciences Po, Ed., *MediTERRA 2012 (english): The mediterranean diet for sustainable regional development.* Paris: CIHEAM, 2012.

[6] M. Canakci and I. Akinci, "Energy use pattern analyses of greenhouse vegetable production," *Energy*, vol. 31, no. 8–9, pp. 1243–1256, Jul. 2006, doi: 10.1016/j.energy.2005.05.021.

[7] M. Omid, F. Ghojabeige, M. Delshad, and H. Ahmadi, "Energy use pattern and benchmarking of selected greenhouses in Iran using data envelopment analysis," in *Energy Conversion and Management*, Jan. 2011, vol. 52, no. 1, pp. 153–162. doi: 10.1016/j.enconman.2010.06.054.

[8] Q. Ali, M. R. Yaseen, and M. T. I. Khan, "Energy budgeting and greenhouse gas emission in cucumber under tunnel farming in Punjab, Pakistan," *Scientia Horticulturae*, vol. 250, pp. 168–173, May 2019, doi: 10.1016/j.scienta.2019.02.045.

[9] S. A. Kalogirou, *Solar Energy Engineering: Processes and Systems*. Academic Press, 2013.

[10] M. Planck, "On the Law of Distribution of Energy in the Normal Spectrum," p. 11.

[11] H. C. Eckstrom and Christoph. Schmelzer, "The Wien Effect: Deviations of Electrolytic Solutions from Ohm's Law under High Field Strengths.," *Chem. Rev.*, vol. 24, no. 3, pp. 367–414, Jun. 1939, doi: 10.1021/cr60079a001.

[12] "Reference Air Mass 1.5 Spectra." https://www.nrel.gov/grid/solar-resource/spectra-am1.5.html (accessed Apr. 11, 2022).

[13] D. Waaijenberg, "Design, construction and maintenance of greenhouse structures," in *Acta Horticulturae*, Jun. 2006, vol. 710, no. 710, pp. 31–42. doi: 10.17660/ActaHortic.2006.710.1.

[14] F. W. Went, “The Effect of Temperature on Plant Growth,” *Annu. Rev. Plant. Physiol.*, vol. 4, no. 1, pp. 347–362, Jun. 1953, doi: 10.1146/annurev.pp.04.060153.002023.

[15] S. R. Adams, K. E. Cockshull, and C. R. J. Cave, “Effect of Temperature on the Growth and Development of Tomato Fruits,” *Annals of Botany*, vol. 88, no. 5, pp. 869–877, Nov. 2001, doi: 10.1006/anbo.2001.1524.

[16] U. Feller and I. I. Vaseva, “Extreme climatic events: impacts of drought and high temperature on physiological processes in agronomically important plants,” *Frontiers in Environmental Science*, vol. 2, p. 39, 2014, doi: 10.3389/fenvs.2014.00039.

[17] Md. A. Hasan, J. U. Ahmed, T. Hossain, Md. A. K. Mian, and Md. M. Haque, “Evaluation of the physiological quality of wheat seed as influenced by high parent plant growth temperature,” *J. Crop Sci. Biotechnol.*, vol. 16, no. 1, pp. 69–74, Mar. 2013, doi: 10.1007/s12892-010-0056-1.

[18] K. R. Reddy *et al.*, “Morpho-Physiological Characterization of Diverse Rice Genotypes for Seedling Stage High- and Low-Temperature Tolerance,” *Agronomy*, vol. 11, no. 1, Art. no. 1, Jan. 2021, doi: 10.3390/agronomy11010112.

[19] K. Rykaczewska, “The Effect of High Temperature Occurring in Subsequent Stages of Plant Development on Potato Yield and Tuber Physiological Defects,” *Am. J. Potato Res.*, vol. 92, no. 3, pp. 339–349, Jun. 2015, doi: 10.1007/s12230-015-9436-x.

[20] M. M. Peet, “GREENHOUSE CROP STRESS MANAGEMENT,” *Acta Hortic.*, no. 481, pp. 643–654, Jan. 1999, doi: 10.17660/ActaHortic.1999.481.77.

[21] M.-É. Tousignant and M. Delorme, “Connaître le fonctionnement de la plante pour mieux gérer son environnement,” *Québec Vert*, p. 3, Sep. 2006.

[22] T. W. Tibbitts, “Humidity and Plants,” *BioScience*, vol. 29, no. 6, pp. 358–363, Jun. 1979, doi: 10.2307/1307692.

[23] R. I. Grange and D. W. Hand, “A review of the effects of atmospheric humidity on the growth of horticultural crops,” *Journal of Horticultural Science*, vol. 62, no. 2, pp. 125–134, Jan. 1987, doi: 10.1080/14620316.1987.11515760.

[24] R. E. Kendrick and G. H. M. Kronenberg, *Photomorphogenesis in Plants*. Springer Science & Business Media, 2012.

[25] P. R. Burkholder, “The Rôle of Light in the Life of Plants. I. Light and Physiological Processes,” *Botanical Review*, vol. 2, no. 1, pp. 1–52, 1936.

[26] J. Nemhauser and J. Chory, “Photomorphogenesis,” *Arabidopsis Book*, vol. 1, p. e0054, Aug. 2002, doi: 10.1199/tab.0054.

[27] A. A. Arsovski, A. Galstyan, J. M. Guseman, and J. L. Nemhauser, “Photomorphogenesis,” *Arabidopsis Book*, vol. 10, p. e0147, Jan. 2012, doi: 10.1199/tab.0147.

[28] B. Thomas and D. Vince-Prue, *Photoperiodism in plants*. Elsevier, 1996.

[29] H. Lambers, F. S. Chapin, and T. L. Pons, “Photosynthesis,” in *Plant Physiological Ecology*, H. Lambers, F. S. Chapin, and T. L. Pons, Eds. New York, NY: Springer, 2008, pp. 11–99. doi: 10.1007/978-0-387-78341-3_2.

[30] T. Cardona, S. Shao, and P. J. Nixon, “Enhancing photosynthesis in plants: the light reactions,” *Essays in Biochemistry*, vol. 62, no. 1, pp. 85–94, Mar. 2018, doi: 10.1042/EBC20170015.

[31] R. Albariño, V. D. Villanueva, and C. Canhoto, “The effect of sunlight on leaf litter quality reduces growth of the shredder *Klapopteryx kuscheli*,” *Freshwater Biology*, vol. 53, no. 9, pp. 1881–1889, Sep. 2008, doi: 10.1111/j.1365-2427.2008.02016.x.

[32] H.-J. Jang *et al.*, “Effect of Sunlight Radiation on the Growth and Chemical Constituents of Salvia plebeia R.Br.,” *Molecules*, vol. 22, no. 8, Art. no. 8, Aug. 2017, doi: 10.3390/molecules22081279.

[33] S. Rehana, F. Ahmed, N. Zeba, A. Husna, and F. Hossain, “Effect of sunlight and artificial light on micropropagation of potato (Solanum tuberosum L.) plantlets,” *Arch. Agri. Environ. Sci.*, vol. 3, no. 2, pp. 151–156, Jun. 2018, doi: 10.26832/24566632.2018.030208.

[34] R. Melouki, A. Ouadah, and P. L. Llewellyn, “The CO2 adsorption behavior study on activated carbon synthesized from olive waste,” *Journal of CO2 Utilization*, vol. 42, p. 101292, Dec. 2020, doi: 10.1016/j.jcou.2020.101292.

[35] N. L. Panwar, S. C. Kaushik, and S. Kothari, “Solar greenhouse an option for renewable and sustainable farming,” *Renewable and Sustainable Energy Reviews*, vol. 15, no. 8, pp. 3934–3945, Oct. 2011, doi: 10.1016/j.rser.2011.07.030.

[36] S. Xu, X. Zhu, C. Li, and Q. Ye, “Effects of CO2 enrichment on photosynthesis and growth in Gerbera jamesonii,” *Scientia Horticulturae*, vol. 177, pp. 77–84, Oct. 2014, doi: 10.1016/j.scienta.2014.07.022.

[37] J. A. M. Kromwijk, E. Meinen, and T. A. Dueck, “THE EFFECT OF ELEVATED CO2 ON THE VEGETATIVE AND GENERATIVE GROWTH OF PHALAENOPSIS,” *Acta Hortic.*, no. 1025, pp. 155–161, Mar. 2014, doi: 10.17660/ActaHortic.2014.1025.23.

[38] D. L. Yun, H. J. Kim, and Y. J. Kim, “CO2 enrichment increased leaf initiation and photosynthesis in Doritaenopsis Queen Beer ‘Mantefon’ orchids,” *Hortic. Environ. Biotechnol.*, vol. 59, no. 2, pp. 159–165, Apr. 2018, doi: 10.1007/s13580-018-0025-z.

[39] A. R. Cho, S. J. Song, S. W. Chung, and Y. J. Kim, “CO2 Enrichment with Higher Light Level Improves Flowering Quality of Phalaenopsis Queen Beer ‘Mantefon,’” *Scientia Horticulturae*, vol. 247, pp. 356–361, Mar. 2019, doi: 10.1016/j.scienta.2018.12.030.

[40] L. M. Mortensen, “Review: CO2 enrichment in greenhouses. Crop responses,” *Scientia Horticulturae*, vol. 33, no. 1, pp. 1–25, Aug. 1987, doi: 10.1016/0304-4238(87)90028-8.

[41] J. DOORENBOS, “Guidelines for predicting crop water requirements,” *Food and Agriculture organization. Rome, Irrig. Drainage pap.*, vol. 24, 1975, Accessed: Nov. 04, 2021. [Online]. Available: https://ci.nii.ac.jp/naid/10012763449/

[42] I. Ghiat, H. R. Mackey, and T. Al-Ansari, “A Review of Evapotranspiration Measurement Models, Techniques and Methods for Open and Closed Agricultural Field Applications,” *Water*, vol. 13, no. 18, p. 2523, 2021.

[43] A. Costantino, L. Comba, G. Sicardi, M. Bariani, and E. Fabrizio, “Energy performance and climate control in mechanically ventilated greenhouses: A dynamic modelling-based assessment and investigation,” *Applied Energy*, vol. 288, p. 116583, Apr. 2021, doi: 10.1016/j.apenergy.2021.116583.

[44] I. Lopez-Cruz, E. Fitz-Rodríguez, S. Raquel, A. Rojano-Aguilar, and M. Kacira, “Development and analysis of dynamical mathematical models of greenhouse climate: A review,” *European Journal of Horticultural Science*, vol. 83, pp. 269–279, Nov. 2018, doi: 10.17660/eJHS.2018/83.5.1.

[45] S. A. Ould Khaoua, P. E. Bournet, and G. Chassériaux, “MATHEMATICAL MODELLING OF THE CLIMATE INSIDE A GLASSHOUSE DURING DAYTIME INCLUDING RADIATIVE AND CONVECTIVE HEAT TRANSFERS,” *Acta Hortic.*, no. 718, pp. 255–262, Oct. 2006, doi: 10.17660/ActaHortic.2006.718.28.

[46] H. Majdoubi, T. Boulard, H. Fatnassi, and L. Bouirden, “Airflow and microclimate patterns in a one-hectare Canary type greenhouse: An experimental and CFD assisted study,” *Agricultural and Forest Meteorology*, vol. 149, no. 6, pp. 1050–1062, Jun. 2009, doi: 10.1016/j.agrformet.2009.01.002.

[47] D. K. Fidaros, C. A. Baxevanou, T. Bartzanas, and C. Kittas, “Numerical simulation of thermal behavior of a ventilated arc greenhouse during a solar day,” *Renewable Energy*, vol. 35, no. 7, pp. 1380–1386, Jul. 2010, doi: 10.1016/j.renene.2009.11.013.

[48] R. Nebbali, J. C. Roy, and T. Boulard, “CLIMATE DYNAMIC SIMULATIONS OF A CROPPED GREENHOUSE TUNNEL,” *Acta Hortic.*, no. 893, pp. 581–587, Apr. 2011, doi: 10.17660/ActaHortic.2011.893.60.

[49] D. Piscia, J. I. Montero, E. Baeza, and B. J. Bailey, “A CFD greenhouse night-time condensation model,” *Biosystems Engineering*, vol. 111, no. 2, pp. 141–154, Feb. 2012, doi: 10.1016/j.biosystemseng.2011.11.006.

[50] R. Nebbali, J. C. Roy, and T. Boulard, “Dynamic simulation of the distributed radiative and convective climate within a cropped greenhouse,” *Renewable Energy*, vol. 43, pp. 111–129, Jul. 2012, doi: 10.1016/j.renene.2011.12.003.

[51] J. I. Montero, P. Muñoz, A. Antón, and N. Iglesias, “COMPUTATIONAL FLUID DYNAMIC MODELLING OF NIGHT-TIME ENERGY FLUXES IN UNHEATED GREENHOUSES,” *Acta Hortic.*, no. 691, pp. 403–410, Oct. 2005, doi: 10.17660/ActaHortic.2005.691.48.

[52] X. Wang, J. Luo, and X. Li, “CFD Based Study of Heterogeneous Microclimate in a Typical Chinese Greenhouse in Central China,” *Journal of Integrative Agriculture*, vol. 12, no. 5, pp. 914–923, May 2013, doi: 10.1016/S2095-3119(13)60309-3.

[53] G. D. la Torre-Gea, G. M. Soto-Zarazúa, I. López-Crúz, I. Torres-Pacheco, and E. Rico-García, “Computational fluid dynamics in greenhouses: A review,” *African Journal of Biotechnology*, vol. 10, no. 77, Art. no. 77, 2011, doi: 10.4314/%u.v10i77.%c.

[54] D. Ma, N. Carpenter, H. Maki, T. U. Rehman, M. R. Tuinstra, and J. Jin, “Greenhouse environment modeling and simulation for microclimate control,” *Computers and Electronics in Agriculture*, vol. 162, pp. 134–142, Jul. 2019, doi: 10.1016/j.compag.2019.04.013.

[55] K. Mesmoudi, B. Zitouni, T. Outtas, and P. E. Bournet, “NUMERICAL SIMULATION OF THE AIRFLOW AND TEMPERATURE DISTRIBUTION IN A CLOSED EMPTY VENLO GLASSHOUSE UNDER HOT AND ARID CLIMATE,” *Acta Hortic.*, no. 1008, pp. 235–240, Oct. 2013, doi: 10.17660/ActaHortic.2013.1008.31.

[56] S. Oskin, D. Tsokur, A. Voloshin, K. Grigoryev, and E. Tsokur, “Simulation of thermal processes in greenhouse,” presented at the 20th International Scientific Conference Engineering for Rural Development, May 2021. doi: 10.22616/ERDev.2021.20.TF376.

[57] M. Jazouli, K. Lekouch, A. Wifaya, G. Lahoucine, and L. Bouirden, “CFD Study of Airflow and Microclimate Patterns Inside a Multispan Greenhouse,” *WSEAS TRANSACTIONS ON FLUID MECHANICS*, vol. 16, pp. 102–108, May 2021, doi: 10.37394/232013.2021.16.10.

[58] H. Fatnassi, C. Poncet, M. M. Bazzano, R. Brun, and N. Bertin, “A numerical simulation of the photovoltaic greenhouse microclimate,” *Solar Energy*, vol. 120, pp. 575–584, Oct. 2015, doi: 10.1016/j.solener.2015.07.019.

[59] X. He *et al.*, “Ventilation optimization of solar greenhouse with removable back walls based on CFD,” *Computers and Electronics in Agriculture*, vol. 149, pp. 16–25, Jun. 2018, doi: 10.1016/j.compag.2017.10.001.

[60] A. Saberian and S. M. Sajadiye, “The effect of dynamic solar heat load on the greenhouse microclimate using CFD simulation,” *Renewable Energy*, vol. 138, pp. 722–737, Aug. 2019, doi: 10.1016/j.renene.2019.01.108.

[61] D. Piscia, P. Muñoz, C. Panadès, and J. I. Montero, “A method of coupling CFD and energy balance simulations to study humidity control in unheated greenhouses,” *Computers and Electronics in Agriculture*, vol. 115, pp. 129–141, Jul. 2015, doi: 10.1016/j.compag.2015.05.005.

[62] G. Zhang, Z. Fu, M. Yang, X. Liu, Y. Dong, and X. Li, “Nonlinear simulation for coupling modeling of air humidity and vent opening in Chinese solar greenhouse based on CFD,” *Computers and Electronics in Agriculture*, vol. 162, pp. 337–347, Jul. 2019, doi: 10.1016/j.compag.2019.04.024.

[63] M. Dhiman, V. P. Sethi, B. Singh, and A. Sharma, “CFD analysis of greenhouse heating using flue gas and hot water heat sink pipe networks,” *Computers and Electronics in Agriculture*, vol. 163, p. 104853, Aug. 2019, doi: 10.1016/j.compag.2019.104853.

[64] C. Baxevanou, D. Fidaros, and C. Kittas, “Yearly numerical evaluation of greenhouse cover materials,” *Computers and Electronics in Agriculture*, vol. 149, pp. 54–70, Jun. 2018, doi: 10.1016/J.COMPAG.2017.12.006.

[65] P. Sdringola, S. Proietti, U. Desideri, and G. Giombini, “Thermo-fluid dynamic modeling and simulation of a bioclimatic solar greenhouse with self-cleaning and photovoltaic glasses,” *Energy and Buildings*, vol. 68, pp. 183–195, Jan. 2014, doi: 10.1016/j.enbuild.2013.08.011.

[66] C. Tavares, A. Gonçalves, P. Castro, D. Loureiro, and A. Joyce, “Modelling an agriculture production greenhouse,” *Renewable energy*, vol. 22, no. 1, pp. 15–20, 2001, doi: 10.1016/S0960-1481(00)00030-6.

[67] V. P. Sethi, “On the selection of shape and orientation of a greenhouse: Thermal modeling and experimental validation,” *Solar Energy*, vol. 83, no. 1, pp. 21–38, Jan. 2009, doi: 10.1016/j.solener.2008.05.018.

[68] Q. Altes-Buch, S. Quoilin, and V. Lemort, “Greenhouses: A Modelica Library for the Simulation of Greenhouse Climate and Energy Systems,” Regensburg, Germany, Mar. 2019. doi: 10.3384/ecp19157533.

[69] A. M. Abdel-Ghany and I. M. Al-Helal, “Solar energy utilization by a greenhouse: General relations,” *Renewable Energy*, vol. 36, no. 1, pp. 189–196, Jan. 2011, doi: 10.1016/j.renene.2010.06.020.

[70] K. A. Joudi and A. A. Farhan, “A dynamic model and an experimental study for the internal air and soil temperatures in an innovative greenhouse,” *Energy Conversion and Management*, vol. 91, pp. 76–82, Feb. 2015, doi: 10.1016/j.enconman.2014.11.052.

[71] R. Ben Ali, S. Bouadila, and A. Mami, “Experimental validation of the dynamic thermal behavior of two types of agricultural greenhouses in the Mediterranean context,” *Renewable Energy*, vol. 147, pp. 118–129, Mar. 2020, doi: 10.1016/j.renene.2019.08.129.

[72] M. Taki, Y. Ajabshirchi, S. F. Ranjbar, A. Rohani, and M. Matloobi, “Heat transfer and MLP neural network models to predict inside environment variables and energy lost in a semi-solar greenhouse,” *Energy and Buildings*, vol. 110, pp. 314–329, Jan. 2016, doi: 10.1016/j.enbuild.2015.11.010.

[73] B. Mohammadi, S. F. Ranjbar, and Y. Ajabshirchi, “Application of dynamic model to predict some inside environment variables in a semi-solar greenhouse,” *Information Processing in Agriculture*, vol. 5, no. 2, pp. 279–288, Jun. 2018, doi: 10.1016/j.inpa.2018.01.001.

[74] M. Taki, Y. Ajabshirchi, S. F. Ranjbar, A. Rohani, and M. Matloobi, “Modeling and experimental validation of heat transfer and energy consumption in an innovative greenhouse structure,” *Information Processing in Agriculture*, vol. 3, no. 3, pp. 157–174, Sep. 2016, doi: 10.1016/j.inpa.2016.06.002.

[75] B. H. E. Vanthoor, C. Stanghellini, E. J. van Henten, and P. H. B. de Visser, “A methodology for model-based greenhouse design: Part 1, a greenhouse climate model for a broad range of designs and climates,” *Biosystems Engineering*, vol. 110, no. 4, pp. 363–377, Dec. 2011, doi: 10.1016/j.biosystemseng.2011.06.001.

[76] B. H. E. Vanthoor, P. H. B. de Visser, C. Stanghellini, and E. J. van Henten, “A methodology for model-based greenhouse design: Part 2, description and validation of a tomato yield model,” *Biosystems Engineering*, vol. 110, no. 4, pp. 378–395, Dec. 2011, doi: 10.1016/j.biosystemseng.2011.08.005.

[77] M. S. Ahamed, H. Guo, and K. Tanino, “A quasi-steady state model for predicting the heating requirements of conventional greenhouses in cold regions,” *Information*

Processing in Agriculture, vol. 5, no. 1, pp. 33–46, Mar. 2018, doi: 10.1016/j.inpa.2017.12.003.

[78] F. Rodríguez, L. J. Yebra, M. Berenguel, and S. Dormido, "Modelling and simulation of greenhouse climate using dymola," in *IFAC Proceedings Volumes (IFAC-PapersOnline)*, Jan. 2002, vol. 35, no. 1, pp. 79–84. doi: 10.3182/20020721-6-es-1901.01322.

[79] R. B. Younès and H. Ayeb, "Numerical Simulation of the Thermal Behavior of a Traditional Greenhouse by Using the Theory of the Green's Functions," *Numerical Heat Transfer, Part A: Applications*, vol. 56, no. 11, pp. 914–929, Dec. 2009, doi: 10.1080/10407780903463441.

[80] D. C. Diaz, C. R. Bojacá, and E. Schrevens, "Modeling the suitability of the traditional plastic greenhouse for tomato production across Colombian regions," *Acta Hortic.*, no. 1205, pp. 857–864, Jun. 2018, doi: 10.17660/ActaHortic.2018.1205.109.

[81] S. Candy, G. Moore, and P. Freere, "Design and modeling of a greenhouse for a remote region in Nepal," in *Procedia Engineering*, 2012, vol. 49, pp. 152–160. doi: 10.1016/j.proeng.2012.10.123.

[82] E. Mashonjowa, F. Ronsse, J. R. Milford, and J. G. Pieters, "Modelling the thermal performance of a naturally ventilated greenhouse in Zimbabwe using a dynamic greenhouse climate model," *Solar Energy*, vol. 91, pp. 381–393, May 2013, doi: 10.1016/j.solener.2012.09.010.

[83] E. Fabrizio, "Energy reduction measures in agricultural greenhouses heating: Envelope, systems and solar energy collection.," *Energy and Buildings*, vol. 53, pp. 57–63, Oct. 2012, doi: 10.1016/j.enbuild.2012.07.003.

[84] A. Boccalatte, M. Fossa, and R. Sacile, "Modeling, Design and Construction of a Zero-Energy PV Greenhouse for Applications in Mediterranean Climates," *Thermal Science and Engineering Progress*, vol. 25, p. 101046, Oct. 2021, doi: 10.1016/j.tsep.2021.101046.

[85] E. Alvarez-Sánchez, G. Leyva-Retureta, E. Portilla-Flores, and A. López-Velázquez, "Evaluación del comportamiento térmico de un invernadero asimétrico mediante simulaciones dinámicas," *DYNA (Colombia)*, vol. 81, no. 188, pp. 152–159, Dec. 2014, doi: 10.15446/dyna.v81n188.41338.

[86] S. Lee *et al.*, "Dynamic Energy Exchange Modelling for a Plastic-Covered Multi-Span Greenhouse Utilizing a Thermal Effluent from Power Plant," *Agronomy*, vol. 11, no. 8, Art. no. 8, Aug. 2021, doi: 10.3390/agronomy11081461.

[87] P. Henshaw, “Modelling changes to an unheated greenhouse in the Canadian subarctic to lengthen the growing season,” *Sustainable Energy Technologies and Assessments*, vol. 24, pp. 31–38, Dec. 2017, doi: 10.1016/j.seta.2016.12.004.

[88] X. Gao, H. Yang, Y. Guan, J. Bai, R. Zhang, and W. Hu, “Length Determination of the Solar Greenhouse North Wall in Lanzhou,” *Procedia Engineering*, vol. 205, pp. 1230–1236, Jan. 2017, doi: 10.1016/j.proeng.2017.10.361.

[89] A. Nadal *et al.*, “Building-integrated rooftop greenhouses: An energy and environmental assessment in the mediterranean context,” *Applied Energy*, vol. 187, pp. 338–351, Feb. 2017, doi: 10.1016/j.apenergy.2016.11.051.

[90] S. Bonachela, A. M. González, and M. D. Fernández, “Irrigation scheduling of plastic greenhouse vegetable crops based on historical weather data,” *Irrig Sci*, vol. 25, no. 1, pp. 53–62, Sep. 2006, doi: 10.1007/s00271-006-0034-z.

[91] C. Baglivo *et al.*, “Complete greenhouse dynamic simulation tool to assess the crop thermal well-being and energy needs,” *Applied Thermal Engineering*, vol. 179, p. 115698, Oct. 2020, doi: 10.1016/j.applthermaleng.2020.115698.

[92] T. Talaviya, D. Shah, N. Patel, H. Yagnik, and M. Shah, “Implementation of artificial intelligence in agriculture for optimisation of irrigation and application of pesticides and herbicides,” *Artificial Intelligence in Agriculture*, vol. 4, pp. 58–73, Jan. 2020, doi: 10.1016/j.aiia.2020.04.002.

[93] K. Jha, A. Doshi, P. Patel, and M. Shah, “A comprehensive review on automation in agriculture using artificial intelligence,” *Artificial Intelligence in Agriculture*, vol. 2, pp. 1–12, Jun. 2019, doi: 10.1016/j.aiia.2019.05.004.

[94] D. I. Patrício and R. Rieder, *Computer vision and artificial intelligence in precision agriculture for grain crops: A systematic review*, vol. 153. Elsevier B.V., 2018. doi: 10.1016/j.compag.2018.08.001.

[95] X. E. Pantazi, D. Moshou, and D. Bochtis, “Artificial intelligence in agriculture,” in *Intelligent Data Mining and Fusion Systems in Agriculture*, Elsevier, 2020, pp. 17–101. doi: 10.1016/b978-0-12-814391-9.00002-9.

[96] D. D. Uyeh *et al.*, “A Reinforcement Learning Approach for Optimal Placement of Sensors in Protected Cultivation Systems,” *IEEE Access*, vol. 9, pp. 100781–100800, 2021, doi: 10.1109/ACCESS.2021.3096828.

[97] Y.-Z. Tsai *et al.*, “Application of Random Forest and ICON Models Combined with Weather Forecasts to Predict Soil Temperature and Water Content in a Greenhouse,” *Water*, vol. 12, no. 4, p. 1176, Apr. 2020, doi: 10.3390/w12041176.

[98] D. J. Rustia and T.-T. Lin, “An IoT-based Wireless Imaging and Sensor Node System for Remote Greenhouse Pest Monitoring,” *Chemical Engineering Transactions*, vol. 58, Jan. 2017, doi: 10.3303/CET1758101.

[99] J.-J. Zhou *et al.*, “Evaluating the Performance of Hyperspectral Leaf Reflectance to Detect Water Stress and Estimation of Photosynthetic Capacities,” *Remote Sensing*, vol. 13, no. 11, Art. no. 11, Jan. 2021, doi: 10.3390/rs13112160.

[100] L. Tian *et al.*, “Spectroscopic detection of rice leaf blast infection from asymptomatic to mild stages with integrated machine learning and feature selection,” *Remote Sensing of Environment*, vol. 257, p. 112350, May 2021, doi: 10.1016/j.rse.2021.112350.

[101] A. T. Nieuwenhuizen, J. Kool, H. K. Suh, and J. Hemming, “Automated spider mite damage detection on tomato leaves in greenhouses,” *Acta Hortic.*, no. 1268, pp. 165–172, Jan. 2020, doi: 10.17660/ActaHortic.2020.1268.21.

[102] Y. Wu and L. Xu, “Crop Organ Segmentation and Disease Identification Based on Weakly Supervised Deep Neural Network,” *Agronomy*, vol. 9, no. 11, Art. no. 11, Nov. 2019, doi: 10.3390/agronomy9110737.

[103] R. Pahlavan, M. Omid, and A. Akram, “Energy input-output analysis and application of artificial neural networks for predicting greenhouse basil production,” *Energy*, vol. 37, no. 1, pp. 171–176, Jan. 2012, doi: 10.1016/j.energy.2011.11.055.

[104] F. He and C. Ma, “Modeling greenhouse air humidity by means of artificial neural network and principal component analysis,” *Computers and Electronics in Agriculture*, vol. 71, no. SUPPL. 1, pp. S19–S23, Apr. 2010, doi: 10.1016/j.compag.2009.07.011.

[105] H. Uchida Frausto and J. G. Pieters, “Modelling greenhouse temperature using system identification by means of neural networks,” *Neurocomputing*, vol. 56, no. 1–4, pp. 423–428, Jan. 2004, doi: 10.1016/j.neucom.2003.08.001.

[106] S. Y. Kim, S. M. Lee, K. S. Park, and and K. H. Ryu, “Prediction Model of Internal Temperature using Backpropagation Algorithm for Climate Control in Greenhouse,” *Horticultural Science and Technology*, pp. 713–729, Oct. 2018, doi: 10.12972/kjhst.20180071.

[107] T. W. Moon, D. H. Jung, S. H. Chang, and J. E. Son, “Estimation of greenhouse CO2 concentration via an artificial neural network that uses environmental factors,” *Hortic. Environ. Biotechnol.*, vol. 59, no. 1, pp. 45–50, Feb. 2018, doi: 10.1007/s13580-018-0015-1.

[108] G. Codeluppi, A. Cilfone, L. Davoli, and G. Ferrari, “AI at the Edge: a Smart Gateway for Greenhouse Air Temperature Forecasting,” in *2020 IEEE International Workshop on Metrology for Agriculture and Forestry (MetroAgriFor)*, 2020, pp. 348–353.

[109] L. Miranda, I. Schuch, D. Dannehl, T. Rocksch, R. Salazar, and U. Schmidt, “USING ARTIFICIAL NEURAL NETWORKS TO PREDICT THE CLIMATE IN A GREENHOUSE: FIRST SIMULATION RESULTS ON A SEMI-CLOSED SYSTEM,” *Acta Hortic.*, no. 1099, pp. 137–144, Sep. 2015, doi: 10.17660/ActaHortic.2015.1099.13.

[110] P. M. Ferreira, E. A. Faria, and A. E. Ruano, “Neural network models in greenhouse air temperature prediction,” *Neurocomputing*, vol. 43, no. 1–4, pp. 51–75, Mar. 2002, doi: 10.1016/S0925-2312(01)00620-8.

[111] M. Trejo-perea, G. Herrera-ruiz, J. Rios-moreno, R. Castañeda Miranda, and E. Rivas-araiza, “Greenhouse energy consumption prediction using neural networks models,” *INTERNATIONAL JOURNAL OF AGRICULTURE & BIOLOGY-Araiza*, vol. 11, pp. 1–6, 2009.

[112] M. Neugebauer, J. Hałacz, and T. Olkowski, “A compost heating solution for a greenhouse in north-eastern Poland in fall,” *Journal of Cleaner Production*, vol. 279, p. 123613, Jan. 2021, doi: 10.1016/j.jclepro.2020.123613.

[113] M. Taki, S. Abdanan Mehdizadeh, A. Rohani, M. Rahnama, and M. Rahmati-Joneidabad, “Applied machine learning in greenhouse simulation; new application and analysis,” *Information Processing in Agriculture*, vol. 5, no. 2, pp. 253–268, Jun. 2018, doi: 10.1016/j.inpa.2018.01.003.

[114] H. Yu, Y. Chen, S. G. Hassan, and D. Li, “Prediction of the temperature in a Chinese solar greenhouse based on LSSVM optimized by improved PSO,” *Computers and Electronics in Agriculture*, vol. 122, pp. 94–102, Mar. 2016, doi: 10.1016/j.compag.2016.01.019.

[115] W. Zou, F. Yao, B. Zhang, C. He, and Z. Guan, “Verification and predicting temperature and humidity in a solar greenhouse based on convex bidirectional extreme learning machine algorithm,” *Neurocomputing*, vol. 249, pp. 72–85, Aug. 2017, doi: 10.1016/j.neucom.2017.03.023.

[116] J. Chen, J. Zhao, F. Xu, H. Hu, Q. Ai, and J. Yang, “Modeling of Energy Demand in the Greenhouse Using PSO-GA Hybrid Algorithms,” *Mathematical Problems in Engineering*, vol. 2015, pp. 1–6, 2015, doi: 10.1155/2015/871075.

[117] A. Allouhi, N. Choab, A. Hamrani, and S. Saadeddine, “Machine learning algorithms to assess the thermal behavior of a Moroccan agriculture greenhouse,” *Cleaner*

Engineering and Technology, vol. 5, p. 100346, Dec. 2021, doi: 10.1016/j.clet.2021.100346.

[118] I. F. Odesola, Ezekwem, and Chidozie, "The Effect of Shape and Orientation on a Greenhouse: A Review," *An International Journal of Science and Technology*, vol. 1, no. 1, 2012, [Online]. Available: www.afrrevjo.net/afrrevstech

[119] N. Choab, A. Allouhi, A. El Maakoul, T. Kousksou, S. Saadeddine, and A. Jamil, *Review on greenhouse microclimate and application: Design parameters, thermal modeling and simulation, climate controlling technologies*, vol. 191. Elsevier Ltd, 2019. doi: 10.1016/j.solener.2019.08.042.

[120] E. M. A. A. ElBialy *et al.*, "Design challenges of agricultural greenhouses in hot and arid environments – A review," *Engineering in Agriculture, Environment and Food*, vol. 12, no. 1, pp. 48–70, 2018, doi: 10.1016/j.eaef.2018.09.004.

[121] B. Groener *et al.*, "Preliminary Design of a Low-cost Greenhouse with Open Source Control Systems," in *Procedia Engineering*, Jan. 2015, vol. 107, pp. 470–479. doi: 10.1016/j.proeng.2015.06.105.

[122] M. Aissa and S. Bezari, "The orientation effect of the agricultural tunnel greenhouse on aerodynamic and energy properties," presented at the Proceedings of the 2018 5th International Symposium on Environment-Friendly Energies and Applications, EFEA 2018, 2019. doi: 10.1109/EFEA.2018.8617097.

[123] M. Aissa and A. Boutelhig, "CFD Comparative Study Between Different Forms of Solar Greenhouses and Orientation Effect," *International Journal of Heat and Technology*, vol. 39, pp. 433–440, Apr. 2021, doi: 10.18280/ijht.390212.

[124] R. Kim, I. Lee, U. Yeo, and S. Lee, "Evaluation of various national greenhouse design standards for wind loading," *Biosystems Engineering*, vol. 188, pp. 136–154, Dec. 2019, doi: 10.1016/j.biosystemseng.2019.10.004.

[125] J. Chen, Y. Ma, and Z. Pang, "A mathematical model of global solar radiation to select the optimal shape and orientation of the greenhouses in southern China," *Solar Energy*, vol. 205, pp. 380–389, Jul. 2020, doi: 10.1016/j.solener.2020.05.055.

[126] A. Rasheed, J. W. Lee, and H. W. Lee, "Development and Optimization of a Building Energy Simulation Model to Study the Effect of Greenhouse Design Parameters," *Energies*, vol. 11, no. 8, Art. no. 8, Aug. 2018, doi: 10.3390/en11082001.

[127] A. Belkadi, D. Mezghani, and A. Mami, "Energy Study Of A Greenhouse And Optimisation Of The Choice Of Shape And Covering Material: Based On An Improved

Static Model," *Engenharia Agricola*, vol. 41, no. 3, pp. 297–310, 2021, doi: 10.1590/1809-4430-ENG.AGRIC.V41N3P297-310/2021.

[128] M. S. Ahamed, H. Guo, and K. Tanino, "Energy-efficient design of greenhouse for Canadian Prairies using a heating simulation model," *Int J Energy Res*, vol. 42, no. 6, pp. 2263–2272, May 2018, doi: 10.1002/er.4019.

[129] H. Ghasemi Mobtaker, Y. Ajabshirchi, S. F. Ranjbar, and M. Matloobi, "Solar energy conservation in greenhouse: Thermal analysis and experimental validation," *Renewable Energy*, vol. 96, pp. 509–519, Oct. 2016, doi: 10.1016/j.renene.2016.04.079.

[130] H. G. Mobtaker, Y. Ajabshirchi, S. F. Ranjbar, and M. Matloobi, "Simulation of thermal performance of solar greenhouse in north-west of Iran: An experimental validation," *Renewable Energy*, vol. 135, pp. 88–97, May 2019, doi: 10.1016/j.renene.2018.10.003.

[131] U. Çakir and E. Şahin, "Using solar greenhouses in cold climates and evaluating optimum type according to sizing, position and location: A case study," *Computers and Electronics in Agriculture*, vol. 117, pp. 245–257, Sep. 2015, doi: 10.1016/j.compag.2015.08.005.

[132] N. Choab, A. Allouhi, A. E. Maakoul, T. Kousksou, S. Saadeddine, and A. Jamil, "Effect of Greenhouse Design Parameters on the Heating and Cooling Requirement of Greenhouses in Moroccan Climatic Conditions," *IEEE Access*, vol. 9, pp. 2986–3003, 2021, doi: 10.1109/ACCESS.2020.3047851.

[133] M. J. Gupta and P. Chandra, "Effect of greenhouse design parameters on conservation of energy for greenhouse environmental control," *Energy*, vol. 27, no. 8, pp. 777–794, Aug. 2002, doi: 10.1016/S0360-5442(02)00030-0.

[134] A. Gupta and G. N. Tiwari, "Performance evaluation of greenhouse for different climatic zones of India," *SESI Journal: Journal of the Solar Energy Society of India*, vol. 12, no. 1, p. 45, 2002.

[135] N. Kumari, G. N. Tiwari, and M. S. Sodha, "Performance Evaluation of Greenhouse having Passive or Active Heating in Different Climatic Zones of India," . *Agricultural Engineering*, p. 19, 2007.

[136] R. D. Singh and G. N. Tiwari, "Energy conservation in the greenhouse system: A steady state analysis," *Energy*, vol. 35, no. 6, pp. 2367–2373, 2010, doi: 10.1016/j.energy.2010.02.003.

[137] V. P. Sethi, "On the selection of shape and orientation of a greenhouse for composite climates," *International Journal of Sustainable Energy*, vol. 28, no. 1–3, pp. 45–58, Sep. 2009, doi: 10.1080/14786450802452621.

[138] G. N. Tiwari and A. Gupta, “A comparison in performance of greenhouses with various shapes: a parametric study,” *International Journal of Ambient Energy*, vol. 23, no. 3, pp. 136–148, Jul. 2002, doi: 10.1080/01430750.2002.9674882.

[139] Y. Shen and S. L. Yu, “COOLING METHODS FOR GREENHOUSES IN TROPICAL REGION,” *Acta Hortic.*, no. 578, pp. 323–327, Jun. 2002, doi: 10.17660/ActaHortic.2002.578.40.

[140] L. Long and H. Ye, “How to be smart and energy efficient: A general discussion on thermochromic windows,” *Sci Rep*, vol. 4, no. 1, p. 6427, May 2015, doi: 10.1038/srep06427.

[141] S. D. Rezaei, S. Shannigrahi, and S. Ramakrishna, “A review of conventional, advanced, and smart glazing technologies and materials for improving indoor environment,” *Solar Energy Materials and Solar Cells*, vol. 159, pp. 26–51, Jan. 2017, doi: 10.1016/j.solmat.2016.08.026.

[142] N. Katsoulas, A. Bari, and C. Papaioannou, “Plant responses to UV blocking greenhouse covering materials: A review,” *Agronomy*, vol. 10, no. 7, 2020, doi: 10.3390/agronomy10071021.

[143] A. M. Abdel-Ghany, I. M. Al-Helal, S. M. Alzahrani, A. A. Alsadon, I. M. Ali, and R. M. Elleithy, “Covering Materials Incorporating Radiation-Preventing Techniques to Meet Greenhouse Cooling Challenges in Arid Regions: A Review,” *The Scientific World Journal*, vol. 2012, p. e906360, May 2012, doi: 10.1100/2012/906360.

[144] A. Al-Mahdouri, M. Baneshi, H. Gonome, J. Okajima, and S. Maruyama, “Evaluation of optical properties and thermal performances of different greenhouse covering materials,” *Solar Energy*, vol. 96, pp. 21–32, 2013, doi: 10.1016/j.solener.2013.06.029.

[145] A. Al-Mahdouri, H. Gonome, J. Okajima, and S. Maruyama, “Theoretical and experimental study of solar thermal performance of different greenhouse cladding materials,” *Solar Energy*, vol. 107, pp. 314–327, 2014, doi: 10.1016/j.solener.2014.05.006.

[146]. C Arcidiacono, A. D’Emilio, R. Mazzarella, and C. Leonardi, “COVERING MATERIALS TO IMPROVE GREENHOUSE MICROCLIMATE DURING SUMMER IN HOT CLIMATES,” *Acta Hortic.*, no. 719, pp. 247–254, Sep. 2006, doi: 10.17660/ActaHortic.2006.719.27.

[147] M. C. Subin, J. S. Lourence, R. Karthikeyan, and C. Periasamy, “Analysis of materials used for Greenhouse roof covering - structure using CFD,” *IOP Conf. Ser.: Mater. Sci. Eng.*, vol. 346, p. 012068, Apr. 2018, doi: 10.1088/1757-899X/346/1/012068.

[148] M. C. Subin, R. Karthikeyan, C. Periasamy, and B. Sozharajan, “Verification of the greenhouse roof-covering-material selection using the finite element method,” 2020, vol. 21, pp. 357–366. doi: 10.1016/j.matpr.2019.05.462.

[149] B. M. Erhioui, A. Gosselin, X. Hao, A. P. Papadopoulos, and M. Dorais, “Greenhouse Covering Materials and Supplemental Lighting Affect Growth, Yield, Photosynthesis, and Leaf Carbohydrate Synthesis of Tomato Plants,” *Journal of the American Society for Horticultural Science*, vol. 127, no. 5, pp. 819–824, Sep. 2002, doi: 10.21273/JASHS.127.5.819.

[150] A. R. Alharbi *et al.*, “DE EFFECT OF CLEAR AND DEFUSE GLASS COVERING MATERIALS ON FRUIT YIELD AND ENERGY EFFICIENCY OF GREENHOUSE CUCUMBER GROWN IN HOT CLIMATE,” *asphc*, vol. 20, no. 3, pp. 37–44, Jun. 2021, doi: 10.24326/asphc.2021.3.4.

[151] E. Baeza, S. Hemming, and C. Stanghellini, “Materials with switchable radiometric properties: Could they become the perfect greenhouse cover?,” *Biosystems Engineering*, vol. 193, pp. 157–173, 2020, doi: 10.1016/j.biosystemseng.2020.02.012.

[152] D. Harjunowibowo, D. Yate, S. A. Omer, and S. B. Riffat, “Reducing greenhouse energy consumption using novelty rooftop: a simulation,” Jul. 2017, Accessed: Nov. 19, 2021. [Online]. Available: https://nottingham-repository.worktribe.com/output/872842

[153] B. Cemek, Y. Demir, S. Uzun, and V. Ceyhan, “The effects of different greenhouse covering materials on energy requirement, growth and yield of aubergine,” *Energy*, vol. 31, no. 12, pp. 1780–1788, Sep. 2006, doi: 10.1016/j.energy.2005.08.004.

[154] B. Cemek and Y. Demir, “Testing of the condensation characteristics and light transmissions of different plastic film covering materials,” *Polymer Testing*, vol. 24, no. 3, pp. 284–289, May 2005, doi: 10.1016/j.polymertesting.2004.11.007.

[155] Chr. Lamnatou and D. Chemisana, “Solar radiation manipulations and their role in greenhouse claddings: Fresnel lenses, NIR- and UV-blocking materials,” *Renewable and Sustainable Energy Reviews*, vol. 18, pp. 271–287, Feb. 2013, doi: 10.1016/j.rser.2012.09.041.

[156] J. Hu and X. Yu, “Adaptive Greenhouse with Thermochromic Material: Performance Evaluation in Cold Regions,” *J. Energy Eng.*, vol. 146, no. 4, p. 04020032, Aug. 2020, doi: 10.1061/(ASCE)EY.1943-7897.0000685.

[157] C. Baxevanou *et al.*, “Simulation of radiation and crop activity in a greenhouse covered with semitransparent organic photovoltaics,” *Applied Sciences (Switzerland)*, vol. 10, no. 7, 2020, doi: 10.3390/app10072550.

[158] R. Gupta, G. N. Tiwari, A. Kumar, and Y. Gupta, “Calculation of total solar fraction for different orientation of greenhouse using 3D-shadow analysis in Auto-CAD,” *Energy and Buildings*, vol. 47, pp. 27–34, Apr. 2012, doi: 10.1016/j.enbuild.2011.11.010.

[159] S. M. Dragićević, “Determining the optimum orientation of a greenhouse on the basis of the total solar radiation availability,” *Thermal Science*, vol. 15, no. 1, pp. 215–221, 2011, doi: 10.2298/TSCI100220057D.

[160] C. Stanciu, D. Stanciu, and A. Dobrovicescu, “Effect of Greenhouse Orientation with Respect to E-W Axis on its Required Heating and Cooling Loads,” *Energy Procedia*, vol. 85, pp. 498–504, Jan. 2016, doi: 10.1016/j.egypro.2015.12.234.

[161] C. Chen *et al.*, “A computational model to determine the optimal orientation for solar greenhouses located at different latitudes in China,” *Solar Energy*, vol. 165, pp. 19–26, May 2018, doi: 10.1016/j.solener.2018.02.022.

[162] W. M. El-Maghlany, M. A. Teamah, and H. Tanaka, “Optimum design and orientation of the greenhouses for maximum capture of solar energy in North Tropical Region,” *Energy Conversion and Management*, vol. 105, pp. 1096–1104, Nov. 2015, doi: 10.1016/j.enconman.2015.08.066.

[163] C. Stanciu, D. Stanciu, and A. Dobrovicescu, “Effect of Greenhouse Orientation with Respect to E-W Axis on its Required Heating and Cooling Loads,” in *Energy Procedia*, 2016, vol. 85. doi: 10.1016/j.egypro.2015.12.234.

[164] E. Cuce, D. Harjunowibowo, and P. M. Cuce, *Renewable and sustainable energy saving strategies for greenhouse systems: A comprehensive review*, vol. 64. 2016. doi: 10.1016/j.rser.2016.05.077.

[165] M. Taki, A. Rohani, and M. Rahmati-Joneidabad, *Solar thermal simulation and applications in greenhouse*, vol. 5. 2018. doi: 10.1016/j.inpa.2017.10.003.

[166] S. Gorjian *et al.*, “A review on opportunities for implementation of solar energy technologies in agricultural greenhouses,” *Journal of Cleaner Production*, vol. 285, p. 124807, Feb. 2021, doi: 10.1016/j.jclepro.2020.124807.

[167] H. A. Ahemd, A. A. Al-Faraj, and A. M. Abdel-Ghany, *Shading greenhouses to improve the microclimate, energy and water saving in hot regions: A review*. 2016. doi: 10.1016/j.scienta.2016.01.030.

[168] M. S. Ahamed, H. Guo, and K. Tanino, “Energy saving techniques for reducing the heating cost of conventional greenhouses,” *Biosystems Engineering*, vol. 178, pp. 9–33, Feb. 2019, doi: 10.1016/j.biosystemseng.2018.10.017.

[169] A. Vadiee and V. Martin, “Energy management strategies for commercial greenhouses,” *Applied Energy*, vol. 114, pp. 880–888, Feb. 2014, doi: 10.1016/j.apenergy.2013.08.089.

[170] R. H. E. Hassanien, M. Li, and F. Yin, “The integration of semi-transparent photovoltaics on greenhouse roof for energy and plant production,” *Renewable Energy*, vol. 121, pp. 377–388, Jun. 2018, doi: 10.1016/j.renene.2018.01.044.

[171] F. Hosseini-Fashami, A. Motevali, A. Nabavi-Pelesaraei, S. J. Hashemi, and K. Chau, “Energy-Life cycle assessment on applying solar technologies for greenhouse strawberry production,” *Renewable and Sustainable Energy Reviews*, vol. 116, p. 109411, Dec. 2019, doi: 10.1016/j.rser.2019.109411.

[172] A. Yano and M. Cossu, “Energy sustainable greenhouse crop cultivation using photovoltaic technologies,” *Renewable and Sustainable Energy Reviews*, vol. 109, pp. 116–137, Jul. 2019, doi: 10.1016/j.rser.2019.04.026.

[173] M. Cossu *et al.*, “Agricultural sustainability estimation of the European photovoltaic greenhouses,” *European Journal of Agronomy*, vol. 118, p. 126074, Aug. 2020, doi: 10.1016/j.eja.2020.126074.

[174] K. Ezzaeri *et al.*, “Performance of photovoltaic canarian greenhouse: A comparison study between summer and winter seasons,” *Solar Energy*, vol. 198, pp. 275–282, Mar. 2020, doi: 10.1016/j.solener.2020.01.057.

[175] G. Trypanagnostopoulos, A. Kavga, Souliotis, and Y. Tripanagnostopoulos, “Greenhouse performance results for roof installed photovoltaics,” *Renewable Energy*, vol. 111, 2017, doi: 10.1016/j.renene.2017.04.066.

[176] J. Chen, F. Xu, B. Ding, N. Wu, Z. Shen, and L. Zhang, “Performance analysis of radiation and electricity yield in a photovoltaic panel integrated greenhouse using the radiation and thermal models,” *Computers and Electronics in Agriculture*, vol. 164, p. 104904, Sep. 2019, doi: 10.1016/j.compag.2019.104904.

[177] T. Huang, H. Li, G. Zhang, and F. Xu, “Experimental Study on Biomass Heating System in the Greenhouse: A Case Study in Xiangtan, China,” *Sustainability*, vol. 12, no. 14, Art. no. 14, Jan. 2020, doi: 10.3390/su12145673.

[178] C. Bisaglia, E. Romano, M. Cutini, and F. Nucci, “CONVERSION OF A HIGH-DEMANDING THERMAL-ENERGY LEVEL GREENHOUSE FROM CONVENTIONAL OIL HEATING SYSTEM TO WOOD-BASED RENEWABLE SOURCES HEATING SYSTEM FOR TROPICAL PLANTS PRODUCTION IN MEDITERRANEAN CONDITIONS,” *Acta Hortic.*, no. 893, pp. 421–428, Apr. 2011, doi: 10.17660/ActaHortic.2011.893.40.

[179] A. Ali *et al.*, “Development of a Low-Cost Biomass Furnace for Greenhouse Heating,” *Sustainability*, vol. 13, no. 9, Art. no. 9, Jan. 2021, doi: 10.3390/su13095152.

[180] J. Riahi, S. Vergura, D. Mezghani, and A. Mami, “Smart and Renewable Energy System to Power a Temperature-Controlled Greenhouse,” *Energies*, vol. 14, no. 17, Art. no. 17, Jan. 2021, doi: 10.3390/en14175499.

[181] M. Esen and T. Yuksel, “Experimental evaluation of using various renewable energy sources for heating a greenhouse,” *Energy and Buildings*, vol. 65, pp. 340–351, 2013, doi: 10.1016/j.enbuild.2013.06.018.

[182] Y. Thomas, L. Wang, and A. Denzer, “Energy Savings Analysis of a Greenhouse Heated by Waste Heat,” *Proceedings of the 15th IBPSA Conference*, Aug. 2017, doi: 10.26868/25222708.2017.713.

[183] “SAMLAB - Home.” https://samlab.dibris.unige.it/en/ (accessed Apr. 10, 2021).

[184] “ERDE - Home.” http://www.erde.it/ (accessed Jan. 06, 2022).

[185] T. Day, “Degree-days: theory and application,” *The Chartered Institution of Building Services Engineers*, vol. 106, 2006.

[186] “AMBIENTE IN LIGURIA: METEO.” http://www.cartografiarl.regione.liguria.it/SiraQualMeteo/script/PubAccessoDatiMeteo.asp (accessed Apr. 30, 2021).

[187] E. U. Finlayson, D. K. Arasteh, C. Huizenga, M. D. Rubin, and M. S. Reilly, “WINDOW 4.0: Documentation of calculation procedures,” Lawrence Berkeley Lab., CA (United States), LBL-33943; TA-309, Jul. 1993. doi: 10.2172/10112503.

[188] ISO. 2003. ISO 15099:2003, “Thermal performance of windows, doors, and shading devices – Detailed calculations.” International Organization for Standardization.

[189] G. N. Walton, *Thermal analysis research program reference manual*. US Department of Commerce, National Bureau of Standards Washington, DC, USA, 1983.

[190] H. C. Hottel and A. F. Sarofim, *Radiative transfer*. McGraw-Hill, 1967.

[191] M. Mirsadeghi, D. Cóstola, B. Blocken, and J. L. M. Hensen, “Review of external convective heat transfer coefficient models in building energy simulation programs: Implementation and uncertainty,” *Applied Thermal Engineering*, vol. 56, no. 1, pp. 134–151, Jul. 2013, doi: 10.1016/j.applthermaleng.2013.03.003.

[192] L. Peeters, I. Beausoleil-Morrison, and A. Novoselac, “Internal convective heat transfer modeling: Critical review and discussion of experimentally derived correlations,” *Energy and Buildings*, vol. 43, no. 9, pp. 2227–2239, Sep. 2011, doi: 10.1016/j.enbuild.2011.05.002.

[193] "Engineering Reference," p. 1741.

[194] I. Beausoleil-Morrison, "The adaptive simulation of convective heat transfer at internal building surfaces," *Building and Environment*, vol. 37, no. 8, pp. 791–806, Aug. 2002, doi: 10.1016/S0360-1323(02)00042-2.

[195] S. Frankenstein and G. Koenig, "FASST Vegetation Models," *Cold Regions Research and Engineering Laboratory*, no. December, p. 56, 2004.

[196] P. Eskilson, "Thermal Analysis of Heat Extraction Boreholes," Doctoral Thesis, University of Lund, 1987. [Online]. Available: https://www.osti.gov/etdeweb/biblio/7778302

[197] M. Fossa, "Correct design of vertical borehole heat exchanger systems through the improvement of the ASHRAE method: Science and Technology for the Built Environment: Vol 23, No 7," *Science and Technology for the Built Environment*, vol. Volume 23, 2016, doi: 10.1080/23744731.2016.1208537.

[198] M. Fossa, D. Rolando, and P. Pasquier, "Pulsated Thermal Response Test experiments and modelling for ground thermal property estimation," in *Proceedings of the IGSHPA Research Track 2018*, Sep. 2018, pp. 1–9. doi: 10.22488/okstate.18.000021.

[199] S. Morchio and M. Fossa, "On the ground thermal conductivity estimation with coaxial borehole heat exchangers according to different undisturbed ground temperature profiles," *Applied Thermal Engineering*, vol. 173, p. 115198, Jun. 2020, doi: 10.1016/j.applthermaleng.2020.115198.

[200] C. C. Tang, "Modeling Packaged Heat Pumps in a Quasi-steady State Energy Simulation Program," May 2005, Accessed: May 05, 2021. [Online]. Available: https://shareok.org/handle/11244/10075

[201] Priarone, Silenzi, and Fossa, "Modelling Heat Pumps with Variable EER and COP in EnergyPlus: A Case Study Applied to Ground Source and Heat Recovery Heat Pump Systems," *Energies*, vol. 13, no. 4, p. 794, Feb. 2020, doi: 10.3390/en13040794.

[202] A. De Miguel, J. Bilbao, R. Aguiar, H. Kambezidis, and E. Negro, "Diffuse solar irradiation model evaluation in the North Mediterranean Belt area," *Solar energy*, vol. 70, no. 2, pp. 143–153, 2001, doi: 10.1016/S0038-092X(00)00135-3.

[203] T. Amegroud, "Morocco's Power Sector Transition: Achievements and Potential," *IAI Working Papers 15*, pp. 1–21, Apr. 2015.

[204] R. E. S. for the M. & A. RES4MED&Africa, "COUNTRY PROFILE MOROCCO 2018," *Names*, 2004.

[205] T. Kousksou *et al.*, “Renewable energy potential and national policy directions for sustainable development in Morocco,” *Renewable and Sustainable Energy Reviews*, vol. 47, pp. 46–57, Jul. 2015, doi: 10.1016/J.RSER.2015.02.056.

[206] “Plan Maroc vert : Premières perspectives sur la stratégie agricole Ministère de l’Agriculture,” 2008.

[207] Ministère de l’agriculture pêche maritime du développement rural et des eaux et forêts, “L’agriculture en chiffre_Plan Maroc vert.”

[208] R. Harbouze, J.-P. Pellissier, J.-P. Rolland, and W. Khechimi, “Rapport de synthèse sur l’agriculture au Maroc,” CIHEAM-IAMM, Research Report, 2019. Accessed: Jan. 11, 2022. [Online]. Available: https://hal.archives-ouvertes.fr/hal-02137637

[209] A. Dakkina, “Changement climatique et énergie, Atelier sur l’efficaté énergétique dans le batiment en zone tropical, témognage du Maroc.” ADEREE, 2013.

[210] “Réglement thermique de construction au Maroc (RTCM).” Agence Nationale pour le Dévelopemen des Energies Renouvelables et de l’Efficacité Energétique, 2014.

[211] C. Kittas and A. Bailie, “Determination of the spectral properties of several greenhouse cover materials and evaluation of specific parameters related to plant response,” *Journal of Agricultural and Engineering Research*, vol. 71, no. 2, pp. 193–202, Oct. 1998, doi: 10.1006/jaer.1998.0310.

[212] S. Nicola, G. Tibaldi, and E. Fontana, “TOMATO PRODUCTION SYSTEMS AND THEIR APPLICATION TO THE TROPICS,” *Acta Hortic.*, no. 821, pp. 27–34, Mar. 2009, doi: 10.17660/ActaHortic.2009.821.1.

[213] E. du Plessis, T. Workneh, and M. Laing, “Greenhouse cooling systems and models for arid climate,” in *Sustainable agriculture reviews*, Springer, 2015, pp. 181–215.

[214] “Food and Agriculture Organization of the United Nations.” https://www.fao.org/land-water/databases-and-software/crop-information/tomato/en/ (accessed Jan. 25, 2022).

[215] S. Frankenstein and G. Koenig, “FASST Vegetation Models,” *Cold Regions Research and Engineering Laboratory*, no. December, p. 56, 2004.

[216] *Site web officiel de l’ONEE - Branche Electricité*. Accessed: Feb. 12, 2021. [Online]. Available: http://www.one.org.ma/FR/pages/interne.asp?esp=1&id1=2&id2=35&id3=11&t2=1&t3=1

[217] W. Baudoin *et al.*, “Good agricultural practices for greenhouse vegetable crops: principles for mediterranean climate areas,” *FAO plant production and protection paper (FAO)*, 2013.

[218] S. Theodoridis, “Chapter 18 - Neural Networks and Deep Learning,” in *Machine Learning*, S. Theodoridis, Ed. Oxford: Academic Press, 2015, pp. 875–936. doi: 10.1016/B978-0-12-801522-3.00018-5.

[219] C. K. I. Williams, “Prediction with Gaussian Processes: From Linear Regression to Linear Prediction and Beyond,” in *Learning in Graphical Models*, M. I. Jordan, Ed. Dordrecht: Springer Netherlands, 1998, pp. 599–621. doi: 10.1007/978-94-011-5014-9_23.

[220] H. Drucker, C. J. Burges, L. Kaufman, A. Smola, and V. Vapnik, “Support vector regression machines,” *Advances in neural information processing systems*, vol. 9, pp. 155–161, 1997.

[221] Y. Freund and R. E. Schapire, “Experiments with a new boosting algorithm,” in *icml*, 1996, vol. 96, pp. 148–156.

[222] M.-F. Li, X.-P. Tang, W. Wu, and H.-B. Liu, “General models for estimating daily global solar radiation for different solar radiation zones in mainland China,” *Energy Conversion and Management*, vol. 70, pp. 139–148, Jun. 2013, doi: 10.1016/j.enconman.2013.03.004.

[223] M. Despotovic, V. Nedic, D. Despotovic, and S. Cvetanovic, “Evaluation of empirical models for predicting monthly mean horizontal diffuse solar radiation,” *Renewable and Sustainable Energy Reviews*, vol. 56, pp. 246–260, Apr. 2016, doi: 10.1016/j.rser.2015.11.058.

[224] Z. Bounoua, L. Ouazzani Chahidi, and A. Mechaqrane, “Estimation of daily global solar radiation using empirical and machine-learning methods: A case study of five Moroccan locations,” *Sustainable Materials and Technologies*, p. e00261, Feb. 2021, doi: 10.1016/j.susmat.2021.e00261.

Annex 1. Systems specifications of SamLab greenhouse (shading, natural ventilation, geothermal and PV systems).

Shading/reflecting system				
Thickness				0.001 m
Shade to glass distance				0.05 m
Conductivity				0.1 W/m. °C
Solar transmittance				0.5
Solar reflectance				0.4
Operable windows				
Total area				63 m²
Control temperatures	Max indoor			60 °C
	Min indoor			16 °C
	Max outdoor			30 °C
	Min outdoor			16 °C
Photovoltaic modules				
Technology				Polycrystalline
Total area				22 m²
Shaded area				11 m² (50%)
Temperature coefficient				0,43%/K
Efficiency of active area				17%
Ground coupled heat pump				
Number of boreholes				6
Borehole length				100 m
Borehole diameter				0.032 m
Heat pump	Heating PLF 95%	Inlet temperature		10 °C
		Outlet temperature		55 °C
		Nominal capacity		28 kW
		COP		3.7
		Equation fit coefficients	A_1	-2.7274
			A_2	-1.9571
			A_3	5.6563
			B_1	-4.9581
			B_2	5.5621
			B_3	0.0031
	Cooling PLF 100%	Inlet temperature		20 °C
		Outlet temperature		7 °C
		Nominal capacity		34.4 kW
		EER		5.29
		Equation fit coefficients	D_1	8.2047
			D_2	3.1824
			D_3	-10.2275
			E_1	4.7551
			E_2	-3.7212
			E_3	-0.0276

Annex 2. Annual air-conditioning cost for different combinations (Shape/cover) for the six climatic zones depending on greenhouses external surface.

		Shape (1)	Shape (2)	Shape (3)	Shape (4)	Shape (5)	Shape (6)	Shape (7)	Shape (8)	Shape (9)
Cost MAD/m²(external surface)/year	**Zone 1 (Agadir)**									
	Glass	89.87	90.11	89.96	117.51	94.09	89.71	86.46	91.87	87.10
	LDPE	88.51	88.73	88.56	115.55	92.58	88.33	85.01	90.31	85.66
	BPE	82.22	82.46	82.01	107.61	85.84	81.50	78.59	83.63	79.63
	EVA	90.14	90.34	90.25	117.57	94.33	90.17	86.71	92.06	87.22
	Zone 2 (Tangier)									
	Glass	94.75	95.05	94.57	123.15	98.76	93.70	89.82	95.52	91.09
	LDPE	94.06	94.34	93.81	122.03	97.96	92.97	89.00	94.64	90.34
	BPE	87.23	87.53	86.78	113.35	90.64	85.66	82.03	87.40	83.73
	EVA	95.91	96.17	95.70	124.34	99.95	94.98	90.92	96.60	92.13
	Zone 3 (Fez)									
	Glass	112.66	113.24	112.09	144.43	117.12	108.02	105.09	110.07	106.87
	LDPE	112.72	113.29	112.06	144.25	117.14	107.99	104.99	109.90	106.87
	BPE	105.43	105.99	104.57	135.07	109.28	100.42	97.77	102.45	99.96
	EVA	113.16	113.84	112.81	144.27	117.55	107.77	105.14	109.67	107.33
	Zone 4 (Ifran)									
	Glass	128.25	129.06	127.44	162.48	132.79	120.94	117.96	122.85	120.64
	LDPE	129.18	129.97	128.25	163.37	133.73	121.73	118.65	123.53	121.47
	BPE	120.05	120.81	118.99	151.94	123.92	112.63	109.91	114.49	112.94
	EVA	131.55	132.34	130.63	166.30	136.28	124.12	120.92	125.86	123.67
	Zone 5 (Marrakech)									
	Glass	104.56	104.97	104.48	135.75	109.03	102.71	99.70	105.15	100.77
	LDPE	103.34	103.71	103.20	133.95	107.64	101.47	98.38	103.75	99.49
	BPE	96.32	96.71	95.96	125.14	100.13	93.98	91.35	96.45	92.84
	EVA	105.03	105.38	104.94	136.03	109.47	103.36	100.12	105.53	101.09
	Zone 6 (Errachidia)									
	Glass	113.66	114.21	113.12	146.25	117.68	109.18	106.74	112.01	108.88
	LDPE	112.67	113.18	112.05	144.75	116.57	108.24	105.66	110.89	107.87
	BPE	105.72	105.92	104.91	136.15	109.18	101.15	98.99	104.01	101.42
	EVA	114.38	114.88	113.79	146.82	118.38	110.01	107.30	112.55	108.88

Terminology

[i] Law of Wien: states the relationship between the temperature of a blackbody (an ideal substance that emits and absorbs all frequencies of light) and the wavelength at which it emits the most light.

[ii] Stomatal resistance: it characterizes the capacity of the plant to resist on the transport of different quantities, such as water vapor, CO_2 from or to stomata. In other words, as much as stomata resistance is important the plant's leaves pores aperture is low and inversely.

[iii] Photosynthesis: is the process of converting carbon dioxide and water into organic material by using solar energy, and then producing oxygen.

[iv] Photomorphogenesis: the set of changes that the plant undergoes due to the influence of the variation of light, i.e., plants' color, size, etc. Otherwise stated, it is the plant's reaction to the variation in light [26], [27].

[v] Photoperiodism: the reaction of plants to changes in daylength that has been considered as a major factor in plant's seasonal regulation. It can also be defined as a mechanism for the plants for measuring time [28].

[vi] Near East and North Africa countries: Algeria, Cyprus, Egypt, Jordan, Lebanon, Libya, Malta, Morocco, the Palestinian Authority, the Syrian Arab Republic, Tunisia, and Turkey.